

University of Windsor

Scholarship at UWindor

Electronic Theses and Dissertations

Theses, Dissertations, and Major Papers

2008

Investigation of cohesive and interfacial properties of structural adhesive materials by advanced acoustic methods

Ina A. Seviaryna
University of Windsor

Follow this and additional works at: <https://scholar.uwindsor.ca/etd>

Recommended Citation

Seviaryna, Ina A., "Investigation of cohesive and interfacial properties of structural adhesive materials by advanced acoustic methods" (2008). *Electronic Theses and Dissertations*. 7883.
<https://scholar.uwindsor.ca/etd/7883>

This online database contains the full-text of PhD dissertations and Masters' theses of University of Windsor students from 1954 forward. These documents are made available for personal study and research purposes only, in accordance with the Canadian Copyright Act and the Creative Commons license—CC BY-NC-ND (Attribution, Non-Commercial, No Derivative Works). Under this license, works must always be attributed to the copyright holder (original author), cannot be used for any commercial purposes, and may not be altered. Any other use would require the permission of the copyright holder. Students may inquire about withdrawing their dissertation and/or thesis from this database. For additional inquiries, please contact the repository administrator via email (scholarship@uwindsor.ca) or by telephone at 519-253-3000ext. 3208.

NOTE TO USERS

This reproduction is the best copy available.

UMI[•]

**INVESTIGATION OF COHESIVE AND INTERFACIAL PROPERTIES
OF STRUCTURAL ADHESIVE MATERIALS
BY ADVANCED ACOUSTIC METHODS**

by
Ina A. Seviaryna

A Dissertation
Submitted to the Faculty of Graduate Studies
through the Department of Chemistry and Biochemistry
in Partial Fulfillment of the Requirements for
the Degree of Doctor of Philosophy at the
University of Windsor

Windsor, Ontario, Canada

2008

© 2008 Ina A. Seviaryna



Library and Archives
Canada

Published Heritage
Branch

395 Wellington Street
Ottawa ON K1A 0N4
Canada

Bibliothèque et
Archives Canada

Direction du
Patrimoine de l'édition

395, rue Wellington
Ottawa ON K1A 0N4
Canada

Your file *Votre référence*
ISBN: 978-0-494-57645-8
Our file *Notre référence*
ISBN: 978-0-494-57645-8

NOTICE:

The author has granted a non-exclusive license allowing Library and Archives Canada to reproduce, publish, archive, preserve, conserve, communicate to the public by telecommunication or on the Internet, loan, distribute and sell theses worldwide, for commercial or non-commercial purposes, in microform, paper, electronic and/or any other formats.

The author retains copyright ownership and moral rights in this thesis. Neither the thesis nor substantial extracts from it may be printed or otherwise reproduced without the author's permission.

AVIS:

L'auteur a accordé une licence non exclusive permettant à la Bibliothèque et Archives Canada de reproduire, publier, archiver, sauvegarder, conserver, transmettre au public par télécommunication ou par l'Internet, prêter, distribuer et vendre des thèses partout dans le monde, à des fins commerciales ou autres, sur support microforme, papier, électronique et/ou autres formats.

L'auteur conserve la propriété du droit d'auteur et des droits moraux qui protègent cette thèse. Ni la thèse ni des extraits substantiels de celle-ci ne doivent être imprimés ou autrement reproduits sans son autorisation.

In compliance with the Canadian Privacy Act some supporting forms may have been removed from this thesis.

While these forms may be included in the document page count, their removal does not represent any loss of content from the thesis.

Conformément à la loi canadienne sur la protection de la vie privée, quelques formulaires secondaires ont été enlevés de cette thèse.

Bien que ces formulaires aient inclus dans la pagination, il n'y aura aucun contenu manquant.


Canada

Declaration of Co-Authorship/Previous Publications

I. Co-Authorship Declaration

I hereby declare that this thesis incorporates material that is a result of joint research undertaken in collaboration with Adrian Fabre and Fedar Severin under the supervision of Professor Elena Maeva. The collaboration results are covered in Chapter 6 of this Dissertation where the contribution of the co-authors was primarily through statistical analysis of the acoustic images performed by Adrian Fabre and code building for 2D FFT analysis of acoustic images performed by Fedar Severin. This dissertation also contains material that has been previously published in co-authorship. All incorporated material is a result of the author's own work that was performed and written by the author. In all cases, the key ideas, primary contributions, experimental designs, data analysis and interpretation and writing were performed by the author.

I am aware of the University of Windsor Senate Policy on Authorship and I certify that I have properly acknowledged the contribution of other researchers to my thesis. I certify that, with the above qualification, this thesis and the research to which it refers is the product of my own work.

II. Declaration of Previous Publications

This dissertation includes material from 4 original papers that have been previously published, as follows:

| Thesis chapter | Publication title | Publication status |
|----------------|---|--------------------|
| Chapter 2 | Maeva, E.; Severina, I.; Bondarenko, S.; Chapman, G.; O'Neill, B.; Maev, R.; Severin, F. Acoustical methods for the investigation of adhesively bonded structures: A review, <i>Canadian Journal of Physics</i> 2004 , 82, 981-1025. | Published |
| Chapter 3 | Maeva, E.; Severina, I.; Bondarenko, S.; Chapman, G.; O'Neill, B.; Maev, R.; Severin, F. Acoustical methods for the investigation of adhesively bonded structures: A review, <i>Canadian Journal of Physics</i> 2004 , 82, 981-1025 | Published |
| Chapter 5 | E. Yu. Maeva, I. Severina, G. B. Chapman, Analysis of the degree of cure and cohesive properties of the adhesive in a bond joint by ultrasonic techniques, <i>Research in Non-destructive Evaluation</i> , 18, n. | Published |

| | | |
|-----------|---|-----------|
| | 2, 2007 , p 121-138 | |
| Chapter 6 | E. Yu. Maeva, I. Severina, G. B. Chapman, Analysis of the degree of cure and cohesive properties of the adhesive in a bond joint by ultrasonic techniques, <i>Research in Non-destructive Evaluation</i> , 18, n. 2, 2007 , p 121-138 Severina, I. A.; Fabre, A. J.; Maeva, E. Y. In Acoustic imaging of microstructure and evaluation of the adhesive's physical, mechanical and chemical properties changes at different cure states, <i>Acoustical Imaging</i> ; 2007 Vol. 28, Plenum publishing Corp., pp. 367-374. | Published |
| Chapter 7 | Maeva, E.; Severina, I.; Bondarenko, S.; Chapman, G.; O'Neill, B.; Maev, R.; Severin, F. Acoustical methods for the investigation of adhesively bonded structures: A review, <i>Canadian Journal of Physics</i> 2004 , 82, 981-1025. Maeva, E. Y.; Severina, I. A.; Chapman II, G. B.; Severin, F. M.; O'Neill, B.; Maev, R. G. Acoustic visualization of the interface deterioration in the adhesive bond joint; (ed. W. Arnold and S. Hirsekorn), <i>Acoustical Imaging</i> ; 2004 Kluwer Academic Publishers, Netherlands, publishing Corp., Vol. 27, pp. 99-104. | Published |

I certify that I have obtained a written permission from the copyright owner to include the above published material in my thesis. The Publishers of the papers are fully acknowledged in the thesis by citations. Copies of the Copyright Transfer Agreements and Permissions are included in the Appendix A. I certify that the above material describes work completed during my registration as a graduate student at the University of Windsor.

I declare that, to the best of my knowledge, my thesis does not infringe upon anyone's copyright nor violate any proprietary rights and any ideas, techniques, quotations, or any other material from the other people included in my thesis, published or otherwise, are fully acknowledged in accordance with the standard referencing practices. I certify that, as the Canada Copyright Act specifies, all copyrighted material is used as fair dealing without infringement for the purpose of review and acknowledgment is made to the source.

I declare that this is a true copy of my thesis, including any final revisions, as approved by my thesis committee and Graduate Studies office, and that this thesis has not been submitted for a higher degree to any other University or Institution.

INVESTIGATION OF COHESIVE AND INTERFACIAL PROPERTIES OF THE STRUCTURAL ADHESIVE MATERIALS BY ADVANCED ACOUSTIC METHODS

by
Ina A. Seviaryna

Chemistry Program

ABSTRACT

This research study has examined the feasibility of using acoustic methods for evaluation of the adhesive mechanical properties. The first method is based on the measurement of bulk longitudinal sound velocity during the process of the adhesive cure reaction. Glass transition temperature T_g depends on the extent of reaction of adhesive polymerization; acoustic parameters reflect viscoelastic properties of the material. Acoustic characteristics such as sound velocity or attenuation reflect changes in the adhesive mechanical properties and predict cohesive strength of the adhesive joint. Experimental results show the validity of this assumption. Methodology for monitoring the viscoelastic properties of the adhesive was developed. It was shown that sound velocity in epoxy adhesive correlates with the cohesive strength of the adhesive.

The second method is scanning acoustic microscopy which quantitatively allows visualization of the intact adhesive/steel interface. Changes in the microstructure on the intact metal-adhesive interface were investigated. Two dimensional Fourier transforms allow us to determine the main sizes of the granular structure which is $200\mu\text{m}$. It was shown that changes in brightness of the images correspond to changes in the reflection coefficient on the adhesive/metal during polymerization reaction. Adhesive adjacent to the interface has Young's modulus slightly higher than the adhesive in the middle of the layer. Conditions optimal for visualization of the major defects of the adhesive structure were determined. The capability of scanning acoustic microscopy to detect and dynamically monitor small changes in both structure of the metal/epoxy interface and bulk adhesive material was demonstrated.

*To my parents,
Alexander and Galina Bravseвич*

ACKNOWLEDGEMENTS

There are many people whom I would like acknowledge and thank for their help and support with this research project.

First and foremost, I would like to thank my research advisor Dr. Elena Maeva for her guidance and intellectual support throughout my studies. Without her never ending ideas, this study would never been completed. Her enthusiasm, warm words of encouragement and everyday optimism have helped me to make this dissertation possible. She is a very kind person and excellent teacher.

I would like to express my respect to Dr. Roman Gr. Maev for introducing me to the world of acoustic microscopy and giving me so much credit when I just started to study acoustics. I need to mention that it is he who encouraged me to continue my education. It is amazing how this very busy person can find time for every student. I would like thank him for generating a very creative and comfortable work atmosphere in the NSERC Industrial Research Chair in Applied Solid State Physics and Material Characterization.

I would like to thank my Examination Committee Members Dr. Alex Adronov, Dr. Wladyslaw Kedzierski, Dr. Keith Taylor, Dr. Holger Eichhorn, Dr. William Baylis and Dr. Elena Maeva for their valuable advice and time.

I would also like to thank Mr. John Robinson for his assistance in electron microscopic analysis of the samples. I would like to thank C.-K. Jen and Jacques Tatibouet for hosting me at the acoustic lab in Industrial Material Institute in Boucherville for two weeks, where experiments for Chapter 5 were performed and for their valuable suggestions in my work.

Many thanks go to my husband and colleague Dr. Fedar Severin for hours of discussion of some aspects of my research, his valuable advice, encouragement and for just being together and supporting me through these years. I express my thankfulness to

my son Roman for giving me the joyful time of being Mom and for his patience while I was busy doing research. I would also like to thank my parents whom this dissertation is dedicated.

I express my gratitude to Sarah Beneteau for her generosity and kindness to me. Her guidance has helped me to improve my English. I am grateful to Graduate Secretary of Chemistry & Biochemistry Department Marlene Bezaire for the academic guidance through the years of my study. Thanks are also due to all CIRAMC members for enjoyable work and collaboration.

I also must acknowledge NSERC for funding this Project and DaimlerChrysler (both US and German sides) for the collaboration and financial support in this Project.

TABLE OF CONTENTS

| | |
|---|-------|
| DECLARATION OF CO-AUTHORSHIP/PREVIIOUS PUBLICATIONS | iii |
| ABSTRACT | v |
| DEDICATION | vi |
| ACKNOWLEDGMENTS | vii |
| LIST OF FIGURES | xii |
| LIST OF TABLES | xvii |
| LIST OF ABBREVIATIONS | xviii |
| I. Introduction | 1 |
| 1.1. Importance of the Adhesive Bonding with Structural Adhesives. | 1 |
| 1.2. Factors that Influence the Adhesive Joint Microstructure and Strengths | 2 |
| 1.3. Problem Statement. | 4 |
| 1.4. Goals of Research | 6 |
| 1.5. Novelty | 7 |
| 1.6. Dissertation Outline | 8 |
| II. Review of Literature. Adhesion Models and Mechanisms | 9 |
| 2.1. Epoxies as Structural Adhesives | 9 |
| 2.1.1. Techniques for Monitoring of Physical and Chemical Properties During Adhesive Cure | 17 |
| 2.2. Models and Mechanisms of Adhesion | 19 |
| 2.2.1. Adhesive and Cohesive Forces. Factors Contributing to Joint Strength | 19 |
| 2.2.2. Wettability | 20 |
| 2.2.3. Mechanical Interlocking Model | 22 |
| 2.2.4. Adsorption Theory | 23 |
| 2.2.5. Electrostatic Theory | 29 |
| 2.2.6. Diffusion Theory | 32 |
| 2.2.7. Weak boundary Layer Model | 34 |
| 2.3. Adhesion at Polymer/Metal Interface | 36 |
| III. Viscoelastic Properties of Cross-linked Polymers and Methods of Their Evaluation. | 41 |
| 3. 1. Elastic Moduli. Stress and Strain. | 41 |
| 3.2. Dependence of Viscoelastic Properties of Cross-linked Amorphous Polymers on Temperature. Glass Transition Temperature (T _g). | 43 |
| 3.3. Effect of Polymerization Reaction on Polymer's T _g . Gelation and Vitrification | 48 |
| 3.4. Acoustic Wave Propagation in Isotropic Elastic and Viscoelastic Materials. | 50 |
| 3.5. Sound Velocity and Absorption | 51 |

| | |
|--|-----|
| 3.6. Relation of Acoustic Parameters to Chemical Structure and Physical Properties of Polymers | 54 |
| 3.7. Acoustic Methods for Adhesive Joint Evaluation | 55 |
| 3.7.1. Pulse-Echo Technique. | 56 |
| 3.7.2. Scanning Acoustic Microscopy | 62 |
| IV. Materials and Methods | 68 |
| 4.1. Epoxy Adhesive Systems | 68 |
| 4.1.1. Two-Component System | 68 |
| 4.1.2. One-Component Epoxy System | 70 |
| 4.1.3. Preparation of the Adhesive Bond Joints. | 74 |
| 4.2. Experimental Procedures | 75 |
| 4.2.1. Differential Scanning Calorimetry (DSC) | 75 |
| 4.2.2. Density/Specific Volume Determination | 76 |
| 4.2.3. Microhardness Measurement | 76 |
| 4.2.4. Adhesive Joint Strength Measurement. | 79 |
| 4.3. Acoustic Methods. | 81 |
| 4.3.1. The basic Principles of the Acoustic Method | 81 |
| 4.3.2 Acoustic Transmission Mode for Measuring Adhesive Properties | 82 |
| 4.3.3. Reflection mode for measuring acoustic properties. | 84 |
| 4.3.4. Calculation of Elastic Moduli Values of Adhesives | 87 |
| 4.3.5. Monitoring of the Adhesive Properties During Polymerization Reaction. | 87 |
| 4.3.6. Acoustic Thermal Characterization of Adhesive | 88 |
| 4.3.7. Scanning Acoustic Microscopy. | 90 |
| 4.3.8. Acoustic Imaging of Intact metal/Epoxy Interface | 94 |
| V. Evaluation of Cohesive Properties of the Structural Adhesives. | 96 |
| 5.1 Adhesive Cure Monitoring for Two-Component system. Preliminary Experiments | 98 |
| 5.2. Investigation of Viscoelastic Properties of Completely Cured Adhesive. | 106 |
| 5.3. Isothermal Cure Monitoring of One-Component Adhesive System | 113 |
| 5.4. Continuous Heating cure of One-Component Adhesive System | 122 |
| 5.5. Study of Changes in T_g Temperature During Adhesive Polymerization | 128 |
| 5.6. Cohesive Strength of Structural Adhesives | 132 |
| VI. Microstructure of the Adhesive-Metal Interface | 136 |
| 6.1. Microstructure on the Intact Epoxy Adhesive-Steel Interfaces. | 136 |
| 6.2. Analysis of the Adhesive Layer Cross-Section in Adhesive Bond Joints | 148 |
| VII. Analysis of the Adhesive Joints Deterioration | 151 |
| 7.1. Major Defects Appear in Adhesive Joints | 152 |
| 7.1.1. Scanning Acoustic Microscopy for Defects Evaluation in Adhesive Bond Joints | 154 |
| 7.2. Effect of Water | 157 |

| | |
|---|-----|
| 7.2.1. Mechanisms of Water Action | 157 |
| 7.2.2. Effect of Water on the Adhesive Joints with Cured Epoxy Adhesive | 159 |
| 7.2.3. Effect of Moisture on Uncured Epoxy Adhesive Joints | 167 |
| 7.3. Accelerated Aging of the Adhesive Bond Joints | 170 |
| 7.4. Effect of Stress | 174 |
| 7.4.1. Normal Tensile Load for the Adhesive Bond | 175 |
| 7.5. Joint Preparation | 177 |
| 7.5.1. Contaminations of the Substrate | 177 |
| 7.5.2. Improper Cure Conditions | 180 |
| VIII. CONCLUSIONS | 181 |
| REFERENCES | 183 |
| APPENDIX A: Copyright Permissions | 195 |
| VITA AUCTORIS | 199 |

LIST OF FIGURES

| | | |
|--------------|--|----|
| Figure 1.1. | Schematic representation of the adhesive bond joint. | 2 |
| Figure 2.1. | Two-dimensional schematic showing various stages of cure. | 10 |
| Figure 2.2. | Structure of diglycidyl ether of bisphenol A resin (DGEBA). | 10 |
| Figure 2.3. | General reaction between epoxy and hardener. | 11 |
| Figure 2.4. | Cross-linking site between epoxy and DDA. | 12 |
| Figure 2.5. | Mesomeric structures of DDA | 12 |
| Figure 2.6. | Reaction of DDA with epoxy resin. | 13 |
| Figure 2.7. | Etherification of secondary hydroxyl groups. | 13 |
| Figure 2.8. | Proposed mechanisms for epoxy cure with DDA by Sounders et al. | 14 |
| Figure 2.9. | Proposed mechanisms for epoxy cure with DDA by Zahir. | 15 |
| Figure 2.10. | Proposed mechanisms for epoxy cure with DDA by Gilbert et al. | 15 |
| Figure 2.11. | Proposed mechanisms for epoxy cure with DDA by Pfitzmann et al | 16 |
| Figure 2.12. | Cohesive and adhesive types of failure. | 20 |
| Figure 2.13. | The equilibrium forces balance according to the Young's equation. | 21 |
| Figure 2.14. | Types of surface irregularities, (right). Sufficient wetting (a) and poor wetting (b), (left) (after Fourche). | 22 |
| Figure 2.15. | Electrical double layer at the polymer-metal interface. | 29 |
| Figure 2.16. | Electron donor-acceptor pairs (after Hays). | 29 |
| Figure 2.17. | Interdiffusion of adhesive (a) and substrate (b) molecules. | 32 |
| Figure 2.18. | Schematic representation of metal substrate surface regions. | 37 |
| Figure 2.19. | The water and oxide layers on the metal surface. M-metal, O- oxygen, O:-water, O ·-hydroxyl group. | 38 |
| Figure 2.20. | Interaction of water and organic molecules with zinc oxide. | 38 |
| Figure 2.21. | Polysiloxane network formation at the metal surface. | 40 |
| Figure 3.1. | Phase shift between stress and strain during sinusoidal deformation of polymers. | 42 |
| Figure 3.2. | Regions of viscoelastic behavior of amorphous cross-linked polymer | 43 |
| Figure 3.3. | Effect of cross-link density on the physical state of the epoxy adhesive | 45 |
| Figure 3.4. | Time-temperature-transformation diagram for typical epoxy based adhesive | 59 |
| Figure 3.5. | Time representation of the echoes. | 57 |
| Figure 4.1. | Mechanism of cross-linking reaction between PU and epoxy resins. | 74 |

| | | |
|--------------|---|-----|
| Figure 4.2. | Intermolecular hydrogen bonding between epoxy and polyurethane | 74 |
| Figure 4.3. | Sample for lap shear experiment. | 75 |
| Figure 4.4. | Configuration of the Vickers microhardness indenter. | 77 |
| Figure 4.5. | Contact geometry for Vickers indenter at (A) zero load, (B) maximum load and (C) complete unload, h is residual penetration | 88 |
| Figure 4.6. | Load-unload curve for microhardness testing. | 78 |
| Figure 4.7. | Zwick Z150 material testing machine (left) and specimen grips for tensile lap shear test (right). | 80 |
| Figure 4.8. | Tensile test profile. | 80 |
| Figure 4.9. | Schematic representation of reflected and transmitted waves in the sample. | 82 |
| Figure 4.10. | Schematic representation of the sound wave propagation (a). Ultrasonic polymer characterization system (b). | 83 |
| Figure 4.11. | Experimental setup for the pulse-echo mode. 1-buffer rod, 2-heating tape, 3-adhesive sample, 4-thermocouple, 5- temperature controller, 6- pulse-receiver. | 84 |
| Figure 4.12. | Schematic representation of the reflections origin (a) and typical A-scan (b). | 85 |
| Figure 4.13. | Test cell design for two-component adhesive. | 86 |
| Figure 4.14. | Temperature profile for investigation of temperature dependence of the epoxy on different cure stages. | 88 |
| Figure 4.15. | Schematic representation of the principle of acoustic scanning (a) and Tessonics AM1102 scanning acoustic microscope (b). | 90 |
| Figure 4.16. | Schematic representation of the acoustic image formation: A-scan (a), B-scan (b) and C-scan (c). | 91 |
| Figure 4.17. | Schematic image of the acoustic lens. | 92 |
| Figure 5.1. | Pulse-echo waveforms for uncured epoxy (a), at gelation time (b) and cured (c) epoxy. | 99 |
| Figure 5.2. | Individual acoustic A-scans before (a), in the middle (b) and at the end of epoxy polymerization reaction (c). Left –original oscillograms, right-oscillograms after matched filtration. | 100 |
| Figure 5.3. | Acoustic signature of curing process and individual A-scans before reaction (1), in the middle of process (2) and for completely polymerized epoxy (3). t_1 is the acoustic reflection from the top of the epoxy cell, t_2 is the reflection from the bottom of the cell. | 102 |
| Figure 5.4 | Change of the sound velocity (top) and attenuation (bottom) during epoxy-amine polymerization reaction. Epoxy-amine ratio: —-1:1; - - - 1:2 (h-r excess),1:0.5 (h-r limit). | 104 |
| Figure 5.5. | Change of the storage longitudinal elastic modulus (top) and loss longitudinal modulus (bottom) during epoxy-amine polymerization reaction. Notations as for Figure 5.4. | 105 |
| Figure 5.6. | Change of the loss tangent during epoxy-amine polymerization reaction. Notations as for Figure 5.4. | 106 |

| | | |
|--------------|--|-----|
| Figure 5.7. | Temperature dependence of longitudinal sound velocity and attenuation of the completely cured adhesive. | 108 |
| Figure 5.8. | Temperature dependence of the elastic moduli of the completely cured adhesive. | 108 |
| Figure 5.9. | Temperature dependence of loss factor of the completely cured adhesive | 109 |
| Figure 5.10. | DSC scan for cured adhesive | 111 |
| Figure 5.11 | Thermodilatometry analysis. Temperature dependence of specific volume of the completely cured adhesive. | 111 |
| Figure 5.12. | Representative curve of sound velocity and attenuation versus temperature in the region of the Tg of epoxy adhesive. Numbers are assigned as in Table 5.1. | 112 |
| Figure 5.13. | Changes in longitudinal sound velocity (top) and attenuation (bottom) during adhesive polymerization at different temperatures. | 115 |
| Figure 5.14. | Changes in longitudinal storage modulus (top) and loss modulus (bottom) during adhesive polymerization at different temperatures. | 117 |
| Figure 5.15. | Changes in loss tangent during adhesive polymerization at different temperatures. | 118 |
| Figure 5.16. | Acoustic extent of adhesive polymerization reaction. | 119 |
| Figure 5.17. | Thermal scans of the adhesives polymerized at different temperatures (100, 120, 140, 160, and 180°C). | 122 |
| Figure 5.18. | Changes of sound velocity (1) and attenuation (2) during continuous heating cure. Straight line shows temperature profile. Heating rate is 10 °C/min. | 123 |
| Figure 5.19. | Changes of adhesive density during continuous heating cure. | 124 |
| Figure 5.20. | Changes in adhesive loss L'' (1) and storage L' (2) moduli during non-isothermal cure. Heating rate is 10 °C/min | 125 |
| Figure 5.21. | Acoustic properties of the adhesive cured at constant heating rate. | 125 |
| Figure 5.22. | Longitudinal elastic moduli of the adhesive cured at constant heating rate. | 126 |
| Figure 5.23. | Loss tangent modulus of the adhesive cured at constant heating rate. | 127 |
| Figure 5.24. | Changes in thermo-acoustic parameters of the epoxy with increasing reaction temperature. Maximal temperature of cure: 1-50°C, 2-70°C, 3-100°C, 4-130°C, 5-160°C, 6-190°C, 7-210°C. | 129 |
| Figure 5.25. | Changes of the loss factor $\tan \delta$ maximum during cure. Indexes are as in Fig. 5.24. | 130 |
| Figure 5.26. | Changes of the loss factor $\tan \delta$ maximum during cure. | 130 |
| Figure 5.27. | Correlation of the sound velocity of the epoxy and the $\tan \delta$ maximum. | 131 |
| Figure 5.28. | Dependence of the joint strength on time of the cure at 180°C (1) and 120°C (2). | 134 |
| Figure 5.29. | Dependence of the joint strength and longitudinal sound velocity on the time of the adhesive cure at 180°C. | 134 |

| | | |
|--------------|---|-----|
| Figure 5.30. | Correlation of longitudinal sound velocity of the adhesive to joint strength. | 135 |
| Figure 6.1. | Development of the microstructure of metal-adhesive interface during polymerization reaction at 180°C. 250 MHz. samples were cured for 0 (a), 10 (b) and 35 (c) min. (d)-image of the interface cured at 200°C for 45 min. | 139 |
| Figure 6.2. | Minimum (left) and maximum (right) intensity as a function of cure time. | 140 |
| Figure 6.3. | Reflection coefficient for steel-adhesive interface during polymerization reaction. | 140 |
| Figure 6.4. | Histograms and cross sections of the acoustic images on Figure 6.1 (a), cured (b) and aged (d) adhesive. | 142 |
| Figure 6.5. | 2D Fourier transform to the acoustic images (Figure 6.1.b). | 143 |
| Figure 6.6. | Analysis of the granular structure on the acoustic image in Figure 6.1. (b). | 144 |
| Figure 6.7. | 2D Fourier transform of acoustic images of the adhesive-metal interfaces from Figure 6.1. | 145 |
| Figure 6.8. | Analysis of the granular structure on the acoustic image in Figure 6.1. | 146 |
| Figure 6.9. | Destructive test results. Strength of the adhesive joints. | 147 |
| Figure. 6.10 | Scanning electron micrographs of fracture surface of tensile test. (a)-properly cured adhesive, (b)-thermally degraded adhesive. x1500 magnification | 147 |
| Figure 6.11. | Acoustic images of the adhesive joint cross section. Adhesive layer thickness is 0.3 mm. Adhesive was hardened at 180 °C during (a)-10 min,(b)-30 min. (c)-adhesive was hardened at 200 °C during 45 min. | 148 |
| Figure 6.12. | Young's modulus values measured across the adhesive layer in adhesive bonds. | 150 |
| Figure. 7.1. | Typical defects and different layers in adhesively bonded joints. | 153 |
| Figure. 7.2. | The A-scan obtained on steel-epoxy-steel adhesive bonding for good quality adhesive. Focal point tuned to first interface. Pulse 1 is the reflected from the steel-epoxy interface; arrow shows the adhesive layer thickness. | 156 |
| Figure. 7.3. | The A-scan obtained on steel-epoxy-steel adhesive bonding for aged adhesive. Pulse 1 is the reflected from the steel-epoxy interface; arrow shows the adhesive layer thickness. | 156 |
| Figure 7.4. | Schematic sketch of the hydrolysis mechanisms that going on in DDA-cured epoxy adhesive during hydrothermal aging (a)18 and in uncured epoxy adhesive (b) 197. | 159 |
| Figure 7.5. | Tensile test results for adhesive joints immersed in water at 20 and 80 °C. Wet samples are shown in gray, dried after immersion samples are white color. | 160 |
| Figure 7.6. | Typical stress-strain curves for normal (solid line) and degraded (dashed line) adhesive joint. | 161 |

| | | |
|--------------|---|-----|
| Figure 7.7. | Joint strength for properly cured (1), undercured (2) and overcured epoxy adhesive before (black) and after (gray) water exposure. | 162 |
| Figure 7.8. | Water uptake and bond strength for epoxy adhesive. | 162 |
| Figure 7.9. | Correlation of the water uptake by epoxy adhesive in the joint and the joint strength. | 163 |
| Figure 7.10. | Young modulus determined by dynamic microhardness method for the adhesive exposed to water. | 164 |
| Figure 7.11. | Acoustic scans of the steel/epoxy interface at day 1 (left) and day 7 (right). Microvoids are shown by arrows. | 165 |
| Figure 7.12. | Histograms of the images on the Fig. 7.11. | 165 |
| Figure 7.13. | Appearance of the voids on the steel/epoxy interface in the adhesive joints immersed in water for 3 days (a) and for 8 days (b). | 167 |
| Figure 7.14. | Microvoids at the interface (left) and inside (middle) the epoxy layer as a result of the waster sorption by uncured epoxy adhesive. Electron microscopy image of fracture surface is shown for comparison (right). | 168 |
| Figure 7.15. | Electron images of the fracture surface for normal adhesive (left) and adhesive immersed into water before cure reaction (right). | 169 |
| Figure 7.16. | Acoustic C-scans of the steel/epoxy interface (left) and middle part of the adhesive layer (right) after accelerated aging procedure | 171 |
| Figure 7.17. | Acoustic image of the adhesive/metal interface structure at late stages of the accelerated aging. | 171 |
| Figure 7.18. | The acoustic images of the intact (left) and degraded (middle and right) steel/epoxy interface. | 172 |
| Figure 7.19. | Images shown in the Figure 7.18 presented in pseudo color scale | 172 |
| Figure 7.20. | Histograms and profiles of the images presented at the Figure 7.18. | 173 |
| Figure 7.21. | Destructive test results. | 173 |
| Figure 7.22. | Deformation of the voids at the adhesive/metal interface due to stress. 1-stress was not applied, 2 and 3-stress was applied in the direction shown by arrow. | 174 |
| Figure 7.23. | Appearance of cavities in the adhesive layer due to joint clamp been removed before adhesive solidification. | 175 |
| Figure 7.24. | Experimental setup. | 175 |
| Figure 7.25. | Acoustic images of the steel/epoxy interface at the increasing load. | 176 |
| Figure 7.26. | Acoustical images of the adhesion problems caused by oil (a) and Teflon (b) contamination on the interface. | 189 |
| Figure 7.27. | Acoustic image of the adhesive joint with uncured adhesive area. | 180 |

LIST OF TABLES

| | | |
|------------|---|-----|
| Table 4.1. | Composition of two-component adhesive system | 69 |
| Table 4.2. | Composition of BETAMATE adhesive. | 71 |
| Table 4.3. | Characteristics of the acoustic lens. | 95 |
| Table 5.1. | Determination of Tg value by acoustic method. | 112 |
| Table 5.2. | Gelation time for structural adhesives cured at different temperatures. | 121 |
| Table 6.1. | Distribution of the Young's modulus across the adhesive joint | 149 |
| Table 7.1. | Acoustic properties of the adhesion contaminants. | 178 |

LIST OF ABBREVIATIONS

| | |
|--------------|--|
| ABUS | Angle Beam Ultrasonic Spectroscopy |
| BDMA | benzyl dimethylamine |
| CW | continuous wave |
| DGEBA | diglycidyl ether of bisphenol A |
| DDA | dicyandiamide |
| DMA | dynamic mechanical analysis |
| DSC | differential scanning calorimetry |
| EGS | electro galvanized steel |
| FT | Fourier transform |
| FTIR | Fourier transform infrared |
| GPC | Gel Permeation Chromatography |
| ICTAC | International Confederation of Thermal Analysis and Calorimetry |
| IR | infrared |
| IPN | Interpenetrating networks |
| LVDT | linear voltage differential transformer |
| MH | microhardness |
| MIBK | methyl isobutyl ketone |
| MSDS | material safety data sheet |
| PET film | polyethylene terephthalate film |
| PU | polyurethane |
| RUS | resonance ultrasound spectroscopy |
| SAM | scanning acoustic microscopy |
| TBA | torsion braid analysis |
| TETA | triethylenetetramine |
| TOF | time of flight |
| TTT | time-temperature-transition |
| VDA | Verband der Automobilindustrie (Ger.), Association of the Automotive Industry in Germany |
| WLF equation | Williams-Landel-Ferry equation |
| XPS | X-ray photoelectron spectroscopy |

CHAPTER I

Introduction

1.1. Importance of the Structural Adhesive Bonding.

“An adhesive may be defined as a material which, when applied to the surfaces of materials, joins them together and resist separation”. This definition for adhesives was proposed by Kinloch in 1987⁷. Expanded use of adhesive bond joints in complex technological structures during recent years is caused by both development of new adhesive materials and broadening of material applications. Structural adhesives are widely used in the aerospace, automotive, and marine industries. Structural adhesives are defined as materials that transmit significant mechanical loads and become integrated into the whole structure of the product. The main requirement for structural adhesives is high strength, durability and long service life. Usually, structural adhesive systems have tensile strength greater than 10 MPa. Another important feature is the ability to maintain its load bearing ability for very long periods. Requirements for structural adhesives include chemical stability as well as resistance to temperature and moisture variations. Figure 1.1 shows places in the car where adhesive joints are used today.

The use of structural adhesives offers many advantages when compared with other more traditional joining methods such as welding, riveting, and mechanical fasteners¹. Some of them are:

- enhanced strength and stiffness;
- uniform distribution of the load stress;
- ability to join dissimilar materials;
- corrosion resistance;
- significant decrease in weight.

Epoxy adhesives are the widest class of adhesive materials and it is expected to grow over the next decade. Today, epoxies are widely used in many industries including aerospace, electrical/electronic, automotive, construction, transportation. Epoxy-based

adhesives provide strong bonding between similar and dissimilar materials such as metals, glass, ceramics, wood, cloth, and many types of plastics. Epoxies offer low shrinkage, low creep, and high performance over a wide range of usage temperatures without any by-products released during cure. The market consumes 25,000 MT of epoxies in North America in 2001 and worth almost \$500 million².

As the adhesive's mechanical properties are an extremely important parameter for structural adhesive joint performance and reliability, achieving high strength at the adhesive/metal interface and in the adhesive itself is the most important task for chemistry, physics and engineering.

1.2. Factors that Influence the Adhesive Joint Microstructure and Strength.

Adhesion science is a multidisciplinary subject which involves physics, chemistry and engineering. Adhesion is a phenomenon of the interaction that appears between two dissimilar materials when they come in into the close contact ² while cohesion refers to the attractive forces between the atoms of the adhesive material. The adhesive joint consists of several layers (Figure 1.1) and strength of the whole system is determined by its weakest link. Failure may occur on the metal/metal oxide interface, metal oxide/adhesive interface, inside the metal oxide layer (adhesive type) or inside the adhesive or metal (cohesive type) but study of the failure locus is beyond this research study.

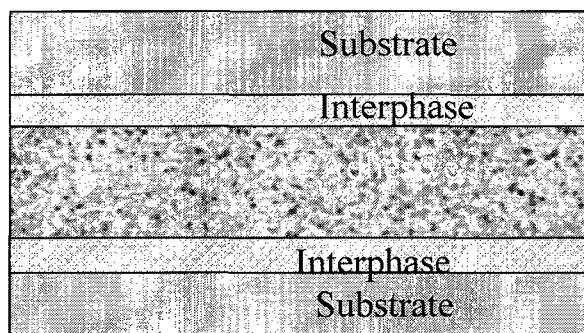


Figure 1.1. Schematic representation of the adhesive bond joint.

The most intriguing section in adhesion science is the nature and formation of the interfacial region between the adhesive and the substrate. Knowledge of formation of the adhesion interphase is important from both a fundamental and practical point of view. Today, there is no general agreement on the nature of the interphase, mechanisms of its formation and relation to the durability of the joint³. The main reasons are the difficulties of direct studies of the interphase region and its complicated nature specific to the type of substrate and adhesive.

Properties of the both substrate and adhesive are accountable for proper adhesion. The substrate should have a rough surface on the microscopic level and be clean from contaminants. The adhesive must wet the substrate; in other words, the substrate's surface tension must be higher than surface tension of the adhesive: $\gamma(\text{substrate}) > \gamma(\text{adhesive})$.

While adhesion technologies become more advanced, the cohesive strength takes on special significance. Most of the structural adhesives are based on cross-linked polymers. The major parameters that control the structural adhesive's physico-mechanical properties and, therefore, cohesion strength are the adhesive's free volume a glassy-state, cross-linked network structure and the macroscopic inhomogenities such as microvoids inside the adhesive. The factors that determine these parameters affecting adhesive strength are:

- type of prepolymer resin and hardener and their molar ratio;
- number and nature of functional groups in resins and hardeners, density of cross-linking;
- mechanism of polymerization;
- curing conditions which determine extent of reaction (degree of curing)-humidity, temperature, time.

Proper rheology of the adhesive is also important. The adhesive must be fluid enough to fill all surface irregularities but when applied it should become a solid material with good mechanical strength. Furthermore, some engineering factors like joint

geometry, bond line thickness, and residual stress in the adhesive play significant roles in the joint's reaching maximum strength.

1.3. Problem Statement.

There have been a lot of investigations in new adhesive material compositions and application during the last twenty years². However, the adhesive bonding method is still not as widely accepted as it deserves.

One of limiting factors that restricts the increased use of adhesives in industry is that long term strength and durability of the adhesive bond joint are unclear. Adhesive joints may suffer from environmental attacks when exposed to service conditions. The increased use of structural adhesives has led to a need to predict the lifetimes of these materials. To predict durability of the adhesive joint, it is necessary to understand the relations between the composition, structure, deformations and mechanical response of the adhesive and substrate and how this relation is modified by environmental factors. In many adhesive applications there is a need for understanding how the chemical and physical factors influence the adhesive viscoelastic, mechanical properties and the entire joint performance.

Another problem is the lack of adequate screening, testing and qualification procedures⁴. While growth of adhesive bonding technology continues, the reliability of adhesive bond joints often remains inconsistent. Quality control of adhesive joints becomes a critical part of the production. The necessity for quality assessment of the joints by non-destructive techniques increases with the development of more improved adhesive bonding technologies, which leads to a more wide-spread use in rapid manufacturing and assembly processes. However, before the test procedures can be created, a comprehensive understanding of the adhesive's behavior in various conditions is necessary.

Ultrasonic testing is widely used in industry to reveal structural defects and evaluate mechanical parameters of the materials. Conventional ultrasonic methods have been widely used to non-destructively inspect the adhesive bond joints for detection of

large defects such as voids. The main advantages of the acoustic technique are an ability to be used for optically opaque and electrically non-conducting materials. The ultrasonic method is quick, precise, non-destructive and non-hazardous. Although the acoustic technique is still the most reliable method for non-destructive defect detection, it is not widely used as an analytical tool for evaluating the cohesive joint strength in on-line applications and, in general, for material characterization. Nonetheless, there have been several applications of ultrasound waves in polymeric materials and processes reported in the past two decades^{1,5,6}. The chemical and physical processes that occur during adhesive cure are not fully understood yet. Application of the ultrasonic technique for characterization of the adhesive hardening reaction would represent a contribution in understanding of the complex process of adhesive cure. Practical interpretation of the ultrasonic data obtained for adhesive cure reaction needs a deeper theoretical groundwork, especially with regard to local physico-mechanical properties.

Mechanical properties of polymers are mostly studied by dynamic mechanical analysis (DMA) in laboratory study. As ultrasonic methods are the most popular in industry, it is also important to characterize adhesive properties by this method. Additionally, acoustics allow not only a study of bulk properties but also an investigation of local properties of the material with resolution depending on the ultrasonic hardware.

A more advanced technique, high resolution scanning acoustic microscopy (SAM), is able to visualize non-destructively the microstructure of the material, as well as investigate the distribution of the different physico-mechanical properties throughout the material comprising the bond joint structure under interrogation and the adhesive/substrate interface. This ultrasonic method yields an assessment of the physico-mechanical properties of the material, such as density, elasticity and viscosity. The interface imaging technique is not limited to the adhesive /steel interface but can also be used for imaging of the other boundaries between materials with dissimilar viscoelastic properties.

1.4. Goals of the Research.

It is important to understand the dynamics of the evolution of viscoelastic properties for structural thermosetting adhesives. The work in this dissertation is aimed at contributing to the knowledge in this area. It is necessary to study the viscoelastic and mechanical properties of the commercial structural adhesive during its polymerization reaction at different temperatures. Since the curing reaction rate is high, the ultrasonic method with a high rate of data acquisition should be used. This study is aimed at characterizing changes in the acoustic, viscoelastic and mechanical properties in an epoxy-based dicyandiamide hardened structural adhesive with the ultrasonic technique and to demonstrate how the acoustic parameters correlate with cohesive strength of the adhesive joint. This correlation could help in identification of some causes that contribute to a joint failure and lead to their elimination by improvements in adhesion process.

The objectives of this study are:

- ❑ to characterize non-destructively viscoelastic properties of an commercial structural adhesive with the ultrasonic technique ;
- ❑ to establish a correlation between acoustic parameters of the adhesive system and the adhesive joint performance;
- ❑ to develop methodology of acoustic characterization of a glass transition region in an epoxy adhesive polymer;
- ❑ to visualize non-destructively the microstructure of the intact adhesive/steel interface with high resolution acoustic microscopy and detect changes in the interface images that appear during the adhesive curing reaction;
- ❑ to establish and apply methods of quantitative analysis of the structure on the acoustic images;
- ❑ to investigate the influence of environmental factors on the adhesive interface and joint strength to show the applicability of SAM to visualize the structural defects which appear in adhesive bonds.

The final goal is to develop a general methodology for the non-destructive characterization of the curing behavior of the structural adhesive and for evaluation of its cohesive and interfacial properties, which has both scientific and practical interest.

1.5. Novelty.

Despite the many advantages of the acoustic methods, they are still not widely used as a tool for material characterization. Often researchers restrict their study by only evaluating the acoustic parameters, without extending data analysis to the viscoelastic behavior of the polymers. This dissertation examines development of the cohesive properties during cure reaction in commercial one component epoxy adhesive. The influence of reaction temperature and other reaction conditions on the cohesive properties and network structure are investigated from a chemistry perspective. Changes in the acoustic parameters and viscoelastic moduli are brought into correlation with change of glass transition temperature and cohesive strength of the joint is determined by destructive tests. Most of the work is performed in reflection acoustic mode, which is convenient for industrial applications, as it only requires access to one side for testing.

The method of matched filtration is used successfully to maximize a signal to noise ratio during a gelation stage in the polymerization reaction when sound attenuation increases dramatically. This approach improves the ability to detect the exact position of the reflected signal and increases precision of the acoustic measurement.

Most metal/adhesive interface studies are related to an aluminum bonding which is significantly different from steel/adhesive one, the most widely used in automotive industry these days. This work investigates the changes that occur in the intact acoustic steel/epoxy interface structure with scanning acoustic microscopy. The good quality adhesive joint interface is relatively homogeneous and produces a low contrast acoustic image. This accounts for a small number of the publications related to the intact imaging of the metal/adhesive interfaces. Nevertheless, the statistical image processing can provide valuable information about the interface state. It is shown that the intensity of the acoustic images reflects changes in the adhesive's elasticity. Contrast ratio and specific

size of the grains on the image is evaluated in this study. Two dimensional Fourier transform is used to evaluate the granular structure of the epoxy/metal interface and characterize the size of the microstructural components.

The changes in the acoustic images of the intact steel/structural epoxy interface are investigated under the influence of various environmental factors: moisture, elevated temperature and stress. All major defects that appear in the adhesive joints are visualized with SAM technique.

1.6. Dissertation Outline

This dissertation consists of the eight chapters. Chapter 2 reviews the structures of the major components and reactions involved in the curing process of epoxy-dicyandiamide-based adhesives. Mechanisms and models of adhesion in general and the specific case of adhesion on a steel substrate are reviewed as well. Chapter 3 gives a review of the viscoelastic properties of the polymers and the basic theory of bulk acoustic wave propagation in polymers.

Chapter 4 gives details of experimental setups as well as the descriptions of the materials and techniques used in this study. This includes the principles of scanning acoustic microscopy. Chapter 5 presents experimental results about the monitoring of evolution of an adhesive's viscoelastic properties during polymerization at isothermal or continuous heating rate conditions. Acoustic experimental data are compared with destructive test results. Obtained results demonstrate correlation between longitudinal sound velocity in the adhesive and cohesive strength in the adhesive joint. Chapter 6 analyses images of the adhesive/steel interfaces obtained with scanning acoustic microscopy. Images of the interface were performed at different curing times. Quantitative analysis of the images is given and discussed with relation to the changes that occur in the adhesive during the polymerization reaction. Chapter 7 analyses the influence of various environmental factors on adhesive bond joint structure and adhesive joint strength. Conclusions of the work are given in Chapter 8.

CHAPTER II

Review of Literature. Adhesion Models and Mechanisms.

2.1. Epoxies as Structural Adhesives

The structural adhesives are typically formulated from thermosetting resins that require chemical cross-linking. The most popular structural adhesives are epoxies, which have wide application in automotive, aerospace and marine industries. One of the advantages of the epoxy adhesives is absence of any volatile compounds during polymerization reaction. Epoxies are a very broad class of adhesives; they can be bonded to a wide variety of substrates and can be easily modified. The unique ability of the epoxy ring to react with a wide variety of reactants gives epoxy adhesives wide prevalence in many fields.

An epoxy adhesive system is composed of epoxy resin and hardener (curing agent). The type of resin and curing agent and their ratio define the degree of cross-linking and types of chemical bonds, which in turn determine the final properties of the product (chemical resistance and mechanical performance). Epoxy adhesives can be a one component system, where hardener is incorporated into the resin, or multiple component adhesives. The first system is usually cured at elevated temperatures while the latter can be cured at either room or elevated temperatures. Elevated temperatures provide higher shear strength and better environmental resistance. Other components of the adhesive system are fillers, polymers, rubbers and co-reacting resins to adjust viscosity and thermal expansion coefficient.

The curing reaction of epoxy –based adhesives is a formation of three-dimensional networks during chemical reaction between epoxy and hardener. A schematic representation of thermoset cure is shown in Figure 2.1. To form a three-dimensional network, hardener functionality should be greater than two. For simplicity, only difunctional and trifunctional co-reactants are illustrated. Reaction starts with monomers. The polyaddition reaction proceeds via simultaneous linear growth and

branching to an increasingly more viscous material and continues with the formation of a gelled but incompletely cross-linked network (Figure 2.1.(c)). Final cure occurs when the network is completely cross-linked.

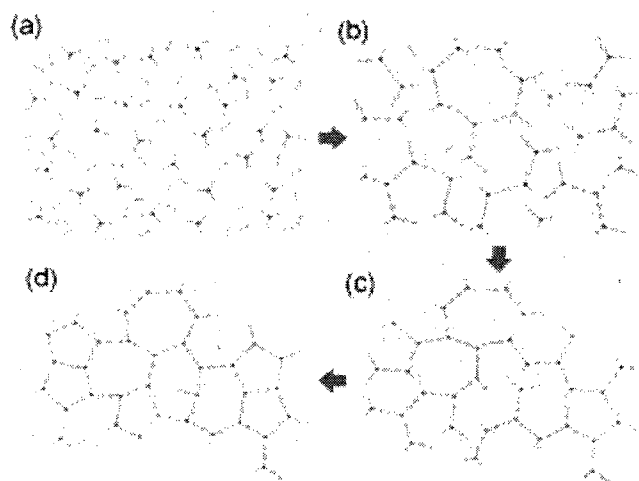


Figure 2.1. Two-dimensional schematic showing various stages of cure ⁸.

In liquid epoxies, the epoxy to resin ratio is quite high and they are polymerized by addition reaction between terminal oxirane ring and compounds containing active hydrogen. The solid resins with high molecular weight of the prepolymers are able to provide only partial polymerization throughout epoxy rings; large amount of hydroxyl groups provide additional branching points. These resins may be considered as polyol resins with terminal epoxy groups. Most epoxy formulations use the diglycidyl ether of bisphenol A resin (Figure 2.2).

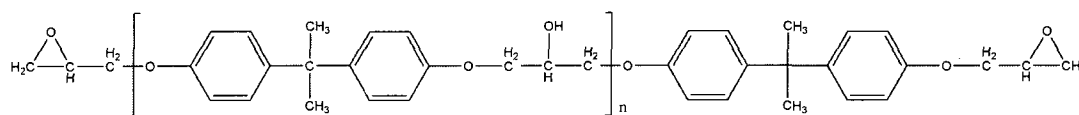


Figure 2.2. Structure of diglycidyl ether of bisphenol A resin (DGEBA).

The epoxy resin contains reactive epoxy groups, which are more reactive than regular non-cyclic ethers $R-OR'$, where R and R' are alkyl groups. This increased reactivity is due to epoxy ring strain. Epoxy can be cured with many compounds-aliphatic or aromatic amines, polyamides and anhydrides. The type of hardener affects the

adhesive network and its cohesive properties. Hardeners work as either catalytic or coreactive curing agents. Catalytic agents serve as an initiator for epoxy homopolymerization or accelerator for other curing agents. A typical catalytic agent is tertiary amine. Coreactive agents act as monomer in polymerization reaction.

The epoxy curing reaction involves electrophilic attack on the oxygen atom or nucleophilic attack on the epoxy ring carbon atom⁹. General reaction of epoxy resin with reagent HR' include oxirane ring opening (Figure 2.3):



Figure 2.3. General reaction between epoxy and hardener.

In this reaction, the attacking group donates a pair of electrons to the atom with lowest electron density, the methylene group. Presence of hydroxyl containing components promotes interaction of the amine with epoxy by making the carbon atom more sensitive to nucleophilic attack. A typical reaction between aliphatic amine hardener and epoxy resin involves an additional reaction between the epoxy ring and primary amine. Following this, secondary amine reacts with another epoxy group.

Dicyandiamide (DDA) was chosen as a major hardener for this research because it is a typical hardener which is widely used as a latent curing agent for single component epoxy systems. This is a crystalline solid, which is soluble in water but insoluble in low polarity liquids, including epoxy resins. Dicyandiamide polymerizes epoxy rapidly at elevated temperatures via a complex sequence of reactions. During polymerization, it interacts with epoxy and hydroxyl groups by all four nitrogen-containing groups yielding a highly cross-linked adhesive (Figure 2.4). Some authors proposed a DDA functionality different from 4¹².

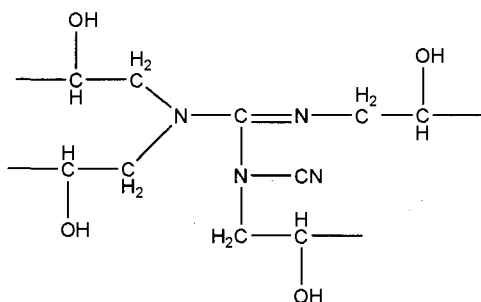


Figure 2.4. Cross-linking site between epoxy and DDA.

The polymerization reaction between epoxy and DDA has been studied in the last decades¹³⁻¹⁵. Despite a large quantity of publications, the detailed mechanism of curing is not fully understood due to its very complex nature. DDA exists in two tautomeric forms as well as in the form of carbodiimide tautomer, cyanamide or melamine form¹⁶ (Figure 2.5). Since DDA initially presents itself in the reactive mixture in its crystalline form, the beginning of the reaction with epoxy coincides with the onset of the dissolution of DDA; this fact also complicates kinetics of the curing reaction.

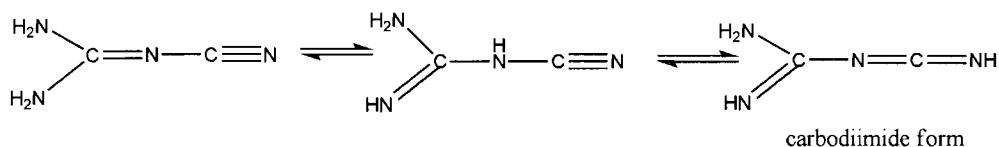


Figure 2.5. Mesomeric structures of DDA¹⁶.

Several possible reactions between epoxy and DDA have been proposed. Reaction products and their ratio depend on temperature of reaction, presence of accelerator and amine/epoxy ratio. First stages of curing are usually accelerated by tertiary amines or dimethyl urea compounds. At higher temperatures, reaction rate does not depend on presence of the accelerator.

Kinetics of the epoxy cure reaction with amines is complex due to the formation of large amounts of hydroxyl groups which catalyze this reaction. First, an addition reaction occurs between N-H bond and epoxy ring, where secondary hydroxyl groups are formed (Figure 2.6).

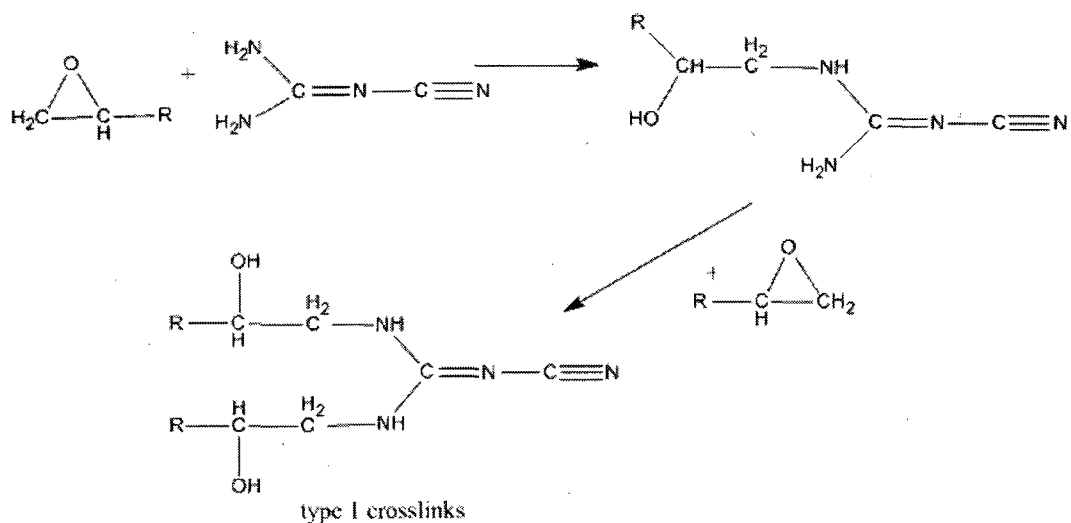


Figure 2.6. Reaction of DDA with epoxy resin.

Hydroxyl groups formed or hydroxyl groups already existing in the epoxy prepolymer react with epoxide groups in additional etherification. This homopolymerization reaction is catalyzed by tertiary amines or hydroxyl groups. Etherification of secondary hydroxyl groups occurs later and only at elevated temperatures (Figure 2.7).

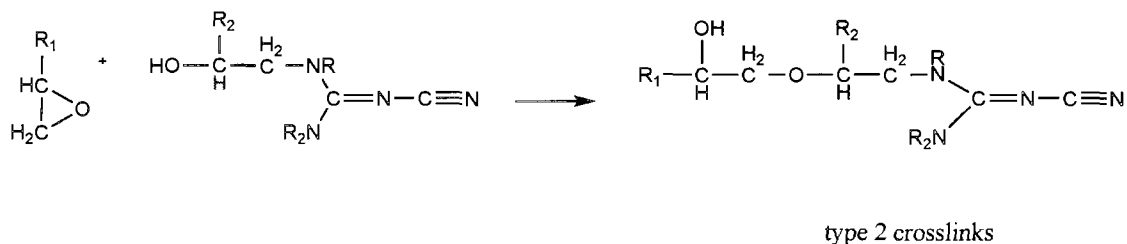


Figure 2.7. Etherification of secondary hydroxyl groups.

Thus, first type of cross-linking forms additional OH groups whereas etherification reaction consumes hydroxyl groups and forms of the ether bonds. Diminishing of the OH groups in the cured adhesive increases its sustainability to water.

These two reactions are typical for any amine hardeners. In the case of DDA, some specific reactions forming cyclic structures also take place at temperatures higher than 140°C. Different mechanisms were proposed. The free DDA molecule is used in

reaction schemes for simplicity purpose, while actually some of the N–H bonds may have already reacted with epoxy groups in the reactions shown above. Sounders et al¹⁸ suggested inter- and intramolecular rearrangements of iminoether with higher probability of the former¹⁸ (Figure 2.8). Type 3 cross-link is formed in this reaction.

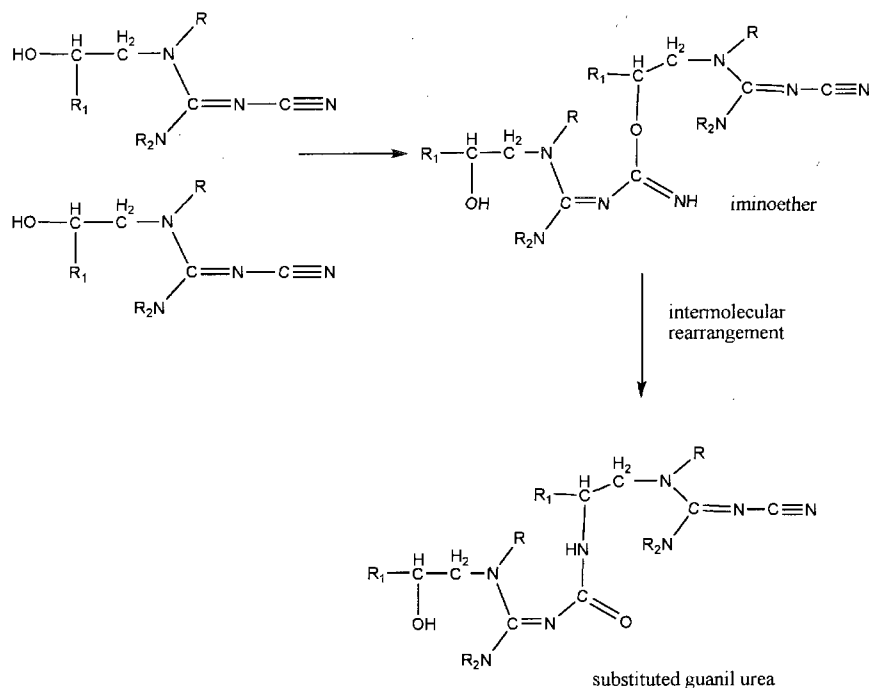


Figure 2.8. Proposed mechanisms for epoxy cure with DDA by Sounders et al ¹⁸.

Zahir proposed an intramolecular mechanism with hydroxyl/cyano addition and further separation of cyanamide to form tautomeric 2-iminooxazolidine and 2-aminooxazoline rings¹⁷ (Figure 2.9). According to Zahir, reaction of epoxy with DDA leads to two types of products: dialkyl cyanamide and derivatives of 2-amine-2-oxazolidine (or 2-imino-oxazolidine).

Gilbert et al. proposed a mechanism where hydroxyl groups adds across C=N bond with loss of ammonia and form iminooxazolidine ring. Later, the imino group is hydrolyzed by water to form a five-membered cyclic urethane ring^{17, 18} (Figure 2.10). Ammonia then acts as a trifunctional hardener.

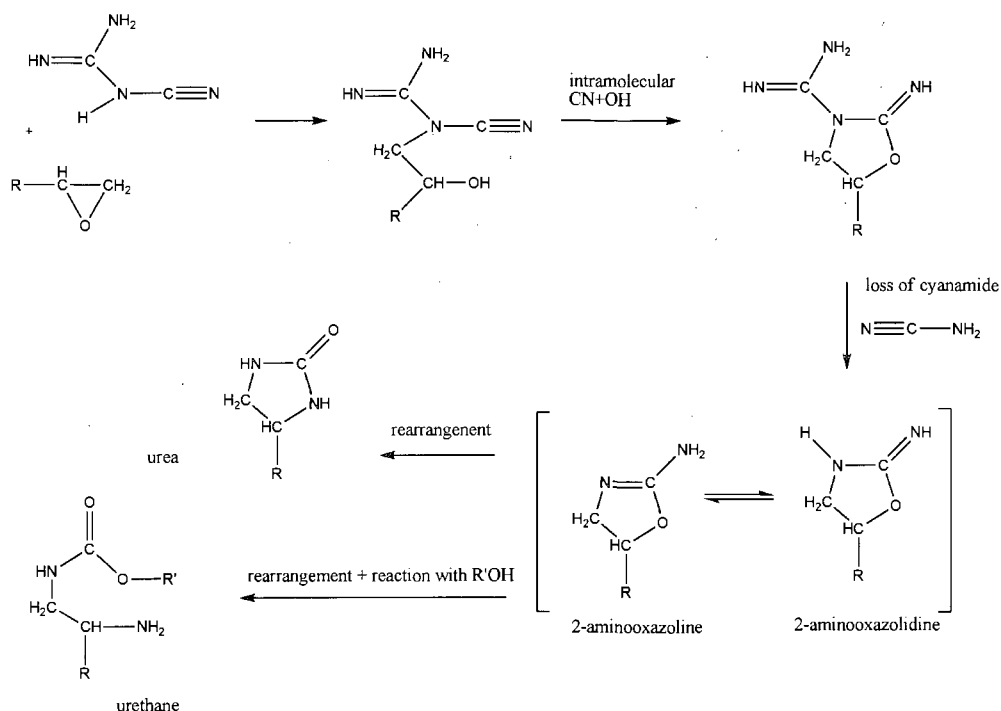


Figure 2.9. Proposed mechanisms for epoxy cure with DDA by Zahir¹⁷.

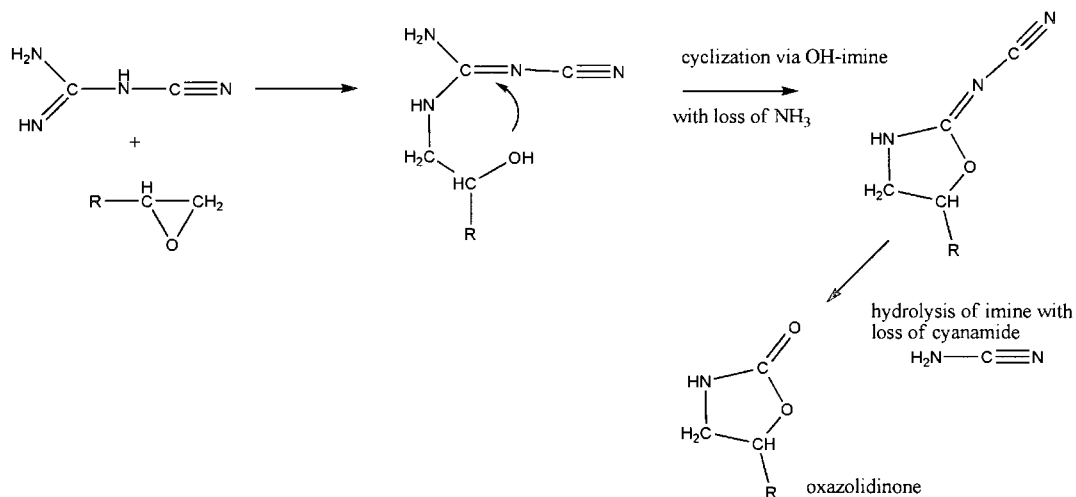


Figure 2.10. Proposed mechanisms for epoxy cure with DDA by Gilbert et al.^{17, 18}.

Pfitzmann et al. proposed a combined approach. He suggested formation of tautomeric oxazoline and oxazolidine rings by reaction of C=N bond with epoxides ring¹⁵ (Figure 2.11). The carbodiimide form of DDA forms oxazoline structures at elevated temperatures. The amide form of DDA reacts in the same way as amines. Two

overlapped reactions occur depending on tautomerization of DDA. Pfitzmann also showed disappearance of nitrile groups through rearrangement to form a melamine structure at high temperatures.

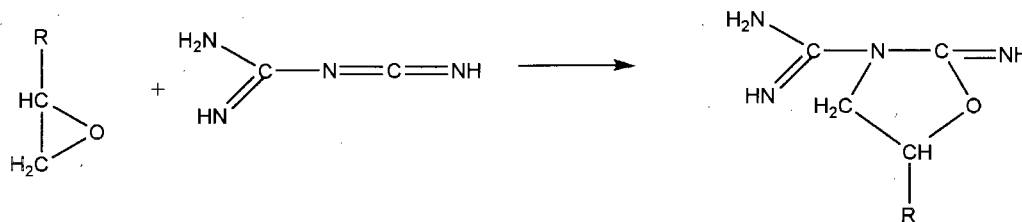


Figure 2.11. Proposed mechanism for epoxy cure with DDA by Pfitzmann et al ¹⁵.

Thus, three types of the cross-linkage are possible in the epoxy/DDA system. The first is formed as a result of additional reaction of epoxy and amine group. The second one is formed as a result of the etherification reaction of epoxy and OH groups. The third type is formed as a result of the reaction between cyano groups with hydroxyl groups in epoxy and specific only for reaction with dicyandiamide. The reaction temperature controls the occurrence of these reactions.

Epoxy systems may contain various additives to provide certain desired properties to the system. Catalysts are used to promote or accelerate a reaction. They include nucleophilic agents like halide ions, tertiary amines and Lewis acids. Diluents are used to reduce viscosity and provide proper wetting of the substrate. Lower viscosity is important for better wetting and penetration into the micro roughness of the surface. Diluents containing functional groups (reactive diluents) participate in a chemical reaction and are incorporated into the cross-linked network reducing cross-linkage density. The monofunctional epoxy diluents are "chain stoppers" since they inhibit formation of the cross-links. Non-reactive diluents work mostly as plasticizers. Fillers are the most common group of additives. They are used to modify physical/mechanical properties of the system (strength, density, electro-conductivity, thermal resistance). Fillers do not usually provide any influence on glass transition temperature (T_g). Aluminium, calcium sulphate, carbon black, copper, graphite, glass microballs, mica, quartz, silica, and sand are used as fillers.

Epoxy adhesives have excellent chemical resistance. However, they are brittle and show low elongation to fracture. Tougheners form a distinct phase in the system and work as crack inhibitors and cause an increase of elastic modulus. Incorporation of the plasticizing additives (polyamides, polyglycol diepoxides, polysulphides) helps to overcome the brittleness of epoxy adhesives. Introduction of rubber leads to formation of the two-phase system with improved toughness. Rubber exists as discrete particles 1000-2000Å in diameter, with functional groups, which covalently bind the epoxy matrix ¹⁹. Two phase adhesives show a combination of high strength and highly reduced brittleness.

2.1.1. Techniques for Monitoring of Physical and Chemical Properties During Adhesive Cure.

Since proper adhesive hardening depends on multiple parameters, such as temperature, time, resin-to-hardener ratio, etc., monitoring and assuring the progress of the curing process is essential. Effective monitoring requires tracking the development of the epoxy network architecture that plays a significant role in the mechanical behavior of the adhesive. Cure monitoring means real-time tracking of the physical state and chemical reactions that occur during cure. Such on-line monitoring will provide efficient cure temperature-time optimization.

Epoxy cure reaction involves transformation of the liquid prepolymer in the beginning of the reaction, into the solid product. The most common techniques used for cure monitoring include:

- direct evaluation of the active groups:
- evaluation of the extent of reaction:
- measurement of physical or mechanical properties.

Chromatographic or spectroscopy methods allow us to evaluate concentration of the reactive groups: epoxy or hardener. More complex systems, however, contain more than one type of reactive group. After the gel stage where epoxy becomes a solid and is no longer soluble in solvents, chromatographic methods can not be applied and other

techniques must be used. For Fourier transform infrared (FTIR) spectroscopy method, 915 cm^{-1} absorption band is assigned to the epoxy ring but IR spectra of the epoxy – hardener adhesive system are very complex. IR and FT Raman methods are not sensitive to the concentration of the reactive groups in the last stages of the reaction, where most of the strength of the adhesive is developed^{8, 20}. These techniques are mostly used for characterization of the uncured or partially cured adhesives.

Dynamic scanning calorimetry estimates the extent of the reaction; it is widely used for epoxy cure reaction monitoring^{21, 22}. Despite wide use of this method for epoxy (and other thermosets) cure monitoring, it is not accurate after the gel point⁸. The gelation stage can not be detected by thermal method, as it does not involve any change in reaction kinetics. This method also allows us to measure T_g of the material, which was proposed to be used as a measure of the reaction extent, as this parameter correlates with the estimate of the extent of reaction^{23, 24}.

Another approach is to measure the changes in physical properties (rheological, dielectrical or elastic) during the reaction. Rheological methods are not suitable for the post-gel stages as viscosity tends to infinity and the material obtains viscoelastic properties. Only methods measuring physical properties allow detecting gel point like such as a dynamic mechanical analysis^{21, 25, and 26}.

Among the techniques used to monitor adhesive hardening, acoustic examination should be listed first due to its simplicity, sensitivity and safety. Direct correlation of the material's elastic properties with acoustic response provides a solid basis for estimation of the adhesive's condition. Evaluation of the adhesive's acoustic properties as it cures allows us to monitor changes that occur in the material and thus, estimate its cohesive properties. Acoustic techniques have been used by researchers to analyze elastic properties and to study in-process molecular network development^{24, 27-29}. Guyott and Cawley³⁰ determined elastic modulus of the adhesive with ultrasonic spectroscopy. Younes et al. confirmed by comparing different monitoring methods that acoustic method is suitable to monitor different stages of adhesive cure, particularly the post-cure³¹. The application of ultrasonic methods for cure monitoring has been used mostly for analysis

of the evolution of ultrasonic properties during reaction and no any correlation with adhesive's final performance were made.

2.2. Models and Mechanisms of Adhesion

The adhesion phenomenon describes the event when two surfaces are stuck together. The study of the adhesion mechanism began in the 1920's when MacBain and Hopkins introduced the mechanical interlocking mode³². In spite of numerous papers, which have reported on the problems with adhesives made of plastic materials, fundamental knowledge about the adhesion processes is still not well developed, and no global approach or theory describes all adhesion phenomena in detail. This lack of a general theory may be explained by the fact that the formation of adhesively bonded joints involves a great number of associated and interdependent processes. The bonding of the adhesive is the sum of a number of mechanical, physical, and chemical forces that overlap and influence one another.

Adhesion between solid materials results from intermolecular interactions. There are generally accepted adhesion models: mechanical theories, diffusion theories, electrostatic theories and adsorption theories³³. Fourche³⁴ gives a similar classification, but also includes a model of weak boundary layers which, despite some criticism leveled at it in the past³⁵, remains important for explaining some cases of poor adhesion. Each theory is useful in some specific cases but none of them is a universal one. It should be noted that the adsorption theory is the most generally accepted adhesion mechanism.

2.2.1. Adhesive and Cohesive Forces. Factors Contributing to Joint Strength

The strength between adhesive and adherend is a result of both adhesive and cohesive forces among the molecules of two materials. Adhesive forces hold two separate materials together while cohesive forces hold together molecules of the same material. Both forces originate from interaction existing between molecules and atoms. The main forces involved in adhesion are³: Van der Waals forces (physical adsorption), hydrogen forces (strong polar interaction), ionic, covalent forces (chemisorption).

The type of failure mode, adhesive or cohesive, (Figure 2.13) depends on the degree of interfacial surface attachment. In the boundary region, strength of the

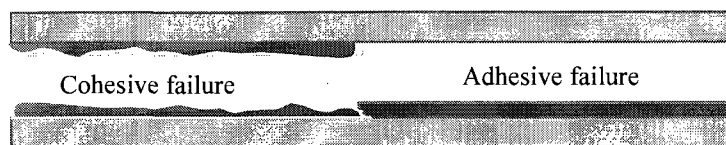


Figure 2.12. Cohesive and adhesive types of failure.

interfacial contact is less than cohesive strength. The strength of the bond is controlled by the interfacial forces and adhesive type of failure is observed. The transitional region shows high sensitivity of the bond strength to the degree of surface attachment. At this stage, usually mixed failure is observed. After a certain degree of saturation of surface attachment, interfacial strength is much higher than cohesive strength. This region is characterized by cohesive failure. Any increase in degree of surface attachment will not lead to increase of bond strength any more.

To obtain a good adhesion, it is necessary to obtain a good intermolecular contact in the interface. The major reason of strength loss is usually due to the failure of the molecules to approach each other within the bonding distance (approx. a few angstroms). However thoroughly the surface is prepared, it still has irregularities on a molecular level, which will not be filled with adhesive, and thus, prevent full contact between adhesive and substrate.

Another factor that should be considered is wetting of a substrate with adhesive.

2.2.2. Wettability

For a liquid-solid interface, proper contact between two phases can be obtained by liquid wetting the solid surface. Several comprehensive reviews ³⁵⁻³⁷ have presented major results regarding wetting and wettability studies of polymers.

The equilibrium balance of forces at contact between three material phases (Figure 2.13) is given by Young's equation³⁵:

$$\gamma_{SV} = \gamma_{SL} + \gamma_{LV} \cos \theta, \quad (2.1)$$

where γ_{LV} is the liquid free surface energy, γ_{SV} the solid free surface energy, γ_{SL} the solid-liquid interfacial free energy, and θ the contact angle between the solid-liquid interface. Usually, surface tension and/or interfacial tension parameters are substituted for free energy.

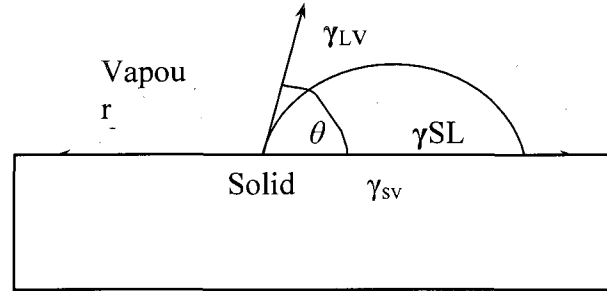


Figure. 2.13. The equilibrium forces balance according to the Young's equation.

For wetting to occur spontaneously, the conditions $\theta=0^\circ$ and

$$\gamma_{SV} \geq \gamma_{SL} + \gamma_{LV} \quad (2.2)$$

must apply. If the γ_{SL} is not significant, this criterion can be simplified to $\gamma_{SV} \geq \gamma_{LV}$, or

$$\gamma_{SUBSTRATE} \geq \gamma_{ADHESIVE}, \quad (2.3)$$

i.e. adhesive will spread on the substrate when the surface free energy of the substrate is greater than that of the adhesive.

For proper wetting of the substrate, both viscosity of the adhesive and its surface energy are important. Poor wetting causes less contact area between substrate and adhesive and more stress regions at the interface and, accordingly, adhesive joint strength decreases. So, it is essential that adhesive is in liquid form to fill all irregularities and reach sufficient contact with the substrate.

2.2.3. Mechanical Interlocking Model

The mechanical interlocking (or hooking) model is one of the earliest and simplest adhesion theories, which was introduced by MacBain in 1925³². The model involves the mechanical (physical) interlocking between irregularities of the substrate surface and the cured adhesive at the macroscopic level. Three types of irregularities are possible (Figure 2.15), although only type *b* may form mechanical interlocking³³. In cases of surface irregularities of types *a* or *c*, the adhesive strength depends on the direction of the applied force because only mechanical hooking is present. Mechanical interlocking is strongly affected by the roughness, porosity, and irregularities of the surface, but only under sufficient wetting of the substrate by the adhesive (Figure 2.14). Poor wetting results in less actual contact area between substrate and adherent. In fact, the non-wettability of substrate's surfaces can prohibit adhesive bonds from forming at all. Hence, for strong adhesion, the adhesive must not only wet the substrate but also have the proper rheological characteristics for penetrating into its pores in a reasonable time. Low

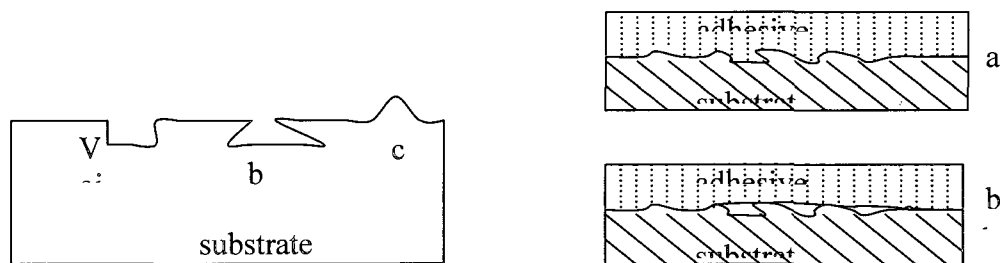


Figure 2.14. Types of surface irregularities, (right)³³. Sufficient wetting (a) and poor wetting (b), (left) (after Fourche³⁴).

adhesive viscosity promotes greater interfacial strength due to its faster and more complete penetration into the microvoids and pores.

Mechanical interlocking is a major factor in the adhesion of fibrous or porous materials such as textiles³⁸, wood³⁹, and paper well as natural rubber to steel adhesion³⁵. Later, in a number of works⁴⁰⁻⁴³ the importance of the physical interlocking at the microscopic level was demonstrated where porosity or micro-roughness of the surface provides a “composite-like” interphase with adhesive. Surface treatment of the

polyethylene significantly improves adhesion quality⁴⁴ due to irregularities of the fiber's surface and increased interfacial area. Thus, interlocking on macro and micro scale is an important factor in achieving good adhesion.

Despite its obvious appeal, the model of mechanical interlocking cannot be considered as a universal adhesion theory because good adhesion can occur even between perfectly smooth-surfaced adherents. Moreover, this theory does not consider any factors which occur on the molecular level at the adhesive/substrate interface. Later, roughness on a smaller scale has attracted attention⁴⁵ with Allen showing a correlation of the bond strength with pore depth on the surface of aluminum oxide. It was also shown that atomic scale surface roughness has a large influence on adhesion in nanometer contacts which lead to breakdown of continuum contact theory⁴⁶.

Thus, mechanical interlocking should only be considered as a composite attribute in the overall view of adhesion mechanisms. This model can be effectively applied in situations where the substrates are impermeable to the adhesive and where the surface of the substrate is sufficiently rough.

2.2.4. Adsorption Theory

It is well known that for good adsorption, effective wetting is essential to provide close contact between two substrates. As good adhesion can be only achieved with proper interfacial contact, it is necessary to consider how interfacial contact between surfaces can be achieved. The adsorption theory is the most generally accepted model which was introduced by Sharpe and Schonhorn⁴⁷ and considers adhesion as result of the intermolecular or interatomic forces at the interface between adhesive and substrate after their intimate contact. Forces between adhesive and substrate can be primary (ionic, covalent or metallic) or secondary (van der Waals, hydrogen bond). The theory includes several models which sometimes are considered as separate theories: the wetting, rheological and chemical adhesion ones.

The most common interaction at the adhesive-substrate interface results from van der Waals forces. These are long range forces (effective from distance of 10Å) which

consist of dispersion and polarization components. Van der Waals forces directly relate to fundamental thermodynamic parameters, such as the free energies of the adhesive and substrate, and allow a reversible work of adhesion of the materials to be calculated for the materials in contact. Thermodynamic aspects are described by Dupr  e's equation ³⁵ which expresses the thermodynamic work of adhesion W_A as

$$W_A = \gamma_{LV} + \gamma_{SV} - \gamma_{SL}. \quad (2.4)$$

where γ_{LV} is the liquid free surface energy, γ_{SV} the solid free surface energy, γ_{SL} the solid-liquid interfacial free energy, and θ the contact angle between the solid-liquid interface.

Combination of equations (2.1) and (2.4) gives the Young-Dupr  e equation

$$W_A = \gamma_{LV}(1 + \cos \theta). \quad (2.5)$$

Sharpe and Schonhorn ⁴⁷ have shown that the adhesive joint strength is influenced by the ability of the adhesive to spread spontaneously on the surface when the joint is initially formed. Hamaker developed a theory for the calculation of the attraction energy between two phases 1 and 2 ⁴⁸

$$W_A^{vdW} = \Delta G_{12} = -\frac{A_{12}}{12\pi l^2} \quad (2.6)$$

where A_{12} is the Hamaker coefficient, and l the distance between phases. If the phases are solids or liquids,

$$A_{12} = \frac{3}{2}kT \sum_{n=0}^{\infty} \left[\frac{\varepsilon_1(i\omega_n) - 1}{\varepsilon_1(i\omega_n) + 1} \right] \left[\frac{\varepsilon_2(i\omega_n) - 1}{\varepsilon_2(i\omega_n) + 1} \right] \quad (2.7)$$

where k is Boltzmann's constant, T the temperature, and ε_1 and ε_2 are the macroscopic dielectric susceptibilities of the phases 1 and 2 that are a function of frequency ω_n with quantum number n of relevant oscillation.

Acid-base interaction is a major factor among short range (< 0.2 nm) intermolecular forces and involves hydrogen bonding, electron donor-acceptor or electrophile - nucleophile interaction. Fowkes⁴⁹ proposed that interfacial tension γ may be expressed by two terms: a dispersive component, γ^d , and a polar component, γ^p :

$$\gamma = \gamma^d + \gamma^p. \quad (2.8)$$

The dispersive component is directly concerned with the Lifshitz – van der Waals interaction; while the polar component represents all the short-range non-dispersive forces, including hydrogen bonds and covalent bonds. According to Fowkes⁴⁹⁻⁵¹ and Owend and Wendt⁵²,

$$\gamma_{12} = \gamma_1 + \gamma_2 - 2\sqrt{\gamma_1^d \gamma_2^d} - 2\sqrt{\gamma_1^p \gamma_2^p}, \quad (2.9)$$

and adhesion work for dispersive forces is

$$W_A^{LW} = 2\sqrt{\gamma_1^d \gamma_2^d}, \quad (2.10)$$

where γ_1^d, γ_2^d are dispersive components of the surface free energy of the substrates 1 and 2, while γ_1^p and γ_2^p are the polar components.

The work of the adhesion in the case of acid-base (a-b) interaction W_A^{a-b} is, according to Fowkes⁴⁹,

$$W_A^{a-b} = -f n^{a-b} \Delta H^{a-b}, \quad (2.11)$$

or can be calculated by combining Eqs. 17, 20, and 22

$$W_A^{a-b} = \gamma_2 (1 + \cos \theta) - 2\sqrt{\gamma_1^d \gamma_2^d}, \quad (2.12)$$

where f is the correction factor (to convert the heat of interfacial acid-base interaction into free energy) which is close to unity, n^{a-b} is the number of acid-base pairs involved per unit area, ΔH^{a-b} the enthalpy of acid-base complex formation.

Therefore W_A may be determined from measurements of the contact angle using groups of standard liquids with known γ^d and γ^p values^{49, 52, 53}. Fowkes's approach is criticized nowadays for substantial overestimation of the apolar, or dispersive forces⁵⁴.

In order to describe better the polar component in terms of acid-base interaction this approach was later extended by van Oss, Chaudhury, and Good (VCG methodology)^{48, 55, 56}.

$$\gamma = \gamma^{LW} + \gamma^{a-b}, \quad (2.13)$$

where γ^{LW} is the Lifshitz – van der Waals component and γ^{a-b} is the acid-base component of the interfacial energy.

The contribution of the acid-base interaction to the interfacial energy is subdivided into two terms regarding donor functionality: the electron acceptor γ^+ and electron donor γ^- ⁴⁸. Then, the acid-base contribution to the interfacial energy can be determined:

$$\gamma_{12}^{a-b} = 2(\sqrt{\gamma_1^+} - \sqrt{\gamma_1^-})(\sqrt{\gamma_1^-} - \sqrt{\gamma_2^-}). \quad (2.14)$$

If the surface involves both Lifshitz-van der Waals and acid-base interactions, the total interfacial tension between two phases is expressed as:

$$\gamma_{12} = \gamma_1 + \gamma_2 - 2\sqrt{\gamma_1^{LW}\gamma_2^{LW}} - 2\sqrt{\gamma_1^+\gamma_2^-} + \sqrt{\gamma_1^-\gamma_2^+}. \quad (2.15)$$

Combination of Eqs. 15, 19 27 yields the expression:

$$\gamma (1 + \cos\theta) = 2\left(\sqrt{\gamma_1^{LW} \gamma_2^{LW}} + \sqrt{\gamma_1^- \gamma_2^+} + \sqrt{\gamma_1^+ \gamma_2^-}\right). \quad (2.16)$$

Adhesion work can be calculated as

$$W_A = 2\left(\sqrt{\gamma_1^{LW} \gamma_s^{LW}} + \sqrt{\gamma_l^+ \gamma_s^-} + \sqrt{\gamma_l^- \gamma_s^+}\right). \quad (2.17)$$

According to the literature, two different approaches can be used to obtain information about the acid-base nature of surfaces from wetting measurements. In the first approach suggested by Fowkes⁵⁷, the acid-base properties of solid surfaces can be measured by the calculation of the work of adhesion against model acidic or basic liquids. In the second approach, described by Good and van Oss⁵⁸, a main parameter characteristic for each solid is calculated from measurements of wetting and contact angle. Eq. 2.16 then allows for the determination of the surface energy components of the solid by measuring the contact angle of the solid substrate with liquids of known surface tension components. Data reveals that Good and van Oss' approach to the evaluation of the γ^+ and γ^- components of the solid surface free energy shows that most surfaces are overwhelmingly basic with a small acidic component, so-called "catastrophe of basidity"⁵⁹. In this connection, some researchers, e.g., Berg⁶⁰, suggest that to verify the method a more complete understanding of the wetting processes involving many interfaces and colloid phenomena is needed. Later, Della Volpe and Siboni⁶¹ resolved this problem: they proposed to compare acidic components with acidic ones only and basic with basic, use a wide set of solvents and emphasize that a complete and coherent definition of the calculation procedures is required. Lee⁶² proposed a unified Lewis acid-base approach to adhesion to complement original Fowkes and VCG methodologies. According to this approach, hydrogen bonding and polarization components exist simultaneously in the case of substantial adsorption. "Basidity" of most polymers was explained as a result of vapour adsorption on polymer surface.

Connor et al.⁶³ have proposed a criterion for optimum adhesion between two phases based on maximizing the wetting tension. It has been shown, that the maximum wetting tension is obtained when the substrate and adhesive surface energies are very

high and equal. For example, in the acid-base approach, such a situation occurs when the Lifshitz-van der Waals components of the substrate and adhesive are equal and when the acidic component of one phase is equal to the basic component of the other phase. Comparison of these results and experimental data from other sources suggests that the wetting tension can be used as a criterion for optimum adhesion.

Sometimes, covalent bonds make a major contribution to adhesion strength. This chemical bonding model was first proposed to explain coupling agents' action. This type of interaction provides high strength but only a small amount of molecules are involved in this interaction. This mechanism was demonstrated in the rubber-brass adhesion³⁴. Silane promoters are also designed to bond chemically the substrate with the adhesive. Covalent bonds are mostly formed in the case of metal oxide -polymer interfaces as a result of charge transfer from the metal to the polymer. C-O-metal oxide complexes are known to be a general characteristic of metal-polymer interfaces.

For adhesively bonded joints, there is a relation between the thermodynamic work of adhesion, W_A , and total work of fracture, F . Recently, Penn and Defex⁶⁴ have determined W_A from contact angle measurements made at room temperature with the adhesive in the liquid state and have established the relation between W_A and F . Values for F were determined from inverted blister tests conducted at temperatures low enough for the adhesive to be in the solid state. Because the thermodynamic work of adhesion, W_A , represents the energy required for reversible separation of the two materials at the interface, and because F includes the energy required for both reversible and irreversible processes during separation, the excess of F over W_A represents the energy consumed by the irreversible processes that occur in the specimen during loading and fracture. This excess, $(F - W_A)$, was found⁶⁴ to increase exponentially with W_A and was attributed to the orientation hardening of the substrate within a very thin layer adjacent to the interfacial plane.

2.2.5. Electrostatic Theory

The basis of the electrostatic theory of adhesion was developed by Deryaguin and coworkers⁶⁵ and is based on the difference in electro-negativities of adhesively bonded materials. According to this model, the adhesive-substrate system can be considered as a capacitor, whose plates consist of the electrical double layer, which occurs when two materials of different nature come into contact (Figure 2.15)^{34, 65, 66}.

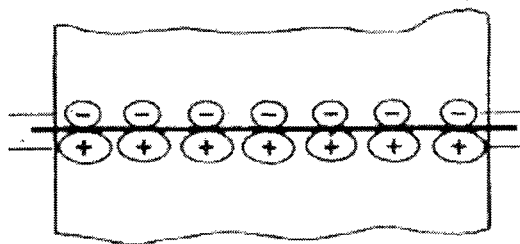


Figure 2.15. Electrical double layer at the polymer-metal interface³⁴.

The electrical double layer forms when electrons cross the interface thereby creating regions of positive and negative charge. According to the electrostatic theory⁶⁶, these electrostatic forces at the interface account for of the attraction between the adhesive and the substrate.

Hays⁶⁷ considered electrostatic adhesion of two materials (donor and acceptor) between anions and cations for two cases: a) when average distance r between cationic and anionic groups is smaller then distance a between donor-acceptor pairs (Figure 2.16), $r < a$; and b) when $r > a$.

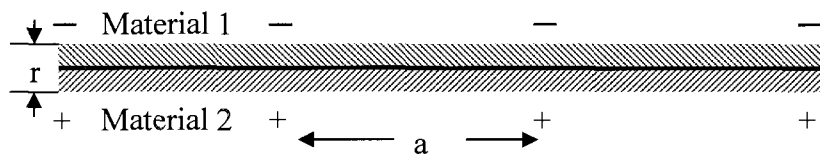


Figure 2.16. Electron donor-acceptor pairs (after Hays)⁶⁷.

For case when $r \ll a$, the electrostatic attractive force F_e between cation and anion pair is equal to

$$F_e = e^2 / (4\pi k \epsilon r^2), \quad (2.18)$$

and the adhesive force per unit area is

$$P_{r < a} = N F_e = N e^2 / (4\pi k \epsilon r^2), \quad (2.19)$$

where e is the electron charge, k the interfacial dielectric constant for the two materials, ϵ the permittivity of the medium, and N the density of the anion-cation pairs per unit area. In the case when the distance between donor and acceptor groups is comparable to the donor-acceptor pair distance, the attractive force between cation and anion increases because of electric field from adjacent dipoles. And for the case when $r \gg a$, the electrostatic force and adhesive force per unit area are

$$F_e = N e^2 / (2k \epsilon_0), \quad (2.21)$$

$$P_{r > a} = n F_e = N^2 e^2 / (2k \epsilon_0). \quad (2.22).$$

Hays ⁶⁷ has established that the electrical contribution to the adhesion is comparable or even greater than the van der Waals component if the density of anion-cation parts is approximately $10^{17}/\text{m}^2$ or greater.

Adhesion between two materials when one of the contacting parts has a certain radius of curvature is important in many technological processes ⁶⁸. Adhesion between these two materials has a more complicated nature. In areas of close contact, the adhesive force is similar to the one for the planar configuration. Outside this area, the total adhesion force, F_a , consists of the Lifshitz-van der Waals force, F_{vdW} , the electrostatic force, F_e , as well as capillary and double layer forces, with only the Lifshitz-van der Waals and electrostatic forces playing a major role ⁶⁹:

$$F_a = F_{vdW} + F_e. \quad (2.23)$$

For a rigid spherical particle with radius r and uniformly distributed surface charge Q , the Coulomb electrostatic image force is ⁶⁷

$$F_e = \alpha Q^2 / 16\pi\epsilon r^2, \quad (2.24)$$

where ϵ is permittivity of the medium surrounding the particle, and α a coefficient which depends on the particle dielectric constant k_p .

It is assumed that a spherically symmetric charge distribution can be modeled as a single charge point, Q , in the center of this sphere. Values of F_e computed using this model are usually lower than the corresponding measured values ^{70, 71}. To solve this problem, the concept of a non-uniform distribution of the charge was proposed ⁶⁸. Feng and Hays ⁶⁸ note that the non-uniform distribution of surface charge and, particularly, the high charge density in the contact region enhance the magnitude of the electrostatic image force. Czarnecki and Schein ⁷⁰ modeled the charge distribution as a set of point charges and introduced additional electrostatic force components due to the charges' proximity to the plane; in this case, the total electrostatic force was found to be 2.2 times higher than that calculated with Eq. (2.24). It was shown that the critical height for material microstructure exists above which the air film remains intercalated under the contact area ². Lhernould and co-authors demonstrated importance of the surface topography on electrostatic interaction, which is reduced with roughness increase³. They have developed an analytical model for evaluation of electrostatic forces with integrated roughness parameters.

The other force which makes a major contribution to adhesion is the van der Waals force, which originates from the molecular interaction due to various polarization mechanisms. For the same rigid spherical particle, the van der Waals force can be calculated as

$$F_{vdW} = Ar / (6h^2), \quad (2.25)$$

where A is the material-dependent Hamaker constant, and h is the minimum distance between the two materials. The value of the van der Waals force depends also on the surface roughness and decreases as the roughness increases.

Weaver has shown that a considerable electrostatic constituent of adhesion depends both on time and temperature⁷². Despite numerous studies, the role and magnitude of the electrostatic force in adhesion is still being debated. Nowadays, however, more and more authors^{68, 69, 73} have come to the conclusion that the values of both the van der Waals and the electrostatic forces can vary in a range over one order of magnitude depending upon the particle size and surface properties (roughness and charge distribution). This could be “the primary reason for controversial results reported in the literature when the comparison conditions were not specified adequately”⁶⁸.

The main limitation of the electrostatic model is the fact that it is applicable mostly to the cases of incompatible materials such as a polymer and a metal. Moreover, because the electrostatic model requires a large number of parameters for predicting adhesion processes, it has found little practical use in engineering.

2.2.6. Diffusion Theory

The diffusion theory was proposed by Voyutski⁷⁴, who explained adhesion as the result of interdiffusion of the macromolecules of the two polymeric materials at the interface as illustrated in Figure 2.17.

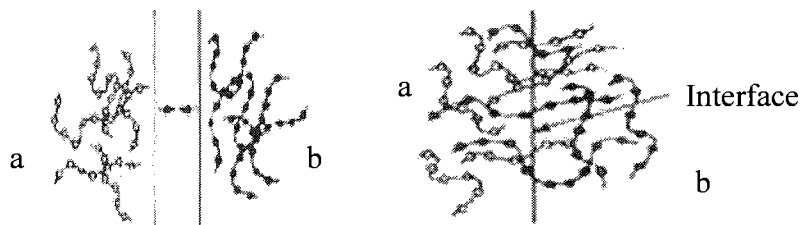


Figure 2.17. Interdiffusion of adhesive (a) and substrate (b) molecules.

According to the diffusion theory both the adhesive and substrate must be polymers, which are mutually miscible and compatible. The theory asserts that two

specimens of polymers which are placed in contact under a constant assembly pressure will diffuse together following Fick's laws of diffusion. In the case when concentration remains constant with time (steady state), flux (F_x) in the direction x is proportional to the concentration c gradient,

$$F_x = -D \left(\frac{\partial c}{\partial x} \right), \quad (2.26)$$

where D is the diffusion constant.

When concentration varies with time, Fick's second law determines the diffusion constant as

$$\left(\frac{\partial c}{\partial t} \right) = D \left(\frac{\partial^2 c}{\partial x^2} + \frac{\partial^2 c}{\partial y^2} + \frac{\partial^2 c}{\partial z^2} \right). \quad (2.27)$$

According to Lee³⁵, the molecular diffusion constant D can be calculated as

$$D\eta = (A\rho kT/36)(R^2/M), \quad (2.28)$$

where η is the bulk viscosity, A -Avogadro's number, ρ -density, k -Boltzmann's constant, T the absolute temperature.

It is shown that interdiffusion is optimal when the solubility characteristics of both polymers are equal^{75, 76}. The chain length of the macromolecule, concentration, and temperature all have a significant influence on the mobility of the macromolecules and therefore on interdiffusion process and on the adhesive strength⁷⁴.

Although increasing attention is being paid to the study of the interdiffusion process, the kinetic performance of the diffusion mechanism is still difficult to predict and not completely understood at present. Vasenin⁷⁷ developed the kinetic concept of adhesion based on Fick's first law. This quantitative model states that the amount of material diffusion in a given direction across an interface is proportional to the contact time and gradient of concentration. Later, the diffusion kinetics were rewritten in light of

the reptation theory of de Gennes⁷⁸ and later extended by several authors^{79, 80}. Reptation theory has made much progress in the fundamental understanding of the molecular dynamics of polymer chains and has been applied to study the tack, healing, and welding of polymers.

From the contact time, t , and the gradient of polymer concentration parameters, it is possible to evaluate the depth of interpenetration, x , and the number of macromolecular chains crossing the interface $L_o(t)$ ³⁵,

$$x(t) \approx t^{\frac{1}{4}} N^{-\frac{1}{4}} \quad (2.29)$$

$$L_o(t) \approx t^{\frac{3}{4}} N^{-\frac{7}{4}} \quad (2.30)$$

where N is number of monomers per chain in the polymer.

A direct relation exists between the concentration gradient and the contact time. Vassenin studied the peel energy for joints bonded with polyisobutylenes of different molecular weights and has established that peel strength is proportional to the contact time $t^{\frac{1}{2}}$.

Finally, however, according to the literature, the diffusion model of adhesion is not thought to contribute to adhesion if the substrate polymers are crystalline or highly cross-linked or if contact between two polymeric phases occurs far below their glass transition temperature. It has also been found to be of limited applicability if the adhesive and substrate are not soluble.

2.2.7. Weak Boundary Layer Model

The model of weak boundary layers was proposed by Bikerman⁸¹, who claims that adhesive joints almost never fail exactly at the interfaces but at a weak boundary layer inside the adhesive or substrate. The author distinguishes several types of weak boundary layers: trapped air, contaminations at the interface, reaction products between

adhesive components, or between components and medium. The theory proposes that clean surfaces can give sufficiently strong bonds with adhesive, but some contaminants result in a layer formation which is cohesively weak. Entrapment of air, impurities, low molecular weight compounds, cohesively weak oxide layer on the substrate surface, chemical deterioration of the coating can cause weak boundary layers³.

The availability of the solid surface results in a decrease of the molecular mobility in the boundary layer as a result of the conformation set limiting and adsorption interactions of the polymer molecules with a solid at the boundary. This fact has also been confirmed by several researchers^{82, 83} for the filled epoxy polymers. It has been shown that geometric limitation of the number of possible macromolecule conformations close to the surface of the particles plays a fundamental role in the change of molecular mobility. As described by Duprée⁸⁴, two factors limit the molecular mobility of chains close to the boundary: the adsorption reaction of macromolecules with the surface and the decrease of their entropy. Close to the interface, the macromolecule cannot adopt the same conformation number as in bulk, so that the surface limits the molecular geometry. Hence the number of states available to the molecule in the surface layer decreases. Therefore, limitations of the molecular conformation are the basic reason for the molecular mobility decreasing close to the interface.

Lee³⁵ draws attention to Bikerman's assertion⁸¹ that in any case of low strength with apparent residue-free separation, weak boundary layers are the main reason. But it was asserted⁸⁵ that a weak boundary layer is a sufficient condition for low strength, but it is not a necessary condition. Although the Bikerman's model has been criticized by several authors, e.g.³⁵ in the past, it is now admitted^{66, 86} that many cases of poor adhesion can be attributed to a weak interfacial layer.

Recently, Yang et al.⁶⁶ applied successfully both models of weak boundary layers and mechanical interlocking for studying composite structures with weak bonding defects by testing adhesively bonded, double lap-shear, and tensile specimens. They have shown that a vibration damping and frequency measurement is an effective instrument for non-

destructive detection of damage or degradation in adhesively bonded joints of composite structures.

Kalnins and Ozolins⁸⁶ studied structure and some other characteristics of the boundary layer of the polyolefin adhesive, which forms the adhesion bond with steel under conditions of contact thermo-oxidation. They have observed that the adhesion interaction of a polyolefin melt with steel leads to the formation of a cohesively weak polymer boundary layer. The structure of the boundary layer is less organized in comparison with the bulk structure, a fact that agrees well with the conception of a weak boundary layer offered by Bikerman^{3, 81}.

2.3. Adhesion at Polymer/Metal Interface.

Sharpe⁸⁷ has extended Bikerman's weak boundary layer theory into a interphase concept. The existence of the region adjacent to the boundary which has different chemical, physical and mechanical properties from those of the bulk is now generally accepted. Presence of the solid surface may prevent adhesive molecule segments from taking certain configurations. Some chemical or physical interaction of the substrate and adhesive may also lead to different material properties at the interphase. The interphase region has variable thickness, which depends on the nature of the both the substrate and adhesive. The nature of interphase region is an important factor in determining the properties of adhesive bonds. Knowledge of formation of the adhesion interphase is important from both fundamental and practical points of view. Today there is no general agreement on the nature of the interphase, mechanisms of its formation and relation to the durability of the joint. The main reasons are difficulties of direct studies of the interphase region and its complicated and substrate/adhesive specific nature.

The surface of metals is believed to consist of regions which have no clearly defined boundaries between them (Figure 2.18). They are a, metal oxide, hydroxide layer and absorbed water layer. In addition, there are contaminants like oils, lubricants, corrosion inhibitors. All these layers are not separate mechanically from one another, but mixed together to form an inhomogeneous structure, which is involved in formation of

the adhesive interphase. Because these layers are relatively thick, they are mostly responsible for the adhesion between the substrate and adhesive.

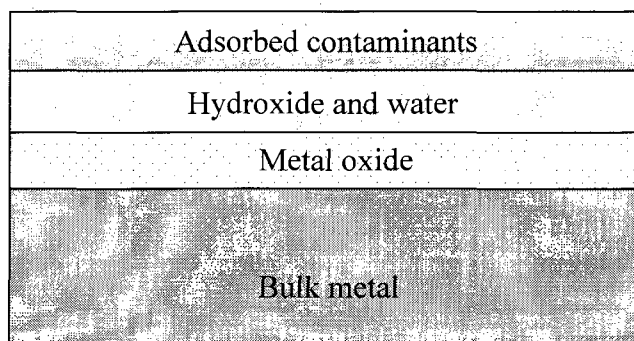


Figure 2.18. Schematic representation of metal substrate surface regions.)

Based on the adhesion theory, direct interaction of the adhesive components with the substrate surface should be considered. Mechanical interlocking on the micro level, acid-base model and molecular bonding are considered the main mechanisms of the adhesion for metal/epoxy systems. Secondary or van der Waals forces account for 75-100% of the molecular cohesion in most non-structural adhesion cases¹⁰. Epoxies usually form strong chemical bonds with metal surfaces. Adhesion is also formed by hydrogen bonding across the interface³⁵. It is shown that the epoxy-metal interface strongly depends on the content of the hydroxyl groups and does not depend on epoxy or hydrocarbon groups content.

Water, almost always presents at the substrate surface in physisorbed or chemisorbed stage, is what makes the substrate surface reactive. The cations react with water forming hydroxyl groups which are readily form hydrogen bonds.

As only steel substrates will be used in this research study, only formation of the interface for steel-epoxy resin-amine hardener will be considered further.

Zinc oxide on a galvanized steel surface, like many other oxides, carries hydroxyl groups. It was shown that oxygen in the metal oxide hydrates to form hydroxyl groups. One half to two-thirds of water molecules dissociate on the oxide surfaces to form hydroxyl groups. Water is also adsorbed on iron oxide by physisorption with a small

amount of water dissociating to form hydroxyl groups. Oxide layer morphology is significantly different from the bulk metal substrate (Figure.2.19).

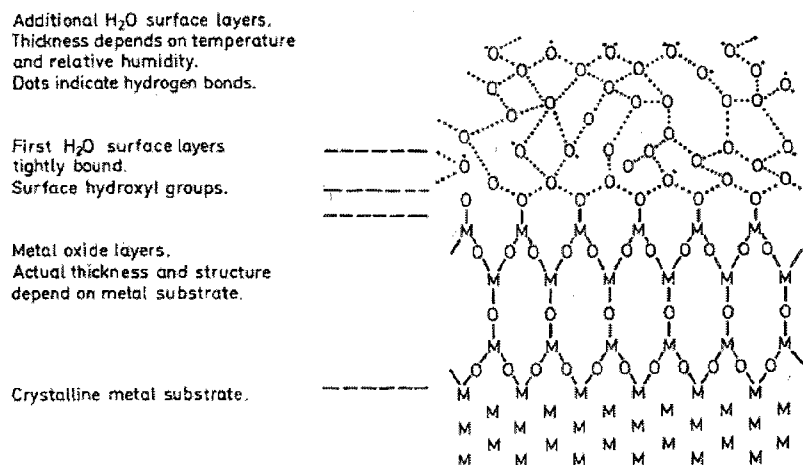


Figure 2.19. The water and oxide layers on the metal surface ⁸⁸. M-metal, O-oxygen, O:-water, O :-hydroxyl group.

Epoxy-based adhesives have plenty of polar groups, which are able to interact with the metal surface. Potentially, there are four possible adsorption sites: benzene ring, epoxy ring, oxygen or hydroxyl group, formed during cure reaction or already present in the adhesive prepolymers. Nakazawa et al. showed that model epoxy compounds are adsorbed mainly via C-O bond scission to form surface phenoxy compounds ⁹⁰. The same bonding occurs on the iron oxide surface. Formation of the interfacial chemical bonds contributes to the adhesion of epoxy resins to cold-rolled steel (CR), galvanized steel (GI), and galvanized steel (GA) sheets (Figure 2.20) ⁹¹.

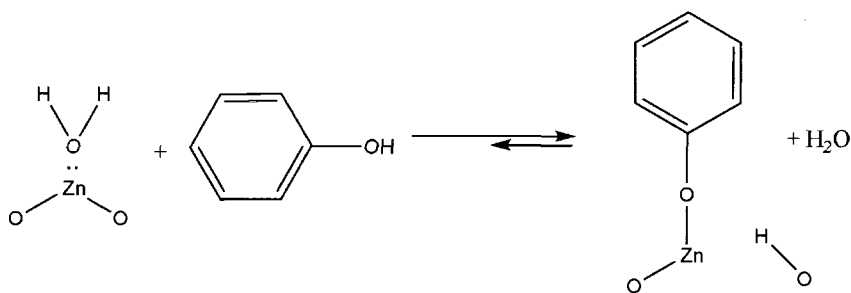


Figure 2.20. Interaction of water and organic molecules with zinc oxide ⁹⁰.

The adhesion of epoxy resin to metal is also due to chemical bond formation between metal oxide surfaces and epoxy oxygen during epoxy ring opening reaction. It is necessary to note that when a zinc oxide surface is covered with water, epoxy ring opening reaction is less efficient ⁹².

The presence of many hydroxyl groups along the epoxy resin chain contributes to a strong adhesion to metal as a result of their binding with metal oxides on the surface. When applied on the metal substrate, epoxy resin and amine hardener react with metal oxides and hydroxide to form chemical bonds ⁹².

Nigro and Ishida ⁹⁴ suggested a chemical reaction on the steel interface, when epoxy /BF₃-monoethylamine system was applied. Gaillard has shown a catalytic effect of zinc ions from the galvanized surface of the steel substrate on epoxy polymerization reaction ⁹⁵. Both epoxy monomers and dicyandiamide were adsorbed on the aluminum surface ⁹⁶. DDA monomers were absorbed by acidic protons of the aluminum oxide while epoxy monomer adsorption was due to epoxy ring opening. Other authors also have shown adsorption and chemical reaction of the curing agent on the metal/adhesive system interface ^{97, 98}.

Carter ⁹⁹ et al. have shown formation of the interphase with unique molecular structure when DGEBA/dicyandiamide adhesive systems were cured in contact with aluminum or electrogalvanized steel (EGS) substrates. In case of EGS substrate, DDA chemically reacts with the substrate and is reduced to carbodiimide compound ((NH₂)₂CH-N=C=N-Zn...) in presence of metallic zinc at elevated temperatures but not in presence of steel or zinc oxide. This fact was supported by theoretical studies ¹⁰⁰. Kinzler ¹⁰¹ has suggested that carbodiimide compounds migrate toward the bulk adhesive creating an interphase. No evidence was found for amine protonation. Bremont applied micro- XPS analysis to the epoxy/DDA interface and has suggested acid/base reaction between dicyandiamide and hydroxylated surface of galvanized steel ¹⁰². It was also shown that organo-metallic precipitates formed as a result of the reaction of metal ions with the hardener are not completely dissolved during the cure cycle and form a separated phase ⁹². Thus, DDA reacts covalently with epoxy and substrate. These covalent bonds

are significant for adhesive joint strength and durability as they introduce a stronger interaction between substrate and adhesive.

Presence of the coupling agents improves significantly the bond strength and its resistance to moisture. The most widely used coupling agents are organosilanes which have following structure $R-Si-(OR_1)_3$ where R is organofunctional group reacting with matrix and R_1 is a functional group which react with substrate. First, hydrolysis occurs.

Then, hydrolyzed organosilanes react with OH groups on the metal oxide surface and OH groups of the silane. As a result, a polysiloxane network is formed (Fig. 2.21)⁹.

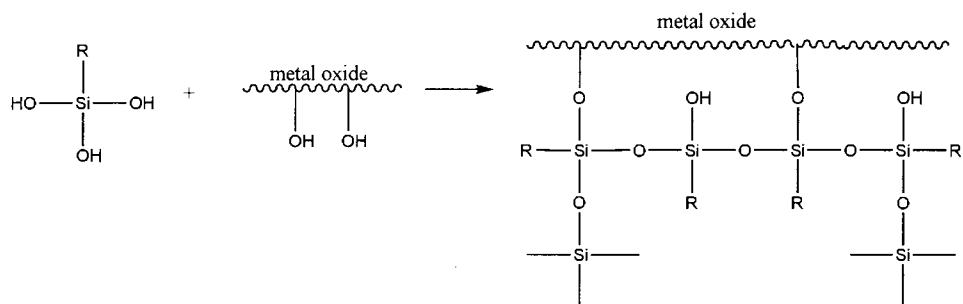


Figure 2.21. Polysiloxane network formation at the metal surface⁹.

Gettings and Kinloch⁷ have shown the presence of Fe-O-Si bonds on the interface. Organofunctional group R reacts with epoxy resin to connect the metal oxide covalently with the epoxy network. At the other end, epoxy penetrates into the silane layer and forms cross-linked interpenetrating network⁷.

Thus, structural adhesives are used to form structural bonds in load-bearing joints. These materials are employed in applications where they have to withstand prolonged impact and peel stress. Adhesive joint strength is controlled by the fundamental properties of the adhesive system such as cohesive strength of the adhesive, rheological properties, and surface attachment characteristics. Adhesion between solid materials results from intermolecular interactions. The generally accepted adsorption theory considers adhesion as result of the intermolecular or interatomic forces at the interface between adhesive and substrate after their intimate contact.

CHAPTER III

Viscoelastic Properties of Cross-Linked Polymers and Methods of Their Evaluation.

Polymers have well developed viscoelastic properties showing characteristics of both solids and liquids that lead to unique physical and mechanical properties. The nature of viscoelasticity is due to molecular movement of polymer chains. Polymer's viscoelastic behavior depends on the time and rate of the force applied and on the external conditions such as temperature and pressure. The main parameters that describe the viscoelastic properties of polymers are their elastic moduli which have direct relation to the acoustic parameters of the polymers.

3. 1. Elastic Moduli. Stress and Strain.

Material deformations cause changes in distance between particles, which in turn induce a force. The relationship between stress and strain is an internal material property. For most solids, the relation between stress σ and strain ε can be represented by Hook's law in its simple form: $\sigma = E\varepsilon$ where E is elastic modulus.

If a periodically changing stress is applied to the viscoelastic material

$$\sigma = \sigma_0 \sin \omega t ,$$

where ω is an angular frequency and σ_0 is the amplitude of stress, the strain will change sinusoidally, but with phase shift,

$$\varepsilon = \varepsilon_0 \sin(\omega t - \delta) \tag{3.1}$$

where ε_0 is an amplitude of the strain and δ is phase shift between stress and strain (Figure 3.1). The stress that changes according to a sinusoidal and does not coincide in phase with the strain can be resolved into two components, one of which will be in phase with the strain and the other will differ from it in phase by $\pi/2$.

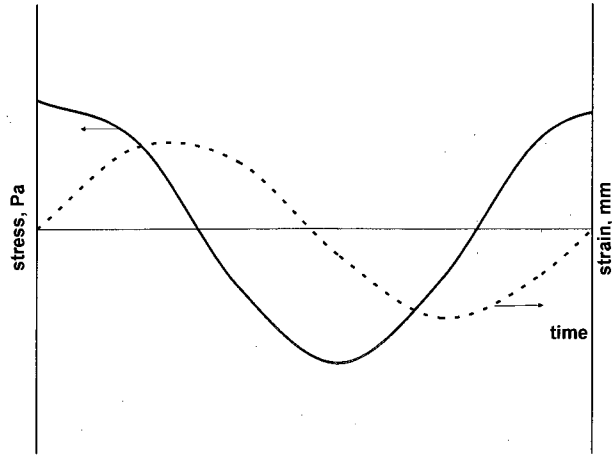


Figure 3.1. Phase shift between stress and strain during sinusoidal deformation of polymers.

In cases of viscoelastic materials, stress changing according to a periodic law can be expressed as

$$\sigma = E^* \varepsilon \quad (3.2).$$

Here E^* is the complex elasticity modulus which is equal to

$$E^* = E' + iE'' \quad (3.3)$$

where E' is the storage modulus of elasticity and E'' is the loss modulus¹⁰³.

The storage modulus is a real part of the elasticity modulus and usually equal to stress component, which is in phase with strain. This modulus reflects energy gained and lost by the polymer per cycle. The loss modulus E'' is the ratio between stress component, which is lagging in phase by $\pi/2$ from the strain, and the value of strain. This modulus characterizes that part of energy that usually dissipates or transforms to heat during the oscillations. It shows the contribution of the viscous component in the polymer properties. In a physical sense the storage modulus is related to the stiffness of the material and elastic behavior of the polymer whereas the loss modulus is reflected in the damping capacity of the material and its viscous action.

The useful parameter that measures the ratio of the lost energy to the stored one is the loss tangent or loss factor

$$\tan \delta = \frac{E''}{E'} \quad (3.4).$$

The loss factor determines some macroscopic polymer properties like damping of free vibrations, attenuation of propagated waves, and width of resonance response¹⁰⁴. The loss tangent is a measure of dissipation of energy and can serve as an index of viscoelasticity.

3.2. Dependence of Viscoelastic Properties of Cross-linked Amorphous Polymers on Temperature. Glass Transition Temperature (T_g).

Amorphous cross-linked polymers show a wide range of elastic properties that depend on temperature and time. Typical elastic behavior of the cross-linked polymer is shown in Figure 3.2. The storage modulus decreases in a sigmoidal manner as temperature increases. At a certain point, the modulus falls rapidly then becomes almost

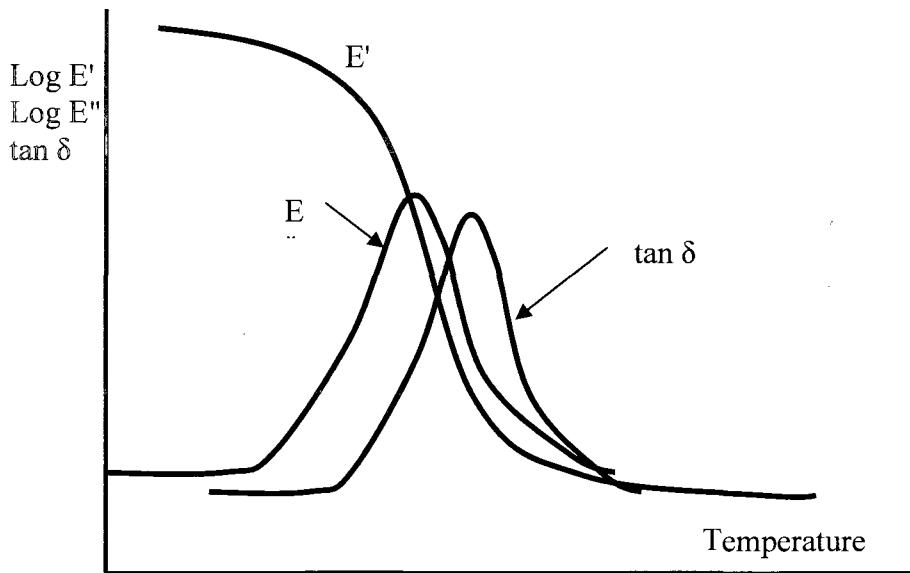


Figure 3.2. Regions of viscoelastic behavior of amorphous cross-linked polymer.

constant at the rubbery state. The elastic modulus can decrease by 3 orders in a temperature range of 20-40 degrees at the transition from glass to rubbery state ¹⁰⁶. the loss modulus E'' and loss factor $\tan \delta$ have their maxima, but the $\tan \delta$ maximum appears several degrees higher than that of E'' . The temperature at which the $\tan \delta$ peak appears is usually accepted as a glass transition temperature value in DMA analysis. Other physical parameters of the polymers, such as thermal expansion, heat capacity, conductivity, refractive index, and tensile strength, also have significant changes in the glass transition region. In the rubbery state, mechanical properties do not change significantly with further temperature increase. In this state, polymers are able to recover significant deformations. It is interesting that most of amorphous polymers in the rubbery state have similar a value of Young's modulus, in the range of 2-4 GPa ¹⁰⁴. Young's modulus in a polymer's rubbery state E_0 is related to the polymer network structure and can allow calculating the cross-link density Q

$$E_0 = \frac{3\rho RT}{M_c} = 3QRT \quad (3.5)$$

where R is universal gas constant, M_c is molecular weight of the section of polymer chain between two cross-links, ρ is the density and T is temperature ¹⁰³. Thus, this is a direct method to characterize cross-linked adhesive network structure. The molecular weight of the polymer chains between cross-links, M_c , determines cohesive properties and physical state for the epoxy adhesive (Figure3.3.).

The value of the loss modulus characterizes behavior of the material during mechanical damping like vibrations. A rapid increase in loss modulus indicates significant increase in polymer structural mobility, which permits motion of the large polymer chains. In this state, the cross-linked adhesive is soft and not able to serve as a load bearing structure.

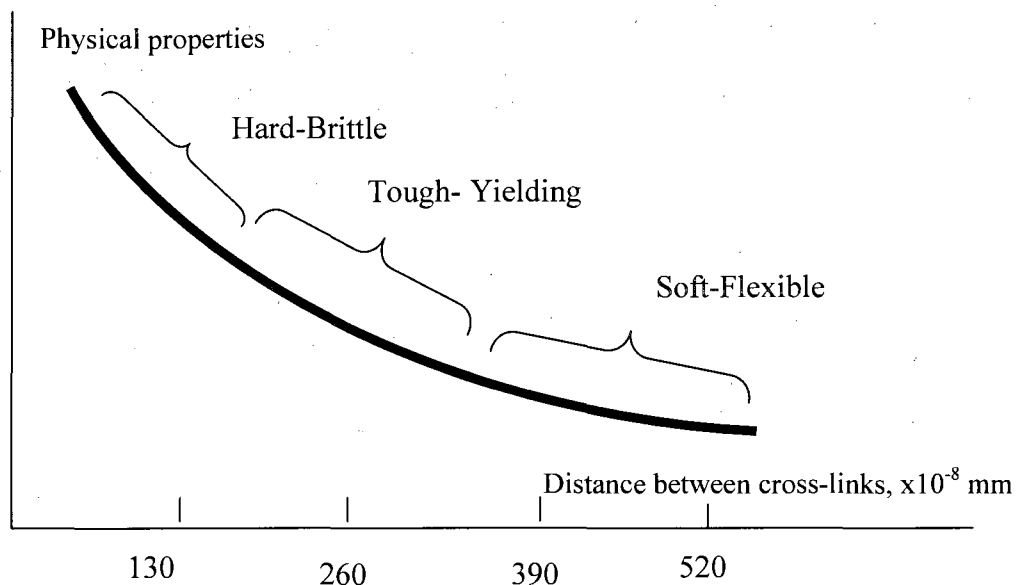


Figure 3.3. Effect of cross-link density on the physical state of the epoxy adhesive.³

Differences in viscoelastic behavior can be explained on the basis of molecular mobility. In a polymer's glassy state, randomly oriented molecules have very limited movement of chain segments. Only local vibrational motions of small units of the main chain or side groups are typical for the glassy state; and the amplitude of vibrations is small. Stiffness of the material relates to small displacements of the molecules from their equilibrium positions. An increase in temperature leads to acceleration and increased flexibility of molecular and segmental motion and to an increase of free volume. There is significant change in flexibility of polymer chains and in the energy of intermolecular interaction at the glass transition. Transformation is due to unfreezing the segmental mobility. In the rubbery region, molecular motions are conformational changes due to rotations around the bond angles. On the molecular level, glass transition involves the beginning of long range coordination in molecular motion. In the glassy state, only 1-4 atoms are involved in motion, while about 10-50 atoms are in movement in the glass transition region⁷⁹. Thus, any small deformations of polymer in the glassy state should be associated with extension and shortening of bond distances and small variations of bond

angles, while in the rubbery region deformations they are associated with conformational rotations.

Glass transition is a transition of second order where the primary thermodynamic functions (enthalpy, entropy, volume) are continuous. A shift in volume or entropy functions is observed at the glass transition⁷⁹. Another distinction is that glass transition occurs in a certain temperature range rather than at a specific value.

The borderline between glassy and rubbery states of an amorphous polymer is the glass transition temperature T_g . There are several definitions of this parameter. More often it is defined as a temperature at which viscosity of the polymer reaches 10^{13} P or as a temperature, below which the segmental motion of polymer molecule is frozen³. Glass transition temperature (T_g) is one of the most important characteristics for amorphous thermosetting polymers, which determine their application. Intensive studies show a relation between the glass transition temperature and the molecular structure of a polymer, which then relates to its elastic constants. The glass transition temperature grows with an increase of cross-linkage density. Cross-linked polymers are characterized by widening of the glass transition region. The degree of cross-linking correlates with elastic modulus and glass transition temperature¹⁰⁴. A correlation between T_g and conversion of the reaction was confirmed for DGEBA and diamine cyclohexane⁸. Thus, T_g can be used as a reliable measure of conversion.

The viscoelastic properties of cross-linked polymers are a function of temperature and frequency of periodical stress applied. Certain property characteristics can be achieved at low temperature or high frequency. This phenomenon is known as time-temperature superposition and can be used to build the “master curve” of viscoelastic properties as a function of frequency or temperature. The shift factor for this curve is described by Williams-Landel-Ferry equation (WLF equation) which is valid polymer's viscoelastic properties at temperatures above T_g ¹⁰⁵

$$\log a_T = -\frac{C_1(T - T_g)}{C_2 + T + T_g} \quad (3.5a)$$

where T is temperature, T_g is glass transition temperature, $a_T = \eta/\eta_g$ is the shift factor, η and η_g is viscosity at T and T_g , C_1 and C_2 are universal constants and equal 17.4K and 51.6K correspondingly for many polymers¹⁰⁶. Viscosity may be replaced by any other free volume-related polymer property such as relaxation times τ or modulus G ; constants values will be different in this case. The WLF equation is a useful tool for estimating physical events in the transition region. The WLF equation is valid only in the temperature range from T_g to $T_g + 100$ °C.

There are several experimental ways to determine glass transition temperature based on the measurements of basic thermal, physical, or mechanical properties. Glass transition is rather a temperature range than a single temperature value (10–15 degrees for uncross-linked polymers and even wider for filled or cross-linked polymers). It is necessary to note that the T_g value varies with different methods of measurement, time, changing of parameters, and thermal history of the sample. Some techniques detect the beginning of transition, whereas others measure its middle point. The slower the rate of temperature change, the lower the value of glass transition. Traditionally, T_g is determined by thermal expansion measurements. Later, other techniques were proposed: differential scanning calorimetry (DSC), thermodielectric, dynamic mechanical analysis (DMA) or torsion braid analysis (TBA). Acoustic methods are successfully used to determine T_g temperature¹⁰³. This technique as well as other dynamic methods such as dynamic mechanical analysis allows us to measure the value of “dynamic” glass transition, which is important for short term deformations like impacts. T_g measured by dynamic methods usually has a slightly higher value than when measured by static methods. The value of T_g , determined by mechanical methods, depends on the frequency of measurement. This is associated with the phenomenon of “dynamic” glass transition, which is influential by a relaxational nature of the transition from rubbery to the glassy state.

The glass transition region is usually broad for cross-linked and crystalline polymers and T_g is not very distinguished and sometimes may be difficult to detect by static methods because the C_p change is of the order of 10–30% while change in modulus is often of the order of 10^3 ¹⁰⁷.

3.3. Effect of Polymerization Reaction on a Polymer's T_g . Gelation and Vitrification.

At the starting point of polymerization, monomers are in a liquid state. Epoxy cure reaction with amine hardener is a step-growth polymerization, a complex process in which three-dimensional linkages are formed throughout the polymer. To form a cross-linked polymer, functionality of the monomers must be greater than two. There are two critical points in the cross-linking polymerization reaction –gelation and vitrification.

Gelation (or gel point) is the reaction stage when a cross-linked polymer with a three-dimensional network is formed. As the reaction proceeds, molecular weight of the reacted branched molecules increases. At a certain point (gelation) chains become linked together into the network with infinite molecular weight. At this point, soluble oligomers become viscoelastic solids, which would only swell in solvents. This transformation is quick and irreversible. Gelation is a chemical phenomenon.

Another important event is vitrification which is important characteristic of the reacting thermosetting system. When polymerization begins and molecular weight and cross-linking density increases, molecular mobility becomes more and more restricted. This leads to increase in the glass transition temperature of the reacting system. When T_g of the reacting system approaches and exceeds the reaction temperature, the polymer transforms into a glassy state (vitrifies). Vitrification may happen both before and after gelation, forming ungelled or gelled glass correspondingly. This is a reversible process and reaction can further proceed if the temperature reached will be higher than T_g of the system.

As the time to gelation or vitrification depends on reaction temperature, this parameter is critical for the extent of the reaction. Gillham¹⁰⁹ has developed a time-temperature-transition (TTT) diagram for the reaction, which is a map of different states during isothermal cure reaction at various cure temperatures (Figure 3.4). It helps to understand all changes in the polymer structure that occur and compare properties of the thermoset polymers. The diagram has three important temperatures: T_{g0} , glass transition

temperature of the uncured system, $_{gel}T_g$, temperature where gelation and vitrification happen simultaneously and $T_{g\infty}$ glass transition temperature of fully cured system. Vitrification and gelation curves divide the graph into four sections: liquid, ungelled glass, gelled glass, and gelled rubber.

The vitrification line has S-shaped form due to increased reaction rate at higher temperatures. Gelation time decreases in exponential manner as temperature increases. The temperature of the reaction determines what event happens first, vitrification or gelation. Curing the adhesive to full conversion involves changing of the glass transition temperature from T_{g0} to $T_{g\infty}$. In the early stages, the reaction is kinetically controlled. If temperature of the reaction is between T_{g0} and $_{gel}T_g$, the reaction proceeds until the T_g of the system reaches the reaction temperature. Reagents vitrify and the reaction rate becomes diffusion controlled so gelation point may not be reached.

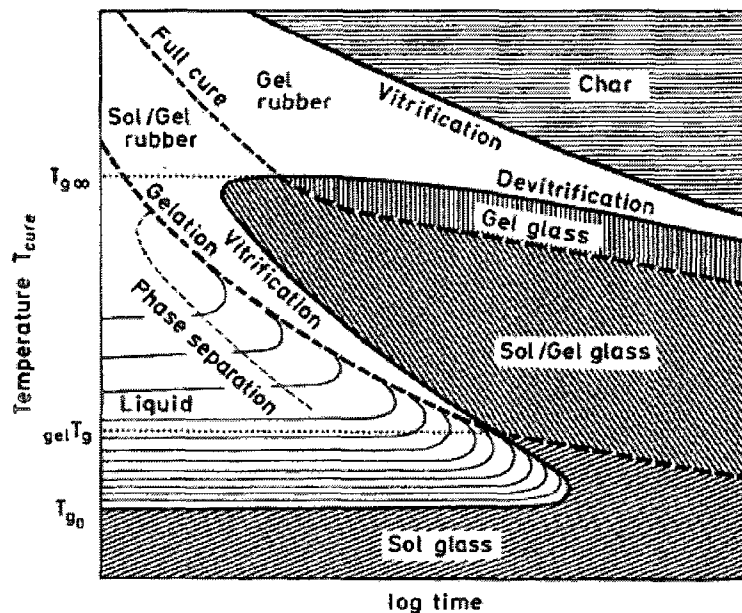


Figure 3.4. Time-temperature-transformation diagram for typical epoxy based adhesive ¹⁰⁹.

If the temperature of the reaction is between $_{gel}T_g$ and $T_{g\infty}$, the system vitrifies after gelation and reaction stops before its completion, which may result in insufficient development of the material's cohesive properties and failure of the adhesive joint. If the cure reaction occurs at a temperature higher than $T_{g\infty}$, the system will not vitrify and the

reaction proceeds to the end. However, the material may start to degrade, which can lead to the lowering of T_g value and losing some mechanical properties. It follows from this diagram that to obtain a fully polymerized system, it is necessary to perform the reaction at a temperature higher than the glass transition temperature of the fully cured system. A TTT diagram is a useful way to show the relationship between cure conditions and adhesive structure and properties.

3.4. Acoustic Wave Propagation in Isotropic Elastic and Viscoelastic Materials.

Acoustic measurement is a form of dynamic mechanical measurement, though sometimes the latter term is reserved for low frequency. Acoustic refers to periodic pressure waves. The propagation of a sound wave can be described from the equations expressing the laws of conservation of mass, impulse and energy. These equations have the following form ¹⁰³:

$$\frac{\partial \rho}{\partial t} + \rho \frac{\partial v_x}{\partial x} = 0 \quad (3.6)$$

$$\rho \frac{\partial^2 u}{\partial t^2} - \frac{\partial \sigma_{xx}}{\partial x} = 0 \quad (3.7)$$

$$\rho c_v \frac{\partial T}{\partial t} - \frac{T \alpha_v}{\rho} K_T \frac{\partial \rho}{\partial t} = - \frac{\partial q_x}{\partial x} \quad (3.8)$$

where ρ is density of the medium, v_x is a x-component of the velocity of the particles, u is displacement of points of a body in deformation (strain), σ_{xx} is a diagonal element of the stress tensor, c_v is specific heat capacity at constant volume, T is absolute temperature, α_v is a coefficient of thermal expansion ($\alpha_v = \frac{1}{V} \left(\frac{\partial V}{\partial T} \right)_p$ where V is specific volume), K_T is isothermal bulk modulus $K_T = -V \left(\frac{\partial p}{\partial V} \right)_T$, q_x is component of vector of heat flux density ($\bar{q} = -\chi T$ where χ is the thermal conductivity coefficient).

In cases of small deformations, the relation between displacements and components of the stress tensor can be described by Newton's law

$$\sigma_{ij} = c_{ijkl} \frac{\partial u_k}{\partial x_l} \quad (3.9).$$

In this case, the equation (3.7) can be expressed in the form

$$\rho \frac{\partial^2 u_i}{\partial t^2} = c_{ijkl} \frac{\partial^2 u_k}{\partial x_l \partial x_j} \quad (3.10).$$

which is called the wave equation. For isotropic media this equation falls into two parts

$$\rho \frac{\partial^2 u_1}{\partial t^2} = (\lambda + 2\mu) \frac{\partial^2 u_1}{\partial x_1^2} \quad (3.11)$$

$$\text{and } \rho \frac{\partial^2 u_2}{\partial t^2} = \mu \frac{\partial^2 u_2}{\partial x_1^2} \quad (3.12),$$

which describe propagation of longitudinal and shear waves correspondingly. In a longitudinal wave, the polymer particles vibrate in the direction of wave propagation. Shear wave moves polymer particles perpendicularly to the direction of propagation. The standard solution for this equation is a sinusoidal wave that describes the wave propagation in one direction with constant speed $u = u_0 \sin(kx - \omega t)$, where ω is angular frequency and $|k| = \frac{2\pi}{\lambda}$, -wave number. Taking into account the thermal and density changes during wave propagation, described by eq.(3.6)-(3.8), variations of sound velocity are small and can be omitted in most cases.

3.5. Sound Velocity and Absorption.

In cases of a wave propagating through the material along the x-axis, displacement of the particles u should be described by

$$u = u_0 e^{i\omega t - \sigma x} \quad (3.14)$$

where u_0 is the amplitude of displacement, t is time, σ is a complex wave number

$\sigma = \alpha + i \frac{\omega}{c}$ where α is absorption coefficient and c is velocity of elastic wave.

In infinite media where wavelength is considerably less than the dimensions of the body, velocity of the longitudinal wave, in which the particle vibration occur in the same direction as wave propagation, is described by following expression

$$c_L = \sqrt{\frac{L}{\rho}} = \sqrt{\frac{E}{\rho} \frac{(1-\sigma)}{(1+\sigma)(1-2\sigma)}} \quad (3.15)$$

where, ρ is density of polymer, L is the longitudinal (or compression) modulus of elasticity and σ is Poisson's ratio. Both compression and shear deformations contribute to the longitudinal modulus value:

$$L = B + \frac{4}{3}G \quad (3.15a)$$

where K is a bulk modulus and G is a shear modulus

If the wave propagates in thin strips of materials and wavelength is larger than lateral dimension of the body, wave velocity will be described as

$$c_L = \sqrt{\frac{E'}{\rho}} \quad (3.16)$$

where E' is Young's modulus.

Velocity of the shear wave can be represented as

$$c_T = \sqrt{\frac{G'}{\rho}} \quad (3.17)$$

where G' is dynamic shear modulus.

Absorption is a measure of the energy removed from a sound wave as a result of conversion to heat as the wave travels through the polymer. In this sense it relates to the loss modulus. In contrast to absorption, the term attenuation includes energy loss due to scattering and reflection as well as absorption. Elastic waves attenuate significantly in polymer materials. The attenuation constant can be found from the formula

$$\alpha = \frac{1}{x_2 - x_1} \ln \frac{A_1}{A_2} \quad (3.18)$$

where A_1 and A_2 are amplitude values for vibrations of the particles at x_1 and x_2 coordinates. Absorption per wavelength is related to the loss factor of the material¹¹⁰

$$\tan \delta = \frac{E''}{E'} = \frac{\alpha \lambda}{\pi} \quad (3.18a)$$

It is to be noted that equations (3.15) - (3.17) are valid only in the cases when sound attenuation per wavelength is relatively small. In general cases, the relationship between elastic modulus and acoustic parameters is described by the following formula¹⁰³:

$$L^* = \frac{\rho c^2}{\left(1 - i \frac{\alpha c}{\omega}\right)^2} \quad (3.19)$$

Then, the longitudinal storage and loss moduli are equal to:

$$L' = \frac{\rho c_L^2 \left[1 - \left(\frac{\alpha \lambda}{2\pi}\right)^2\right]}{\left[1 + \left(\frac{\alpha \lambda}{2\pi}\right)^2\right]^2}; \quad L'' = \frac{2\rho c_L^2 \left(\frac{\alpha \lambda}{2\pi}\right)}{\left[1 + \left(\frac{\alpha \lambda}{2\pi}\right)^2\right]^2} \quad (3.20)$$

Moduli and acoustic parameters in polymers depend on the acoustic frequency. Deformation in a polymer produced by stress depends on time that the stress is applied. For acoustic frequencies, stress is applied for a very short time; so only a small part of the polymer is deformed. This causes only a small strain compared with classical static or Dynamic Mechanical Analysis (DMA). Measurements using ultrasonic waves probe motions of the polymer on the short length scales, while low frequency methods probe large-scale motions. Elastic moduli measured at ultrasonic frequencies are usually higher than the static moduli.

In viscoelastic materials, temperature and frequency dependencies are interrelated. As it is impossible to investigate dependence of the viscoelastic properties in a broad frequency range by one technique, the study of temperature dependence seems to be more convenient.

3.6. Relation of Acoustic Parameters to Chemical Structure and Physical Properties of Polymers

Macroscopic properties of a polymer are directly related to its molecular structure. Ultrasound wave propagation in a polymer is governed by many factors, which are important for understanding the molecular mechanisms associated with the polymer's macroscopic behavior. They are degree of polymerization, the degree of crystallization, the extent of cross-linking and/or entanglements, type of side groups, flexibility of the backbone or side groups' structures, and bond angles.

Ultrasonic techniques measure the propagation characteristics of mechanical waves through the polymers. Acoustic response of the polymer is a reflection of the dynamic process that occurs at the molecular level during mechanical deformation. Sound velocity is greatly determined by intermolecular interaction. Increase in velocity can be explained by growth in intermolecular interaction or by change in type of the interaction. There is a correlation between acoustic parameters of a polymer, its chemical composition and structural factors such as the glass transition, cross-link density, or morphology. The magnitude and nature of change in the dynamic elastic modulus and

sound velocity are determined by the bond energy of atoms forming the main chain of the polymer and the energy of interaction between the elements of adjacent polymer chains (intermolecular interaction). Intermolecular interactions have an influence on the moduli of elasticity of the polymer in different physical states. Thus, in the glassy state when intermolecular interactions are significant, dynamic modulus of elasticity is 3-4 orders greater than modulus of the same polymers in the rubbery state, when the energy of intermolecular interactions is lower¹⁰³. Any structural changes, change in the nature of the macromolecular organization or nature of components in polymer compositions have an influence on the effectiveness of the intermolecular interaction. Therefore, they will affect the elastic and acoustic behavior of the polymers. The loss modulus and sound absorption are determined by the type and intensity of the molecular motion. Thus, acoustic measurements can be used as a measure of any of these factors, or to monitor their changes as a function of time or temperature.

Maximum induced particle displacement can be calculated by the following formula¹¹¹:

$$u_0 = \frac{1}{\omega} \sqrt{\frac{2I}{\rho c}} \quad (3.21)$$

where I is intensity, ρ is polymer density, $\omega = 2\pi f$ is angular frequency, c is sound velocity in polymer, I is intensity. With acoustic frequencies in the range of 5-100 MHz and values typical for epoxy polymers (sound velocity - 2400m/s, density 1.1 g/cm³), maximum particle displacement is approximately 1.3×10^{-2} nm. Thus, the acoustic technique stimulates molecular motion on length scales much smaller than the polymer chain size (10nm)¹¹⁰. Hence, in addition to being non-invasive, the technique is non-destructive (does not change the material's properties).

3.7. Acoustic methods for adhesive joint evaluation.

There are many acoustic techniques and approaches used to evaluate quality of the adhesive joints^{1, 112}. Two of them used in this study will be reviewed in details.

3.7.1. Pulse-Echo Technique.

The pulse-echo technique is one of the most widely used methods for inspection of adhesively bonded joints. A wide survey describing the “state of the art” in this field is given by Adams and Drinkwater¹¹³. Usually pulses of compression or shear waves of frequencies in the range 1-20 MHz are stimulated by a piezoelectric transducer. It provides a resolution of about 0.5 – 2.0 mm that enables one to find macroscopic defects but is not sufficient to achieve proper resolution for revealing microscopic defects. Next the pulse is modified by the path taken and energy is reflected by discontinuities such as the adhesive layers. The change in the acoustic impedance of the materials across the interface causes part of the wave to be reflected. As a rule, defects contain air or other low density substance, and they will have very low acoustic impedance relative to the adhesive. Under such conditions the ultrasonic signal will be almost completely reflected. Typically experiments are performed with the transducer positioned such that the ultrasonic pulse generated by the transducer is incident perpendicular to the surface of the specimen. By scanning the interface, information can be obtained about the area of adhesively bonded joints in the ultrasonic beam as well as various types of defects and morphological peculiarities.

A broadband transducer generates a sharp acoustic pulse, which propagates through the structure, and then collects the train of pulses reflecting from each interface. Such displays are commonly called A-scans. The data available from the A-scan includes the times of flight and amplitudes of various reflections, which may be individually gated and analyzed. The correlation between acoustic and mechanical properties is described by the following equations^{103, 114, 115}:

$$Z = C\rho; \quad C_L = \left(\frac{K + \frac{4}{3}G}{\rho} \right)^{\frac{1}{2}}; \quad C_S = \left(\frac{G}{\rho} \right)^{\frac{1}{2}}, \quad (3.21)$$

where Z is the specific acoustic impedance, C_L is the longitudinal sound velocity, C_S is the shear sound velocity, G is the shear modulus, K is the bulk modulus and ρ is the density.

A single A-scan contains quantitative information about the layer thickness, which allows the sound velocity to be calculated. However, our previous investigations¹¹⁶ and work by other researchers show that the complex structure of the reflected waves makes the interpretation of individual A-scans difficult. At the same time, collecting a set of A-scans often makes it clearer which pulse is carrying the useful information.

The basic data may be individually gated and analyzed. Figure 3.5 shows the ultrasonic pulse-echo method which was used for testing the quality of metallic adhesive bonding. A transducer, at normal incidence, works as a transmitter-receiver, i.e. sound from the contact transducer passes through the sample and reflects from the interfaces.

The time representation of the echoes, as seen on the oscilloscope, is shown in Figure 3.7. The measurement of the time delay between two successive echoes permits us to calculate the sample thickness¹¹⁷.

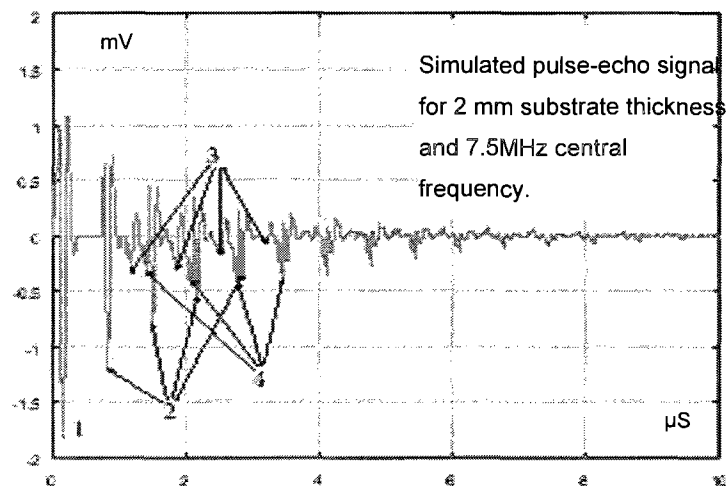


Figure 3.5. Time representation of the echoes. 1-transducer/metal interface, 2-metal/adhesive, 3-adhesive/metal and 4-metal/air interface.

A promising method for the ultrasonic testing of adhesively bonded joints with A-scans in the frequency range of 20-50 MHz has been proposed by Goglio and Rossetto¹¹⁸. They used acoustic methods to detect zones affected by poor adhesion. In these zones the adhesive can be present in the gap between the sheets but bonding does not take place due to insufficient curing or impurities on the interface. The reflected signal has the form of a damped succession of pulses as a result of the ultrasound reverberations inside the metal sheet. The decay, θ , of the signal is defined as the ratio of successive peak amplitudes [70]

$$\theta = \frac{1}{n} \sum_{k=1}^n \left| \frac{Y_{k+1}}{Y_k} \right| = R_m R_l e^{-2\alpha s} \frac{1}{n} \sum_{k=1}^n f(k), \quad (3.22)$$

where Y_k and Y_{k+1} are the amplitudes of the k^{th} and $(k+1)^{\text{th}}$ peaks, n is the number of ratios considered, R_m is the reflection coefficient of the coupling/metal interface, R_l is the reflection coefficient of the metal/adhesive interface, α is the attenuation coefficient of the metal, s is the thickness of the sheet, and $f(k)$ is a function of the peak order k . If $R_l = R_{met}$ (the reflection coefficient for metal-air interface), adhesive is not present; if $R_l = R_{GA}$ (the reflection coefficient for metal-adhesive interface) good adhesion exists. The authors state that their method allows an adhesion index to be evaluated which is related to the reflection coefficient at the adhesive-substrate interface. Statistical distributions of such indices can then be used to develop guidelines for evaluating the quality of adhesion in a sample¹¹⁸.

In a subsequent work, Gogli and Rossetto¹¹⁹ investigated bonded joints with anaerobic adhesives where the thickness of the adhesive layer is nominally zero due to contact pressure between the sheets. In these systems the ultrasonic signals traveling through the interface are not completely damped. In such cases the method based on the decay measurement described above is not suitable because the adhesive layer is negligible or absent. To overcome this problem the authors take the adhesion index to be the ratio of the first peaks reflected from the bonded area after and before bonding. Using this so-called “first-peak” method allows the authors to extend the limits of the pulse-echo technique application to ultrasonic inspection of adhesive joints between sheets of

thickness more than 1 mm, bonded together by an adhesive layer of nominally zero thickness¹¹⁹.

Challis et al.¹²⁰ have applied a transfer matrix approach based on the Thompson and Haskell^{121, 122} formulation for a bonded joint excited by a compression wave probe with a coupling shoe attached. The authors incorporate complex wave numbers in the layers to include the frequency-dependent effects of absorption and phase velocity in the adhesive. One of the difficulties of using the pulse-echo method for investigation of adhesive joints is that the incident signal overlaps and interferes with the reflected signals, thereby making analysis of the received pulse sufficiently difficult. To improve the detectability of the low amplitude echo from the rear adhesive-substrate boundary it was necessary to reduce the amplitude of the reverberation from within the front metal sheet. Challis and co-workers have approximated the behavior of the echo and reverberations expressed in the frequency domain as:

$$H(\omega) = \frac{1}{1 - \alpha e^{-j\omega 2T}}, \quad (3.23)$$

where α is the product of the internal reflection coefficient on either side of the front substrate boundaries and T is the propagation time for the compression wave to cross the area of the sheet. Because the signals are digitized, Eq. (3.23) can be represented in the z -transform domain, commonly used in digital signal processing¹²³, as:

$$H(\omega) = \frac{1}{1 - \alpha z^{-2m}}, \quad (3.24)$$

where m is the number of digitizer time steps equivalent to T . The inverse of this filter has following time-domain equivalent:

$$y_n = x_n - \alpha x_{n-2m}, \quad (3.25)$$

where x_n and y_n are the input and output data, respectively. Eq. (3.25) describes a digital filter which clears away reverberation oscillations and clarifies the output signal from the lower interface. After filtering the data, the signal should only contain the bondline

echoes, which can be processed using conventional pulse location and gating methods. Experiments which have employed this model with 0.7 mm epoxy-1.2 mm steel joint have shown that front disbonds are testable in most cases. However, detection of a disbond from a rear substrate void is also possible after significant signal processing and for restricted combinations of substrate and adhesive thickness. Evaluation of the state of adhesive cure was uncertain due to large errors in the calculations of adhesive impedance in the measurements. Clearly the results of these investigations are highly relevant for the automotive industry, where the non-destructive evaluation of simple substrate metal lap joints is commonly necessary.

Chapman et al.⁶ showed that attenuation of the successive echo amplitudes of sound reverberations in the metal substrate is associated with bond state (bonded or unbonded) on upper substrate-adhesive interface. Phase change occurs on the lower interface in case of improper bonding between adhesive and substrate.

For the inspection of adhesive joints consisting of an aluminum alloy substrate and epoxy adhesive, Vine and co-workers¹²⁴ have used ultrasonic measurements at normal and oblique incidence. The oblique incidence scans have been applied for detecting the same types of defect as the normal incidence technique, except in cases where the resolution was insufficient to detect very small defects. In the case of oblique incidence scans, no defect was detected that could not be observed by means of the normal incidence technique. In comparison to the normal incidence method, the oblique incidence testing tends to be more sensitive to the interlayer characteristics and more complicated to interpret because mode conversion can occur at the various interfaces. The authors applied ultrasonic scans to both two and three layer adhesive joint specimens with a centre frequency of around 50 MHz for normal incidence and 20 MHz for oblique incidence. In the two layer samples, micro-defects and edge disbonds were detected; the latter objects were simple to find by both methods. The micro-defects were detected in areas remote from the edges and these isolated defects took several forms. The normal incidence scans allow for the detection of many of these micro-defects but only the largest of them could be observed in the oblique incidence technique due to the poorer spatial resolution. It was found that in the three layer compositions (4 mm aluminium-0.2

mm epoxy-4 mm aluminum) no micro-defects were detected by any ultrasonic scans by oblique waves. At the same time it is possible to assert that micro-defects can go undetected due to insufficient spatial resolution of the ultrasonic technique ¹²⁴.

An approach which uses ultrasonic normal (7-22 MHz) and oblique (7-28 MHz) incidence techniques has been applied by Moidu, Sinclair, and Spelt ¹²⁵ for the non-destructive durability study of epoxy adhesives using reflection measurements from the interfacial region between the adhesive (thickness at 0.6 mm) and the substrate (1.6 mm-aluminum alloy). They used the spring boundary conditions ¹²⁶ to model the interfacial area with tangential and normal spring constants. As a rule, the spring model has been used in cases where the adhesive and substrate may be treated as connected by normal and tangential linear spring elements ¹²⁷.

Moidu and co-workers¹²⁵ applied the above-mentioned approach for adhesive-substrate systems and showed that shear waves are a more sensitive indicator of the durability of epoxy adhesives than measurements of longitudinal waves with a given frequency at normal incidence. The shear waves at oblique incidence also showed somewhat greater sensitivity to degradation in comparison to shear waves at normal incidence.

In a comprehensive survey of non-destructive testing methods for inspection of adhesively bonded joints, Munns and Georgiou¹²⁸ note that a technique which uses shear stresses is likely to be more sensitive to interfacial properties than a technique which uses compressive stresses. An oblique incidence method commonly works as a practical inspection technique in cases where a high probe frequency is not required. Clark and Hart¹²⁹ have shown that for normal incidence shear waves are more sensitive than longitudinal waves for detecting small liquid-filled gaps in layered systems. Thus, the oblique incidence method can potentially detect the more gross types of defects, such as voids, cracks and disbonds.

3.7.2. Scanning Acoustic Microscopy.

The historical aspects of acoustic microscopy development have been discussed by Quate¹³⁰, while the physical principles and applications of acoustic microscopy have been described in detail by Briggs¹³¹. Acoustic microscopy has been used widely over the last fifteen years for a variety of purposes. Development of mathematical models of ultrasound propagation in heterogeneous and anisotropic systems, including adhesively bonded joints is summarized in^{132, 133}. The increased operating demands of adhesively bonded joints require inspection of thermal, chemical, and mechanical properties with high spatial resolution. Because the contrast of ultrasonic images is mostly determined by the viscoelastic characteristics of the materials under examination, the technique may be used to obtain quantitative information about mechanical material properties^{134, 135}. At the same time, the formation of the adhesively bonded joint involves a great number of factors^{136, 137}. Among these factors must be included the formation of weak layers of different types between the adhesive and the substrate and of internal stresses in the adhesive layer. Determination of these factors depends significantly on the resolution of the scanning acoustic microscope (SAM). The spatial resolution of conventional methods of acoustic microscopy is limited by the wavelength of the ultrasound¹³¹.

Acoustic waves transmitted through the adhesive-substrate system may be used to examine the internal interfaces where the incident sound wave partially reflects back. The most common method of investigation uses an analysis of the reflected intensity of a focused acoustic wave. To accomplish this task, both the emitter and detector of ultrasound are combined on one probe head. If a one-dimensional scan is performed along the line and the echo amplitude is plotted as a function of position, a cross-sectional view of the laminated system, or B-scan, is obtained. If a two-dimensional scan is performed, a planar view of the bonded joints, or C-scan, is produced. In this way it is possible to determine the distribution of defects by scanning the surface of the structure with a transducer. The spatial resolution of the scan depends on the scanning system and the beam width, which is limited by the transducer (or lens) size and curvature and the acoustic wavelength. The depth resolution depends primarily on the wavelength width of

the incident pulse. Generally, higher frequencies increase resolution at the expense of a weaker signal. More details about SAM method will be given in Chapter 4.

Many parameters are involved in the choice of a coupling fluid. The velocity and attenuation of the acoustic waves in the fluid as well as the chemical reactivity of the fluid with the materials constituting the lens and specimen must all be taken into account. Theoretical and experimental investigations regarding the acoustic parameters of coupling fluids in acoustic microscopy are described by Cros, et al.¹³⁸. In this study, the effects of electrolytic solutions of LiOH, NaOH, and KOH in water were considered in order to increase of the sound velocity. This approach is possible because the velocity of compression waves in liquids increases with the strength of the interaction between molecules. Because ion-water interactions tend to be strong, the velocity will increase as a function of the ion concentration, the polarizing capacity of the cations, and polarizability of the anions.

Yamanaka et al.¹³⁹ used SAM for investigation at low temperatures. They used a methanol couplant to design a scanning acoustic microscope that is capable of operating between +30 and -94 °C. It was proven that at a low temperature (-30 °C) the sensitivity of the method is much better than that at the room temperature. Further investigations have shown that resolutions as high as 15 nm can be obtained by SAM operating near absolute zero using 15.3 GHz ultrasound and liquid helium coupling fluid¹⁴⁰.

An alternative to liquid couplant is a solid coupling medium. Transducers of this type commonly use a soft rubber between the transducer and specimen, which conforms to the surface undulations of the test surface when in pressed contact. Billson and Hutchins¹⁴¹ demonstrated the application of a static, solid-coupled, longitudinal-wave probe operating using a synthetic rubber-coupling medium. Drinkwater and Cawley^{142, 143} described a similar probe operating at a frequency range of 3.8 - 7 MHz but composed of a different low-loss rubber. These techniques were capable of operating in pulse-echo mode and showed promise for use in generating C-scan data without the risk of test piece contamination. This approach has shifted development away from the use of low frequency, un-damped, through-transmission devices which use a thin layer of highly

attenuative solid coupling, towards higher frequency, highly damped, pulse-echo devices where the solid coupling is used as a delay line.

During recent years, enormous effort has been exerted to make the transducers sensitive enough to transmit ultrasound without using physical contact^{144, 145}, i.e. air coupling only. Blomme et al. have reported studies on a wide diversity of materials of both low and high acoustical impedance including flaws in an aluminum plate, spot welds on metallic plates, and ultrasonic reflection from an epoxy plate with a copper layer in the frequency range of 0.75 – 2 MHz. One limitation of this technique is that the object must have a flat surface and parallel entrance and exit planes to accommodate the requirement that the measurements occur at normal sound incidence.

The choice of couplant depends on the required resolution and depth penetration as well as the properties of the sample's surface. A survey of the acoustical experiments in this field for last decade indicates that the main way to launch ultrasound into a sample is still to immerse both ultrasonic transducer and test material in a liquid (usually distilled water). However, this immersion technique is not suitable for some metals, wood, paper, or any other porous material, and in these cases air or solid coupling may be used. For extremely high resolution, a coupling medium of low attenuation such as super-fluid liquid helium may be used, although at the cost of higher impedance mismatch and reduced depth penetration. Among limitations of the air coupling technique is an upper bound on the usable ultrasound frequency, (typically below 5 MHz) and consequently the relatively low resolution of this technique.

Acoustic imaging is well suited to the adhesive bond geometry. The amplitude of acoustic pulses reflected from each interface is very sensitive to the physical properties of the media on either side as well as elastic conditions at the boundary itself. The images, obtained using a SAM, demonstrate the possibilities of the technique for detecting various types of defects and also the difficulties in dealing with the metal-polymer acoustic mismatch^{146, 147}.

By using 50 MHz (normal incidence) and 20 MHz (oblique incidence) probes for an aluminum/epoxy interface, Vine, Cawley, and Kinloch¹²⁴ have obtained acoustical images which show that a very large number of line and spot micro-defects can be clearly detected, although a much smaller number are seen on the oblique incidence scan as compared to the normal incidence scan. The authors develop the potential of ultrasonic imaging application for the detection of environmental degradation in aluminum/epoxy adhesively bonded joints. Photographs taken for a specimen exposed to water at 50 °C illustrate those defects as small as 0.5 mm in diameter could be detected at normal incidence, while the minimum detectable size at oblique incidence was around 2 mm.

Cross et al.¹³⁸ investigated 12 μm polyethylene terephthalate (PET) films coated with a 40 nm thick aluminum layer by high frequency (600 MHz) acoustic microscopy. Due to the superficial layer thickness of a few microns, acoustic attenuation was negligible, and images were obtained with the resolution of about 2 – 3 μm in focus. The authors observed the variations of the adhesion with the thermal treatment as a function of the number of unbonded areas. These areas have been characterized as losses of adhesion between the layer of aluminum and PET film. Certainly the acoustic images of the samples show sufficiently rich contrast behavior; however, this technique can be used only for the detection of very thin bonded joints and is inapplicable to the thicker layers of the adhesive and substrate which are common in heavier industries.

In recent decades, quantitative acoustic microscopy has been widely adopted for the evaluation of the adhesively bonded joints. Quantitative acoustic microscopy depends on the variation of the video signal V with the defocus, z , of the lens towards the specimen¹³¹. The $V(z)$ curve is the amplitude of the normal component of the ultrasound returning to the transducer as a function of the distance between the acoustic lens and the sample surface. The oscillating shape of the $V(z)$ curve appears due to interference between the directly reflected central part of the ultrasonic beam and the beam associated with the propagation of leaky Rayleigh waves. The latter are generated provided the opening angle of the lens includes the boundary angle for surface wave generation of the sample under study. It is possible to obtain the Rayleigh wave velocity from the distance Δz between the interference maximum/minimum of the $V(z)$ curve¹⁴⁸:

$$\Delta z = \frac{v_f}{2f(1 - \cos \theta_R)}; \quad \sin \theta_R = \frac{v_f}{v_R} \quad (3.30)$$

where v_f is the sound velocity in the coupling medium, v_R is the Rayleigh wave velocity of the specimen material, θ_R is the boundary angle of surface wave generation, and f is the frequency of the ultrasonic waves. Using the Rayleigh wave velocity, it is possible to obtain the local acoustic impedance with a spatial resolution of a few microns¹⁴⁸.

The $V(z)$ response can be quantified through the Fourier transform method, often used in numerical signal processing. This method allows the velocities of the various acoustic modes to be obtained from the period of the pseudo-oscillations.

Quantitative acoustic microscopy can be adapted to the investigation of adhesion phenomena in thin multilayer structures. Guo et al.¹⁴⁹ have applied the reflectance function of the specimen to calculate the $V(z)$ curve for thin Ti, TiN and Al (1 μm) films on steel substrates (3.5 μm) by 225-MHz line-focus acoustic microscopy. The stiffness characteristics of a non-perfect interface obtained by applying the $V(z)$ measurement model have shown that these characteristics can be used as a tool for an indication of the bond quality between film and substrate. Quantitative acoustic microscopy of thin-film systems at 600 MHz¹⁵⁰ has also confirmed a good correlation between Rayleigh wave velocity and bond strength. While non-destructive evaluation cannot be used for direct measurement of bond strength, the interfacial stiffness is related to this parameter. Hence the results discussed here illustrate the capability of quantitative acoustic microscopy to evaluate the bonding conditions at the interfaces of thin-film systems. However, it is important to note that such correlations have been obtained only for thin (submicron) films and are not practical for the adhesively bonded joints with thickness on the order of 0.5 mm where it is necessary to account for attenuation.

In spite of the fact that acoustic imaging techniques are important tools in non-destructive testing and material evaluation, only a limited number of researchers have used them to investigate adhesive joints. This limited application may be explained by the fact that the presence of the finely layered structure complicates visualization, and these

complications may only be adhesive/substrate thickness and viscoelastic properties of the material considered. It is well known that some composite materials, for example, a glass-reinforced plastic, highly attenuate ultrasound, and, in such cases, the thickness of the material that can be inspected ultrasonically is limited¹²⁸.

CHAPTER IV.

Materials and Methods

4.1. Epoxy Adhesive Systems

Commercial one and two-component adhesive systems were chosen for investigation of the cohesive and interfacial properties. Diglycidyl bisphenol A-based epoxies, hardened with amines, are among the widespread adhesives used in many industries. Polymerization reaction (cure) between epoxy and amine is a quite complex process, which includes several chemical reactions. The typical one is an additional reaction between epoxy ring and primary or secondary amine. The hydroxyl groups formed during epoxy opening or existing react with epoxy groups in addition etherification. Details are discussed in Chapter 2.1. The reaction's stoichiometry and temperature control the final adhesive's microstructure and therefore properties.

One of the problems in studying the commercial adhesive's relation between its structure and its properties is the lack of information about the adhesive's composition. However, the main components of the systems can be identified.

4.1.1. Two-Component System

Two-component epoxy adhesive was used for calibration studies. Composition of the epoxy and hardener components is shown in Table 4.1. The epoxy and hardener are mixed right before the adhesive is used. Two-component adhesives allow us to vary the resin to hardener ratio to evaluate how stoichiometry influences the final adhesive's properties. These systems typically gel within 10-15 minutes and harden after 40-60 minutes. This time interval is enough to monitor all important events with reasonable experiment duration. Although a huge amount of compounds can react with epoxy at room temperature, almost all of them need to be heated to reach a high cure degree⁸. Only aliphatic amines are able to cure epoxy at ambient temperatures with acceptably high cure degree. We conducted preliminary study of the epoxy adhesive hardening reaction to

adjust experimental setups and find the proper acoustic parameters, as conventional acoustic transducers are not resistant to the temperatures higher than 150°C.

Table 4.1. Composition of two-component adhesive system.

| component | CAS# | Amount, wt% |
|--|-------------|-------------|
| Resin | | |
| Epichlorohydrin-4,4'-isopropylidene diphenol resin (Bisphenol A- epichlorohydrin polymer | 25068-38-6 | 60-100 |
| Phenyl glycidyl ether | 122-60-1 | 0.1-1 |
| Hardener | | |
| Polyamide of C ₁₈ unsaturated fatty acid dimers and triethylenetetramine (TETA) | 68410-23-1 | 60-100 |
| N-(2-Aminoethyl) piperazine | 140-31-8 | 10-30 |
| Aliphatic amines | | 10-30 |
| Silica, amorphous, fumed, crystalline-free | 112945-52-5 | 1-5 |

Epichlorohydrin-4,4'-isopropylidene diphenol resin is a typical difunctional epoxide with molecular weight approx. 380. Phenyl glycidyl ether is a mono epoxy-based reactive diluent which modifies viscosity of the epoxy resin and participates in the polymerization.

Polyamide hardeners are based on polymerization reaction between triethylenetetramine (TETA) and a mixture of dimer fatty acid. Dimer fatty acid is a complex mixture of the branched and cyclic products, which consist of C₃₆ diacids and C₅₄ triacids. The schematic of TETA-dimer acid oligomer is shown below. Typical reactions between epoxy resin and aliphatic polyamide hardener is discussed in Chapter 2.1. As the etherification reaction between hydroxyl and epoxy groups occurs only at elevated temperatures, epoxy resin used can be considered difunctional. Bulky alkylene groups make hardener more elastic and increase its adhesive properties because of formation of the hydrogen bonds in the amine region and presence of the low polarity

domains in the fatty regions ¹⁵¹. Fatty acid amides provide additional water and corrosion resistance to the adhesive. At the same time, reactivity of this type of hardener is slower.

Short chain distance of the aliphatic amines provide the adhesive's mechanical strength and resistance to water, while fatty acid polyamides give good adhesion and flexibility due to their secondary amine groups.

N-(2-Aminoethyl) piperazine (N-AEP) contains one primary, secondary and tertiary nitrogen atom. It is used as an additional curing agent and corrosion inhibitor. At ambient temperatures, N-AEP reacts as acyclic homologue triethylenetetramine (TETA) with rapid gelation and high exotherm (Reaction 2.3)¹⁵². However, full cure is not possible with N-AEP at room temperature. The addition of silica provides dimensional stability, thermal conductivity and moisture resistance.

4.1.2. One-Component Epoxy System

As a structural adhesive system BETAMATE 1469V (Dow) was used for experiments. Widely used in the automotive industry, this is a one-component latent adhesive system, where epoxy resin is premixed with the curing agent. The major components of BETAMATETM are shown in Table 4.2²⁰⁴. Optimal conditions for adhesive cure recommended by the manufacturer are 30 min. at 180 °C.

Dicyandiamide is a hardener which is insoluble in glycidyl ethers at room temperature; it is present in a particle form in the adhesive system at room temperatures but dissolves when heated. This property makes it a widely used curing agent for one-component thermoset epoxy systems with relatively long (up to 6-9 month) pot life. Normally, about 5-8 % DDA is used for liquid epoxy⁴. The end of lifetime of the adhesive material is considered when 5% mass loss or 5% conversion is reached.

Dicyandiamide polymerizes epoxy rapidly at elevated temperatures via a complex sequence of reactions. During polymerization, it interacts with epoxy and hydroxyl groups by all four nitrogen-containing groups yielding a highly cross-linked adhesive.

Table 4.2. Composition of BETAMATE™ adhesive.

| Component(s) | | CAS# | Amount (wt %) |
|---|--|------------|---------------|
| Epoxy-based | Propane, 2,2-bis[p-(2,3-epoxypropoxy)phenyl]-polymers | 25085-99-8 | 15.0 - 25.0 |
| | Phenol, 4,4'-(1-methylethylidene) bis-, polymer with 2,2'-[(1-methylethylidene) bis(4,1-phenyleneoxymethylene)] bis (oxirane), | 25036-25-3 | 30.0 - 40.0 |
| | Epoxy resin P98-344 | | 5.0 – 15.0 |
| | Reaction product: Bisphenol A-(epichlorohydrin) epoxy resin ($M_n \leq 700$) | 25068-38-6 | < 10.0 |
| Aliphatic based urethane polymer P92-500 | | | 10.0 – 20.0 |
| Acetic acid ethenyl ester, polymer with ethenol, cyclic acetal with butanal | | 68648-78-2 | < 10.0 |
| 1-cyanoguanidine/dicyandiamide (DDA) | | 461-58-5 | < 10.0 |
| Methylated silica | | 67762-90-7 | < 10.0 |
| Glycidyl neodecanoate, Mr 228.33 | | 26761-45-5 | < 5.0 |
| Silane, trimethoxy-octyl, hydrolysis reaction product with silica | | 92797-60-9 | < 5.0 |

Some authors proposed DDA functionality different from 4¹². Accelerators such as BDMA (benzyltrimethylamine) or mono- or dichlorophenyl-substituted ureas are also used. Commercial products usually contain tertiary amines to accelerate the reaction and lower the temperature of polymerization.

DGEBA-based prepolymer is a main epoxy resin component. Reactions of the epoxy with DDA were discussed in detail in Chapter.2.1. Concentration of DDA below the stoichiometric ratio is usually used as some epoxy groups are involved in reaction with hydroxyl groups. Low DDA content also results in decreasing of hydroxyl groups at

etherification reaction thus decreasing sensitivity of the adhesive to moisture and increasing cross-link density.

The monoglycidyl ester of neodecanoic acid is used as a diluent for high viscosity epoxy resins. The epoxy functional group, high boiling point and low viscosity allow it to serve as a solvent for uncured adhesive and, at the same time, to be incorporated in the thermoset network. The component modifies the properties of the cured adhesive. Non-polar alkyl groups in neodecanoic acid improve the adhesive's hydrophobicity and stability.

Brittle polymers exhibit poor strength characteristics to high rate impacts because the molecular chains in the material do not have time to absorb most of the energy. Toughness is a characteristic of a material which has both high elongation and tensile strength (maximization of the area under the stress-strain curve). To toughened epoxy, elastomeric modifiers are added that during the curing reaction form a second dispersed phase which stays linked with the epoxy matrix through covalent bonds. It improves impact strength because elastomeric inclusions in the epoxy matrix absorb energy and stop crack propagation. Thus, a complex three-dimensional multiphase structure is formed.

Silica is used as a toughener as well as to improve rheology, dimensional and thermal stability. The methylated silica particles are composed of silica with part of an epoxy network which could form an interpenetrating networks (IPN) structure between the organic and inorganic components with a covalent bond¹⁵³. Silanes work as the coupling agents for adhesion promotion between polymers and inorganic surfaces (Chapter 2.3). Improved adhesion is due to formation of the three-dimensional interphase formed by interdiffusion and chemical reactions between the adhesive and silane layer, forming an IPN. Three or four functional groups substituted on silicon react with substrate to form oxane bonds (M-O-Si where M=Si, Al, Fe, etc.)⁸⁹. Other functional groups react with epoxy. The coupling agent forms a multilayer structure contributing to the interphase structure. The DDA acts as a basic catalyst for the condensation of the silane alkoxides to form cross-linked network⁸⁹. Some inorganic particulate fillers have

been considered as toughening agents. Brittle hollow glass beads are used to improve the toughness of filled epoxy resins and maintain the thickness of the adhesive bond line.

Polyurethane (PU), which has good compatibility with epoxies¹⁵⁴, can be incorporated into the adhesive formulation to improve toughness and increase T_g of the adhesive system¹⁵⁵. Reactive hybrid epoxy-urethane adhesive was initially developed for bonding to oily contaminated steel, but it had shown good adhesion on other substrates as well. It is believed that the oily contaminant located on the substrate is adsorbed into the uncured adhesive and acts as a plasticizer². They have good peel strength and impact properties. The main market for epoxy-polyurethane adhesives is automotive. Isocyanate monomers and prepolymer will react with the hydroxyl groups on epoxy resins to give tough, flexible hybrids. Another advantage is highly improved moisture resistance. The reactivity of isocyanates and epoxy resins are similar, because both can be cured with amines or other hydrogen-containing compounds. The isocyanate reaction is several orders of magnitude faster than the epoxy reaction. So, to toughen epoxy with PU, a mixture of epoxies and urethane oligomers with pendant epoxy groups is used¹⁵⁴. Curing of the pendant epoxy groups unites the urethane and non-urethane components through conventional epoxy reactions to give a tough, durable product. Hawkins has developed another approach¹⁵⁶. A viscous liquid polyurethane resin terminated with hydroxyl groups was obtained first and then blended with a diepoxy resin, dicyandiamide curing agent, and fillers to make a one-component adhesive. During cure, reactions occur between DDA and epoxy as well between the epoxy and the -OH groups on the modifying resin.

Dutta and Karak proposed a mechanism for cross-linking a reaction between PU and epoxy resins in the presence of polyamidoamine hardener¹⁵⁴ (Figure 4.1). Amine groups react with ester groups of PU resin, together with the reaction of the DDA with epoxy and hydroxyl groups. Also, the hydroxyl or urethane groups can react with hydroxyl or epoxy groups in the presence of DDA hardener to form cross-links between two interpenetrating networks. Hydrogen bonding can be formed between hydroxyl groups in the epoxy and C=O groups of the urethane (Figure 4.2).

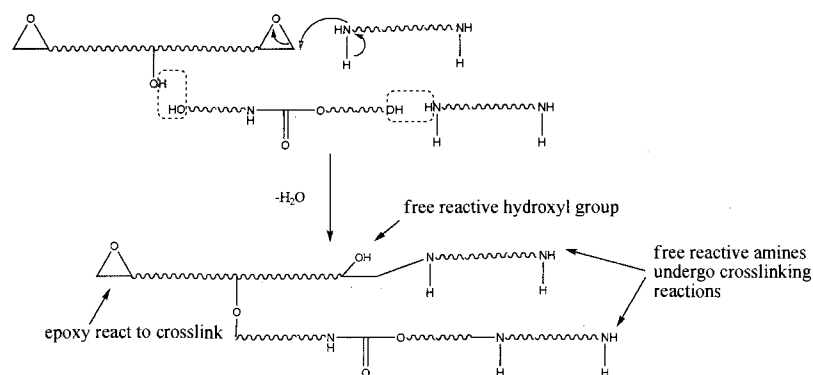


Figure 4.1. Mechanism of cross-linking reaction between PU and epoxy resins¹⁵⁴.

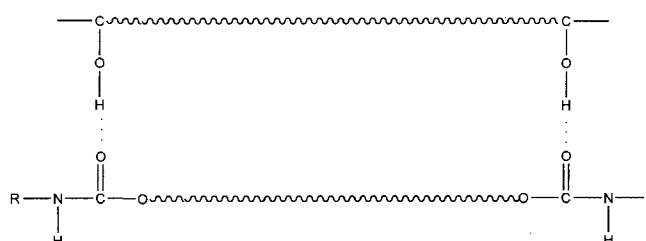


Figure 4.2. Intermolecular hydrogen bonding between epoxy and polyurethane.

Thus, we deal with a complex adhesive system with incomplete knowledge of its chemistry. This formulation allows us to reach a high joint strength together with high toughness; combination of these properties is very important for the structural adhesives used in the automotive industry.

4.1.3. Preparation of the Adhesive Bond Joints.

To evaluate the epoxy's curing effect on adhesive joint's performance, samples were prepared for a single lap shear test (Figure 4.3). Steel plates of 25 mm wide and 100mm long with metal thickness of 1.5mm were used. Metal strips were overlapped over an area of 25x25 mm and bonded with adhesive of 0.3mm thickness to form lap shear specimen. Since the goal of the experiment was to evaluate cohesive strength of the joint, special care was taken to maintain equal level of adhesive strength by thorough substrate surface preparation. Specimens were exposed at different times to certain temperatures to reach different degrees of cure. Temperature of cure reaction varies from

120 to 180⁰C. The same type of samples was used for acoustic imaging of the adhesive/metal interfaces.

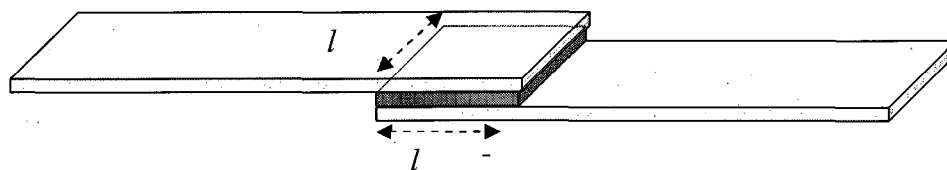


Figure 4.3. Sample for lap shear experiment.

To investigate the internal structure of the adhesive bond, the adhesive joints were cut and cross sections of the joints were mounted into the epoxy mounting system (Buehler) and polished according to the procedure designed for polymers. Prepared cross sections were then investigated by optical and acoustic microscopy techniques to examine morphology of the adhesive layer within the joint.

As degradation of the structural adhesives is slow process, the accelerated degradation test was performed for the adhesive joints (DaimlerChrysler). The goal is to reduce degradation time by increasing relative humidity and temperature. Adhesive bond joint samples were exposed to 2 and 10 degradation cycles recommended by Verband der Automobilindustrie (VDA) (Ger.) to evaluate how the environment affects the quality of the adhesive bonds. Each cycle consists of 24 hrs of salt spray (DIN30021): 50+/- 5g of NaCl; pH 6.5-7.2; 35 °C. 96 hrs of condense cycle (DIN 50017): 400C, 100% humidity (beyond dew point); 48 hrs of recovery (DIN 50018): 18-28 °C. Five samples were tested per each experiment.

4.2. Experimental Procedures

4.2.1. Differential Scanning Calorimetry (DSC)

A differential scanning calorimetry (DSC) method was used to determine the glass transition temperature (T_g) of the adhesives. Analysis was conducted on DSC Q1000 V6.22 (TA Instruments) at Industrial Materials Institute, NRC Canada in

Boucherville. The method involves heating the sample placed in the aluminum holder and the holder itself in a way that the temperatures of both cells are maintained the same. The heat (positive or negative) needed to compensate the chemical reaction or phase transformations that occur with the sample is recorded as a function of time. Positive signals indicate exothermic processes while negative changes refer to endothermic ones.

The test procedure involves dispensing about 10 to 15 mg of the adhesive sample into aluminum pans, which are crimped in a press to give a uniform contact between the disc in the DSC and the pan, avoiding any discontinuities that may lead to anomalous heat flows. The material was scanned with temperature increased from 20 to 250°C with heating rate of 20°C/min and a plot of heat flow vs. sample temperature was obtained. Glass transition was determined as an inflection point in the transition.

4.2.2. Density/Specific Volume Determination

To determine the adhesive's density, the Archimedean principle was applied. Solid immersed in liquid is exposed to the force of buoyancy; value of this force is equal to the weight of the liquid displaced by the volume of the solid.

Samples were weighed in air, and then weighed immersed in distilled water at 22°C using density measuring kit for analytical balances (Sartorius CP). Density was calculated as:

$$\rho = \frac{W_a \rho_l}{W_a - W_l}$$

where W_a is weight of the sample in air, W_l is weight of sample in water, and ρ_l is water density.

4.2.3. Microhardness Measurement.

Hardness can be defined as the ability of a body to resist local surface deformation. Microhardness (MH) of polymers is a complex parameter which related to

the mechanical properties such as moduli, strength, elasticity and plasticity. MH of a polymer measures resistance of the material to plastic deformation and provides information about local strain. Hardness testing has been used to evaluate cure of thermosetting polymers and as a measure of mechanical properties affected by changes in chemical composition, microstructure and aging¹⁵⁷⁻¹⁵⁹. Microhardness measurements are able to detect many morphological changes in polymers since the method is based on plastic straining and directly related to the molecular deformation mechanisms that occur on the polymer surface and depend on the material's morphology¹⁸⁹. Measurement of local hardness is based on penetration force applied to the specimen by an indenter.

The test uses dynamic deformation of the material specimen. During the test, the indenter is pressed into the material under specific conditions (certain force value and time of measurement). Vickers dynamic microhardness test was performed on a Shimadzu Duhammic Ultra-Microhardness Tester DUH-W201S. This test uses a square diamond pyramid, the angles α between non-adjacent faces of the pyramid is 136° (Figure 4.4). Figure 4.5 shows geometry contact with polymer materials for Vickers indenter. Elastic deformation is shown as an instant recovery from profile B to C. Permanent plastic deformation, C, is determined by the polymer structure.

The following procedure was used: load of 50 mN was applied in a controllable rate, held for 5 s and then removed. The imprint size was approximately 15-25 μm . The length of impression was measured with accuracy to $\pm 1 \mu\text{m}$ with an optic microscope equipped right after load-unload cycle. Both diagonals of the indentation were measured

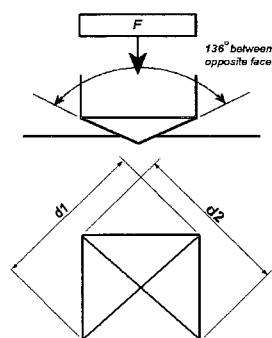


Figure 4.4. Configuration of the Vickers microhardness indenter.

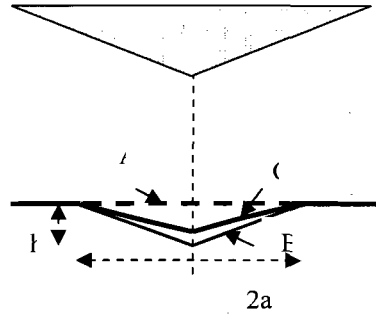


Figure 4.5. Contact geometry for Vickers indenter at (A) zero load, (B) maximum load and (C) complete unload, h is residual penetration.

and the mean of these values was used. The device automatically performs stress-strain curve during load-unload cycles. A typical curve is demonstrated in Figure 4.6.

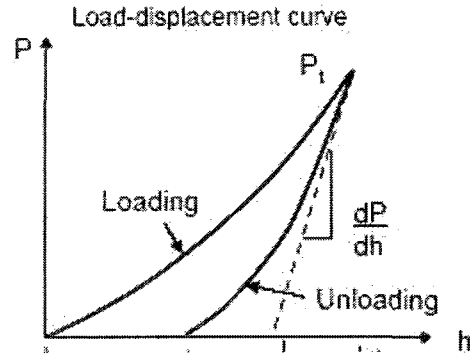


Figure 4.6. Load-unload curve for microhardness testing.

Microhardness (H) was determined with the following formula:

$$H(V) = \frac{2P \sin(\alpha/2)}{d^2} = 1.854 \frac{P}{d^2} \quad (4.1)$$

where P is the force in mN, d is the mean diagonal length of the impression (μm).

The unloading part of the curve can be used for calculating of Young's modulus of the material according to the Sneddon's equation^{160, 189}:

$$E_r = \frac{\sqrt{\pi}}{2} \frac{S}{\sqrt{1.854d^2}} \quad (4.2)$$

where S is stiffness and E_r is the Young modulus of the indenter-specimen system

$$E_r = \frac{(1-\nu^2)}{E} + \frac{(1-\nu_i^2)}{E_i} \quad (4.3)$$

where ν and ν_i is a Poisson's ratios of the specimen and indenter and E and E_i are Young's moduli of the specimen and indenter correspondingly.

Thus, microhardness offers a bridge between microstructure and macroscopic mechanical properties. This method allows us to characterize specific parts of the material on a micrometric scale.

As steel substrate and epoxy adhesive have significantly dissimilar hardness values, steel substrate was removed before preparation of the adhesive joint cross section. Steel surface was sprayed with Teflon before adhesive was applied and then the adhesive joint was cured. Later, the steel plates were removed without disturbing the interface and the adhesive layer was molded into the epoxy hardened at room temperature. Molded samples were polished by special procedure to create flat surface.

4.2.4. Adhesive Joint Strength Measurement.

Standard destructive tests were carried out using Zwick Z150 material testing machine (Figure 4.7) in order to evaluate the epoxy curing effect on adhesive joints performance. A stress-strain test for determining strength of adhesively bonded lap-shear joints by tension loading was performed. The method measures the force required to break a joint and elongation of the specimen, which was prepared as described in Section 4.1.3. The adhesive joint was placed in the grips of the testing machine and pulled with speed 1.3 mm/min. until joint failure. Stress-strain curve was used to determine elongation and yield point (Figure 4.8). Average shear stress, the type of the failure

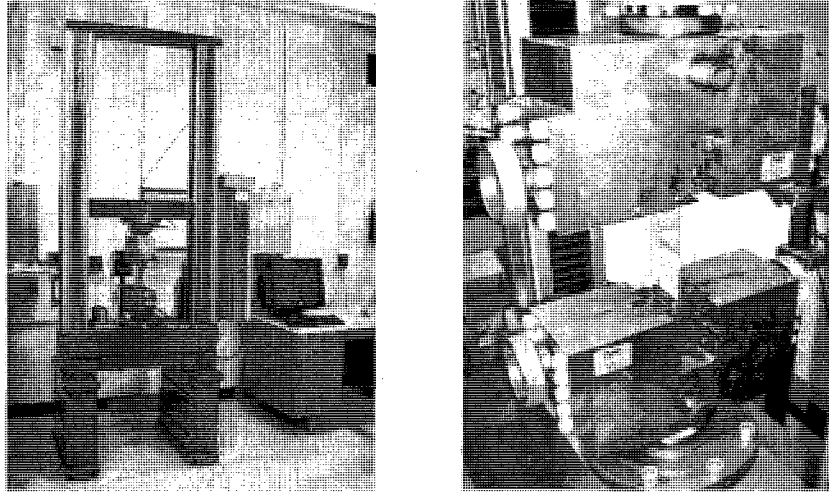


Figure 4.7. Zwick Z150 material testing machine (left) and specimen grips for tensile lap shear test (right).

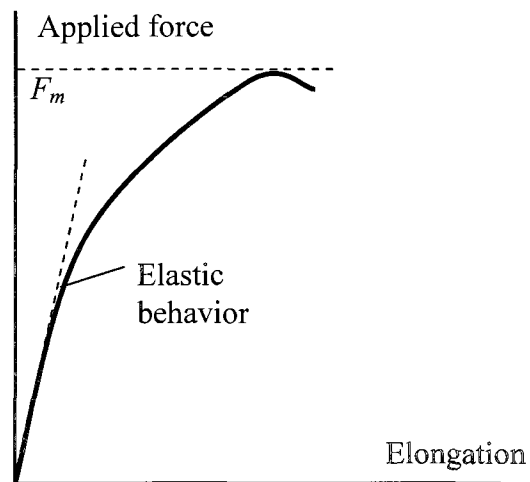


Figure 4.8. Tensile test profile.

(cohesive or adhesive) and characteristics of the samples (adhesive type, bonding conditions) were recorded. Lap shear strength was calculated as:

$$\sigma = \frac{F_m}{A} \quad (4.4)$$

where F_m is highest load applied and A is a bonded area.

Tensile shear strength depends on many factors: adhesive composition, adhesive layer thickness, joint size, cure conditions and other factors. In a series of experiments for cohesive strength evaluation, all conditions of joint fabrication were equal except cure time. We assume that differences in strength value were only due to difference in cohesive properties of the adhesive at various cure states. Bond strength experiments were carried out to show joint cohesive strength as a function of cure degree.

After tensile tests, samples were studied by optical and electron microscopy to examine morphology of the adhesive samples and understand the nature of their failure. Leica optical microscope (Leica materials workstation) was used for analysis of fractured surfaces of the adhesive joints. The fractured surfaces of the cured adhesive joints after adhesion strength evaluation were also observed using a field emission type electron microscope. Test specimens were sputter coated with gold, then placed in a vacuum chamber for viewing on the computer monitor at up to 1500x magnification.

4.3. Acoustic Methods.

4.3.1. The Basic Principles of the Acoustic Method.

The acoustic methods were used to study viscoelastic properties of adhesives. Acoustic measurements involve mechanical excitation by imposing a small cyclic deformation to a sample and measuring the stress response. Acoustic waves are generated by a piezoelectric transducer, which converts an oscillating electric field to mechanical oscillations. Acoustic pulses less than 1 ms in duration are sent through a specimen. Acoustic waves traveling through a polymer specimen were partially reflected and transmitted at each acoustic interface (Figure 4.9) creating the secondary echoes. Each echo reaches the transducer at its specific time depending on depth of this specific interface. The acoustic interface corresponds to physical discontinuity in the material (crack or void) or changes in material viscoelastic properties (adhesive/metal interface, variations in material density).

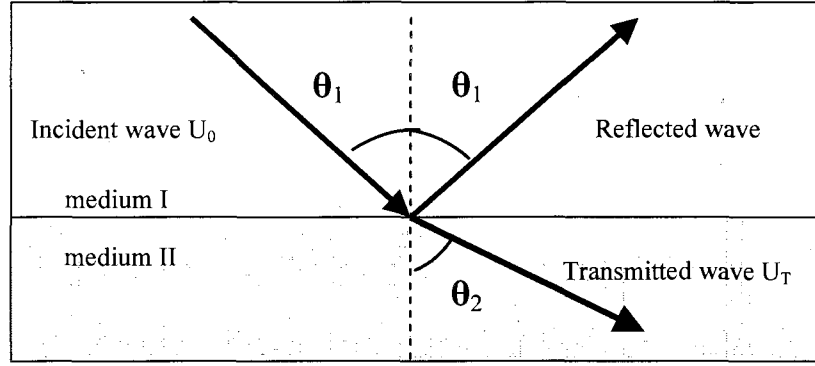


Figure 4.9. Schematic representation of reflected and transmitted waves in the sample.

For $\theta=0$, the amount of transmitted or reflected signal is determined by transmission T and reflection R coefficients, which is described by the following formulas¹¹¹:

$$T_{ij} = \frac{2Z_i}{Z_i + Z_j} \quad (4.1)$$

$$R_{ij} = \frac{Z_j - Z_i}{Z_j + Z_i}, \quad (4.2)$$

where Z is the acoustic impedance, which is a product of density ρ of the material and its sound velocity c : $Z = c\rho$. Both transmission and reflection modes were used to characterize epoxy adhesives.

4.3.2. Acoustic Transmission Mode for Measuring Adhesive Properties.

An ultrasonic polymer characterization system (Industrial Materials Institute, NRC Canada) was used for characterization of the adhesive system at the transmission mode. 2.5 MHz acoustic frequency and pressure of 100 bar were used (Figure 4.10). Uncured or cured adhesive can be used for analysis. To prepare a cured sample, approx. 3g of adhesive was placed into the silicon molds and cured at certain time and temperature regime. Thickness of the samples was in the range of 2-3 mm. The specimen was oriented perpendicular to the sound beam and positioned between the two buffer rods

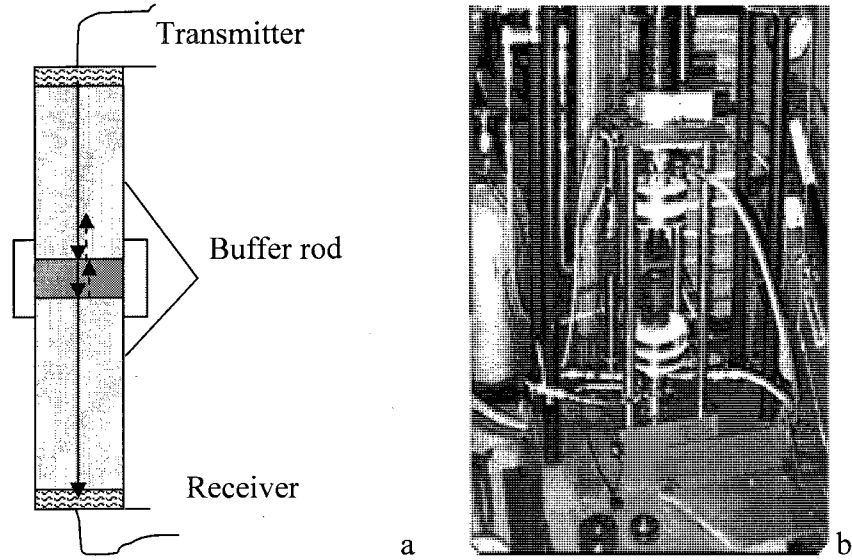


Figure 4.10. Schematic representation of the sound wave propagation (a). Ultrasonic polymer characterization system (b).

and transducers. The specimen was heated to the required temperature and pressure was maintained constant. To compensate for thermal expansion of adhesive, axial displacement of upper buffer rod was performed. Acoustic waves were transmitted through the rod into the specimen; the phase and amplitude of the acoustic waves interacting with the sample were monitored. Acoustic parameters were taken at 10s intervals. A linear voltage differential transformer (LVDT) device incorporated into the system allows us to accurately measure the changes in sample thickness h during heating or cooling, independently of acoustic measurements. Pulses of sound that propagate through the specimen are partially reflected at the specimen interfaces and bounce back and forth with decreasing amplitude. From the time t needed for the echo to travel through the sample and the reduction in its amplitude during this trip, the speed c and absorption α can be calculated:

$$\alpha = \frac{1}{h} \ln \frac{U_1}{U_2} \quad (4.3)$$

$$c = \frac{h}{t} \quad (4.4)$$

where U_1 and U_2 are the values of peak amplitude for the first and second reflections with time delay t and h is specimen thickness. After the experiment, the adhesive sample was cooled to ambient temperature; its mass was recorded, and density of the material was calculated.

4.3.3. Reflection Mode for Measuring Acoustic Properties.

At reflection mode, the same transducer emits and receives the echo reflections from the sample boundaries. Reflection mode was used with the following experimental set up at the ultrasonic frequency of 5 MHz (Figure 4.11). Approximately 1.5-2 g of epoxy was placed in the cylindrical chamber of the specially designed preheated cell. The

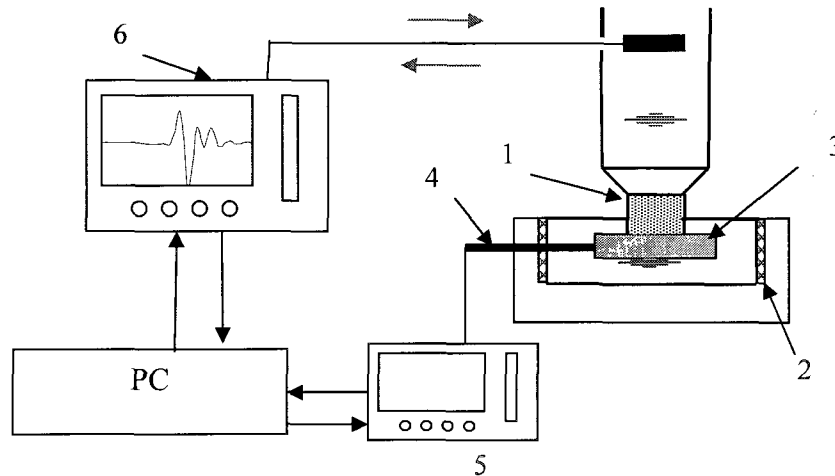


Figure 4.11. Experimental setup for the pulse-echo mode. 1- buffer rod, 2-heating tape, 3-adhesive sample, 4-thermocouple, 5- temperature controller, 6- pulse-receiver.

isothermal conditions were maintained with a Digi-Sence temperature controller. Since cured and especially uncured epoxy is soft at temperatures investigated, good contact was maintained on the buffer rod/epoxy interface without any coupling media. The epoxy samples reached the required temperature within 1-3 min., depending on temperature of cure, following this, recording of data was started. Acoustic parameters were taken at 0.5 min. intervals. The electronic instrumentation includes Panametrics 5073PR pulse-receiver connected to a Tektronix TDS 3032 digital oscilloscope for data acquisition and

further processing. A pulse travels through the buffer rod/epoxy sample/metal substrate multilayer system. Schematic wave propagation through the sample and typical A-scan is shown in Figure 4.12. A simplified test cell (Figure 4.13) was used for study of the two-component adhesive system. Instead of the buffer rod, a water-glycerin mixture was used as a coupling medium to reduce reflection from the coupling medium-epoxy interface. PET film used to separate adhesive from coupling was thin enough so its presence did not create an additional reflected pulse at the coupling-epoxy interface. Flexibility of the PET film allows us to measure variation of the sample's thickness during curing and thus to monitor the material's density changes.

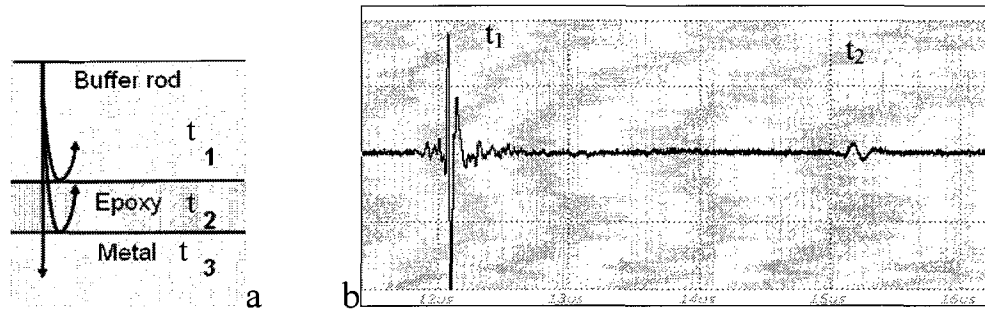


Figure 4.12. Schematic representation of the reflections origin (a) and typical A-scan (b). t_1 -signal reflected from buffer rod/epoxy sample interface, t_2 -signal reflected from epoxy/metal substrate interface, t_3 -signal transmitted into the metal substrate.

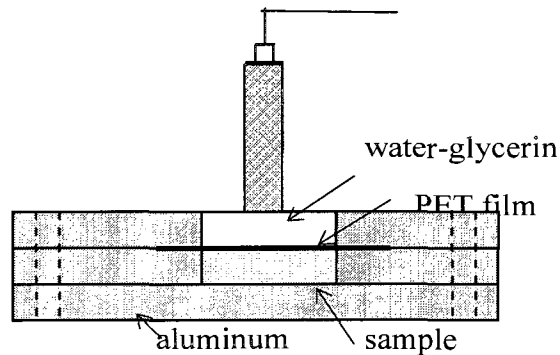


Figure 4.13. Test cell design for two-component adhesive.

Longitudinal sound velocity c_L was calculated according to the formula:

$$c_L = \frac{2d}{\Delta t} \quad (4.5)$$

where d is the thickness of the sample and Δt is time of flight of the upper and lower interface reflections. Thickness of the samples varies between 2.5-3.0 mm. Since temperature stays constant, thickness variations are only due to density changes during epoxy polymerization reaction. It was shown that density increases by only 2-4 % during cure for this type of adhesive, so density and sample thickness variations were neglected.

Only relative attenuation was monitored and used to calculate changes in acoustic attenuation $\Delta\alpha$ according to the following:

$$\Delta\alpha = \frac{1}{2x} \left[\ln \left(\frac{A_{final}}{A_{cure}} \right) + \ln \left(\frac{T_{12cure} T_{21cure} R_{32cure}}{T_{12final} T_{21final} R_{32final}} \right) \right] \quad (4.6)$$

where A_{final} and A_{cure} are the amplitudes of the signal reflected from the lower interface. The subscript *final* identifies data taken at the end of the cure reaction and the subscript *cure* identifies data taken at a certain point of monitoring. T_{12} and T_{21} are the transmission coefficients; R_{23} is a reflection coefficient. l in the subscript corresponds to the epoxy rod, 2 - to the epoxy BETAMATETM, 3 - to the aluminum test cell. The second term of the equation (4.6) takes into account changes in reflection and transmission coefficients during cure, which are mostly due to changes in epoxy sound velocity. Experimentally it was shown that the last term in the formula for attenuation (4.6) varies during the reaction from -0.0013 to 0.008. Thus, the contribution of changes in R and T can be neglected during calculation of the attenuation value. Relative attenuation for completely cured epoxy was then brought into accordance with the absolute attenuation α_{final} value obtained by the acoustic method in transmission mode at corresponding temperature. Thus, absolute attenuation α was calculated as

$$\alpha = \Delta\alpha + \alpha_{final} \quad (4.7).$$

4.3.4. Calculation of Elastic Moduli Values of Adhesives.

For both reflection and transmission modes, if the sample dimension is much larger than the wavelength, propagation is guided by the bulk longitudinal modulus L which relates to bulk (K) and shear (G) moduli¹⁰³ as in equation (3.15).

The data of sound velocity and attenuation are used for calculation of storage L' , loss L'' bulk longitudinal moduli as well as loss factor $\tan \delta$ according to formulae (3.20). For high acoustic frequencies, $\alpha\lambda/2\pi \ll 1$, and effect of the attenuation on sound velocity is small so expressions (3.20) can be simplified as

$$L' = \rho c_L^2 \quad (4.8)$$

$$\text{and } L'' = \frac{2\rho c_L^3 \alpha}{\omega} \quad (4.9)$$

4.3.5. Monitoring of the Adhesive Properties During Polymerization Reaction.

Changes of the viscoelastic properties of the adhesive during the polymerization reaction were monitored by both transmission and reflection modes at constant temperatures or at constant heating rate.

Acoustic degree of conversion was expressed then as:

$$A_{US} = \frac{L' - L_0'}{L_f' - L_0'} 100\% \quad (4.10)$$

where L_f' is bulk longitudinal modulus for the completely cured adhesive, L_0' is the modulus value for the uncured adhesive.

Acoustic parameters of the epoxy adhesive were investigated as a function of material cure degree. This was reached by heating the sample up to, and cooling it down

from, successively increasing temperatures, as shown graphically in Figure 4.14. Each heating phase provides a different cure stage, while each cooling phase allows investigation of the T_g of the system in this particular stage. Heating rate was $5^\circ\text{C}/\text{min.}$, cooling rate was $2^\circ\text{C}/\text{min.}$ All acoustic and elastic parameters were calculated as described in Section 4.3.4.

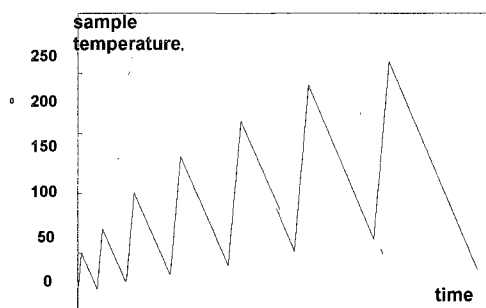


Figure 4.14. Temperature profile for investigation of temperature dependence of the epoxy on different cure stages.

4.3.6. Acoustic Thermal Characterization of Adhesive.

Temperature dependence of the acoustic properties of completely cured adhesive was investigated using an ultrasonic polymer characterization system (Industrial Materials Institute, NRC Canada) in transmission mode. Measurements were performed at cooling state with the rate of $2^\circ\text{C}/\text{min}$ to allow a specimen to reach temperature equilibrium.

Glass Transition is characterized by a step change in many physical properties. Usually, this region covers a range of temperatures, approximately $10\text{-}15^\circ\text{C}$, while highly cross-linked polymers may have even a broader transition region. Due to nature of the ultrasonic method (what will be discussed in Chapter 5), the transition region is even wider. The problem in this case is what value to assign as a T_g and what criterion should be used for specifying this parameter? In DSC method, five characteristic temperatures are usually associated with glass transition at heat flow versus temperature curve: the “onset” temperature, temperature of intercept of extrapolated base line and tangent to steepest slope, temperature of 50% transition, temperature of maximum slope (peak of

derivative plot), and temperature at completion of the transition ¹⁶¹. In recent years the most often used parameter for specifying T_g is a half-vitrification or $T_{0.5}$, the endotherm half-height. It shows good reproducibility and locates a temperature where the thermal transition has approximately reached the inflection point ¹⁶¹. The last approach is quite inapplicable for acoustic studies of structural adhesives because of the broad transition region for acoustic parameters. To determine which acoustic parameter can be set as a T_g , acoustic thermal curves obtained were analyzed and the following characteristic temperatures were defined: the “onset” and “offset” temperatures, peak maximum, and temperature of half-transition. Two approaches were chosen in this research: the point where the dynamic elastic modulus E' begins to drop from its glassy value and the maximum of loss factor $\tan\delta$. Details of T_g value determination will be discussed further in Chapter 5.2.

The proposed method of acoustic monitoring of the adhesive cure reaction and determination of adhesive T_g are among the various thermal analysis techniques. The International Confederation of Thermal Analysis and Calorimetry (ICTAC) defined thermal analysis as “a group of techniques in which a property of a sample is monitored against time or temperature while the temperature of the sample, in a specified atmosphere, is programmed” ¹⁰⁷. It is necessary to note that ultrasonic methods have been used more often during the last decades to monitor chemical reactions or evaluate elastic properties of materials ^{28, 162-164}. The terms “thermoacoustimetry” or “thermoacoustic analysis” (TAA) are sometimes used ¹⁰⁷. This term has not become widely accepted though. At the same time, the Dynamic Mechanical Analysis (DMA) method, which is based on mechanical excitation by imposing a small cyclic deformation in the frequency range of kHz to a sample and measuring the stress response, is widely used by thermal analysts to determine the viscoelastic properties of polymers. It is necessary to note that the only difference between these two techniques is the frequency range: kHz for DMA and MHz for ultrasonic analysis.

4.3.7. Scanning Acoustic Microscopy.

Scanning acoustic microscopy like any other ultrasonic method in material characterization is based on the measurements of the interaction of high-frequency elastic waves with the samples by scanning a transducer along the sample. Some information about SAM is provided in Section 4.3.1. There are several configurations of the acoustic microscope differing in shape of the ultrasonic signal, type and relative position of the transducers, and the methods for displaying the results. In the pulse-echo mode, the same broadband transducer emits a short ultrasonic signal and receives the echo reflections. This mode is specifically useful for imaging of the material's internal structure. The transducer excites the "spike" of a high-voltage pulse for duration of 5-20 ns and produces an acoustic wave containing one or two periods. The wave penetrates through the coupling liquid into the sample and backscatters from the boundaries and voids. Transducer receives the reflected wave and converts it into an electrical signal with the voltage corresponding to the amplitude. After the necessary amplifications, the received signal is digitized at a corresponding sampling rate and stored into the computer memory for analysis (Figure 4.15).

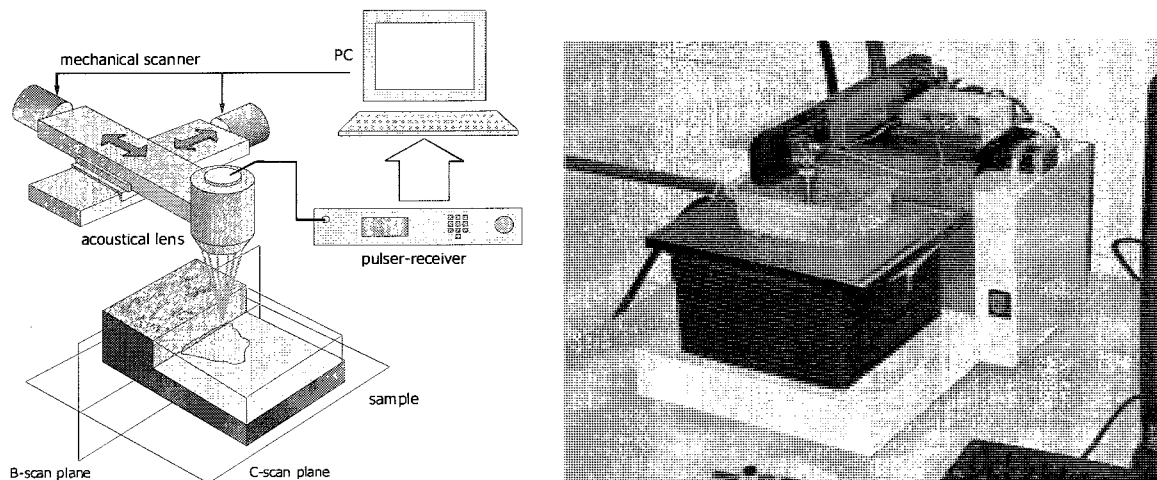


Figure 4.15. Schematic representation of the principle of acoustic scanning (a) and Tessonics AM1102 scanning acoustic microscope (b).

The sequence of the acoustic readings obtained in one particular position of the transducer over the sample surface is called an A-scan. It represents the time dependence

of the reflected signal and usually is plotted in the oscillogram form (Figure 4.16.a). Several oscillograms obtained in equidistant positions of the transducer along a straight line and assembled together into a two-dimensional image represent an acoustic B-scan (Figure 4.16.b). The position of each pixel is related to the position of the transducer (along one axis) and time delay from the initial pulse (second direction). The brightness of the pixel is proportional to the amplitude of the received signal. The B-scan obtained

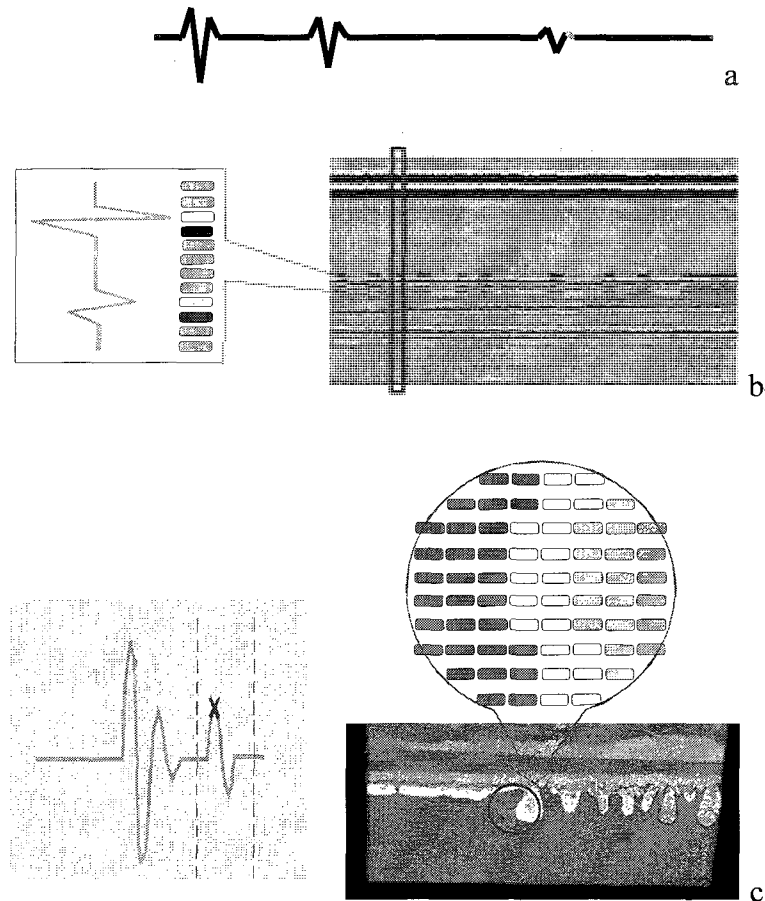


Figure 4.16. Schematic representation of the acoustic image formation: A-scan (a), B-scan (b) and C-scan (c).

during the one-dimensional motion of the transducer provides a vertical cross section of the sample. It is especially useful for the evaluation of the depth-dependent sample structure. Two-dimensional motion of the transducer in the plane parallel to the sample surface gives the possibility to collect acoustic data coming from the sample volume under the scanned area. Line-by-line mechanical raster scanning provides a set of B-scans

combined into three-dimensional cube of data. A horizontal cross-section (C-scan) represents the distribution of reflective properties of the sample at certain acoustic depths (Figure 4.16.c). In practice, the C-scan is formed by the plotting of signal maximum inside the user-defined time window as a two-dimensional function of the transducer position. The color of each pixel on the acoustic image shows this value according to adopted pseudo-color scale. (Figure 4.16)

The main part of the acoustic microscope is a focused transducer (acoustic lens). The acoustic lens consists of a buffer cylinder made from fused quartz with attached piezoelement (Figure 4.17). The outer side of the buffer has a spherical concave surface which provides focusing of the acoustic beam. When the transducer generates plane acoustic waves, they travel through the buffer and are refracted toward the focus when they cross the spherical surface.

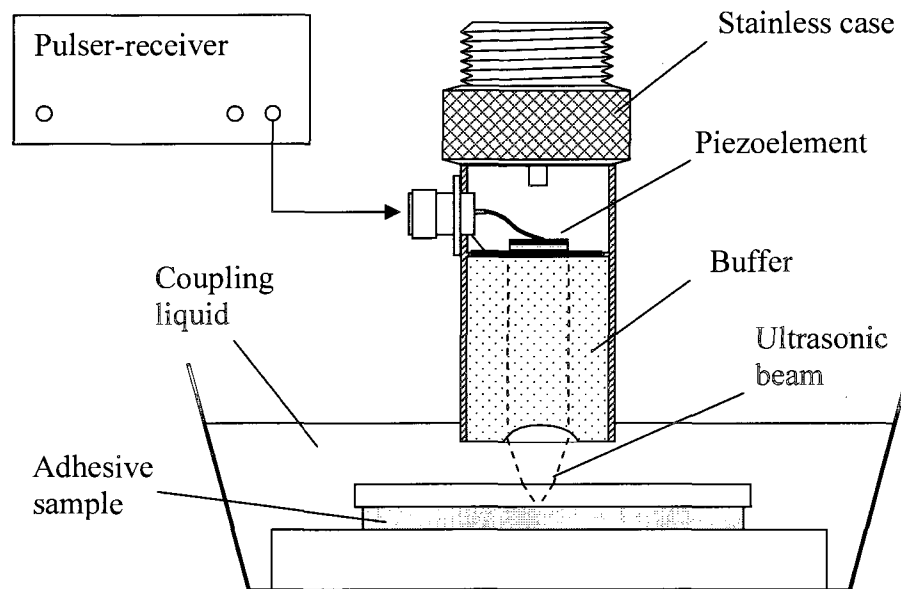


Figure 4.17. Schematic image of the acoustic lens.

The acoustic lens is coupled through an immersion medium to the surface of the sample. This coupling material helps to reduce the extremely high impedance mismatch between the material and air. While there are some cases where the use of couplant can

damage the sample (e.g., fibre webs, textiles or water sensitive specimens), the use of immersion medium is adequate for adhesives and adhesively bonded plates.

Resolution in scanning acoustic microscopy depends on both the material's properties and acoustic hardware. Resolution of the ultrasonic microscopy method is related to the capability to distinguish two close reflectors on the A-scan (axial resolution) or on the C-scan (lateral resolution). For the short pulse signal, both values are proportional to the central frequency of the wave. The resolution of the acoustic microscope is inversely proportional to the lens numerical aperture $N.A. = \sin\theta_0$ where θ_0 is a semi-aperture angle.

Depth of focus defines how far the sample can be moved before the image begins to become blurred. Acoustic depth of focus is equal to ¹⁶⁵:

$$\Delta Z_F = \frac{1.28\lambda}{\sin^2 \theta} = \frac{1.28c}{f} \left(\frac{F}{N.A.} \right)^2 \quad (4.11)$$

where λ is wavelength in the material, c is sound velocity, F is focal length and f is transducer acoustic frequency.

The Rayleigh criteria states “that the images of two points may be considered resolved if the principal diffraction maximum of one falls exactly on the first diffraction minimum of the other”. According to this, and Kino notes ¹³¹, the lateral resolution is determined by focal spot size and equal to the so called Airy radius

$$r_{Airy} = \frac{0.51\lambda}{\sin \theta} = \frac{0.51c}{f} \frac{F}{N.A.} \quad (4.12)$$

In practice, the ideal numerical aperture has never been realized. The SAM typically uses a frequency range of 3 MHz – 2 GHz for focused acoustic waves, which limits the spatial resolution to around a few microns. An increase of the acoustic image resolution cannot always be achieved by an increase of frequency, because the attenuation of the ultrasonic wave is proportional to the square of this frequency. Hence, when a wave of sufficiently

high frequency is used as a probe, the wave may not penetrate far enough inside the specimen for information about its interior to be obtained. The highest frequency level f is determined by attenuation in the coupling fluid

$$f \leq \sqrt{\left(\frac{\alpha_{acc}}{2\alpha_0 q}\right)} \quad (4.13)$$

where α_{acc} is an acceptable attenuation in the coupling media, α_0 is a specific attenuation in liquid per Hz of acoustic frequency and q is minimum focal length which is proportional to velocity. The resolution coefficient R_c is equal to

$$R_c = \sqrt{(c_0^3 \alpha_0)} \quad (4.14)$$

The smaller R_c , the shorter wavelength and better resolution can be achieved.

The axial resolution depends on the duration of the acoustic signal. For an ideal one-period pulse, the minimal distance between two reflectors at which they can be resolved on A-scan is¹¹¹

$$z_{axial} = \frac{\lambda}{2} \quad (4.15).$$

Longer pulses provide less resolution.

4.3.8. Acoustic Imaging of Intact Metal/Epoxy Interface

For non-destructive visualization of the interface microstructure, high resolution scanning acoustic microscopes (Sonix HS-1000 and Tessonics AM1103) were used with 10-250 MHz frequency acoustic lens. Acoustic lens characteristics are presented in the Table 4.3. An 8-bit image of a 1cm² metal-adhesive interface region of each sample was produced. The focal point of the acoustic lens was positioned at the upper or lower metal/adhesive interface. Since the properties of the steel remain constant during the process of adhesive cure, all variations in reflection coefficient value are due only to changes in acoustic impedances of the adhesive. These changes are caused by

modification in either density or sound velocity. Actually, both parameters undergo changes during cure reactions and work together to produce changes in the acoustic images that indicate changes developing in the adhesive during cure. It was shown experimentally that density increases by 2-4% during cure, and all other changes are due to sound velocity modifications.

Statistical analysis of the obtained images is performed with OriginLab 8.0 Pro and MatLab software. Details of the analysis are described in Chapter 6.1.

Table 4.3. Characteristics of the acoustic lens.

| Central frequency, MHz | Focal length, mm | Aperture diameter, mm |
|------------------------|------------------|-----------------------|
| 250 | 5.6 | 3.2 mm |
| 50 | 12.7 | 4.5 mm |
| 25 | 15 | 6.3 mm |
| 20 | 15 | 12.6 mm |
| 15 | 18 | 6.3 mm |

Determination of the longitudinal sound velocity in the adhesive in bond joints was performed at ambient temperatures. A series of measurements was performed at the centre, close to the each edge and in between on each sample. Longitudinal sound velocity was calculated by analyzing the waveform and measuring the time of flight (TOF) between reflection pulses from the upper and lower adhesive/metal interfaces according to formula (4.5). Then, thickness of the adhesive layer was calculated by measuring the overall joint thickness with a micrometer and subtracting the double thickness of the metal plate.

CHAPTER V

Evaluation of Cohesive Properties of the Structural Adhesives.

While consideration of the interfacial forces is critical in adhesion science, the cohesive strength of structural adhesives is also very important for the adhesive joint performance. New bonding techniques, which allow achieving high bonding strengths, result in more cases of cohesive failures now. To obtain adhesive joints with the desired mechanical properties, it is important to understand the process of network formation in cross-linked thermosets as well as to have simple and reliable methods to monitor this process.

Network formation, or cross-linking, of the epoxy adhesive is a complex process in which three-dimensional linkages are formed throughout the polymer during the curing process. While polymerizing, the epoxy undergoes significant changes from a low-molecular weight liquid to a highly cross-linked solid. During the last twenty years, the curing reaction of epoxy adhesives has been studied extensively^{8, 9, 166, and 167}.

The properties of thermoset adhesives are determined by the nature of the prepolymer and hardener structures and density of the cross-linking points. The ratio between prepolymer and hardener determines the number of cross-linking sites and, therefore, strongly controls the network structure. Any structural changes will lead to alteration of the corresponding properties. Despite the fact that the epoxy structure can be derived from the initial epoxy prepolymer and hardener and reaction conditions, very often the adhesive's structure is still unclear. Complex commercial system formulation makes prediction of T_g and establishing structure-mechanical properties relationships more complicated. For industrial applications, evaluation of reaction conversion is equally important along with investigation of changes in the material's physical and mechanical properties. It is known that the adhesive cure degree correlates with the elastic moduli and cohesive strength^{124, 169, 180}, and improper curing (both under- and overcure) can lead to joint failure by cohesion modes. It is usually difficult to determine the extent of cure reaction accurately by percentage of reactive groups. Wang and

Gillham suggested that T_g can be used as a measure of adhesive cure. They introduced the cure parameter C ¹⁶⁸:

$$C = \frac{T_g - T_{g_0}}{T_{g_\infty} - T_{g_0}} \quad (5.1)$$

where T_{g_0} is the glass transition temperature of the uncured system and T_{g_∞} the glass transition temperature of fully cured system. Later Gillham showed that T_g value is related to the fractional conversion and is not dependent on the reaction path of the adhesive cure reaction²³. This makes T_g a convenient parameter for monitoring conversion especially at high conversions¹⁶⁹. Cure conditions (time and temperature) influence the reaction rate and therefore the network structure as well.

Since proper adhesive cure depends on multiple parameters, such as temperature, time, resin-to-hardener ratio, etc., monitoring and assuring the progress of the cure is essential to obtain the quality of a bond joint. Effective in-process control requires effective observation of formation of the epoxy network that plays a significant role in the mechanical behavior of the bond joint. Cure monitoring means real-time tracking of the physical state and chemical reactions that occur during cure, and such on-line monitoring may provide efficient cure temperature-time optimization that will yield joints exhibiting the required aesthetic and structural performance of the assembly.

Conventional ultrasonic methods have been widely used to non-destructively inspect adhesive bond joints for defects. Although this technique is still the most reliable method for non-destructive defect detection, its use for evaluating viscoelastic properties in on-line applications is still quite limited as well as their application in understanding the structure of thermoset networks. Since those critical mechanical properties of the adhesive bond joint, such as strength and modulus, are strongly related to the cure state of the adhesive, an NDE technique which will monitor the state of adhesive cure during and after the process would be quite useful. Acoustic techniques have been used by researchers to analyze elastic properties and to study in-process molecular network development^{27-29, 170}. Most of the work was performed in transmission mode, but this

mode is not convenient for industrial applications because industrial applications usually limit inspection access to only one side of the specimen or workpiece. In this research, both reflection and transmission modes has been applied to monitor the changes in acoustic and elastic properties within the adhesive during the reactions that lead to adhesive polymerization.

This study aims to evaluate the cohesive properties of structural epoxy adhesives through the evaluation of its acoustic and elastic parameters as a function of curing conditions. Another goal is to develop methodology for characterization of curing behavior of a commercial complex structural adhesive system with incompletely known chemistry.

5.1. Adhesive Cure Monitoring for a Two-Component System. Preliminary Experiments.

A two-component adhesive system was used to find the proper acoustic parameters (frequency, transducer configuration) and build an experimental cell to monitor changes of the viscoelastic properties during the polymerization reaction. Another reason was to investigate how the epoxy-hardener ratio influences the final properties of the adhesive, which is impossible for premixed one-component adhesive systems. Figure 5.1 shows typical A-scans in the beginning, during reaction and at the end of reaction. Origin of the reflected signals is explained in Chapter 4.3.1. The first peak t_1 is formed at the couplant-adhesive interface; and the second one, t_2 , at the adhesive-substrate interface. Both position and amplitude of the reflected signals undergo significant changes, which are due to alteration of the epoxy's properties during the reaction. Changes in the second reflection are the most significant because this peak reflects changes in the ultrasound pulse, which propagates twice through the adhesive layer.

During the reaction, both signals move towards each other. Change of the t_1 peak position occurs due to epoxy shrinkage during the cross-linking reaction. The sample's thickness at each point of the reaction can be calculated as:

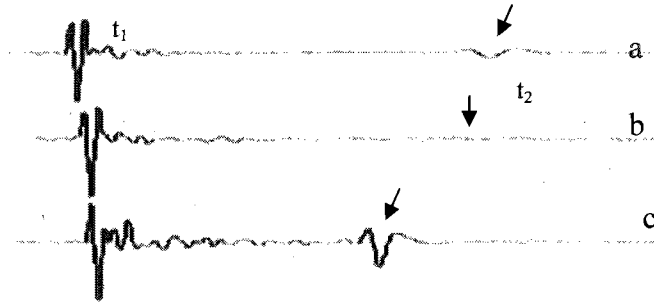


Figure 5.1. Pulse-echo waveforms for uncured epoxy (a), at gelation time (b) and cured (c) epoxy. Arrows show signal t_2 reflected from the bottom of the cell.

$$h = h_s + \frac{c_{Lw}(t_{1i} - t_1)}{2} \quad (5.2)$$

where h_s is the final thickness of the sample measured at the end of experiment, t_{1i} is time delay of the couplant-adhesive peak at the initial point of reaction, t_1 is time delay of the signal reflected from the film at current moment and c_{Lw} is longitudinal sound velocity in water. With knowing how adhesive thickness changes during cure reaction, it is possible to calculate variations in adhesive density.

The lower interface (epoxy-metal substrate) produces reflected signal t_2 , however, its shape is essentially distorted. This is a result of a strong attenuation of high-frequency ultrasound components during the double pass through the unpolymerized epoxy layer. The signal is recognizable in the beginning of the reaction and well defined after completion of the cure process (Figure 5.2 left, a and c). However, almost full disappearance of the signal is observed after polymerization starts. The waveform of the reflected pulse totally differs from conventional sinus-like profile in the middle of the cure process and its amplitude is reduced dramatically (Figure 5.2 b, left). These factors complicate determination of the exact position for a reflected signal. As a result, precision of time of flight (TOF) direct measurement drops.

The special methods of digital signal processing can be applied for extraction of information from the experimental data. The well-known method of matched filtration is commonly used in radar techniques for maximizing the signal to noise ratio in the

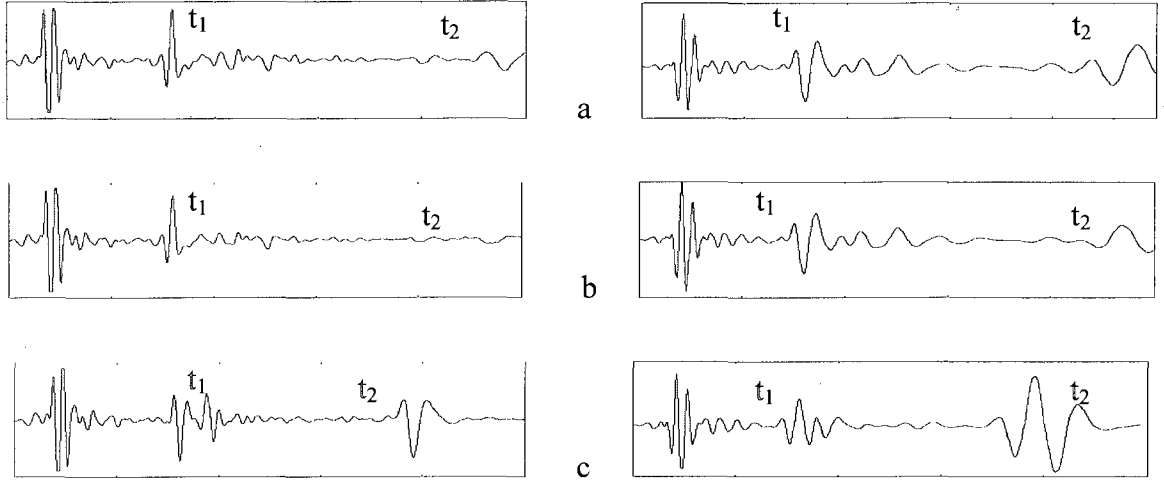


Figure 5.2 .Individual acoustic A-scans before (a), in the middle (b) and at the end of epoxy polymerization reaction (c). Left –original oscillograms, right-oscillograms after matched filtration.

presence of additive stochastic noise ¹¹¹. The ultrasonic pulse-echo setup used in this study is similar to radar applications and meets the same problems. As a result, the filter approach can help to reduce noise component in signal distortion.

Mathematically, application of a matched filter to the analyzed signal is equivalent to convolving the original signal $f(t)$ with time-reversed reference template $f_{ref}(t)$, i.e. calculation of cross-correlation function

$$f_{output}(t) = \int_{-\infty}^{\infty} f(\tau) f_{ref}(t - \tau) d\tau \quad (5.3)$$

where τ is integration time for cross correlation and t is time for the initial function.

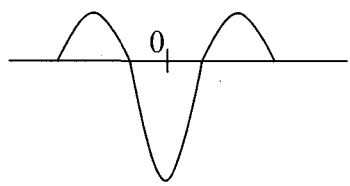
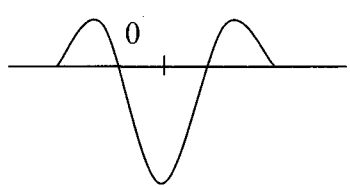
Function (5.3) represents the similarity between the obtained signal and the reference template. When shape of the template corresponds exactly to the signal profile, the output function is a pure Dirac δ function. The finite time segment and then shape distortion causes a blurring effect of the peak. As a result, sensitivity and precision of the method depends on the proper choice of the template.

To design a template, different sinusoidal functions were combined (option a in the Table). Another approach includes the use of a more sophisticated function like *sin*

x/x (option b). The proper choice of the reference template depends on the shape of the reflected signal. This shape is different for different parts of the A-scan, but in the area of maximal disappearance it generally can be described as three sinusoidal half-periods (Fig. 5.2, scan3). The period of the sinusoid varies along the A-scan – shorter for the first reflection pulse and longer for the second one. The amplitudes and durations of these half-periods also are different. The two simplest functions were used during calculations for template modeling:

a)
$$f(t) = \begin{cases} -2 \cos(2\pi \frac{t}{T}), & \text{for } |t| < \frac{T}{4} \\ -\cos(2\pi \frac{t}{T}), & \text{for } \frac{T}{4} < |t| < \frac{3T}{4} \\ 0, & \text{for } \frac{3T}{4} < |t| \end{cases}$$

b)
$$f(t) = \begin{cases} f(t) = -\frac{T}{2\pi} \sin(\frac{2\pi t}{T}), & \text{for } |t| < \frac{3T}{4} \\ 0, & \text{for } \frac{3T}{4} < |t| \end{cases}$$

Comparison of calculated results shows better performance of the template b) in the region of the disappearing second reflected pulse. The period of template signal T is an adjustable parameter, whose optimum value is different for different sections of initial A-scan. To keep resolution on an acceptable level, for both first and second reflected pulses, T was made variable along an A-scan with linear dependence $T(t)$

$$T(t) = T_1 + (t - t_1) \frac{T_2 - T_1}{t_2 - t_1} \quad (5.4)$$

where T_1 and T_2 – periods are optimal for the first and second reflected pulses arrived at time t_1 and t_2 correspondently. They were determined by the maxima of the cross-correlation function in these time regions.

Original A-scans were acquired from ADC device in the form of column of n real numbers. A sequence of m A-scans was combined into a two-dimensional matrix. Then

data were plotted in form of gray-scaled image (Figure 5.3) and processed by the MATHLAB program according to the described algorithm. Results of filtering are presented in the Figure 5.2, right column. The reflected signal t_2 , barely visible on the original Scan b, has a clear maximum now.

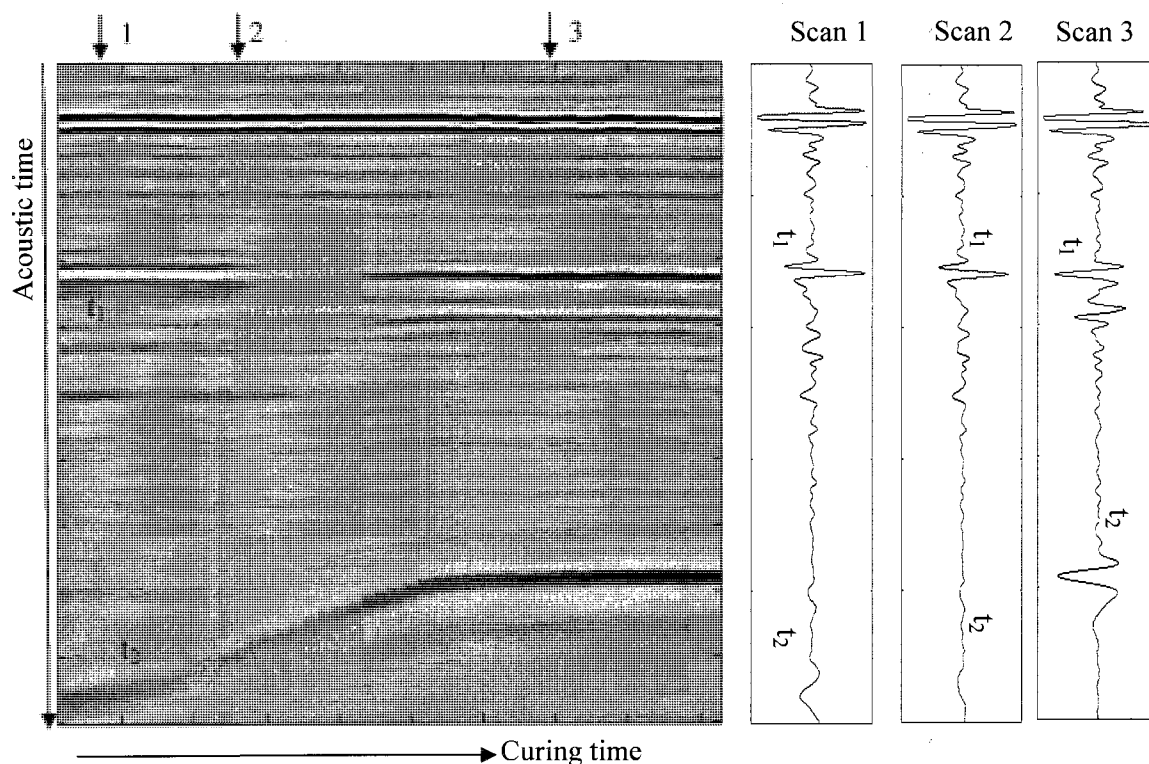


Figure 5.3. Acoustic signature of curing process and individual A-scans before reaction (1), in the middle of process (2) and for completely polymerized epoxy (3). t_1 is the acoustic reflection from the top of the epoxy cell, t_2 is the reflection from the bottom of the cell.

The image on Figure 5.3 represents an acoustic signature of an adhesive polymerization reaction and reflects chemical and physical changes, which occur in the epoxy-amine adhesive system. The first line in the image is formed from reflections from the transducer-couplant interface and does not belong to the adhesive reaction. The next two lines refer to the couplant-adhesive and adhesive-metal substrate interfaces. As mentioned, the line formed by t_2 signal represents the changes that occur in adhesive properties during reaction. Decreasing the distances between lines t_1 and t_2 is due to two processes: decrease in density and cross-linking and polymer network formation during

reaction. As changes in density for structural adhesives vary within 2-4%, the major role in decreasing time of flight (distance between signals) belongs to network formation. Disappearance of the line t_2 after reaction starts indicates a rapid increase in attenuation and is due to formation of branched oligomers. Reflection from the first interface (buffer-epoxy) sometimes has several periods; this structure also remains in the processed A-scan. Position of this peak was determined and assigned to the position of the highest peak in the group. Time of flight was measured as a distance between this peak and maximum of the second signal.

The speed of sound, acoustic attenuation and elastic moduli were calculated from raw data as described in Chapter 4.3.3 and 4.3.4 and results are presented on Figures 5.4-5.6. Figure 5.4 shows that longitudinal sound velocity of the adhesive increases in sigmoidal manner during the cure reaction towards a plateau value. The final value is the highest for the stoichiometric epoxy/hardener ratio. Attenuation increases in the beginning of the reaction, goes through maximum, and decreases. Final values for attenuation for different mixtures are almost equal. Changes in acoustic properties result from modifications in the material's viscoelastic parameters and reflect transformation from low-molecular weight low viscosity mixture of epoxy prepolymer and amine to the cross-linked polymer network as the reaction proceeds. A peak in the attenuation coincides with a sharp increase in sound velocity and relates to multiple oligomer formation before formation of the polymer network¹⁷². As more cross-links are formed after gelation, attenuation decreases but sound velocity and storage modulus continue to rise. An increase in sound velocity relates to the increase in intermolecular interactions.

The ratio epoxy/amine was varied to obtain networks with non-stoichiometric component ratios. Different ratios of adhesive components result in different reaction kinetics and final adhesive properties. Both excess and deficiency of the hardener have sufficient effect on the material's properties. Excess of the hardener leads to earlier gelation time and faster curing but final storage modulus is lower than in the adhesive with stoichiometric ratio. Deficiency of the amine hardener slows down the reaction.

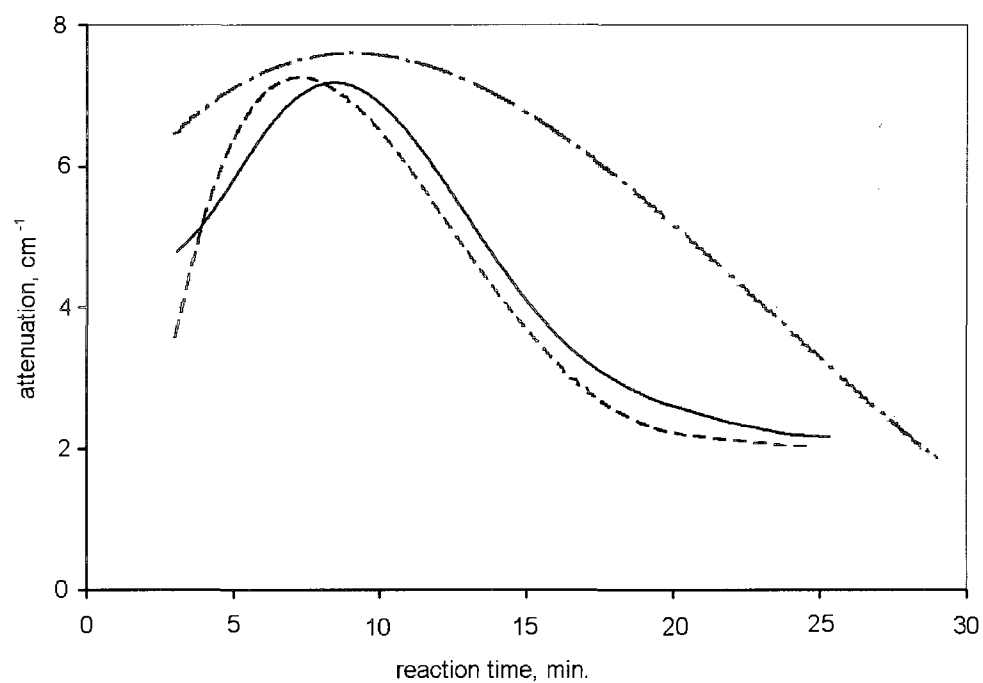
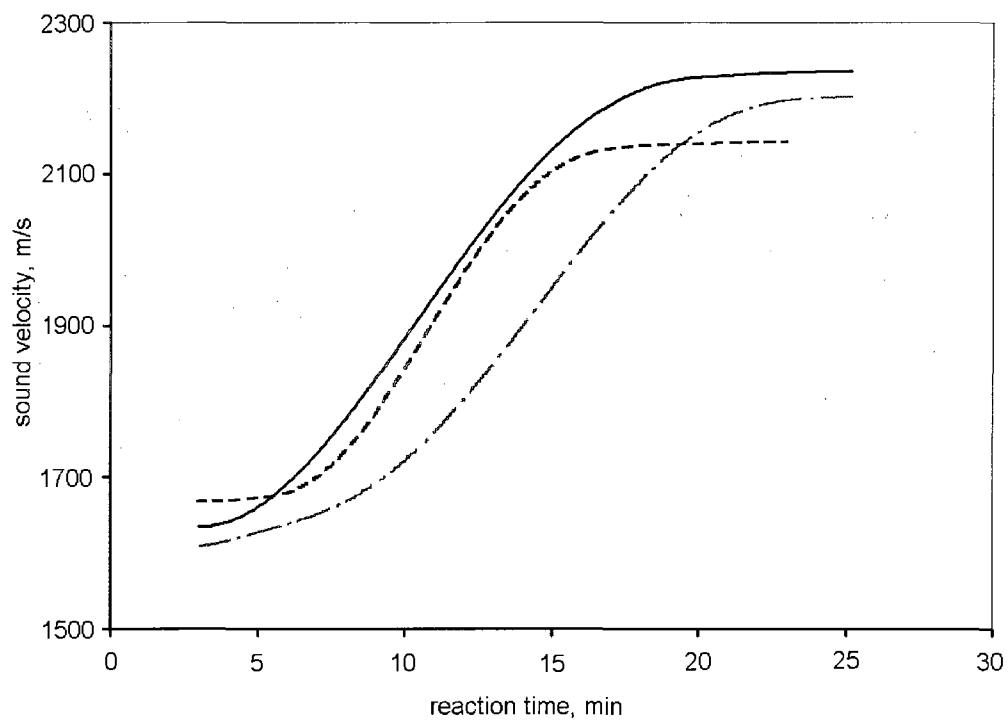


Figure 5.4. Change of the sound velocity (top) and attenuation (bottom) during epoxy-amine polymerization reaction. Epoxy-amine ratio: — 1:1; - - 1:2 (hardener excess), - · - 1:0.5 (hardener limit).

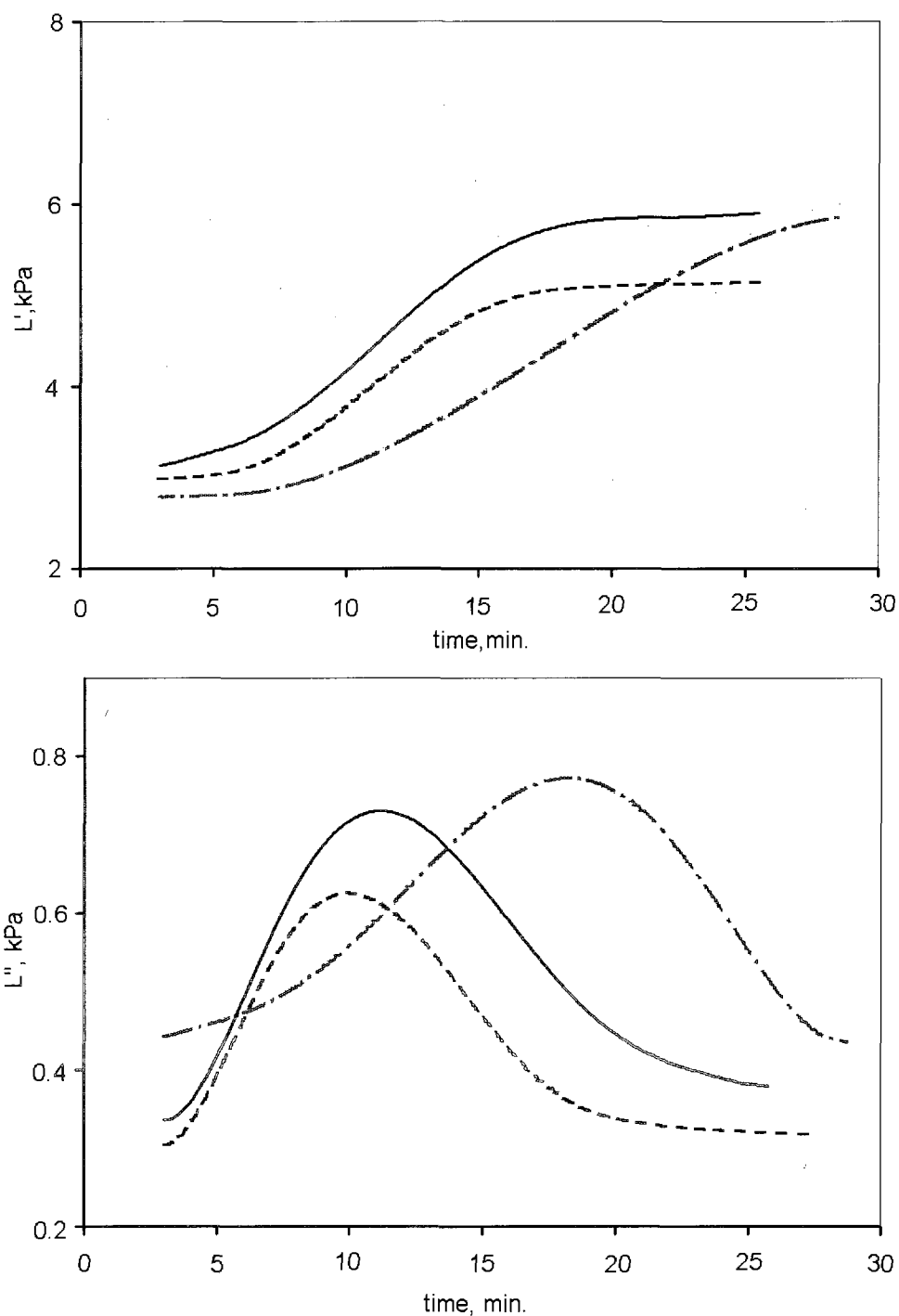


Figure 5.5. Change of the storage longitudinal elastic modulus (top) and loss longitudinal modulus (bottom) during epoxy-amine polymerization reaction. . Epoxy-amine ratio: —1:1; - - 1:2 (hardener excess), - · - 1:0.5 (hardener limit).

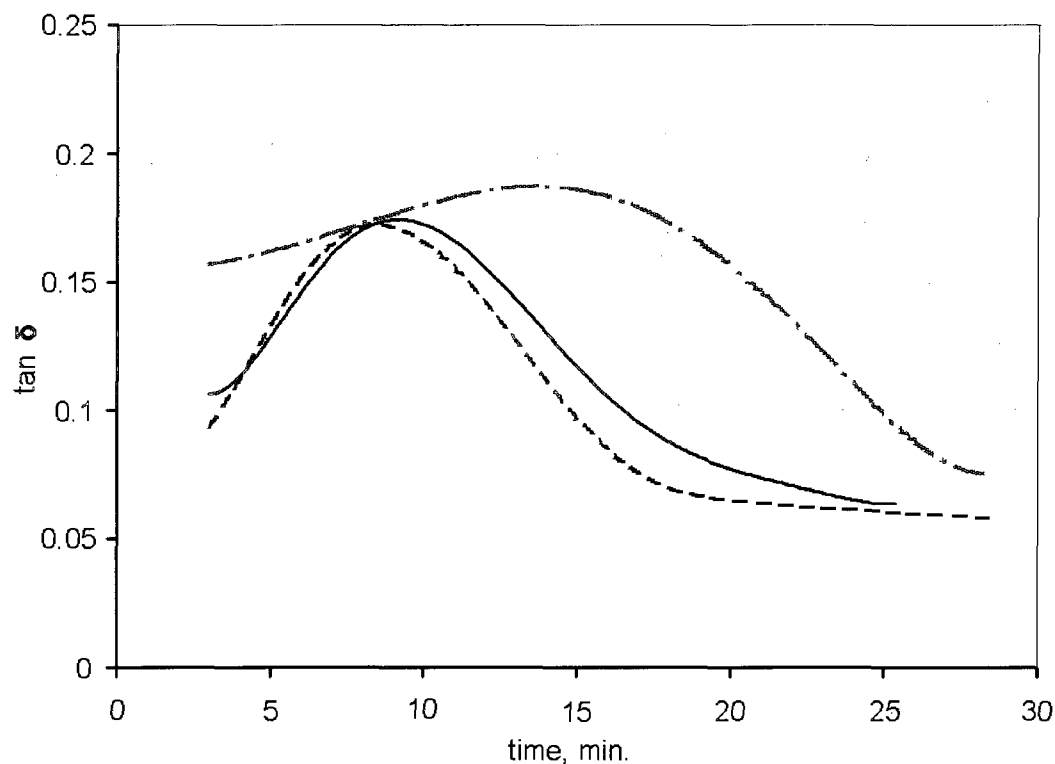


Figure 5.6. Change of the loss tangent during epoxy-amine polymerization reaction. Epoxy-amine ratio: —1:1; - - 1:2 (hardener excess),1:0.5 (hardener limit).

A peak in attenuation appears later and decreases at a slower rate. By 30 minutes of reaction, the storage modulus does not reach a plateau level.

Thus, a non-stoichiometric ratio of adhesive components results in not achieving proper viscoelastic properties and, correspondingly, cohesive strength. Epoxy and hardener must be thoroughly mixed before gelation occurs since after this point, increased viscosity inhibits homogeneous mixing of reactants, which leads to morphological inhomogeneities and defects.

5.2. Investigation of Viscoelastic Properties of Completely Cured Adhesive.

Due to the multiple chemical reactions that occur during epoxy hardening, the structure of epoxy adhesives is complex. Direct structural characterization of epoxide is very difficult so their molecular and physical microstructures are mostly presumed. The

most accessible technique for epoxy adhesive's structural characterization is study of its rubber-like properties above the glass transition.

T_g , is a very useful physical parameter that characterize the adhesive system's behavior. As T_g reflects molecular motion that occurs in a polymeric system, this parameter is useful for considering cohesion, strength and other properties of polymers. Another important direction in the investigation of polymer is the study of temperature dependence of the parameters that characterize polymer viscoelastic properties, such as storage and loss moduli. An acoustic method is proposed for the characterization of the polymer properties as a function of temperature^{103, 173, 174}. Nguyen and co-authors have shown that transition observed at high ultrasonic frequencies involves the same relaxation mechanism as glass transition measured by low frequency DMA technique or static methods²⁸. Although the ultrasonic method is well-known for non-destructive analysis, its application as a thermal analysis technique for measurements of dynamic mechanical properties of polymers has been limited. Most studies were performed on thermoplastics^{173, 175} and only a few publications characterize thermosets¹¹⁵.

Data for changes in acoustic parameters and elastic moduli of the cured adhesive plotted against temperature change are presented on Figures 5.7-5.9¹⁴⁷. Analysis of experimental data shows that it is possible to distinguish three regions of viscoelastic behavior. The largest change in adhesive properties occurs across the glass transition, when the material transforms from a hard glassy solid to the rubbery state. As temperature increases, the sound velocity and moduli drop while the sound attenuation and loss factor increases and show their maxima.

The adhesive's longitudinal sound velocity was calculated to be 2400 m/s at ambient temperature. Both velocity and storage modulus decreases as temperature increases. The velocity curve shows a very slight change of the slope at 45°C, inflection point at 80-83°C and the "offset" transition temperature at 145°C. Such broad transition region is quite unusual. One of the reasons may be interpenetrating networks of epoxy and polyurethane. Bockenfeimer and co-authors have reported presence for broad

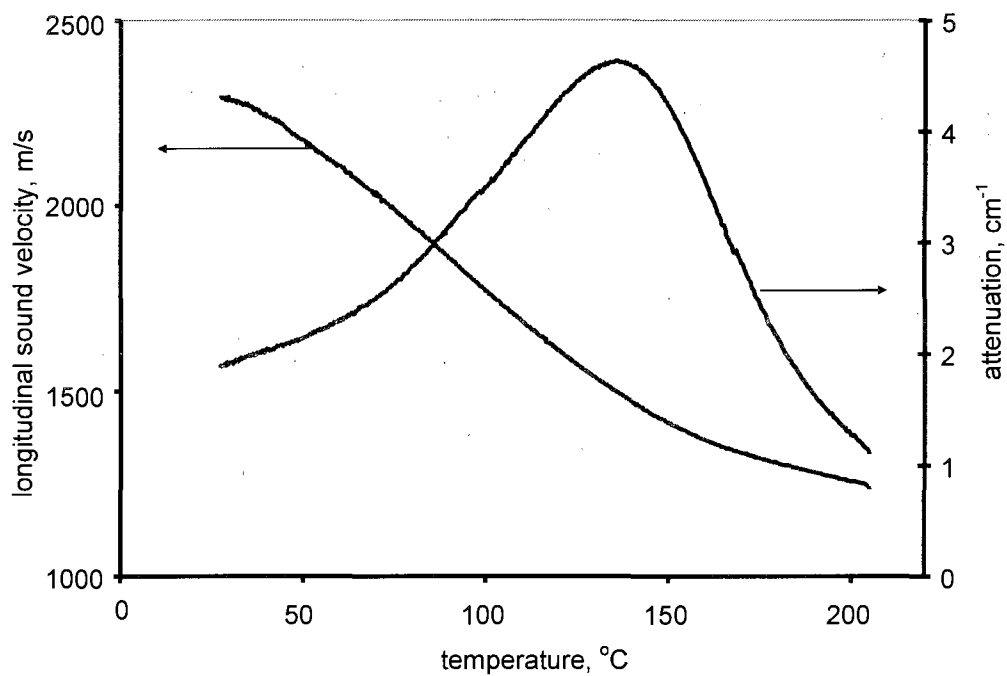


Figure 5.7. Temperature dependence of longitudinal sound velocity and attenuation of the completely cured adhesive ¹⁴⁷.

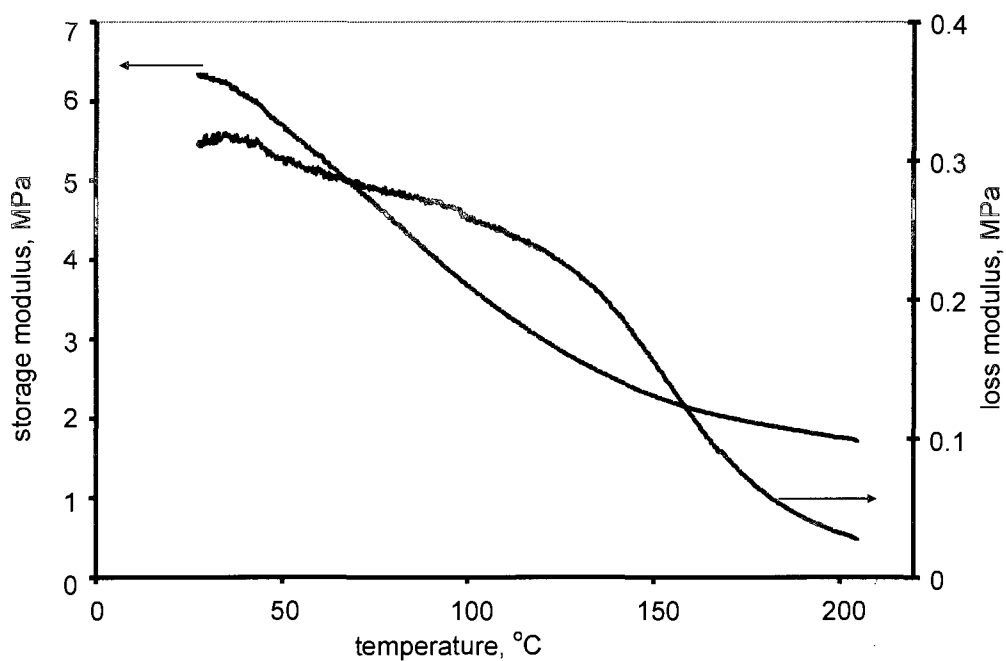


Figure 5.8. Temperature dependence of the elastic moduli of the completely cured adhesive.

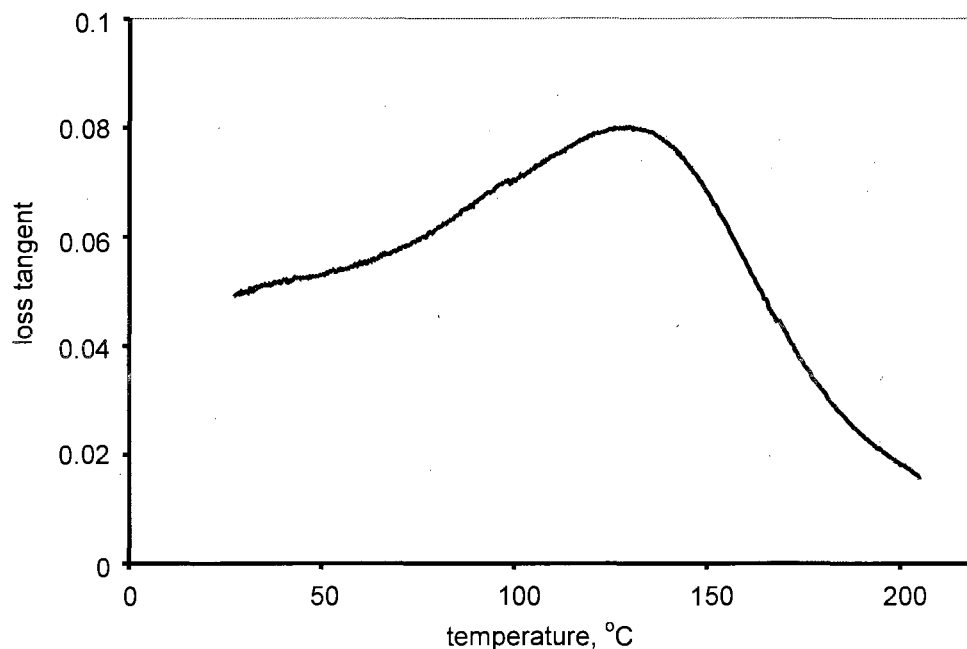


Figure 5.9. Temperature dependence of loss factor of the completely cured adhesive.

glass transition region for epoxy with inhomogenous cross-linking density¹⁰⁴. Another reason rises from the nature of acoustic wave propagation in polymers. White²⁴ also noticed two transitions temperature dependence of sound velocity for DGEBA-DDS (4,4'-diaminodiphenyl sulphone): the first correlated with glass transition and the second one was observed at higher temperatures. He has suggested that both are related to the glass transition, which broadens when examined at ultrasonic frequencies. This effect is mainly pronounced for high molecular weight polymers¹⁷⁴. The nature of this phenomenon was explained by Piche¹⁷³. As known, the longitudinal modulus L is related to bulk K and shear moduli G as

$$L^* = K^* + 4/3G^* \quad (5.5).$$

Piche showed that below T_g , the thermal behavior of the material's sound velocity is governed by the shear modulus G^* while at T_g and higher temperatures, the bulk modulus K^* is more significant and dominates the velocity's temperature dependence. This also leads to the absence of a sharp peak velocity derivative at T_g . On the velocity derivative curve (not shown), the maximum is observed, which is equal to 10m/s/K for the studied

adhesive. Ferry recorded derivative maximum of 25 m/s/K¹⁰⁴. The storage modulus E' shows a pattern similar to velocity dependence with slight change of slope at 50 °C temperature range and “offset” transition temperature at 142°C (Figure 5.9). Significant E' decrease (three times drop) is due to virtual disappearance of the G' term in the eq. 5.5 as epoxy becomes rubbery. The loss elastic modulus also decreases as temperature rises. It shows a slope change at 125°C and does not have any maximum, which is unusual for this parameter. These changes in viscoelastic properties reflect structural rearrangements in transition from glass to rubber state that are due to micro-Brownian motion of the polymer network chains. Sound attenuation and loss factor have well defined maxima at 142°C and 135°C, correspondingly.

The widths of the transition peaks and their position depend on the material, its molecular structure and other parameters. A wider transition region with lower peak intensity is more typical for cross-linked polymers^{106, 176}. The mechanisms of the peak appearance in attenuation have a structural relaxation nature, which involves motion of the molecular chains, or short molecular segments. Relaxation time τ is an important parameter, which is defined as a time required for that system to return to the equilibrium state. Relaxation time is a function of temperature, pressure and frequency. A peak in the sound absorption occurs when frequencies $f \approx 1/\tau$ where f is acoustic frequency and τ is relaxation time.

A DSC scan (Figure 5.10) shows two transitions - at 47.1 and 88.6°C. A specific volume curve obtained by Thermodilatometry (TD) (Figure 5.12) reveals a slope change at 76°C that is assigned as the T_g value. Usually thermal expansion in the rubbery state is about three times that in the glassy state¹⁰⁶. Slope change is much less for the structural adhesives which are designed for a better match of thermal properties of the metal substrates.

To assign T_g temperature based on the acoustic data obtained, the thermoacoustic curves were analyzed (Figure 5.12) and the following characteristic parameters were

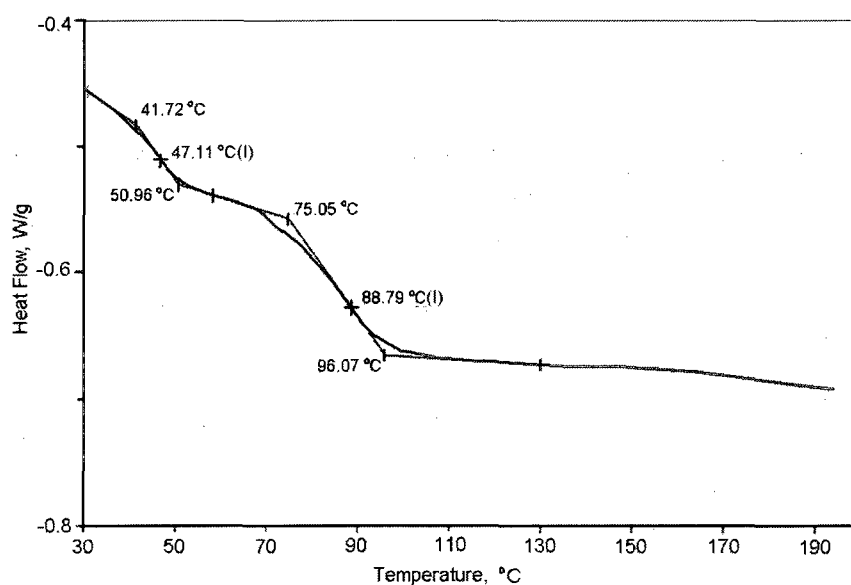


Figure 5.10. DSC scan for cured adhesive.

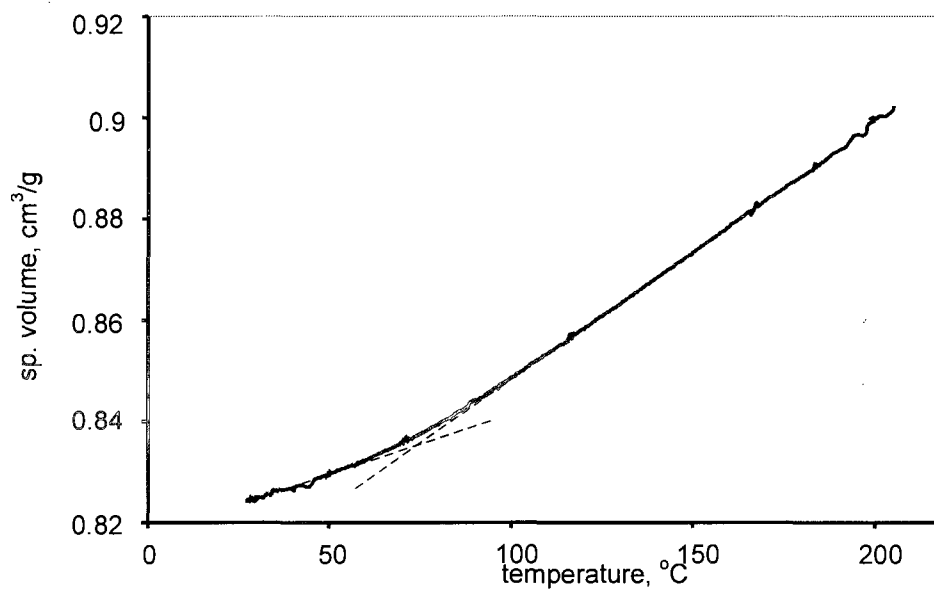


Figure 5.11. Thermodilatometry analysis. Temperature dependence of specific volume of the completely cured adhesive.

determined: “onset” and “offset” temperatures, peak maximum, and temperature of half-transition. Results shown in Table 5.1 indicate that the $\tan \delta$ peak at 135°C corresponds more closely to the peak in attenuation, midpoint of the decreasing E'' curve and offset temperature of the storage modulus. Values of T_g determined as a half-height

of transition for velocity and E' graphs correspond more closely to T_g calculated by DSC. Another transition that occurs at 47.1°C on DSC scan is also reflected in the acoustic measurements as an “onset” temperature for the sound speed and storage modulus. Loss modulus and loss $\tan\delta$ curves have a small shoulder (not shown in the Table 5.1). Slope change for specific volume, which occurs at the lower temperature value that T_g determined by DSC, relates to the “onset” temperature in attenuation and $\tan\delta$ curves. It is necessary to note that T_g measured by the acoustic method is usually observed at slightly higher temperatures than when measured by evaluating specific volume, and close to that when measured by DSC ^{110, 161, 187}.

Table 5.1. Determination of T_g value by acoustic method.

| Method | Adhesive property | Onset (1) | Max (2) | 50 (3) | Offset (4) |
|----------|------------------------------------|-----------|---------|--------|------------|
| Acoustic | Sound velocity, m/s | 45 | n/a | 95 | 145 |
| | Attenuation, cm^{-1} | 72 | 136 | n/a | ----- |
| | Storage elastic modulus, Pa | 45 | n/a | 86 | 140 |
| | Loss modulus, MPa | ----- | 125 | ----- | ----- |
| | Loss factor $\tan\delta$ | 70 | 135 | ----- | ---- |
| TD | sp. Volume, cm^3/g | 72 | ----- | ----- | ----- |
| DSC | Heat flow, W/g | | | 47, 88 | |

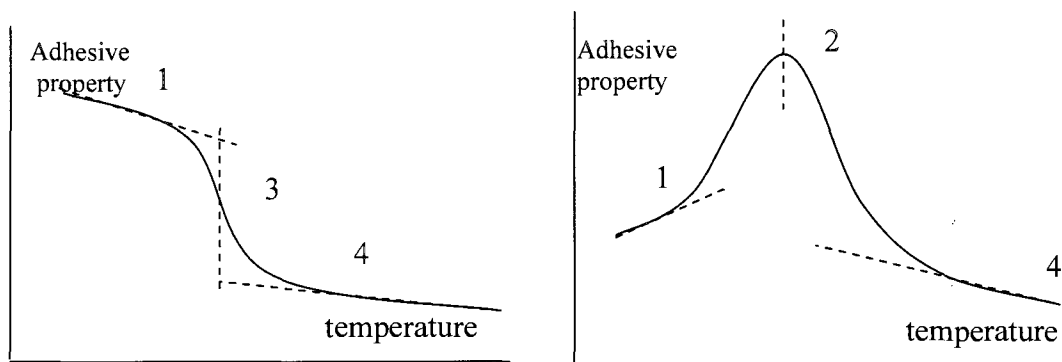


Figure 5.12. Representative curve of sound velocity and attenuation versus temperature in the region of the T_g of epoxy adhesive. Numbers are assigned as in Table 5.1.

Thus, the glass transition region of the structural adhesive covers a wide temperature range from 70°C to 150°C when measured by the ultrasonic method. This highlights the problem of assigning T_g a value. The DSC method usually uses the endotherm half-height. The criteria for selecting of T_g value from DMA (which is the closest method related to acoustics) are usually either a peak in the loss modulus E'' or a peak in $\tan \delta$. The T_g value obtained with the loss factor peak is several degrees higher than peak E'' . For cross-linked polymers where $\tan \delta$ peak is not so pronounced, it is often recommended to consider T_g as the point where the E' starts to drop¹⁷⁷. This point more closely correlates with T_g values determined by other methods and this is the lowest value which is important for structural adhesives. As the acoustic thermal technique is not widespread yet, there is no strict definition of the T_g determination and different points were used as a T_g temperature value: inflection point on the sound velocity vs. temperature curve^{103, 174}, offset point for velocity curve or maximum of loss tangent $\tan \delta$ ²⁸.

It is to be noted that the midpoint of the transition region in the storage modulus curve is the closest to the DSC value for BETAMATE adhesive. However, due to limited temperature range in some experiments for proper T_g determination, it is difficult to measure the midpoint of the transition region on storage modulus curve precisely. Therefore, in this study, a maximum in the loss modulus $\tan \delta$ curve is used as a reference point for T_g . It is necessary to note that T_g determined by other methods is strictly connected to the maximum in $\tan \delta$ from ultrasonic study¹⁷³.

5.3. Isothermal Cure Monitoring of One-Component Adhesive System

Dicyandiamide is not soluble and therefore not reactive at temperatures lower than 140°C¹⁵². The optimal cure regime for BETAMATE adhesive is 30 min at 180 °C. the cure reaction of BETAMATE was studied at the several temperatures higher than 140°C. Figures 5.13-5.15 represent change of acoustic and viscoelastic properties during the adhesive polymerization at temperatures 100, 120, 140, 160 and 180 °C.

During cure reaction, atoms, which have been separated by van der Waals forces, (3-5 Å) participate in the formation of covalent bonds (1-3 Å). This leads to an increase in adhesive density. Although specific volume value does not change significantly due to special composition of structural adhesives to prevent stress appearance on the metal-adhesive interfaces, formation of covalent bonds and cross-linked network is reflected in sound velocity increase. Changes in sound velocity are shown in Figure 5.13. A significant rise in sound velocity is noticeable as the adhesive passed from the uncured stage to the fully cured. Velocity increases in a sigmoidal manner as reaction proceeds reaching a plateau at the end of the reaction. At lower temperatures, 100 °C and 120 °C, the velocity curves have short lag-periods, which correspond to an increase of the molecular weight of the epoxy oligomers. Then velocity increases rapidly at the gel point followed by a slowing down. After 100 minutes of cure, sound velocity of the epoxy remains almost constant; only 4% increase is observed during the next 2 hours. At reaction temperatures of 140 °C and higher, the lag period is not observed; the velocity curve increases rapidly and reaches a plateau. Different final sound velocities illustrate the dependence of sound velocity on temperature. Slopes of the graphs increase with the cure temperature, which indicates higher cure reaction rate.

Sound attenuation curves (Figure 5.13) show their peak in the beginning of the process and decreases afterwards. The peak in attenuation corresponds to the maximum slope in the sound velocity curves for both temperatures. Accordingly Lionetto²⁹ and Alig et al.¹⁶², show the peak in attenuation occurs in either gelation or vitrification. As temperature of the curing is higher than T_g of the cured and especially not cured adhesive, the attenuation peak in this case corresponds to gelation process, where the maximum of the epoxy oligomers chains are formed. Following the formation of a three-dimensional epoxy network leads to decreasing in attenuation.

As reaction temperature decreases, attenuation peak (and accordingly gelation) comes later at cure reaction and becomes wider. Similar widening of the attenuation maximum was noted for two-component adhesives with limit of hardener (Figure 5.4 bottom). A slower reaction rate and widening of attenuation and loss modulus maxima

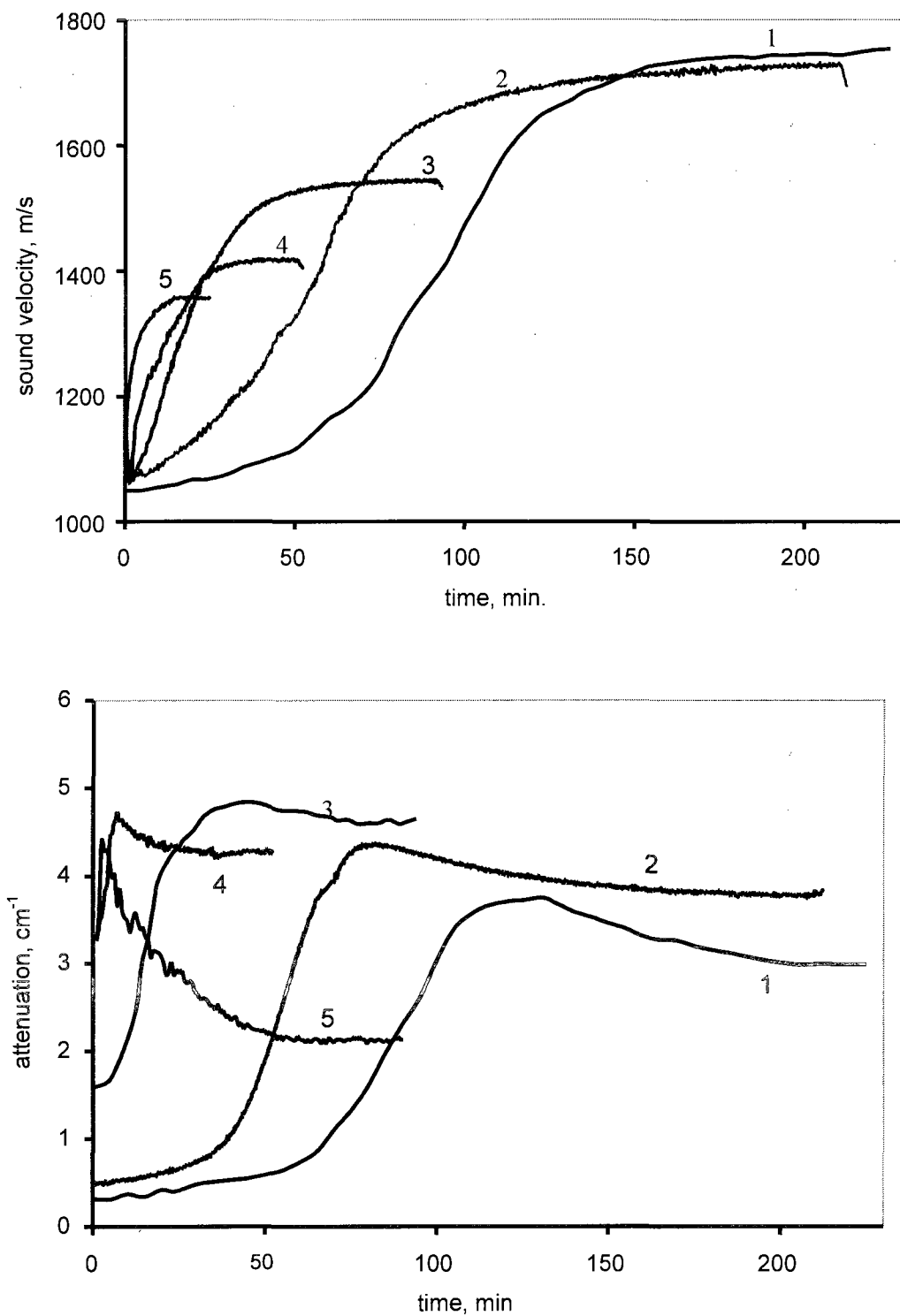


Figure 5.13. Changes in longitudinal sound velocity (top) and attenuation (bottom) during adhesive polymerization at different temperatures¹⁴⁶. 1-100°C, 2-120°C, 3-140°C, 4-160°C and 5-180°C.

may also be explained not only by lower reaction temperature but also by limit of hardener. DDA initially exists in the form of dispersion of crystalline particles in premixed, one-component adhesive and melts at about 140°C ¹⁵². Thus, the main reaction should start with beginning of DDA dissolution. Below that temperature, other reactions occur as a consequence of the presence of accelerators and homopolymerization (etherification of hydroxyl groups) reactions. Another reason for slowing the reaction at 100°C is vitrification and corresponding topological isolation of reactive groups. At higher temperatures, on the contrary, reaction proceeds so fast that it is not possible to record first stages of the reaction, especially at 180°C . The final values of the attenuation tend towards plateaus as well; however, the maximum and final values of attenuation are not proportional to the temperature. The maximum values are observed at 140°C . A little drop in attenuation after reaching the maximum value at 120 and 140°C refers to the relaxation peak for cured adhesive at these temperatures (Figure 5.8). Similar behavior of the epoxy adhesive's properties at different temperatures during the curing reaction was observed by Fremantle and Challis^{120, 172}.

Figure 5.14 shows development of the storage (L') and loss (L'') longitudinal moduli during the curing reaction at different temperatures. Changes of the loss factor $\tan \delta$ are represented in Figure 5.15. Maxima in L'' and $\tan \delta$ occur slightly later than the peak in sound attenuation. Pindinelli et al.²⁷ and Maffezzoli et al.¹⁷⁰ have shown that the most significant changes in longitudinal moduli occur after gelation. According to them, modulus L correlates rather with crosslinking degree than with the extent of the reaction. The former parameter represents the number of joints in the network, which reflects the cohesive properties of adhesive and can be theoretically calculated using the approach of Macosko and Miller^{178, 179}. Johari has shown that an increase in L' during adhesive transformation from liquid to the solid is mostly due to a significant increase in K' . G' also contributes but its magnitude is 2-6 times less than K' ¹⁸⁰.

There is a fundamental difference in morphology between two-component room-temperature cured and heat-cured adhesives. At the room temperature, the curing reaction between epoxy and hydroxyl groups proceeds slowly and hydroxyl groups, formed

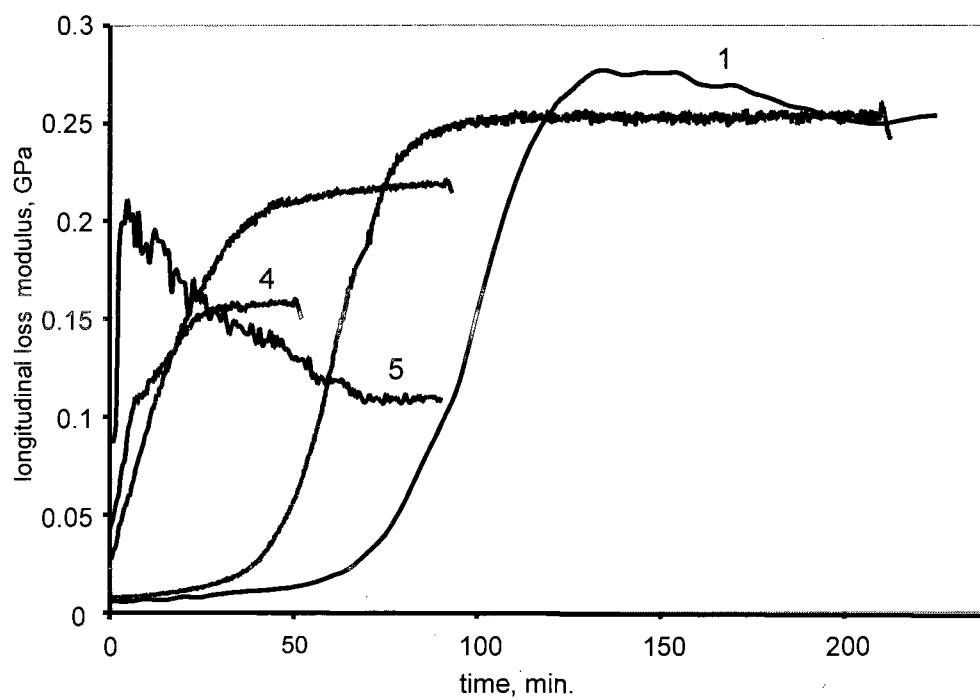
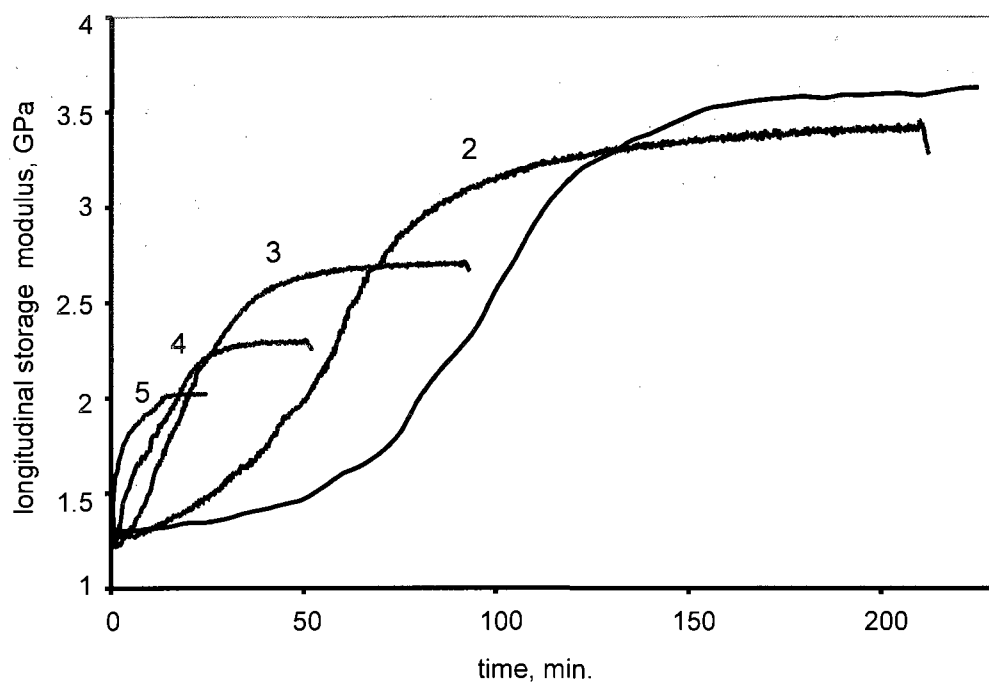


Figure 5.14. Changes in longitudinal storage modulus (top) and loss modulus (bottom) during adhesive polymerization at different temperatures. 1-100°C, 2-120°C, 3-140°C, 4-160°C and 5-180°C ¹⁴⁶.

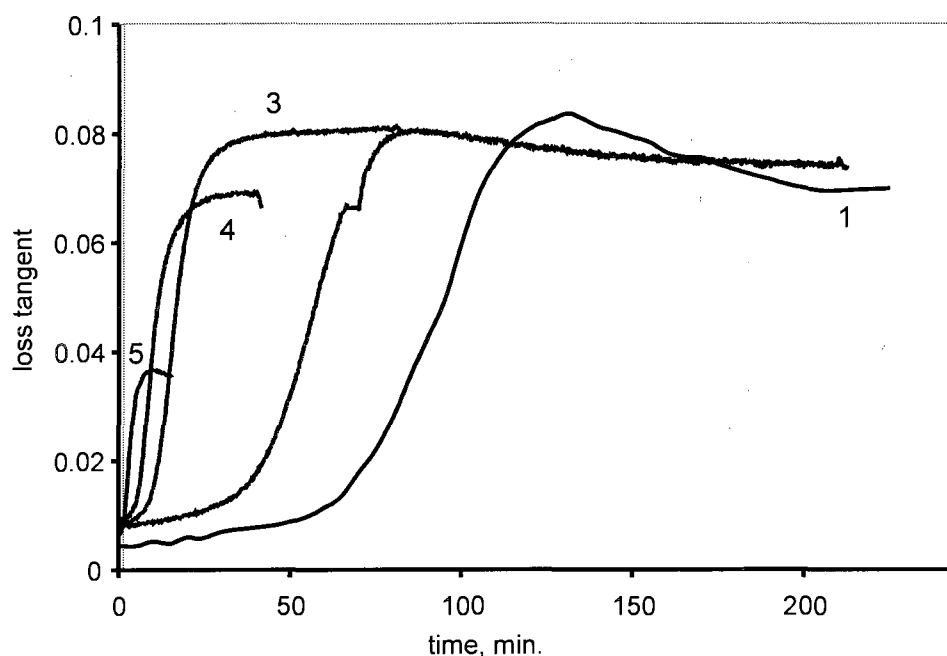


Figure 5.15. Changes in loss tangent during adhesive polymerization at different temperatures.
1-100°C, 2-120°C, 3-140°C, 4-160°C and 5-180°C.

during oxirane ring opening reaction, do not participate in further reaction with oxirane rings. The adhesive with two epoxy functional ends (what is quite typical) can form only two bonds with hardener; and number of cross-links is determined only by functionality of the hardener. In heat cured adhesives, formed hydroxyl groups actively react with epoxy groups. Thus, DGEBA prepolymer acts as a component with functionality 4 or even more. Existing in the prepolymer resin, hydroxyl groups further increase functionality and cross-linking density of the adhesive. Due to different reactivity of the various reaction centres and complexity of number of reactions, the final network structure can be complex and varied. Etherification reaction proceeds more slowly than reaction with amines. Stevens ⁷ have shown that most cross-links involve etherification reactions and thus influence T_g temperature and elastic moduli values.

As acoustic and viscoelastic properties of polymers greatly depend on temperature, direct comparison of the final properties of the adhesives polymerized at different temperatures is not possible. To compare these results and evaluate the cure

state of the adhesive, sound velocity and moduli values were adjusted to their values at corresponding temperatures for completely cured adhesive. Based on these normalized data, ‘mechanical’ reaction extent was calculated as ^{146, 186}

$$\alpha_{US} = \frac{L' - L'_0}{L_f - L'_0} \quad (5.4)$$

where L_f is longitudinal storage modulus for the completely cured adhesive, L'_0 is the longitudinal storage modulus for the uncured adhesive. Data is shown in Figure 5.16.

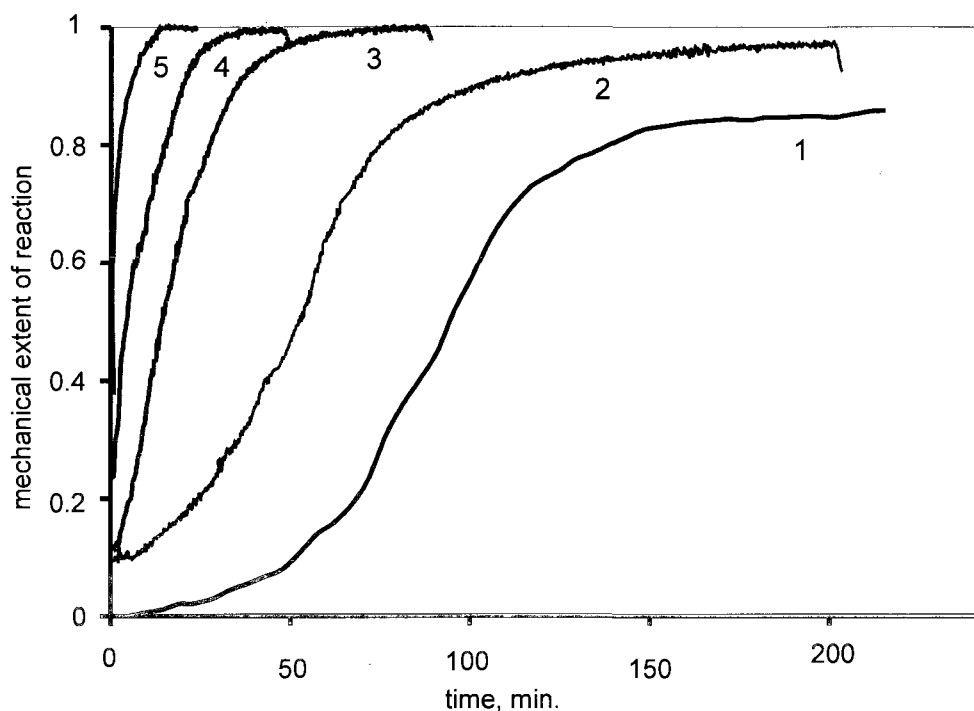


Figure 5.16. Acoustic extent of adhesive polymerization reaction¹⁴⁶. 1-100°C, 2-120°C, 3-140°C, 4-160°C and 5-180°C.

Adhesive cured at temperatures higher than 140°C, reaches complete cure whereas epoxy cured at 120 and 100°C reach only 0.96 and 0.85 cure conversion, correspondingly. Oleinik showed that even at the temperatures slightly lower T_g , reaction extent still may reach 1 for DGER-mPDA network¹⁸¹. He suggested that at $T_{cure} = T \pm 25-30^\circ$ the reacting groups stay mobile and their motion is sufficient to continue reaction. In this study however, even at the temperatures slightly higher than T_g ,

reaction can not proceed to the end due to impossibility of the DDA hardener to participate in the reaction. It is to be mentioned that α_{US} is based on the thermomechanical properties representing cross-linking rather than the degree of the reaction, or functional group ¹⁸².

In general, the amine-epoxy resin curing reactions show complex kinetics with acceleration due to autocatalysis in the beginning of reaction. The later stages may show significant slowdown after gelation when mechanism becomes diffusion-controlled. Usually, if reaction temperature was higher than T_g of the completely cured adhesive and the systems is not hindered from vitrification after gelation.

There are many techniques that determine gelation time in thermosetting polymers. Gel point can be measured by determining the point where the prepolymer is no longer dissolved in solvent. For dielectric measurements, inflection point in the conductivity vs. time curve is used as the gel time. For DMA analysis, the several points can be used as gelation time: the time when G' and G'' are equal, maximum of $\tan \delta$ curve. Often, the point where the loss modulus shows a change in slope is used as well ¹⁷⁷. In this study, gelation time was settled as the time when the maximum in sound attenuation occurs. ‘Mechanical’ conversion of the reaction at the gel time was calculated based on the graph in Figure 5.16. Results are shown in Table 5.2. “Mechanical” conversion at gel time varies from 0.7 to 0.75 at different temperatures. The theoretical value of chemical reaction conversion at the gel point can be approximated as:

$$\alpha_{theor} = \frac{1}{r(F_e - 1)(F_h - 1)} \quad (5.6)$$

where r is molar ratio between epoxy and hardener functional groups participating in the reaction, F_e is a number of functional groups in epoxy and F_h is a number of functional groups in a hardener. DGEBA-based resin has only two oxirane rings but it is important to realize that in heat-cured structural adhesives, hydroxyl groups formed during ring opening reaction or existing in the pre-polymer also actively participate in the reaction with epoxy groups (Figure 2.8). Thus, epoxy functionality should be considered as four

Table 5.2. Gelation time for structural adhesives cured at different temperatures.

| Reaction temperature, °C | Gel time, min. | “Mechanical” conversion at gel time |
|--------------------------|----------------|-------------------------------------|
| 100 | 121 | 0.72 |
| 120 | 75 | 0.73 |
| 140 | 42 | 0.75 |
| 160 | 8 | 0.70 |
| 180 | 3 | 0.75 |

or even higher resulting in more dense network. With $F_e=4$, $F_h=4$ and $r=0.5$, theoretical conversion at gelation time is 0.66. Degree of cure at gel point is usually in the range of 0.58-0.62 which is lower than “mechanical” cure degree determined. It is necessary to remember that DDA is usually used at lower than the stoichiometric ratio amounts, which should increase conversion value. Also, some epoxy groups are involved in homopolymerization reaction.

After being polymerized at a certain temperature, the adhesive samples were heated to 200°C and scanned down to room temperature with cooling rate 2°C/min. to investigate cross-link density. Scans are presented in Figure 5.17. Despite numerous publications^{30, 108, 183} which show that dissimilar polymerization conditions should lead to different network structures, all samples demonstrate equal values of longitudinal storage modulus in the rubbery state and correspondingly equal cross-linking density and identical temperature behavior. One of the reasons of this behavior may be post-cure polymerization, which occurs during heating samples up to 200°C. It is interesting to note that in glass state at ambient temperature, adhesives have slightly different values for the storage modulus. It is known that in the glassy state, the storage modulus of amorphous polymers is determined not by structure or cross-link density but by intermolecular forces¹⁸⁴. Thus, despite the same cross-link density, these epoxies have different structures. A different cure regime leads to various reactivity of not only DDA but also hydroxyl groups, which could be assumed is the reason for structural variation in the glassy state.

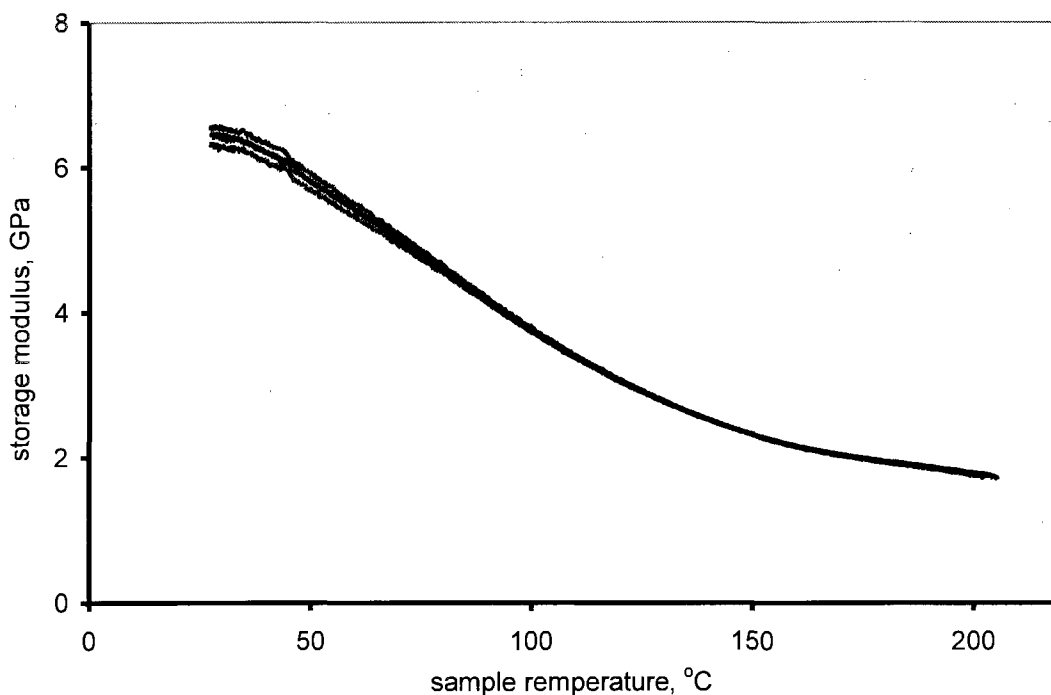


Figure 5.17. Thermal scans of the adhesives polymerized at different temperatures (100, 120, 140, 160, and 180°C).

5.4. Continuous Heating Cure of One-Component Adhesive Systems

Continuous heating cure is one of the ways to investigate viscoelastic properties of the adhesives. As the adhesive is heated at a certain rate, it goes through various states. The acoustic parameters were monitored under continuous heating conditions with a heating rate of 1°C/min. Results of the acoustic velocity and attenuation changes are presented in Figure 5.18¹⁴⁶.

Reaction starts after the adhesive passes the temperature equal to T_g of the initial components. Both sound velocity and attenuation show a change of slope 20 minutes after the experiment begins, which corresponds to the temperature of 58°C. As the reaction proceeds, glass transition temperature T_g of the adhesive increases and, at some point, exceeds the cure temperature. Starting from this point, the adhesive vitrifies and reaction becomes diffusion controlled due to restrictions on diffusion of reactive

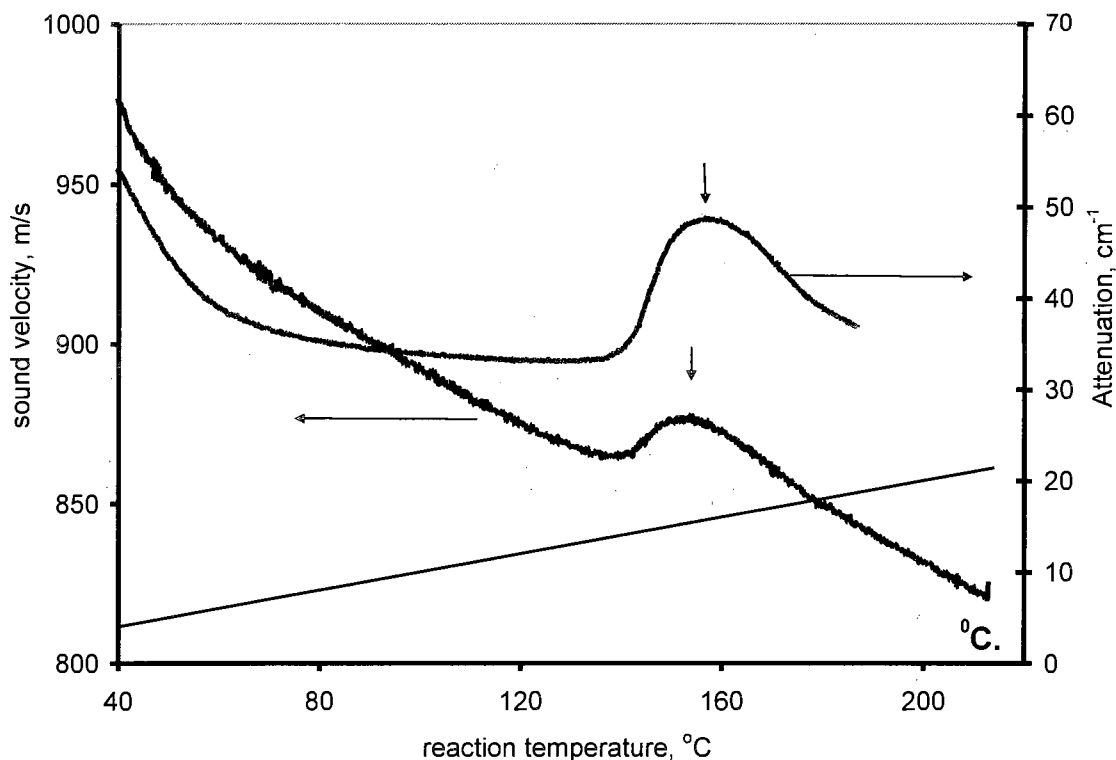


Figure 5.18. Changes of sound velocity (1) and attenuation (2) during continuous heating cure¹⁴⁶. Straight line shows temperature profile. Arrows illustrate residual polymerization. Heating rate is 1°C/min¹⁴⁶.

groups¹⁸⁵. Reaction rate decreases drastically or stops. Region with a linear decrease of the sound velocity corresponds to temperature dependence of these parameters which indicates vitrification of the system. Attenuation stays constant for vitrified adhesive. The effective T_g of the partially cross-linked adhesive will be slightly greater than the temperature at which adhesive has vitrified, as reaction rate slows down gradually after vitrification and cross-link density is not high enough. The reaction may restart again if the reaction temperature becomes higher than T_g of the partially polymerized adhesive and its molecular mobility increases. A sharp increase in sound velocity and attenuation is observed right after temperature of 135 °C is passed. Peaks in both parameters at 135°C represent so-called residual polymerization. A sharp increase in velocity indicates additional cross-linking reaction¹⁸⁶. Renewing the reaction at 135°C again may support the assumption that maxima in attenuation and loss tangent (Figures 5.8 and 5.10) relate to the glass transition phenomenon. Another reason for renewing the reaction at this

temperature is melting of DDA and release of very active hardener for epoxy. After reaction is complete, sound velocity starts to decrease again linearly with heating. The attenuation curve shows a more complex pattern as residual polymerization overlaps with the relaxation peak for a completely cured adhesive, which is observed at 142°C. Changes in epoxy density are shown at Fig. 5.19. Figure 5.20 represents changes in storage L' and loss L'' elastic moduli during non-isothermal cure¹⁴⁶. Both moduli show similar behavior as cure temperature reaches 135°C and exceeds the glass transition temperature T_g .

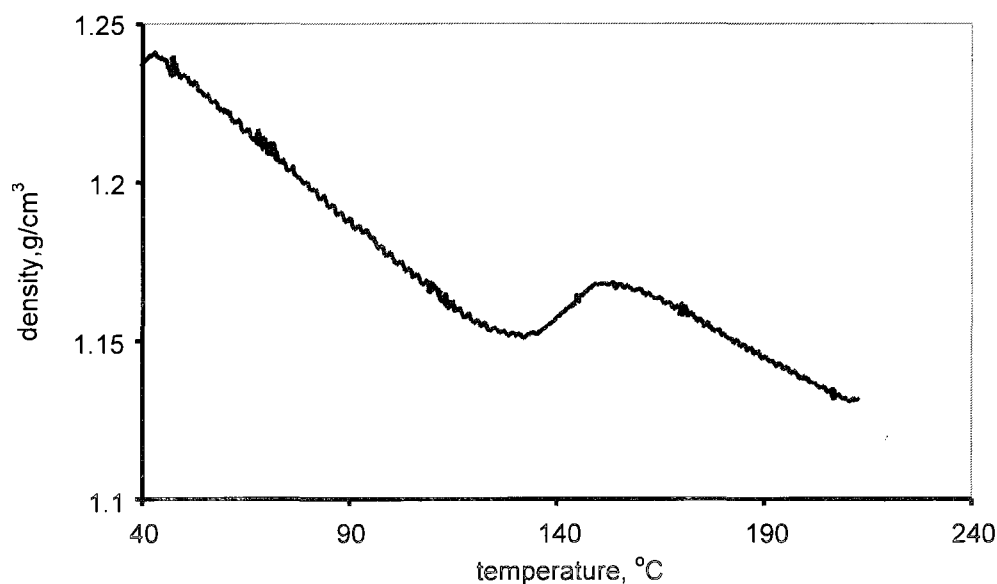


Figure 5.19. Changes of adhesive density during continuous heating cure.

After reaching 210 °C, the epoxy sample was cooled down to room temperature with cooling rate of 2°C/min. Scans are presented in Fig. 5.21-5.23. It is interesting to note appearance of the multiple peaks at lower temperatures on the attenuation and loss tangent curves. The major peak is detected at 147°C, second peak with lower amplitude

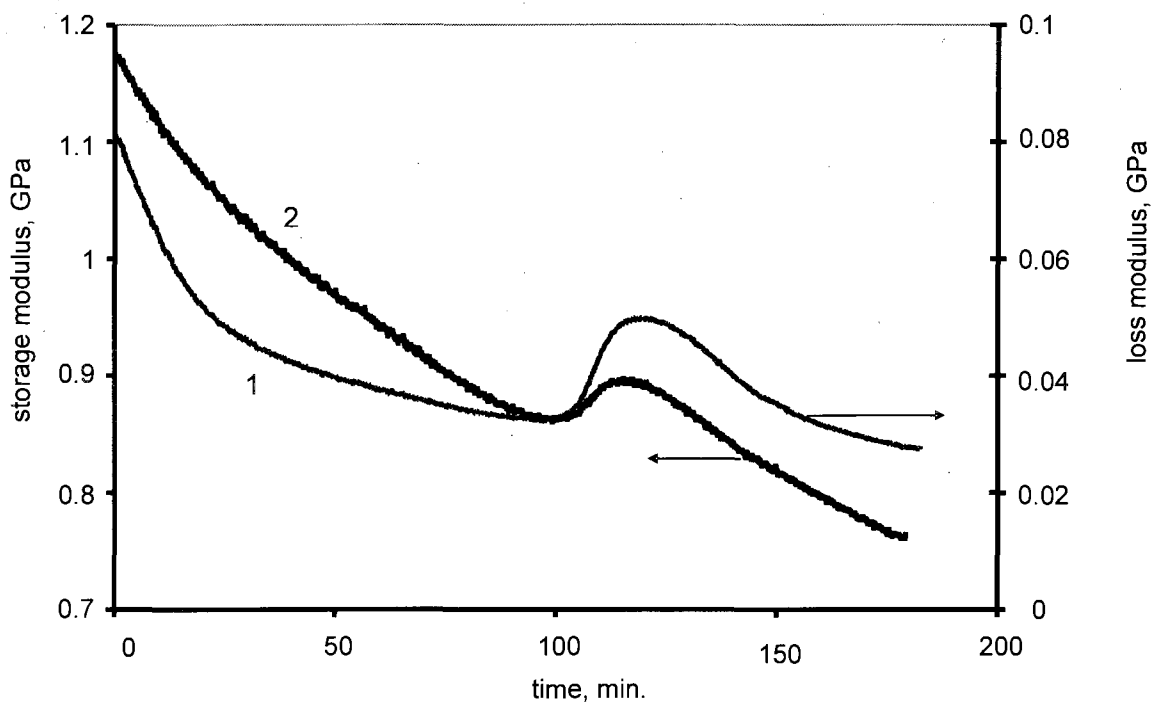


Figure 5.20. Changes in adhesive loss L'' (1) and storage L' (2) moduli during non-isothermal cure¹⁴⁶. Heating rate is 10C/min.

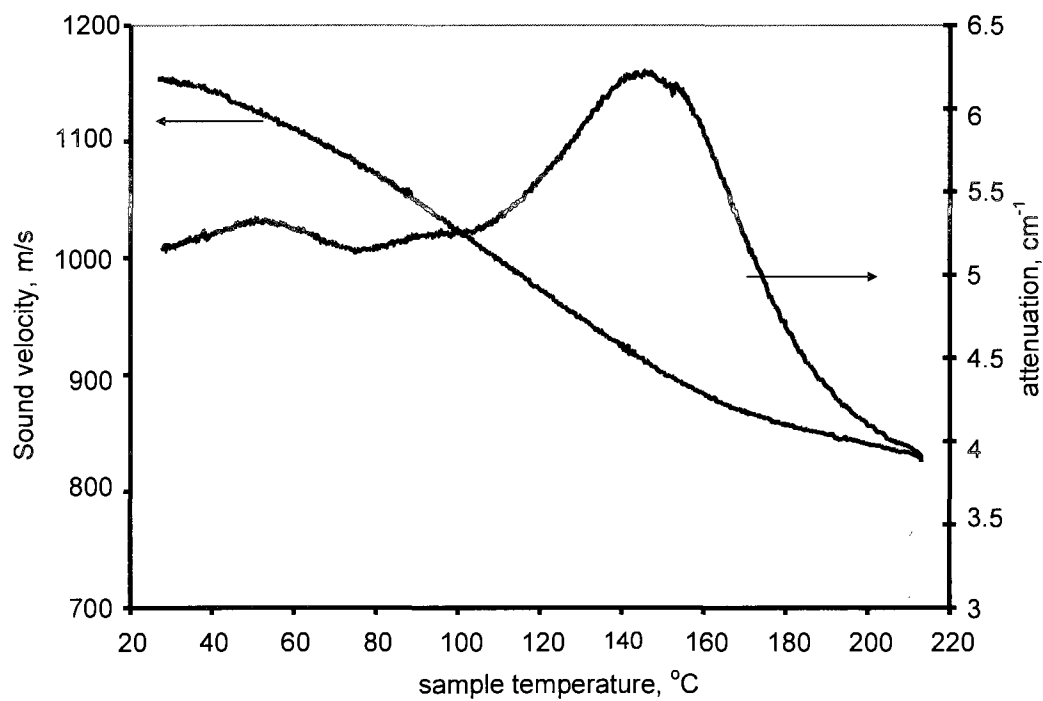


Figure 5.21. Thermoacoustic properties of the adhesive cured at constant heating rate.

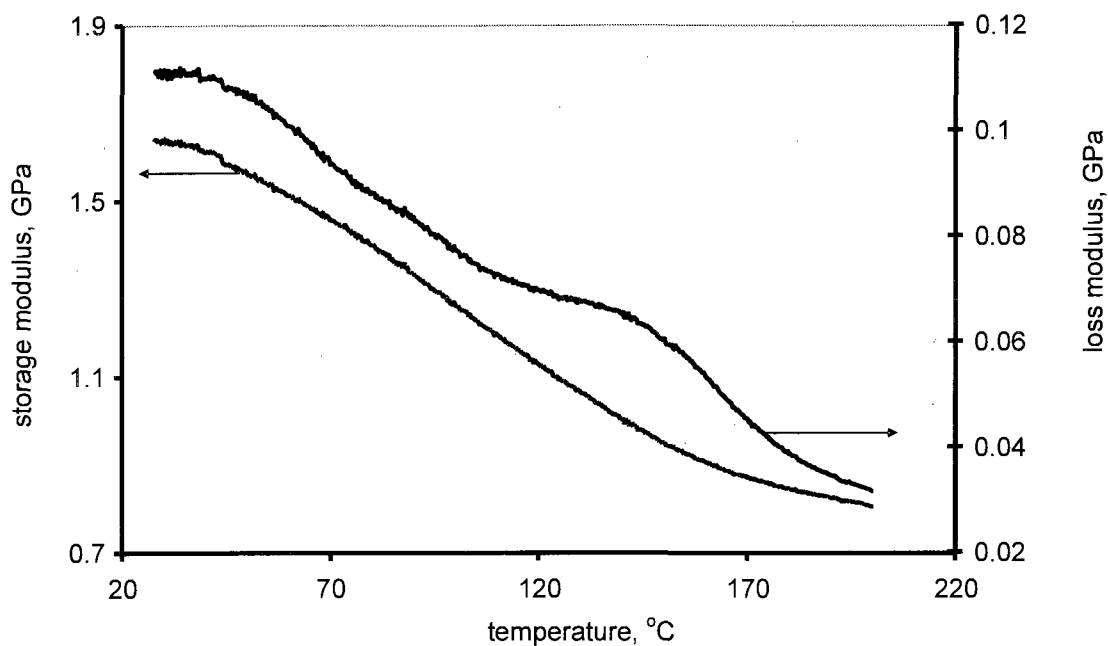
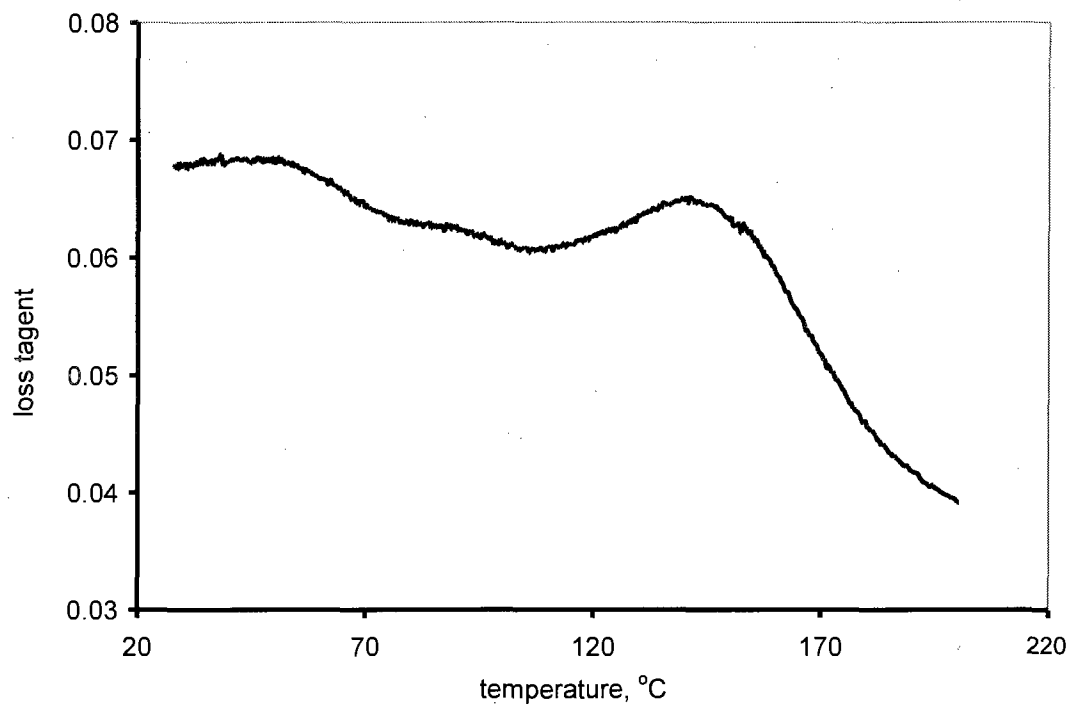


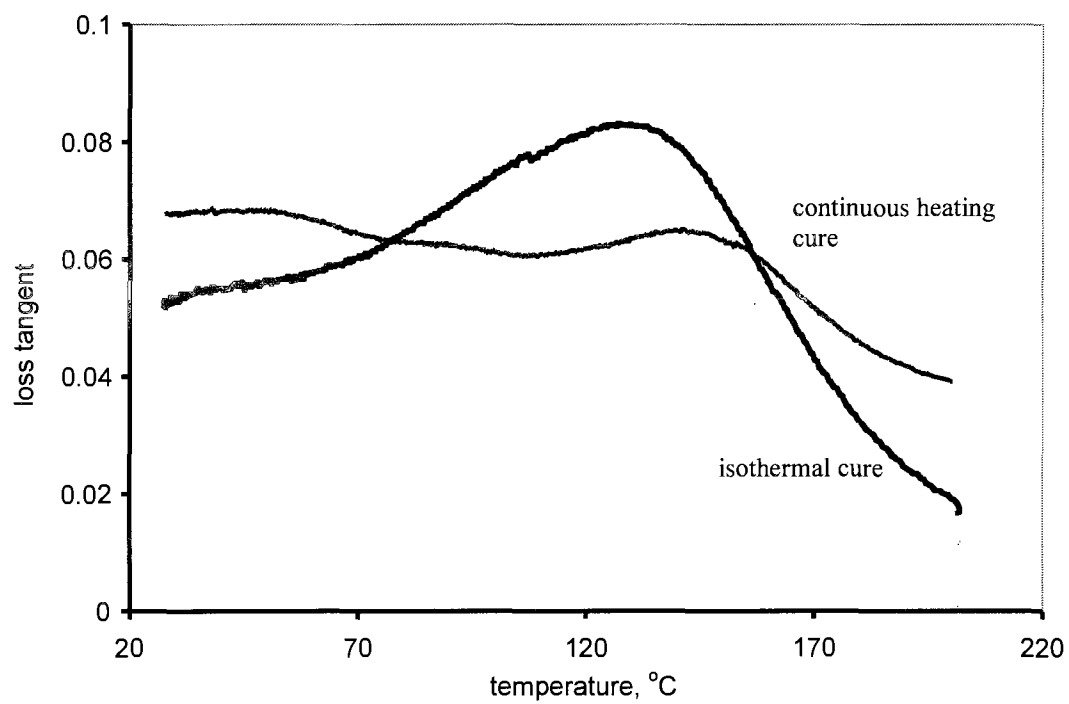
Figure 5.22. Longitudinal elastic moduli of the adhesive cured at constant heating rate.

and small shoulder are visible at 52 °C and 95 °C correspondingly. Figure 5.23 (b) compare temperature scans of the $\tan \delta$ for isothermal and continuous heating cure conditions. The broadening of the relaxation spectrum and appearance of the multiple peaks can be explained by network heterogeneity. Another reason for a second peak

along with unexpectedly low values for elastic moduli might be uncompleted phase separation. Phase separation is usually completed before gelation¹⁹. But in the case of slow heating, the adhesive vitrifies and increased viscosity could inhibit the phase separation.



a



b

Figure 5.23. Loss tangent of the adhesive cured at constant heating rate.

5.5. Study of Changes in T_g Temperature During Adhesive Polymerization

As the glass transition temperature of the cross-linked polymer correlates with conversion of the cure reaction²³, T_g can be used as a reliable measure of conversion. Viscoelastic properties of epoxy adhesive were investigated as a function of reaction conversion. This was reached by heating the sample up to, and cooling it down from, successively increasing temperatures as described in Section 4.3.5. Each heating step provides a different cure state according the TTT diagram and each cooling phase measures the T_g value for this particular state¹⁸⁶. Results are presented in Figures 5.24 and 5.25.

Uncured adhesive has attenuation and loss factor maxima at 32 °C¹⁴⁷. As the reaction temperature increases, the peaks shift to higher temperatures and become wider. One can see from the graphs that all the adhesive properties change in a manner corresponding to cure temperature. The transition loss dispersion decreases in intensity, broadens, and shifts to higher temperatures. Also, the slope of the storage modulus curve decreases. Figure 5.26 shows maximum of the $\tan \delta$ plotted against the cure temperature $T_{\text{cure max}}$. It is to be noted that maximal reaction temperature is higher than T_g values of a partially polymerized system. Again, this abnormality should be related to the nature of hardener, which is present in the reaction system in crystalline form and has a high melting point. Maximal shift in properties occurs when temperature of cure $T_{\text{cure max}}$ reaches 138 °C. After the temperature reaches 170 °C, the peak temperature becomes a constant 142 °C. Maximal increase of temperature of the loss tangent peak could relate melting of DDA and significant increase in reaction rate at this temperature. Therefore, this transition reflects structural changes during cure of the adhesive which are internally linked to the cohesive properties of the adhesive within the bond joint.

Data obtained shows the importance of maintaining proper cure conditions. If the temperature is too low, vitrification may occur or DDA involvement in the reaction may be doubtful. This may result in an undeveloped network structure and low adhesive

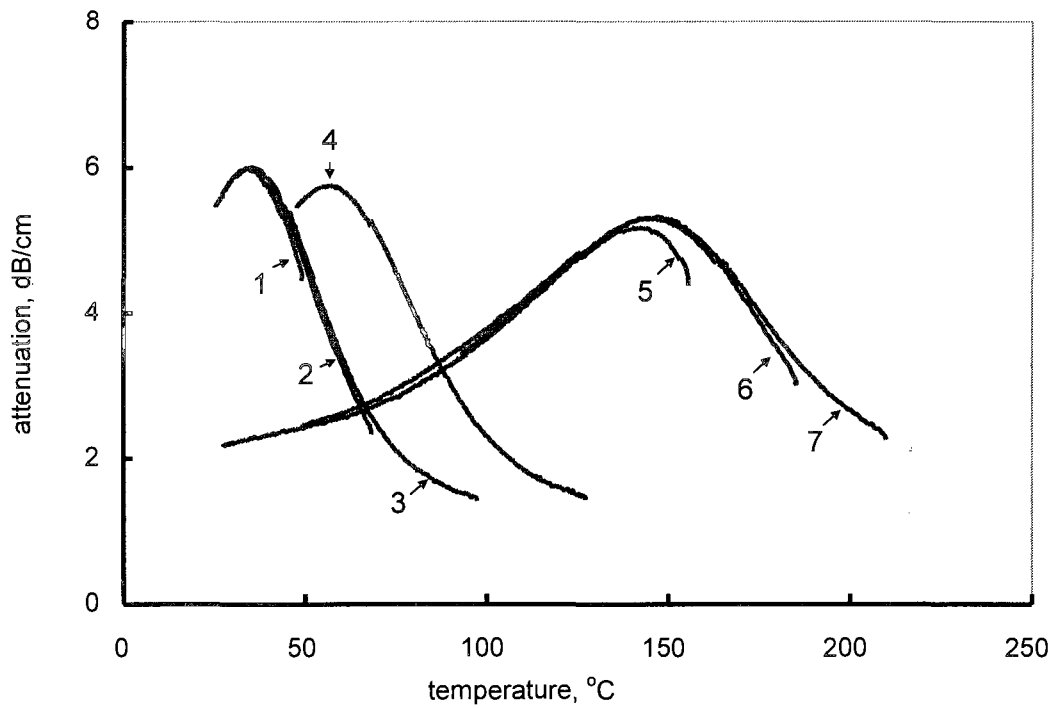
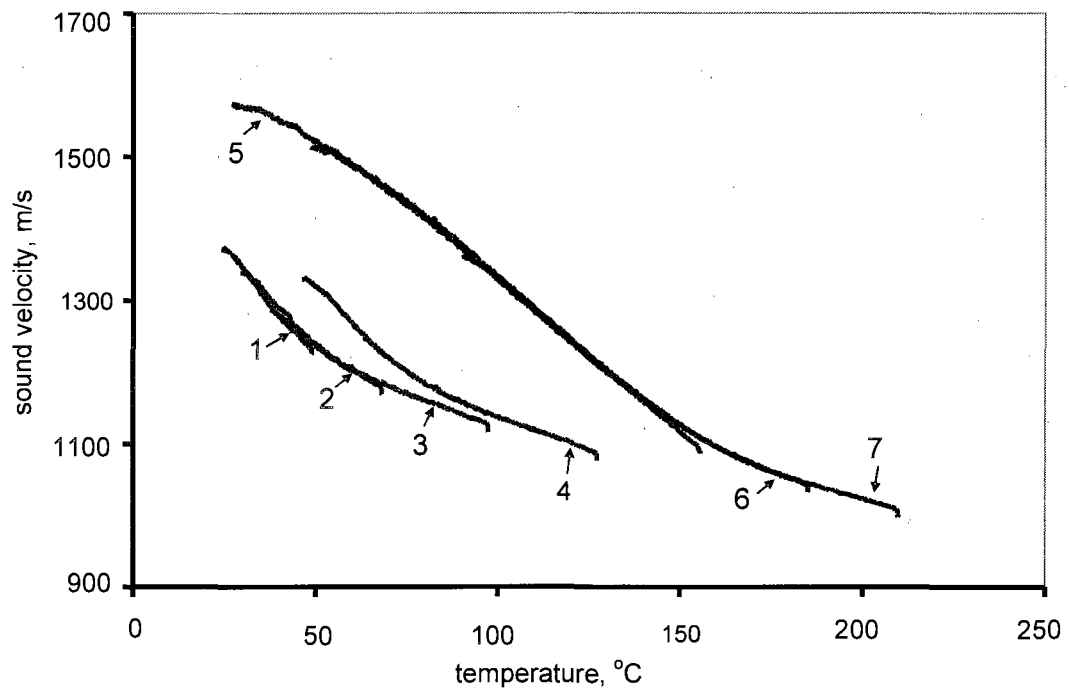


Figure 5.24. Changes in thermo-acoustic parameters of the epoxy with increasing reaction temperature¹⁴⁷. Maximal temperature of cure: 1-50°C, 2-70°C, 3-100°C, 4-130°C, 5-160°C, 6-190°C, 7-210°C.

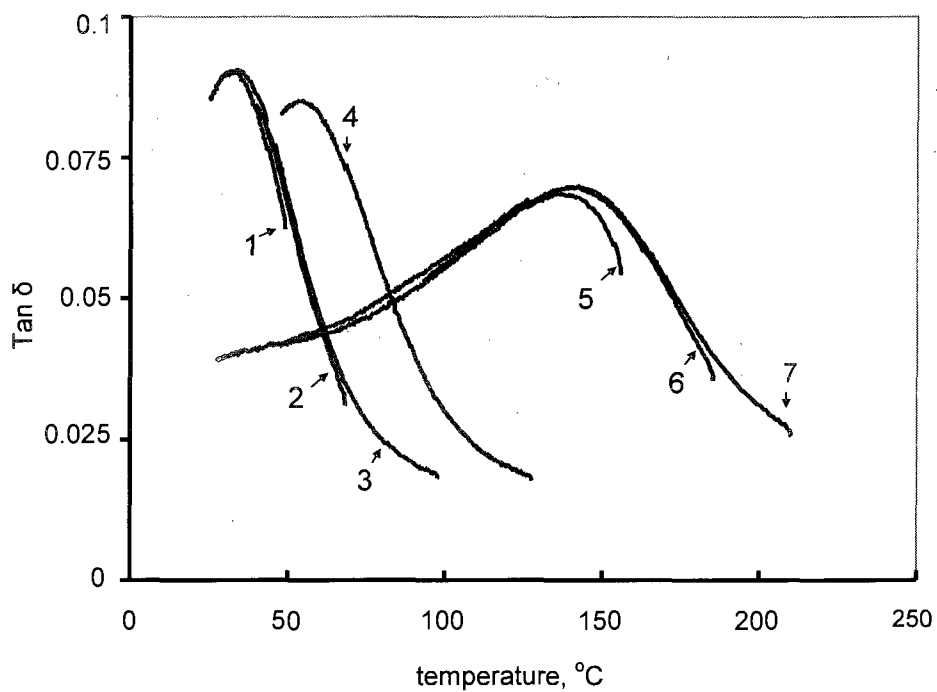


Figure 5.25. Changes of the loss factor $\tan \delta$ maximum during cure. Indexes are as in Figure 5.24¹⁴⁷.

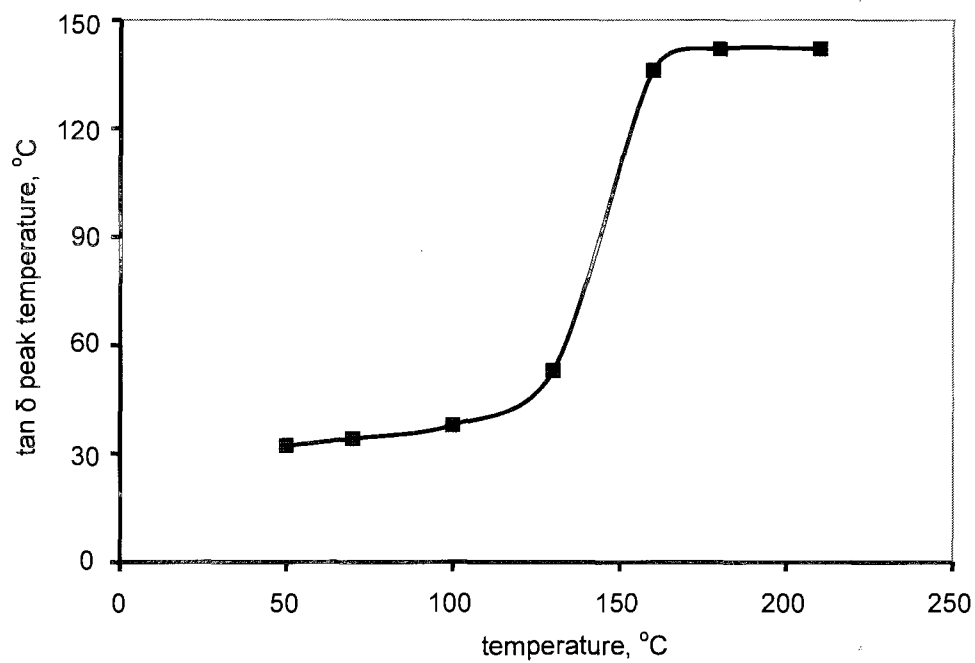


Figure 5.26. Changes of the loss factor $\tan \delta$ maximum during cure¹⁴⁷.

strength. Thus, the curing regime (temperature and time of reaction) determines the kinetics and extent of the reaction.

When plotted against T_g determined as the peak in loss factor $\tan \delta$ curve, sound velocity in the epoxy was found to correlate closely¹⁴⁷, which is represented in Figure 5.27. This linear correlation supports the idea that T_g and cross-link density play the key role in the sound propagation in polymers.

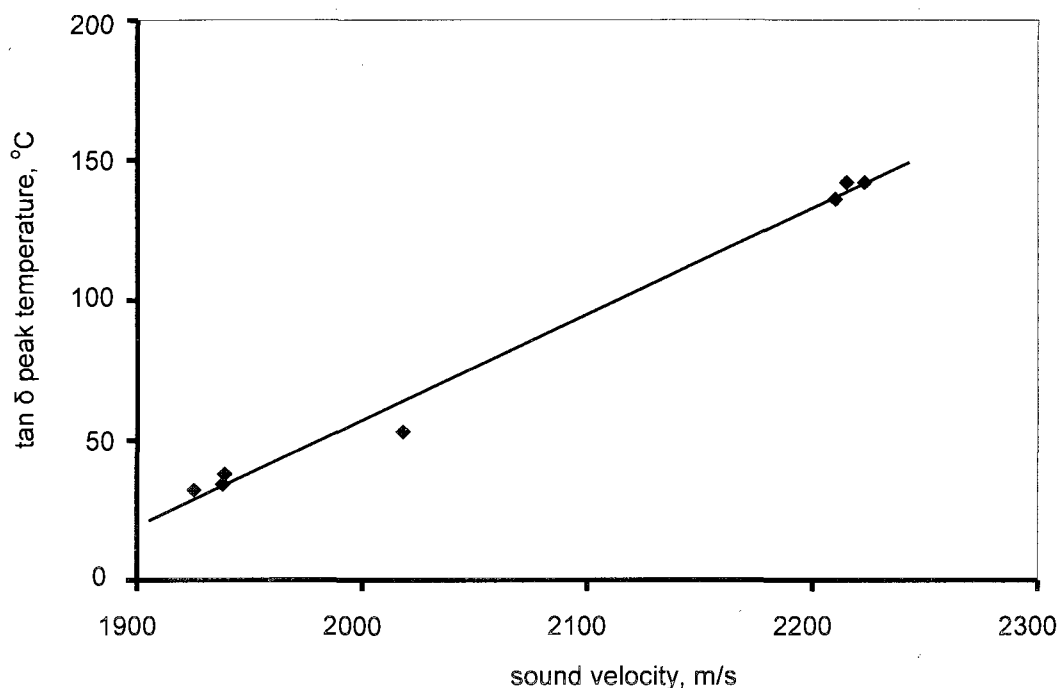


Figure 5.27. Correlation of the sound velocity of the epoxy and the $\tan \delta$ maximum¹⁴⁷.

Thus, transition of the epoxy from viscous liquid (or gel) into solid is accompanied with significant changes in the elastic moduli of the adhesive and, consequently, in its acoustic properties. Measurement of the acoustic parameters of the adhesive can be used for in-line, non-destructive cure monitoring and quantitative evaluation of the cross-linking degree and cohesive properties of the adhesive.

5.6. Cohesive Strength of Structural Adhesives

Cohesive strength of the adhesive depends on attraction forces that exist between particles (molecules) of the adhesive. The type of force (covalent, hydrogen or van der Waals) depends on the nature of the adhesive. The effect of cohesive properties on the adhesive joint strength is measured by bulk effect of the adhesive and by total mechanical properties of the bond joint.

Destructive tests performed after acoustic investigations show that the cohesive strength of the joint correlates with acoustic parameters and “mechanical” reaction extent. Samples cured at 140⁰C and higher show adhesive type of failure with shear strength 12-13 MPa. This indicates that acceptable joint strength is achieved at the reaction extent higher than 95%.

As was mentioned earlier, sound velocity greatly depends on intermolecular interaction. So it is logical to make the assumption that cohesive strength of the adhesive joint should correlate with elastic and acoustic properties of the adhesive ¹⁸². To determine cohesive strength, specimens for lap shear test were prepared as described in Section 4.1.3. A hypothesis was that the increase in sound velocity reflects an increase in intermolecular interaction and growth in cohesive strength of the adhesive. It was suggested that a non-destructive method able to measure elastic modulus of the adhesive can help estimate bond strength ¹⁴⁷. Destructive tests shown in Figure 5.28 confirm this. As seen, sound velocity and joint strength increase in similar manner. For curing conditions of 120 ⁰C, strength of the joint stays low for the first 30 minutes, then, increases sharply and reaches a plateau by 90 min. of cure. At 180 ⁰C, the strength increases sharply from the beginning of the cure reaction and reaches a maximum value by 15 min. This behavior is similar to the changes in longitudinal sound velocity during cure, which is shown in Figure 5.13. It is necessary to note that this type of adhesive failure was observed only after the strength of the joint reaches a plateau (13-14 MPa for 180 ⁰C and 12-13 MPa for 120 ⁰C). The maximal strength reached at 120⁰C is slightly lower than at 180⁰C. This corresponds to the lower extent of the reaction (0.9) reached at 120 ⁰C by cure time 210 min. compared to 0.9 at 180 ⁰C (Figure 5.16). However, this

strength difference is small and both values are acceptable from a technological point of view.

The sound velocity in the adhesive was evaluated non-destructively in the cured samples and then the samples were prepared for destructive tests. Results of both experiments for 180°C are shown in Figure 5.29¹⁴⁷. Sound velocity increases in the same manner as joint strength. A more gradual increase of the velocity in the beginning of cure compared with the curve in Figure 5.29 can be explained by different heating rates of the adhesive in the joint compared with experiment chamber and 1-3 min. delay in data recording in cure monitoring experiments. The maximum values of sound velocity and strength are both reached by 12-15 min. Figure 5.30 demonstrate correlation of the joint strength and sound velocity of the adhesive in the joint¹⁴⁷. Similar correspondence was shown for T_g value (Figure 5.27). It is to be noted that the absence of data in the middle range of both velocity and cohesive strength/ T_g . A possible reason can be the rapid reaction rate at elevated temperatures.

Velocity changes reflect variations in the cross-linking degree of the adhesive during the cure reaction. Joint cohesive strength develops after gelation of the adhesive at the final stages of cross-linking. Correlation of longitudinal sound velocity with cohesive strength was reported earlier¹⁹⁸. Authors have reached variations in cohesive strength by mixing two-part adhesive in different proportions and have observed a linear correlation of the investigated parameters. In this work, different cure degree was reached by varying cure time at constant resin/hardener ratio. Both sound velocity and joint strength reach a plateau at the same time.

Thus, reaching a certain sound velocity indicates development of full cohesive strength of the joint. Cohesive properties of the epoxy adhesive may be indirectly evaluated by monitoring its acoustic parameters. It is not suggested that this technique will provide precise evaluation of the cohesive strength of the joint and may replace other techniques currently used, as cohesive strength depends on many other factors as well. Nevertheless, this method can act as an indicator for reaching optimal cure state of the adhesive at different cure regimes.

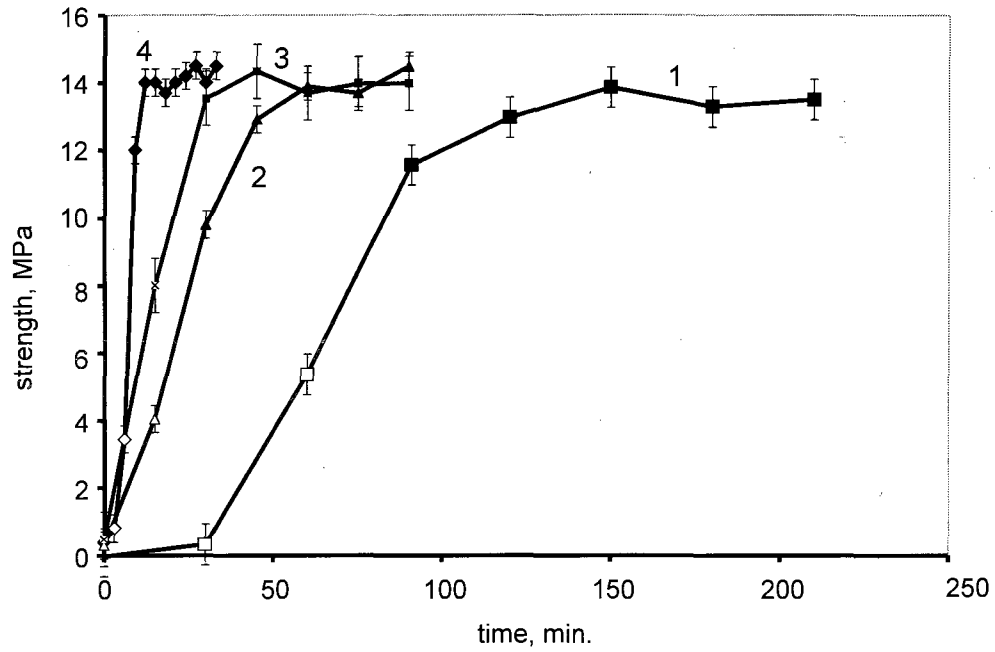


Figure 5.28. Dependence of the joint strength on time of the cure at 120°C (1), 140°C (2), 160°C (3), and 180°C (4)¹⁴⁷. Unfilled data points on the graph (□ ◇ △) represent cohesive type of joint failure; filled ones (■ ◆ ▲) show adhesive failure of the joint.

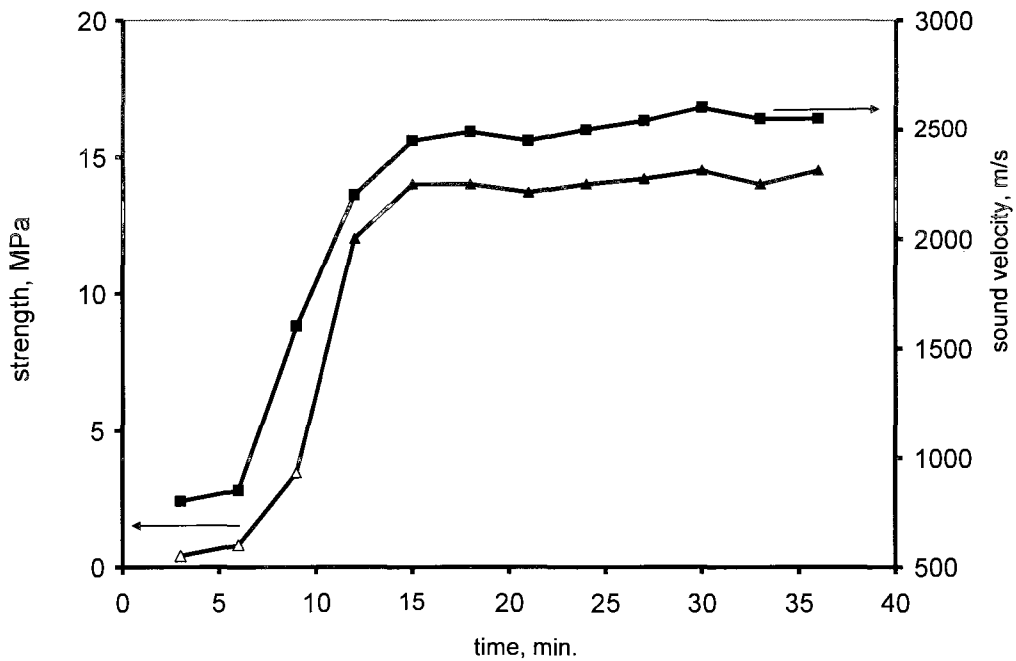


Figure 5.29. Dependence of the joint strength and longitudinal sound velocity on the time of the adhesive cure at 180°C¹⁴⁷.

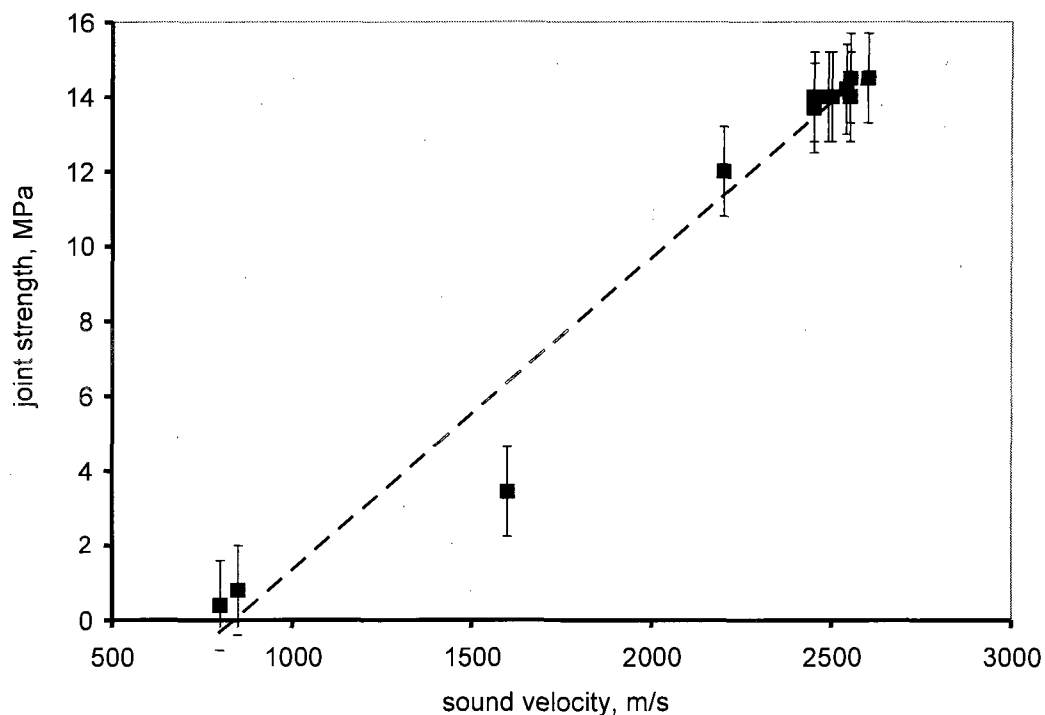


Figure 5.30. Correlation of longitudinal sound velocity of the adhesive to joint strength¹⁴⁷.

On the basis of the information obtained, it can be concluded that the ultrasonic technique is a useful method to characterize viscoelastic properties of structural adhesives and predict cohesive strength of adhesive joints since sound velocity and attenuation reflect changes in mechanical properties of the adhesive. Reaching full reaction conversion is important as meaningful structure-property relationships between different systems can only be made by considering fully cured materials.

CHAPTER VI

Microstructure of the Adhesive-Metal Interface

Scanning acoustic microscopy is suitable for polymer study. The low acoustic impedance Z (compared to the water impedance) allows more ultrasound transmission into material through the surface. Low impedance also means that a small change in this parameter leads to greater variations in the reflection coefficient and correspondingly produces more image contrast. Thus, even little changes in density or elastic properties in the polymer should be detected by scanning acoustic microscopy and visualized as the acoustic images.

On the contrary, metal has high acoustic impedance which creates additional complication for imaging of adhesive joint interfaces. Strong reflection from the steel/adhesive interface leads to the appearance of elastic oscillations in the steel, which attenuate after the initial pulse. These reflections hide the useful pulse reflected from the lower boundary of adhesive layer. With the acoustic impedances for steel and adhesive equal to $4.3 \times 10^7 \text{ kg m}^{-2} \text{ s}^{-1}$ and $3.0 \times 10^6 \text{ kg m}^{-2} \text{ s}^{-1}$, respectively, it becomes obvious, that steel/adhesive interface reflects a lot of acoustic power. The reflection coefficient in this case is equal to $R = 0.87$, whereas the transmission coefficient is $T = 0.5$. The situation is even worse for the water/metal interface. This problem can be overcome by using a coupling liquid with higher impedance. A mixture of glycerol/water was used as a coupling liquid in this study. By try and error approach, the 1 to 5 ratio was chosen because it allows a decrease in the reflection coefficient while the increase in attenuation due to the coupling liquid is still acceptable.

6.1. Microstructure on the Intact Epoxy Adhesive-Steel Interfaces.

The microstructure of bulk adhesive, substrate surface and interface between them influence the strength and performance of the joint in equal manner. The complex nature of the epoxies, especially highly cross-linked structural adhesives complicates studying of the adhesive interface microstructure. Both molecular and physical microstructures are often presumed. It is known that the adhesive's microstructure substantially affects the

mechanical properties of the joint. High resolution acoustic microscopy is able to non-destructively visualize the microstructure of the adhesive material, as well as investigate the distribution of different physico-mechanical properties throughout the material and thus estimate the bond quality. Both aspects are important for examination of changes in the adhesive-adherent interface during the curing process, as well as during the joint lifetime that often undergo to external influences (i.e. load, fatigue, chemical reactions and so on). Visualization of the adhesive joint's microstructure in the form of B- and C-scans provides direct information about the nature, structure and spatial distribution of the defects. The method uses high-frequency acoustic waves that yield an assessment of the physico-mechanical properties of the material, such as density, elasticity and viscosity. The pulse-echo scanning acoustic microscopy method is still the most reliable for examination of internal structural defects in various types of materials.

Six identical single lap joints were prepared to study the formation of microstructure on the metal-adhesive interface. Metal thickness was 0.7 mm; thickness of the adhesive layer was maintained at 0.3 mm with spacers. Each specimen was cured separately for a different length of time, at a constant temperature of 180 °C and was immediately cooled after. This approach allows reaching different cure states of the adhesive. Samples were then scanned with Sonix HS-1000 SAM with acoustic lens of 250 MHz central frequency.

Resolution in acoustic microscopy depends on lens configuration (frequency, focus position) and material properties (stiffness). Therefore, the choice of frequency and imaging conditions depends on the type of material. Lateral resolution l (minimal distance between two distinguishable points) is calculated as (4.15) and equal to 50 μm for 250MHz acoustic frequency. This frequency gives focus depth in steel equal to 650 μm which is sufficient for the focusing directly on the intact metal-adhesive interface of the real joint. Axial resolution (depth of the structures involved in image formation) calculated as (4.18) is 30 μm . This quite low resolution is compensated by the ability to penetrate deep into the adhesive joint and visualize the intact internal structure. Although images with this resolution are not able to provide detailed information about material microstructure, some conclusions still can be made.

Let's now consider the nature of the contrast difference in the images. The reflection coefficient R at the metal-adhesive interface and, correspondingly, values of pixel intensity I on C-scan image depend on the difference of the density and sound velocity of two materials:

$$I \propto \left(\frac{\rho_2 c_2 - \rho_1 c_1}{\rho_2 c_2 + \rho_1 c_1} \right) \quad (6.1).$$

Since the properties of the steel stay constant during the adhesive cure process, the variations in the reflection coefficient value are due to variations in acoustic impedances of the adhesive only. So, these changes are caused by modification in either density or elasticity of the material. Since shrinkage of the adhesive used is very low, we assume that all changes in acoustic impedance are due to variations in elastic moduli.

To visualize the adhesive-steel interface, samples were cured for different times, and then 10x10 mm acoustic images were prepared with SAM at 250MHz acoustic frequency. Figure 6.1 demonstrates the development of microstructure in the epoxy adhesive/metal interface from curing at 180°C¹⁴⁷. It is important to remember that both metal substrate and adhesive contribute to the acoustic image of the interface. However, modifications in the acoustic image arise from changes in adhesive microstructure. The image of the uncured adhesive –metal interface does not have a clearly expressed structure with a small difference in signal intensities. After the material has been exposed to curing conditions, the image has greater contrast, granular structure of the interface appears and becomes completely developed by the end of the curing process (30 min.). Higher sound velocity of the cured adhesive is related to a stronger contact-three-dimensional network adhesive that has increased rigidity. Overcured adhesive, which was exposed to a higher temperature (200°C), becomes more brittle and adhesion strength decreases. The acoustic image of the overcured adhesive-metal interface becomes more fragmentary and starts to reveal regions with higher amplitude of the reflected signal, which indicates a stiffer material and usually corresponds to some physical and chemical changes in the adhesive and/or appearance of micro-defects at the interface. That usually corresponds to physical changes in the material's properties

and/or appearance of micro-defects at the interface and in bulk. Thus, micro-structural characteristics of the adhesive can give important insight on the process of adhesive cure inside the joint.

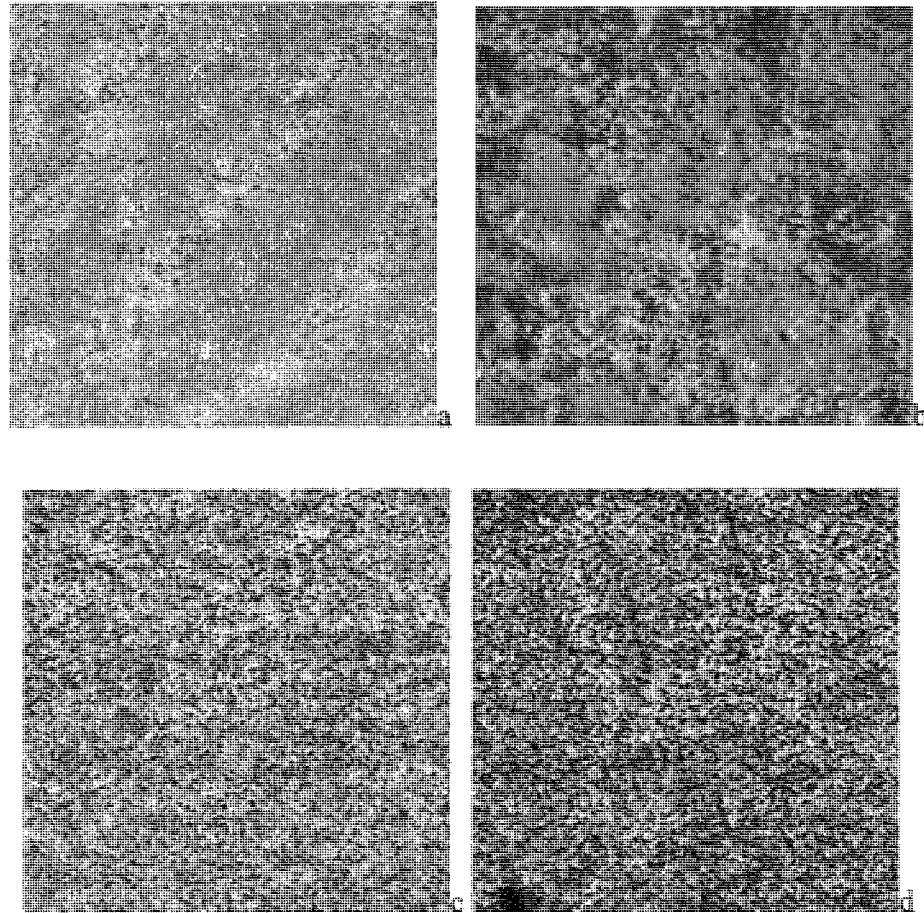


Figure 6.1. Development of the microstructure of metal-adhesive interface during polymerization reaction at 180°C ¹⁴⁷, 250 MHz. samples were cured for 0 (a), 10 (b) and 35 (c) min. (d)-image of the interface cured at 200°C for 45 min.

Each 500x500 pixel image was stored as a matrix in Octave, a software package primarily intended for numerical computations. Each matrix was decomposed into 100 matrices of equal dimensions. Properties such as the minimum value, maximum value, and mean value of the set of matrices were then calculated. Performing measurements on a set of smaller regions allows us to determine many local maxima and minima which in turn enable one to calculate an error bound. The results were then averaged, producing a result representative of the entire 1cm² region. The minimum and maximum intensities of

these images were compared. Figure 6.2 clearly indicates a decrease in both properties during the curing process, as expected¹³⁴. If compared with changes in reflection coefficient measured during isothermal reaction monitoring at this temperature (Figure 6.3), it is easy to see a similar pattern. Thus, intensity of the acoustic images reflects changes in the adhesive's elasticity.

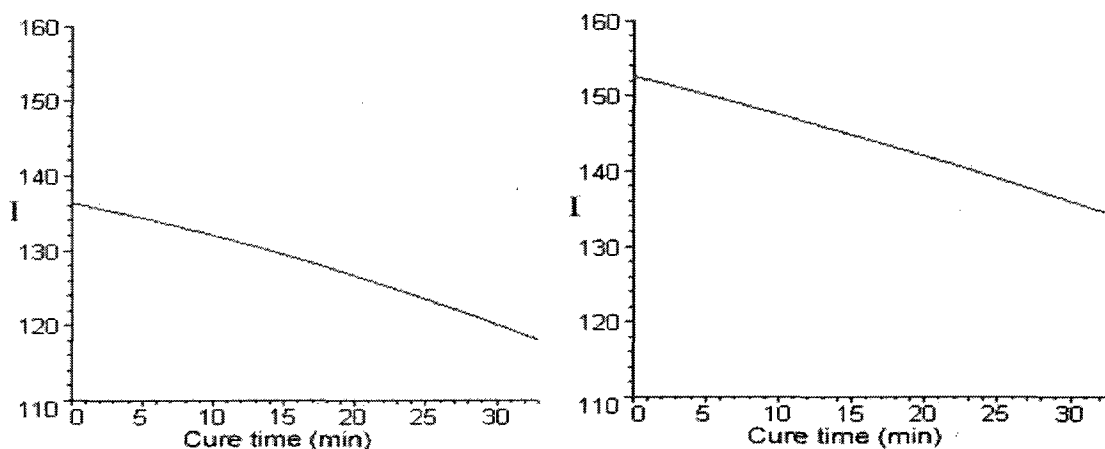


Figure 6.2. Minimum (left) and maximum (right) intensity as a function of cure time¹³⁴ (with kind permission of Springer Science and Business Media).

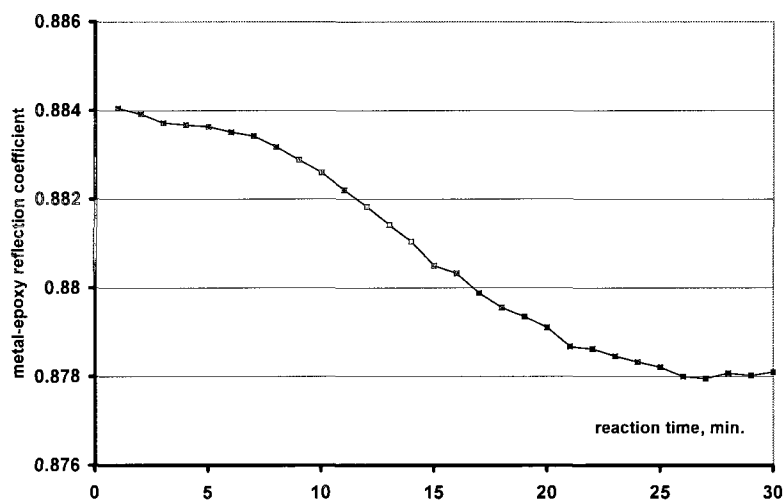


Figure 6.3. Reflection coefficient for steel-adhesive interface during polymerization reaction.

Qualitative description of the acoustic image as a “granular structure” can be supported by quantitative estimation of the structural parameters. Statistical image

processing can provide valuable information about interface state. There are two possible characteristics: contrast ratio and specific size of the grains on the image.

The contrast ratio can be determined by analysis of the image histograms. As was mentioned earlier, the acoustic image actually represents a stochastic spatial distribution of the elastic moduli in the adhesive material. The image histogram, where a number of pixels of certain brightness are presented as a function of the pixel brightness, gives us statistical representation of a distribution of elastic moduli in the adhesive as this parameter is intrinsically related to amplitude of the reflected signal. Width of the histogram shows the contrast ratio of the image.

A commercial adhesive used in this study is toughened material, which forms second-phase particles during hardening. Phase separation is shown on the acoustic images 6.1 (b) and (c) as appearance of granular structure and increasing of histogram standard deviation (SD). Comparison of histograms (a) and (b) on Figure 6.4 shows that during the curing reaction inhomogeneity of the material increases from 9 % to 30%. Another noticeable change is a shift of the median towards the lower values of signal intensity which represents increasing of acoustic impedance of the adhesive material during the curing process. Changes in average acoustic impedance calculated from the histogram's shift correlates well with direct measurements of acoustic properties of the adhesive. Increased sound velocity of the cured adhesive is related to a stronger three-dimensional network in the adhesive that has increased rigidity. Thermal degradation of the adhesive joint, due to exposure to elevated temperatures, leads to further increasing in width of image histogram and strength reduction as shown on Figures 6.1 (c) and 6.4 (c). Cross-sections show the amplitude variations across the images.

Size of the clearly visible objects can be measured directly on the images. However, irregular shape and diffuse boundaries of the grains reduce precision of such measurements. More reliable data may be obtained by application of Fourier transform to the acoustic images. The original nature of acoustic image is digitized by a two dimensional function $f(x,y)$, so a Fourier representation of acoustic image is a statistical distribution of "spatial frequencies" is:

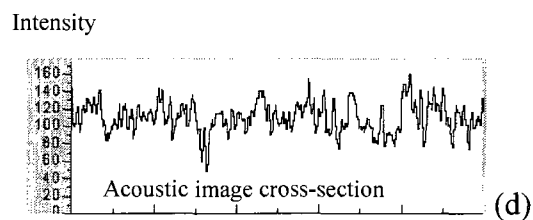
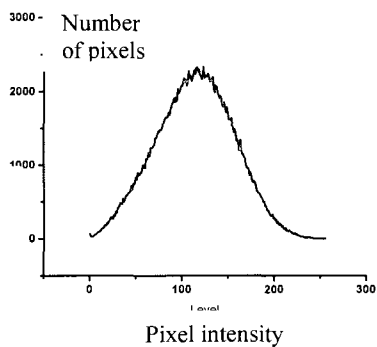
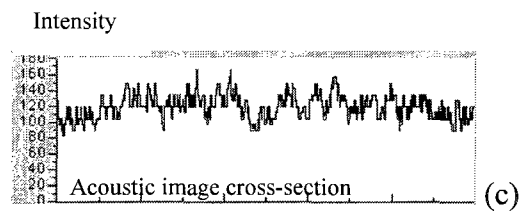
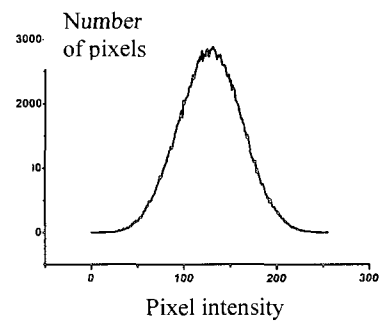
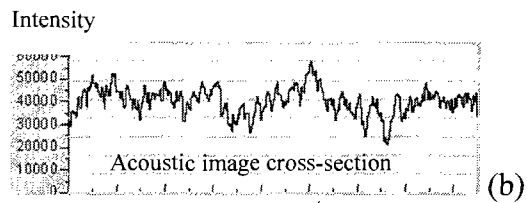
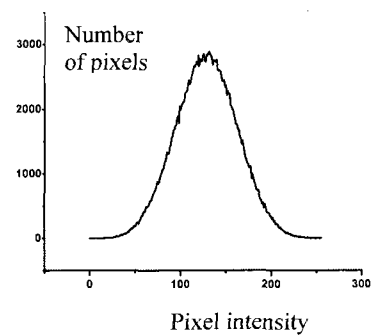
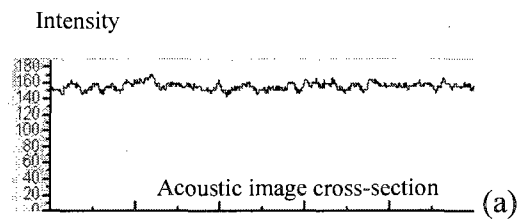
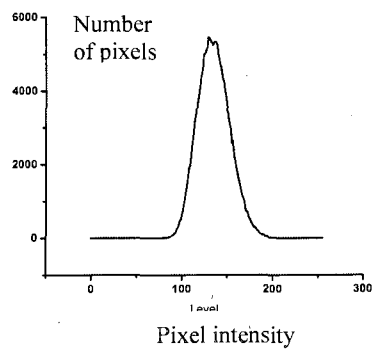


Figure 6.4. Histograms and cross sections of the acoustic images on Figure 6.1.

$$F(\omega_x, \omega_y) = \iint_{-\infty}^{\infty} f(x, y) e^{-i\omega_x x} e^{-i\omega_y y} dx dy \quad (6.2)$$

where ω_x, ω_y – coordinates in frequency domain. These reverse values of periods of regular patterns existing on the acoustic image.

Application of 2D Fourier transform to acoustic images of the adhesive-steel interface produces a matrix of complex number-spatial frequency domain representation. The amplitude of this matrix is shown in Figure 6.5 (a) in the form of a contour map and in Figure 6.5 (b) in the form of a solid surface. Structures with different periods produce peaks with different positions on the diagram.

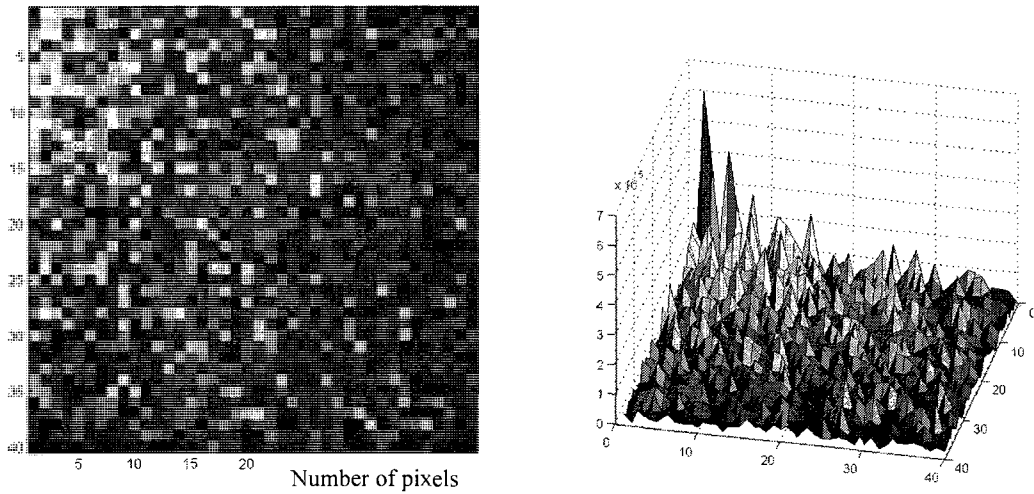


Figure 6.5. 2D Fourier transform of the acoustic images (Figure 6.1.b).

Both dimensions represent a distribution of spatial frequencies along the image; the scale shows the number of periods per full image length. The images are limited by half of the Nyquist frequency. As seen from the images, most of the spectrum is concentrated in the low frequency area. Amplitude distribution is approximately the same in both directions, which illustrates isotropy of the epoxy adhesive on this scale. Figure 6.6 (a) shows an average section of the Fourier matrix along both directions. This one-dimensional curve shows a rise in amplitude at the points with frequency maxima. To clarify this graph interpretation and coordinate data to the interface structure, these

data were recalculated into the pixel periods. Figure 6.6 (b) represents dependency of the spectral amplitude from period of the interface structure. Besides overall increasing in the peaks' amplitude, there are several peaks corresponding to the spatial periods of 10-18 pixels that describe granular interface structure. These peaks describe the presence of the granular structures with average distance between centers $300\mu\text{m}$.

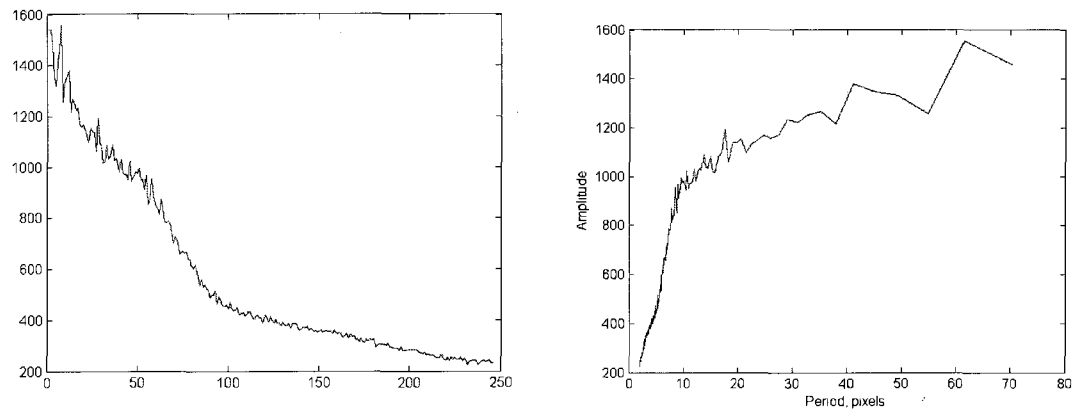


Figure 6.6. Analysis of the granular structure on the acoustic image in Figure 6.1. (b).

Similar analysis of other acoustic images is presented in Figures 6.7 and 6.8. Comparing images, it is easy to see that uncured epoxy is practically uniform and homogenous and its spatial spectrum of the acoustic scan is narrow. During the cure process, inhomogeneity increases. Analysis of the image brightness and size of the granular structures may lead to some conclusions about the nature of these structures. Hollow glass spheres added to the adhesive to increase toughness and maintain adhesive layer thickness, is 0.2-0.3 mm. Silica granules are also 100-200 μm in diameter. Rubber toughened regions are usually significantly smaller in size and beyond the acoustic frequency resolution used. However, it is possible that slight gray variations represent variations in density.

Another possible explanation for epoxy heterogeneity is the nature of the cross-linking agent, DDA, which is added to the adhesive system in a crystalline form. Thus, some degree of heterogeneity can arise from possible incomplete mixing and/or from increased concentration of DDA in microcrystal melting spots. Multiplicity of chemical

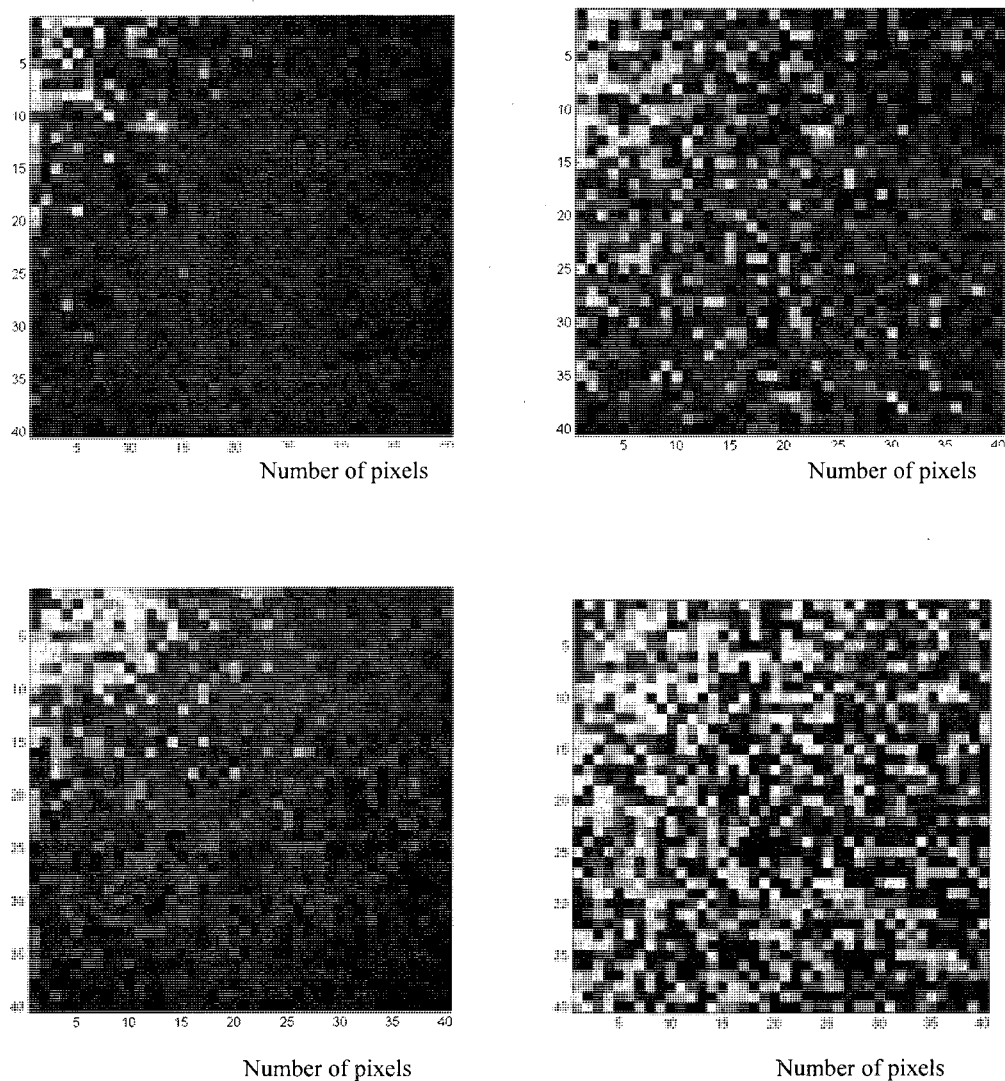


Figure 6.7. 2D Fourier transform of acoustic images of the adhesive-metal interfaces from Figure 6.1. Samples were cured for 0 (a), 10 (b) and 35 (c) min. (d)-image of the interface cured at 200°C for 45 min.

reactions with a different rate involved in adhesive hardening also could lead to the inhomogeneity in the adhesive's microstructure¹⁸⁸.

Overcured epoxy adhesive can be characterized by decreased elasticity. As a result, intrinsic thermo-elastic stresses lead to a partial bond breakage and appearance of micro-cracks and voids. This leads to an overall decrease in adhesive strength. The acoustic image of a thermally damaged interface is very similar in structure and spectrum when compared to the control sample. However, contrast of the image becomes higher and structural elements of larger size appear which correlates with micro-crack

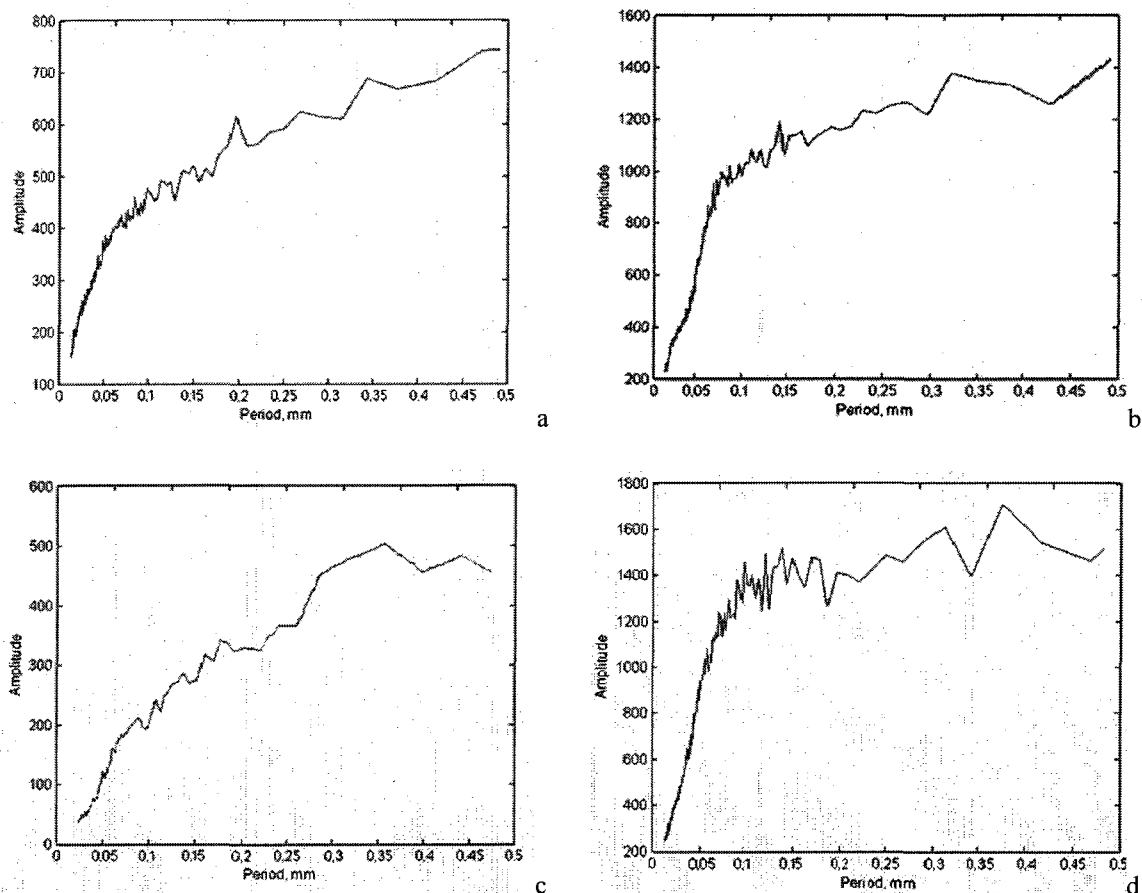


Figure 6.8. Analysis of the granular structure on the acoustic image in Figure 6.1. Samples were cured at 180 °C for 0 (a), 10 (b) and 35 (c) min. (d)-sample was cured at 200°C for 45 min.

formation. Morgan has shown that the major degradation mechanism, for epoxies exposed at elevated temperatures, is dehydration ¹⁶⁷.

Results of destructive tests shown in Figure 6.9 indicate that appearance of the granular structure coincides with a significant increase in joint strength. Degraded adhesive shows decreased strength with combined adhesive and cohesive types of failure; which allows imagining the micro-crack formation not only on the interface, but also in the bulk adhesive layer.

Fracture surface analysis (Figure 6.10) made with electron microscopy is in agreement with the acoustic imaging method. Morphology of the fracture surface shows the presence of two distinct phases. The continuous phase is the epoxy resin and the

other one is the toughener. Silica and glass sphere particles serve as tougheners to stop crack propagation as stated in the MSDS for Betamate. Size of the particles is

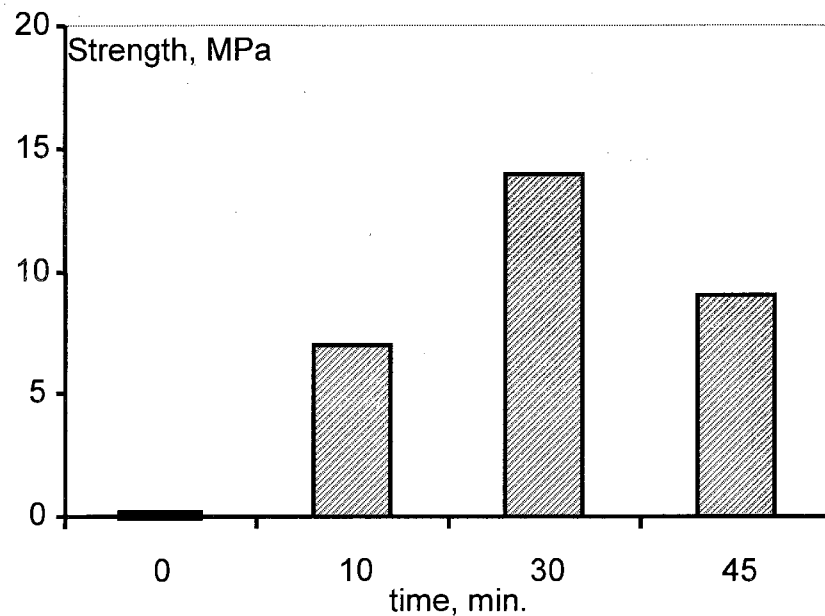


Figure 6.9. Destructive test results. Strength of the adhesive joints.

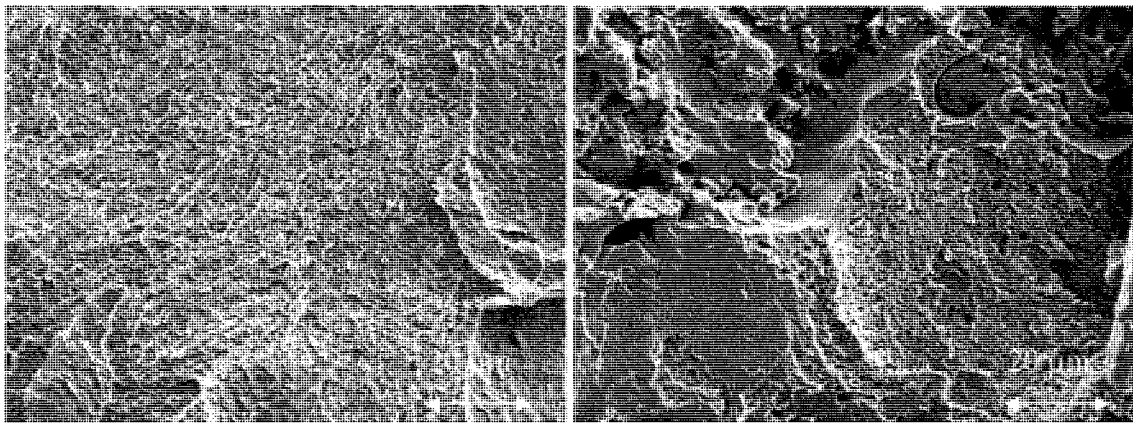


Figure 6.10. Scanning electron micrographs of fracture surface of tensile test. (a)-properly cured adhesive, (b)-thermally degraded adhesive. x1500 magnification.

approximately 100-200 μm . The shallow cavities from the silica particles appear at the surface due to good particle/matrix adhesion. The crack propagates through the matrix above or below the particles. The image of degraded adhesive shows more defects in the structure.

6.2. Analysis of the Adhesive Layer Cross-Section in Adhesive Bonds

Elastic properties of the epoxy adhesive in an adhesive joint were analyzed. A cross-section of the adhesive joint was cut, mounted and polished. Acoustic images of the joint cross-section are shown in Figure 6.11. Due to a huge difference in hardness values between steel and epoxy adhesive, it is almost impossible to develop the proper methodology to prepare these two materials being equally polished for successful interface visualization. On the acoustic images prepared on the Elsam SAM with 400 MHz acoustic lens, the interface line is quite uneven. Darker regions along the interface with the metal are visible on all scans. Darker color on the acoustic image means lower reflection coefficient which is due to higher density and/or sound velocity and correspondingly elastic modulus. Propagated cracks are visible on the thermally degraded epoxy. Most likely they were formed during sample cutting and polishing because of increased material elasticity.

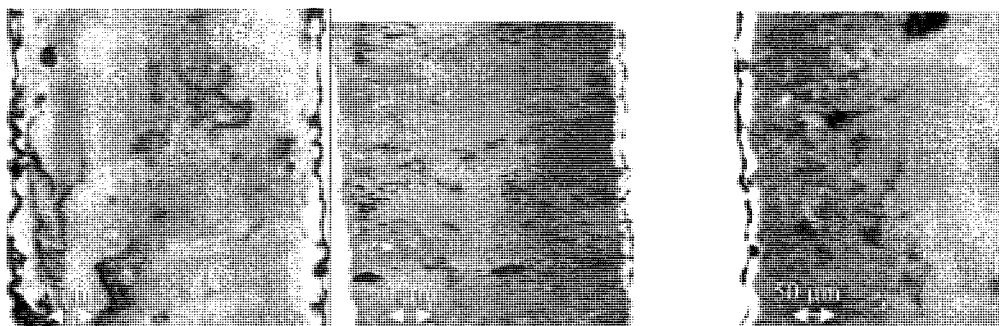


Figure 6.11. Acoustic images of the adhesive joint cross section. Adhesive layer thickness is 0.3 mm. Adhesive was hardened at 180 °C during (a)-10 min, (b)-30 min. (c)-adhesive was hardened at 200 °C during 45 min.

Microhardness (MH) and Young's modulus values were determined by the dynamic microhardness method (Figure 6.12 and Table 6.1). The MH technique is able to provide information about local properties of the material. The stress required to deform the amorphous network involves displacement of bundles of chain segments against the local restraints of secondary bond forces and internal rotations¹⁸⁹. It shows that both Young's modulus and microhardness is slightly higher in the regions close to the interface. For epoxy-silane-glass interface it was shown that epoxy-silane interface has

higher cross-link density than in the bulk epoxy⁷. For epoxies, the hardness value depends on thermal history of the sample and free volume in the material in the glassy state which is physical aging. Increased hardness and elastic modulus is due to increased cross-link density in the regions close to the interfaces. Safavi¹⁹⁰ performed a study of the elastic properties across an epoxy/aluminum interphase with scanning acoustic microscopy and showed that the interphase region has larger acoustic wave velocity parameters than the bulk adhesive what corresponds to higher cross-link density. Koutsky⁸⁹ has found that epoxy adsorbed on a copper substrate surface is replaced later by amine hardener. As a result of this event, a region with high amine concentration and, correspondingly, with higher cross-link density exists closer to the substrate.

These results are contrary to the data about increased concentration of the DDA on metal surface. Preferential adsorption of the amino groups on the zinc oxide surface of the electro galvanized steel lead to imbalanced ratio of epoxy and DDA hardener and therefore to a less dense cross-linked network.

Thus, acoustic images of the metal–adhesive bonds, produced at different stages of the adhesive curing reaction, reflect the structure in bulk and at the interface. Quantitative analysis of the images allows us to track changes in the material.

Table 6.1. Distribution of Young's modulus across an adhesive joint.

| Cure time | 10 min./180 oC (MPa) | 30 min./180 oC (MPa) | 45 min./210 oC (MPa) |
|-----------|----------------------------|----------------------------|-------------------------|
| 1 | 3.41 | 3.30 | 3.33 |
| 2 | 3.01 | 2.75 | 2.73 |
| 3 | 2.79 | 2.72 | 2.84 |
| 4 | 3.01 | 2.75 | 2.73 |
| 5 | 3.41 | 3.30 | 3.33 |

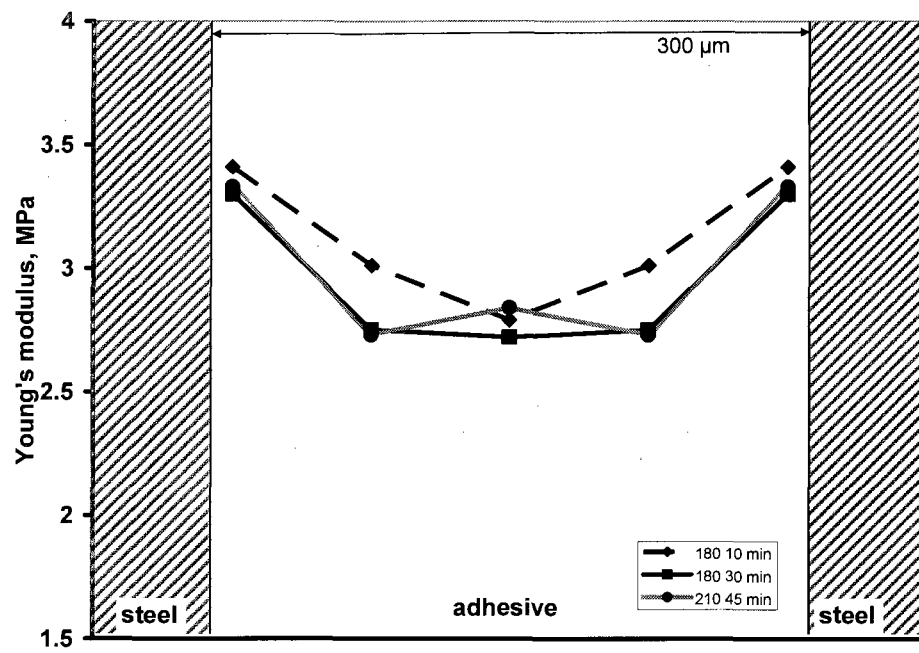


Figure 6.12. Young's modulus values measured across the adhesive layer in adhesive bonds.

CHAPTER VII

Analysis of Adhesive Joint Deterioration

Scientists often define degradation as a “negative change in chemical structure, physical properties as appearance of polymer” (Wool, 1995).

As high strength and load transferring ability are the essential features for structural adhesives; these properties must be retained for the adhesive joint's entire service life. A huge number of publications regarding the modeling and experimental work of an adhesive's behavior under various environmental conditions have been published over the last decades¹⁹¹⁻¹⁹⁵. Despite this fact, there is still a problem in predicting the real service life of structural adhesive joints due to their complex structure and large number of factors that influence the adhesion quality. Another problem is revealing the first stages of degradation early on which often are undetectable by conventional non-destructive techniques.

In most of the cases, the properly prepared adhesive joint is broken cohesively. However, degraded or stressed joints fail at the interface. It is the interface that becomes the most important place for influence of external factors. So, it is important to investigate the interface area to understand how environmental factors influence the adhesive joint's performance. Evaluation of the interfacial region of an adhesive bond joint has significant practical importance as it indirectly indicates the adhesion strength and can reveal appearance of defects in the interface during the production process and after environmental influence. It is important to investigate the adhesive within the joint because the adhesive itself responds entirely differently to environmental factors compared with the joint assembly. A number of methods are used for evaluating the adhesive joint microstructure: visual inspection; light microscopy; electron transmission and scanning microscopy; X-rays; and IR-radiometry; thermography.

Conventional acoustic methods for evaluation of the adhesive joint are based on detection of defects in the interface, which is assumed to lead to a decrease in the joint

strength. There are several reported works that investigate adhesive bond degradation with acoustic techniques. Moidu et al. used open-faced specimens to characterize the water intake¹²⁵. Rokhlin and co-workers found a correlation between the frequency spectrum and joint strength¹⁹⁶. As frequency resonance strongly depends on the specimen configuration it is of little use as a non-destructive technique. Most of the studies were performed with aluminum bonded structures over the last decades, as this substrate was most widely used^{125, 196, and 197}. However, these days steel and other metal substrates have become more utilized.

Today there is no non-destructive method to evaluate the strength of an adhesive joint. Lack of such a method limits widening the use of adhesive joint. Also, no strong correlation exists between adhesion strength and the presence of some defects, both at the interface and in bulk adhesive. The presence of defects and their parameters are more likely to indicate insufficient joint manufacturing than possible joint failure^{113, 146}. However, many structural defects have a negative influence on the integrity of the joint and decrease its strength. The following factors may also have an influence on the adhesion strength: adhesive thickness, joint type and geometry, composition of the adhesive, and substrate surface preparation. There are three main types of adhesion defects: complete absence of the adhesive, poor adhesion and poor cohesive strength.

The objective of this part of the study is an analysis of adhesive joint deterioration under various factors. Another goal is to evaluate the capability of scanning acoustic microscopy to visualize any changes in the interface structure at early stages of the adhesive joint deterioration. Correlation of macro-signs of adhesive joint deterioration with bulk adhesive behavior is sought to be practical importance.

7.1. Major Defects Appear in Adhesive Joints

Classification of defect types can be found in the surveys given by Adams et al. and Munns and Georgiou^{113, 128, 146}. Adams and Cawley¹¹³ classify defects by two types according to their location: defects in the bulk of the adhesive layer and defects at the adhesive-substrate interface. Bulk defects in the adhesive cause a decrease of cohesive

strength because cohesion determines the binding properties of the adhesive. Defects at the adhesive-substrate interface relate to the bonding process reducing the overall adhesive strength.

In a wide review of non-destructive testing of adhesively bonded joints, Adams and Drinkwater¹⁴³ have described three basic types of defects in simple adhesively bonded systems (Fig. 7.1): gross defects, poor adhesion, and poor cohesive strength.

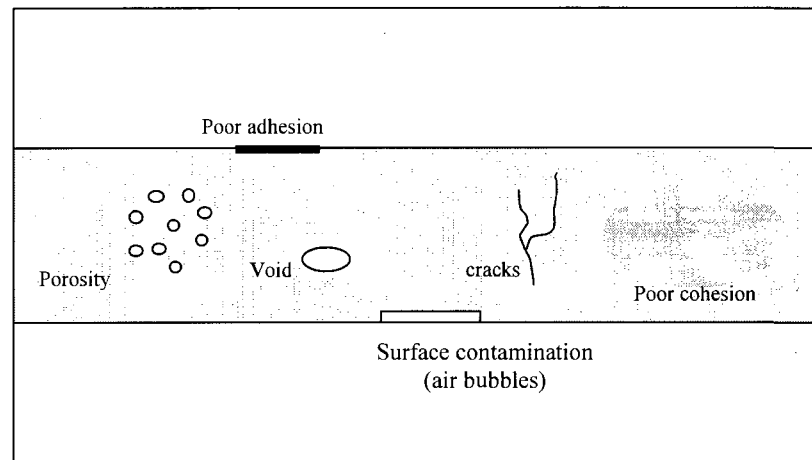


Figure. 7.1. Typical defects and different layers in adhesively bonded joints ¹.

Gross defects include voids, porosity, and cracks. The main reason for voids is the surface roughness and improper surface preparation, which leads to air being trapped in the interface. An insufficient amount of the material can also cause this problem. Cracks in the adhesive are often caused by applied stress or incorrect curing under thermal shrinkage. Surface disbonds can be caused when some degree of curing occurs in the adhesive before it contacts the substrate. Porosity may result from gas released during cure reaction.

Poor adhesion is a separation of the adhesive layer from a substrate due to lack of interaction between adhesive and substrate. It is caused mainly by the presence of contaminants or poor substrate surface preparation. The contaminants may come from the atmosphere, the substrate, or the adhesive. They prevent adhesion but unlike voids there is no air trapped on the interface. One of the sources of the substrate surface impurities is

low-molecular weight substances in the substrate which gradually diffuse to the solid surface and thereby cause marked decreases in adhesive strength. Also, poor adhesive strength may be the result of a weakness at the adhesive-substrate interface or internal stresses of the adhesively bonded joints. No current method is able to detect adhesion strength in the adhesive bond. Most of the non-destructive methods used currently to evaluate quality of the joints are sensitive to the voids of certain diameter only.

Poor cohesive strength is a defect of the bond within the adhesive layer, which appears as a result of insufficient interaction between adhesive molecules. It is often a result of incomplete polymerization in the adhesive due to improper curing conditions: insufficient cure temperature or cure duration, improper adhesive resin/hardener ratio and others. Insufficient mixing of the components is another reason. Exposure of the bond to aggressive environmental factors can also lead to cohesive failure.

7.1.1. Scanning Acoustic Microscopy for Defect Evaluation in Adhesive Bond Joints

The main problems during acoustic evaluation of adhesive joints arise from joint design, operational requirements and adhesive nature. A thin metal sheet (~1 mm) creates strong reverberations in the upper sheet joined with a layer of adhesive, which can hide reflection signal from the lower interface. Highly attenuative adhesive material (0.76 mm^{-1} at 7.5 MHz, and even worse for higher frequencies) also complicates evaluation of the lower interface. A large difference in the acoustic properties of the substrate (steel) and epoxy adhesive causes strong reflection from the first metal-adhesive interface. Another disadvantage of the acoustic method is relatively low contrast of the images – sometimes the difference in reflected amplitude between areas with good bonding and complete absence of the adhesive is approximately 10%. Good quality images of some adhesion defects are difficult to obtain; it requires high qualification skills and the proper choice of instrument settings for each sample. Adaptive digital filtration reduces masking of the 2nd interface signal¹¹⁷; however, uncertainties of adhesive parameters complicate the problem. Some other special methods of the signal processing can acquire more information from A-scans and, therefore, significantly improve quality of the acoustic

image. Resonance or cross-correlation methods achieve higher contrast in the acoustic images, which makes defects in the adhesive joints more detectable. This improves performance of the ultrasonic imaging method and gives a more reliable basis for evaluation of the industrial adhesive bond joints.

In the case of studies with a 20 MHz and higher acoustic frequency focused acoustic lens in a scanning acoustic microscope on flat metal-adhesive-metal samples, it is possible to clearly distinguish the pulse reflected from the steel-adhesive interface from the reverberations in the steel sheet. An ultrasonic signal is highly attenuated in epoxy. Nevertheless, it is possible to visualize the reflection from the lower interface as well in thin adhesive layers. C-scan acoustic images are created by positioning focus on the lower adhesive interface. This approach is the most sensitive to all changes in acoustic parameters of the adhesive layer and clearly shows micro-voids or any significant delaminations or disbonds. Conventional ultrasound instruments produce reflections of pulsed acoustic wave in the form of damping series of oscillations (Fig. 7.2). For a good quality adhesive joint, the form of the A-scan indicates good contact between adhesive and metal substrate on the interface and uniform structure of the adhesive layer between two substrates. A degraded interface (Fig. 7.3) reveals higher amplitude of the signal 1, which indicates an increase of the reflection coefficient and correspondingly a decrease in the adhesive's elasticity. The presence of some noise indicates appearance of non-uniformity in the adhesive layer due to micro-cracks and micro-voids.

Study of the adhesive bond interface with scanning acoustic microscopy provides information not only about an adhesive joint's morphology, presence of defects, their size, location and classification, but also combines the microscopic inspection with a total estimation of the bond quality in one measurement. Both aspects are important for examination of changes in the adhesive-adherent interface due to the influence of external factors (load, fatigue, chemical reactions, and so on) or due to time. As brightness of the image is determined by reflection coefficient on the substrate/adhesive interface, any changes in the adhesive or substrate properties or micro- defect appearance are detected by SAM. Higher frequencies allow us to detect minor changes in an adhesive joint's structure and increase image resolution. Due to lower acoustic impedance of polymers

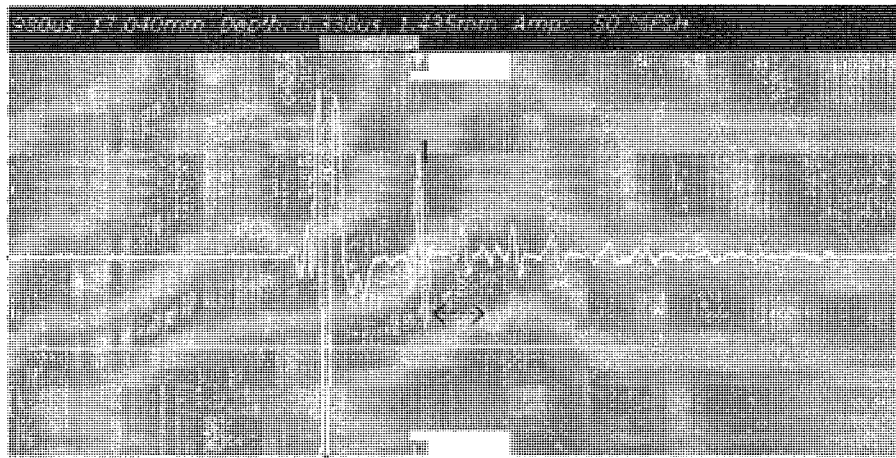


Figure. 7.2. The A-scan obtained on steel-epoxy-steel adhesive bonding for good quality adhesive. Focal point tuned to first interface. Pulse 1 is the reflecting from the steel-epoxy interface; arrow shows the adhesive layer thickness.

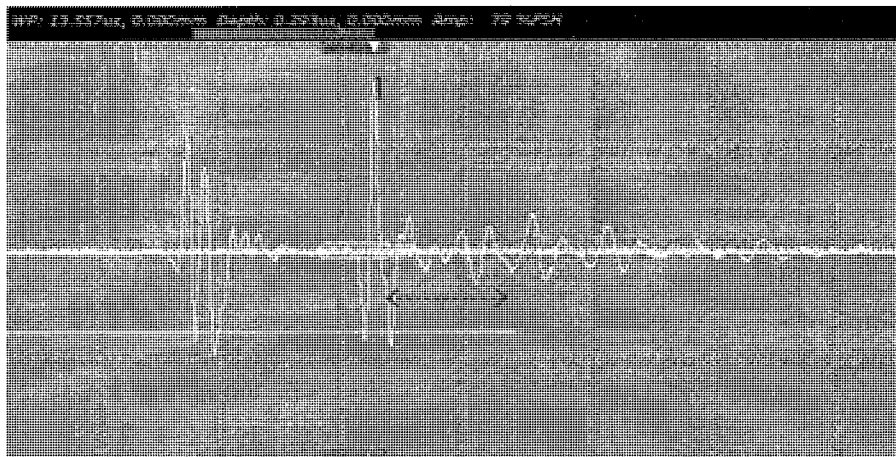


Figure. 7.3. The A-scan obtained on steel-epoxy-steel adhesive bonding for aged adhesive. Pulse 1 is the reflecting from the steel-epoxy interface; arrow shows the adhesive layer thickness.

compared to metals, the SAM imaging method is very sensitive to changes in the adhesive properties. It is able to detect the variation in amplitude within 2-4%. Resolution for the acoustic lens of 20 MHz frequency is equal to 300 μm , for 25 MHz -240 μm , for 50 MHz -120 μm , and for 250 MHz- 30 μm with an acceptable depth of sound penetration in most of the materials. Data obtained will help us to better understand the most important factors contributing to a structural adhesive joint's durability.

7.2. Effect of Water

The result of aggressive environment exposure is the appearance of some modifications in the adhesive structure. These modifications lead to strength loss due to formation of micro-cracks and micro-voids in the adhesive volume as well as on the interface with adherent. The reason for these structure imperfections is the penetration of active substances through the adhesive which change of the adhesive structure at the interface and in the bulk of the joint.

One of the greatest problems in environmental durability of the adhesive joints is their exposure to water in liquid or vapor form¹⁹². Epoxies are rich in polar hydroxyl groups, which make them hydrophilic and sensitive to water exposure. Most thermosetting adhesives are stable in the presence of organic solvents and water at ambient conditions. However, a combination of two factors, water and elevated temperature, exhibits a potential danger. Even at slightly elevated temperatures (60-90°C for epoxy), the adhesives are more sensitive to water penetration than at ambient conditions. Exposure to these conditions causes changes in mechanical properties and loss in cohesive strength of the joint.

To study the influence of water on the quality of the adhesive joints, various approaches are used: total immersion in water at room or elevated temperatures, exposure to high humidity conditions at elevated temperatures, cyclic exposure to elevated temperatures, humidity and drying.

7.2.1. Mechanisms of Water Action

A detailed mechanism of the interfacial attack is unknown. Several theories are proposed: breakage of the secondary bonds and replacement of the adhesive by water, or weakening of the metal oxide layer⁷. Water may penetrate through the adhesive or penetrate along the interface (wicking) or by capillary effect through the cracks and voids (mostly for aged adhesives). Diffusion through the exposed adhesive is the fastest way for water to penetrate into the joint interface¹⁹⁷. Usually, water affects both cohesive and

adhesive properties of the adhesive joint. After entering the joint, the adhesive can be weakened by water by⁷:

- Plasticization (reversible). Moisture is a well-known plasticizer for macromolecules. Water molecules may be adsorbed on the hydrophilic sites or on the surface of excess free volume elements frozen in the glassy structure. The glass transition temperature T_g is lowered as a result of water absorption which leads to decreasing the elastic modulus and cohesive strength.
- Inducing swelling stresses. This stress often compensates for the residual stress that appears in the joint due to epoxy shrinkage and therefore can not significantly contribute to the joint failure.
- Displacing the epoxy adhesive on the interface or hydrating the metal oxide surface. Water breaks hydrogen bonds between the metal oxide and epoxy to form new hydrogen bonds. Thus, epoxy is removed from the interface. This type is more typical for secondary hydrogen bonds.
- Hydrolysis (irreversible). Water can react with the epoxy adhesive by hydrolysis decreasing the cross-link density and cross-linked molecular weight which alters the mechanical properties significantly. In DGEBA/DDA adhesive, the backbone chains can be cut during water immersion and then low molecular weight segments leach out forming micro-voids¹⁹⁸. Xiao also reported the loss of nitrogen-containing functional groups. It was shown that water's ability to form clusters causes irreversible micro-voiding in epoxies especially at high temperatures¹⁹⁹.

Thus, changes in the adhesive's properties become irreversible after a certain point. In incompletely cured adhesives, unreacted chemicals can be leached from the adhesive network. Micro-cracks appear as a result of these two effects.

Substances that have a potential to be hydrolyzed include alkyl halides, amides, epoxides, carboxylic acid esters, phosphate esters, and sulfonic acid esters¹⁹⁷. Fata and Possart¹⁸ did not reveal any sign of hydrolysis for type-1 and -2 crosslinks in the DDA-cured epoxy adhesive systems. They have proposed¹⁸ that water reacts with imino-ethers

that adjacent to the type-3 crosslinks (Figure 7.4 (a)). Water can disrupt the existing epoxy hydrogen bonds, causing swelling of the network. Water molecules can also enter voids (including free volume) that exist in the network and form aggregates.

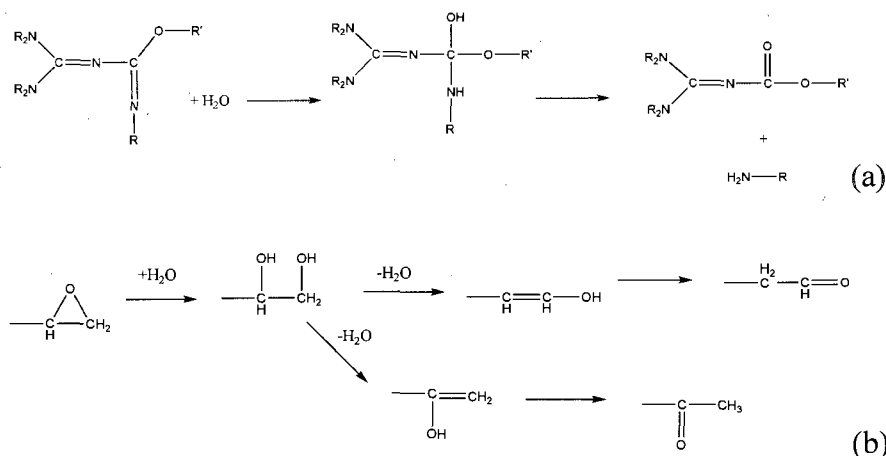


Figure 7.4. Schematic sketch of the hydrolysis mechanisms that going on in DDA-cured epoxy adhesive during hydrothermal aging (a)¹⁸ and in uncured epoxy adhesive (b)¹⁹⁷.

Uncured epoxy adhesive is even more prone to water deteriorating effect (Figure 7.4 (b)). Epoxide can be hydrolyzed to form a diol. Hydrolysis of this group is estimated to occur at a rapid rate, based on data for 14 epoxides at pH 7, as summarized by Harris¹⁹⁷ that ranged in half-life from approximately 1 minute to 8 days. In comparison, the ester group is estimated to hydrolyze at a significantly slower rate. The aqueous base/acid-catalyzed hydrolysis half-life at pH 8 and 7 (25°C) is estimated as 4.4 and 44.3 years, respectively¹⁹⁷.

7.2.2. Effect of Water on the Adhesive Joints with Cured Epoxy Adhesive

The primary mechanism of strength loss is considered to be diffusion of water to the interface and weakening of the oxide layer due to the growth of ferric oxide. Hydrolytic degradation that started at the interface and moved to the bulk adhesive also contributes to a decrease in joint strength²⁰⁰. For steel/epoxy interfaces, bond performance depends on the ability of water to displace the adhesive from the metal oxide layer.

The effect of water on the adhesive bond durability was investigated. Adhesive joints were immersed in water at ambient and elevated temperatures (20 and 80°C). Strength of the joint was measured right after exposure without drying and after samples had been dried overnight. Adhesive joints were prepared with BETAMATE adhesive as described in Chapter 4.1.3. After preparation, some specimens were tested to determine joint strength and others were immersed in water at two temperatures for 6 weeks. Results are presented in Fig. 7.5. For samples immersed in water at ambient temperature, joint strength decreases insignificantly. This effect is reversible as strength is restored after the joint has been dried. This result is consistent with plasticizing effect of water.

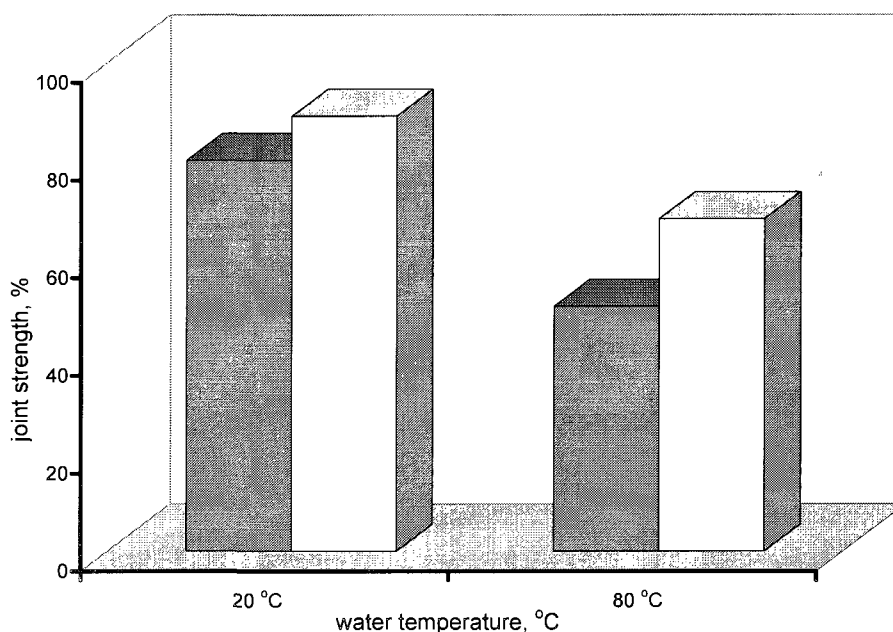


Figure 7.5. Tensile test results for adhesive joints immersed in water at 20 and 80 °C. Wet samples are shown in gray, samples dried after immersion are white. 100% is the strength of the joint that was not exposed to water.

Brewis et al. showed that the major mechanism of adhesive strength loss is due to reversible water plasticization of polymer.²⁰¹ However, water immersion of the adhesive joint at 80°C causes a permanent decrease in joint strength. The reversible water effect is also present. The possible cause of irreversible damage in the adhesive structure at elevated temperatures is formation of micro-voids and cavities¹⁹⁷. This mechanism of damage exists in rigid cross-linked epoxy network, preventing matrix relaxation after

micro-voids are formed. Strain in the adhesive increases (Fig. 7.6) for both temperatures which indicate involvement of the plasticization effect in both cases. The failure mode shifted from cohesive for the control joint to mixed cohesive/interfacial for the sample immersed at room temperature and to pure interfacial for the joints immersed in water at high temperature.

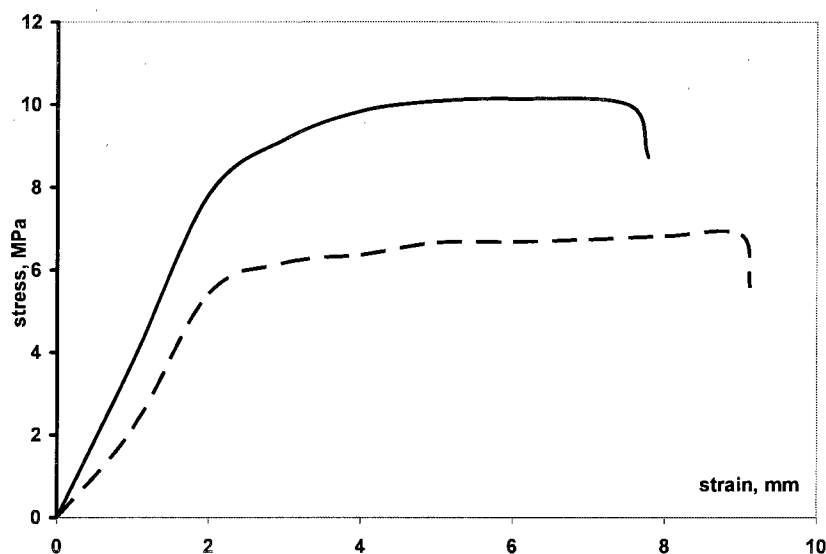


Figure 7.6. Typical stress-strain curves for normal (solid line) and degraded (dashed line) adhesive joint.

It is interesting to study how the adhesive cure conditions affect the durability of the adhesive joints. Strength was measured for the normally cured, undercured (10 min. at 180 °C) and cured at temperature higher than normal (45 min. at 200°C) adhesives joints, which were then exposed to water at 80 °C (Fig. 7.7). Measurements were taken after overnight drying to eliminate reversible effects. The decrease in joint strength for overcured adhesive is significantly higher than for control joint. This fact can be explained by appearance of micro-damage in the exposed to high temperature adhesive matrix that speeds up the water uptake process and its path to the interface. An incompletely cured adhesive joint also shows significant decrease in strength. Epoxy cured at 120 °C is more sensitive to water uptake because it contains unreacted DDA, which becomes preferred sorption (bonding) sites for water. Alkaline products formed later are leached out from the matrix and may react with metal oxides at the interface.

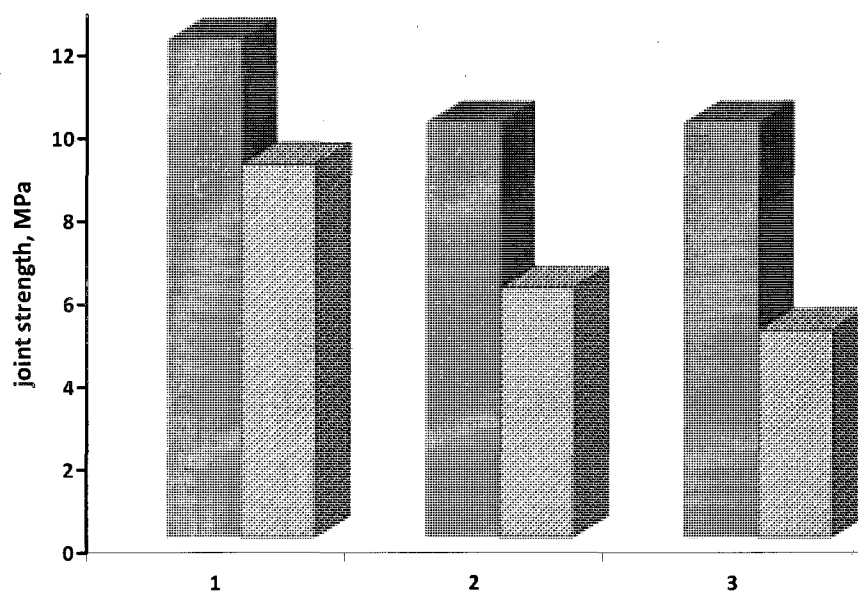


Figure 7.7. Joint strength for properly cured (1), undercured (2) and overcured (3) epoxy adhesive before (black) and after (gray) water exposure.

The dynamics of water uptake and joint strength changes were studied at 80 °C. Water uptake was measured by weighing the samples after removal from water. Joint strength was measured after overnight drying. Results are shown in Fig. 7.8 and 7.9.

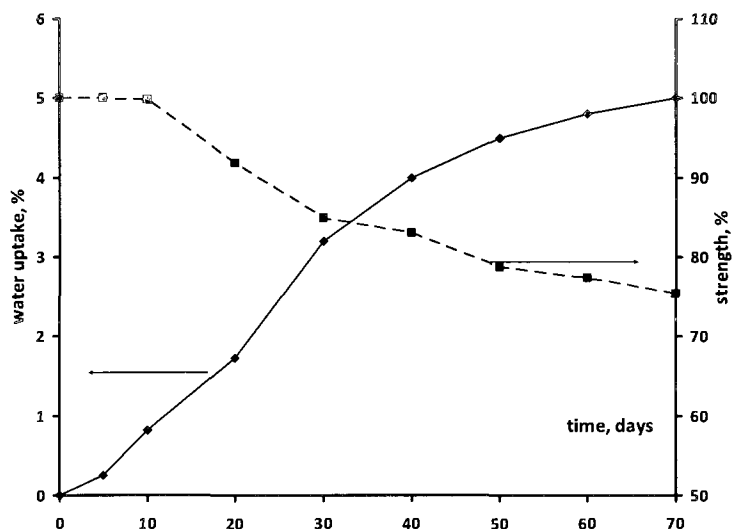


Figure 7.8. Water uptake and bond strength for epoxy adhesive.

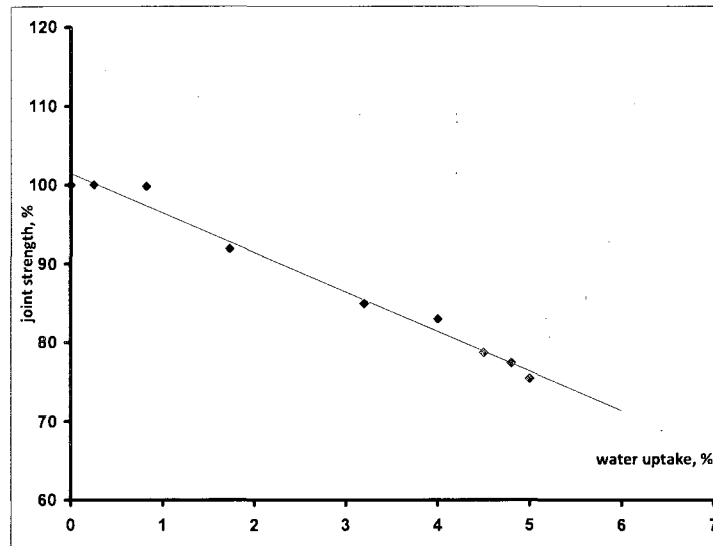


Figure 7.9. Correlation of the water uptake by epoxy adhesive in the joint and the joint strength.

Adhesive joint strength starts to decrease by the 10th day, while water sorption increases linearly from the 1st day. It was shown that water uptake and its distribution within the epoxy/metal joint can be described by diffusion through the adhesive layer with Fick's law¹⁹⁷. It can be assumed that some threshold exists before irreversible changes in adhesive structure start. The type of failure is cohesive for both control samples while mostly interfacial for the wet samples. Even partially cohesive, the wet samples show different structure of the failed surface. Large pieces of the adhesive are present on both steel plates in the degraded joint while normal cohesively fractured surface looks rough due to very small particles of the adhesive on both full surfaces of the substrate. Later, the type of failure becomes interfacial. Fig. 7.10 shows correlation between water uptake by the adhesive joint and an irreversible decrease in joint strength.

Young's modulus of the adhesive measured by the dynamic microhardness method decreases from 2.8 MPa to 2.3 MPa as a result of plasticization or breakage of the bonds. As seen from Figure 7.10, elastic properties and microhardness of the material decreases. The microhardness test results indicate that the loss in elastic modulus mirrors

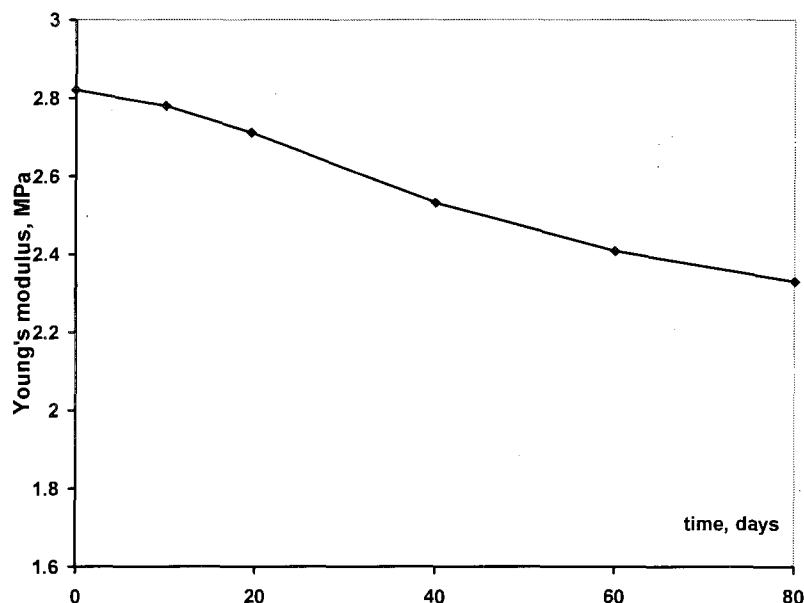


Figure 7.10. Young modulus determined by dynamic microhardness method for the adhesive exposed to water.

the water uptake. This may be due to broken chemical bonds. Despite the fact that specimens for microhardness measurements were molded into an epoxy matrix cured at the room temperature, some surface heating may occur during the samples preparation process (polishing), so it is difficult to estimate contribution of the reversible and irreversible parts of the water effect.

Thus, the results obtained demonstrate that water penetrates into the adhesive joint through the adhesive layer toward the epoxy/steel interface. Degradation that occurs at the interface is most essential for joint strength. These results indicate that during the first stages the degradation process is reversible and is mostly due to epoxy matrix plasticization; the later stages of the ageing process cause irreversible loss in joint strength, which occur mostly at the interface.

To investigate the nature of the epoxy/steel interface and any changes that appear during immersion in water, acoustic scans were prepared. Figure 7.11 demonstrates typical changes that appear at the interface under the influence of water at 80°C¹³⁵. Micro-voids with a size of 30-100 µm are clearly noticeable throughout the interface. Some of them form clusters, which appear closer to the edge of the joint. Histograms (Fig.

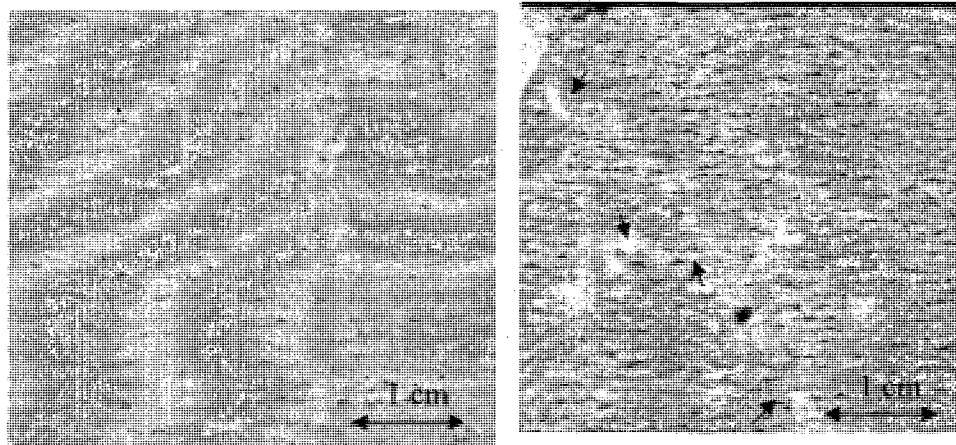


Figure 7.11. Acoustic scans of the steel/epoxy interface at day 1 (left) and day 7 (right) of immersion in water at 80°C¹³⁵ (with kind permission of Springer Science and Business Media). Micro-voids are shown by arrows.

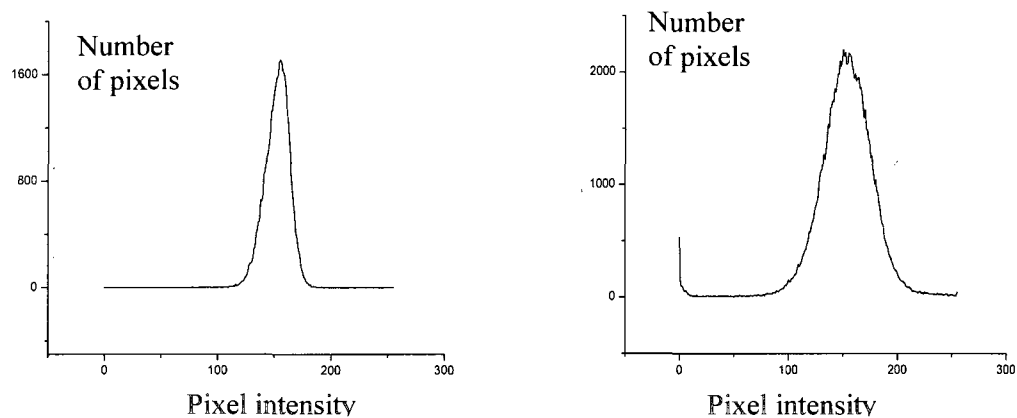


Figure 7.12. Histograms of the acoustic images on the Fig. 7.11.

7.12) show significant widening of the peak. Direct quantitative comparison of the image brightness and reflection coefficient is not possible because other factors contribute to the brightness variations: gain, surface degradation. However, it is necessary to note that there is no noticeable change in reflection coefficient for areas with microdefects compared with well bonded areas. Moidu found only an increase in scatter in the data, but not a significant change in the reflection coefficient during the epoxy's exposure to water¹²⁵.

It is generally accepted that it is the water effect on the interfacial properties that are responsible for the decline in the overall joint strength. The appearance of micro-voids on the acoustic images at the interface coincides with a shift to some degree of interfacial failure in destructive tests. Thus, this phenomenon can be a signal that the joint was exposed to moisture. Substrate corrosion was not noticeable on the time scale of the experiment; it usually starts later and follows rupture of the interfacial interactions.

There are several events that can cause micro-void formation that was discussed earlier: breakage of the secondary bonds at the interface and displacing the adhesive, and hydrolysis of the susceptible linkage that leads to bond breakage or formation of micro-cavities⁷. DDA can act as an absorption centre for water because of its hydrophilic nature⁸⁹. Kinloch⁷ developed another approach to describe the mechanisms of environmental failure of adhesive joints through three stages: water uptake through the interface, loss of the interface integrity and then failure of the adhesive joint. The type of failure is interfacial at the edges and cohesive in the center of the joint. The ratio of the failure types depends on the duration of water immersion. When exposed to temperature of 70-80°C, epoxy adhesive is close to the T_g temperature so stresses cannot be transferred efficiently from one part of the joint to the other and both the material and interface become permanently damaged when they experience any stress. This factor also contributes to micro-void formation.

For epoxy/steel adhesive joints that do not have covalent bonds at the interface, the mechanism of the environmental attack has been found to be via the adhesive displacement with water at the metal oxide interface⁷. Covalent bonds between metal oxides and silane coupling agents or epoxy matrix provide better moisture resistance to the moisture compared with secondary bonds. Water also is adsorbed on the iron oxide by physisorption with a small amount of water dissociating to form hydroxyl groups. Epoxy compounds are adsorbed dissociatively on iron oxide to form surface phenoxy species. Interfacial chemical bonds formed contribute to the adhesion of epoxy resins to cold-rolled steel (CR) and galvanized steel (GA) sheets and prevents water absorption at the interface. Epoxy degrades more rapidly at elevated temperatures for zinc or steel substrates than on aluminum substrates²⁰² since divalent metals have a more basic oxide

surface than the three valence metal oxides which leads to faster dehydrogenation and chain scission.

7.2.3. Effect of moisture on uncured epoxy adhesive joints

The uncured epoxy adhesives absorb water, which has a significant influence on the joint quality after the joint is prepared and adhesive has been cured. Although the main problem of the adhesive's exposure to humid conditions is weak cohesive strength (Figure 7.4) this also has an influence on interface quality as well. When water is present on the zinc oxide, the epoxy ring opening reaction occurs less efficiently than on a dry surface⁹⁰.

Small voids, 50-100 μm in diameter, appear throughout the adhesive layer and at the metal/adhesive interface (Fig. 7.13a). In the case of longer exposure (10 days), micro-

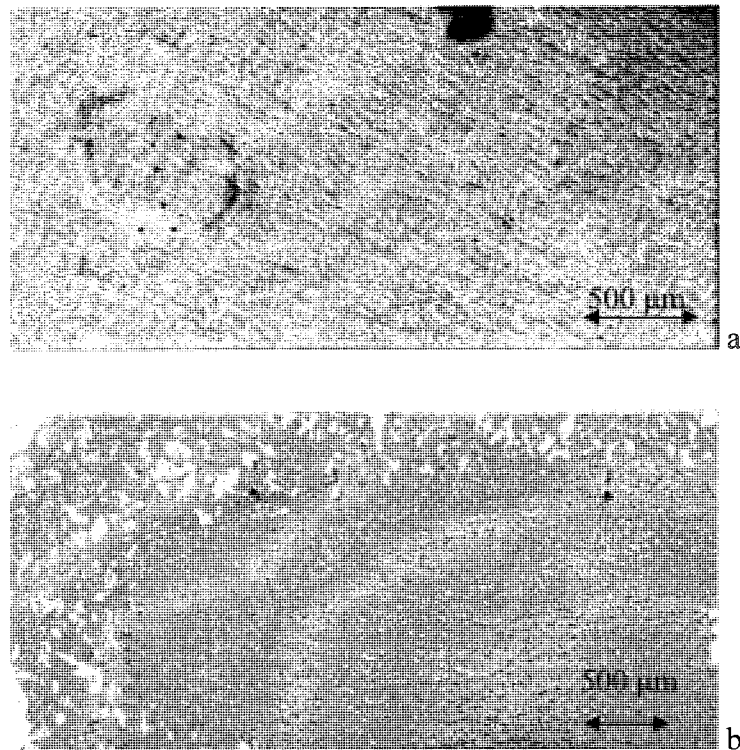


Figure 7.13. Appearance of the voids on the steel/epoxy interface in the adhesive joints immersed in water for 3 days (a) and for 8 days (b)¹⁸⁶.

voids merge forming a 'lace'-like pattern along the edges (Fig. 7.13 b). In both cases, voids are concentrated along the sample's edge, where access to water was provided. The approximate velocity of water penetrating was around 2 mm/day. The center of the sample is free of voids with an undamaged structure.

More details for micro-voids formation are shown in Fig. 7.14. Since the reflection coefficient of steel/air (for the voids) is equal to unity and significantly higher than the reflection coefficient for the steel/epoxy interface, micro-voids appear as light spots. When the electronic data gate is positioned on the lower interface, all voids in the adhesive layer appear above the data gate and disturb the ultrasound propagation. Therefore, micro-voids appear as dark spots on the image of the second interface. Also, it is necessary to note that the middle image in Fig. 7.14 present not a pure lower epoxy/steel interface but rather an integral image of the epoxy/steel interface and the whole epoxy layer.

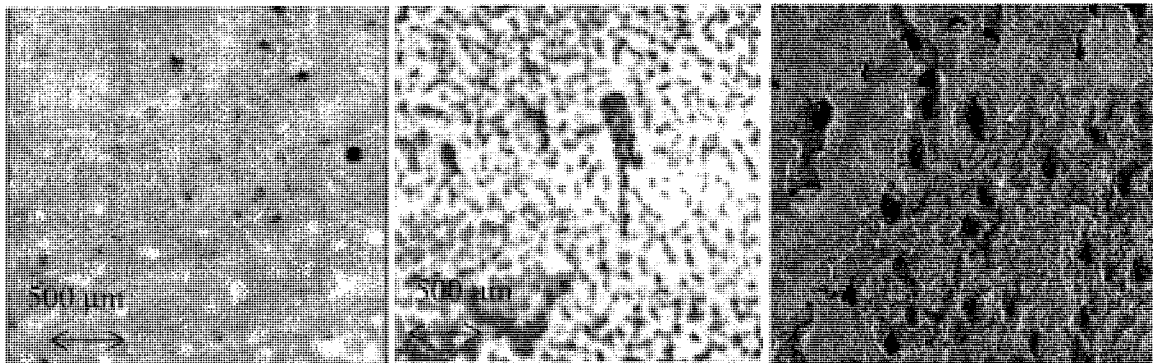


Figure 7.14. Micro-voids at the interface (left) and inside (middle) the epoxy layer as a result of water sorption by uncured epoxy adhesive. Electron microscopy image of fracture surface is shown for comparison (right).

Images in Fig. 7.14 indicate that the porosity inside the adhesive is much higher than at the interface. 674 pores are present inside the adhesive layer while only 36 are present at the interface. Assuming the thickness of the adhesive layer is even and equal to 200 μm, only one pore with an average size of 200 μm can be present at a certain point. This allows us to calculate the porosity distribution in the adhesive layer volume. With the volume of the adhesive layer equal to 145 mm³, the distribution of the pores is 4.34 micro-voids per mm³.

Morphology of the fracture surfaces analyzed with electron microscopy show the cohesive type of joint failure in both cases (Figure 7.15). However, immersed in water before curing, the adhesive reveals poor adhesion between the epoxy matrix and glass spheres while the control joint breaks through the epoxy matrix. Higher magnification images show poor phase separation during the network formation and poor cohesion in the adhesive for the material immersed in water.

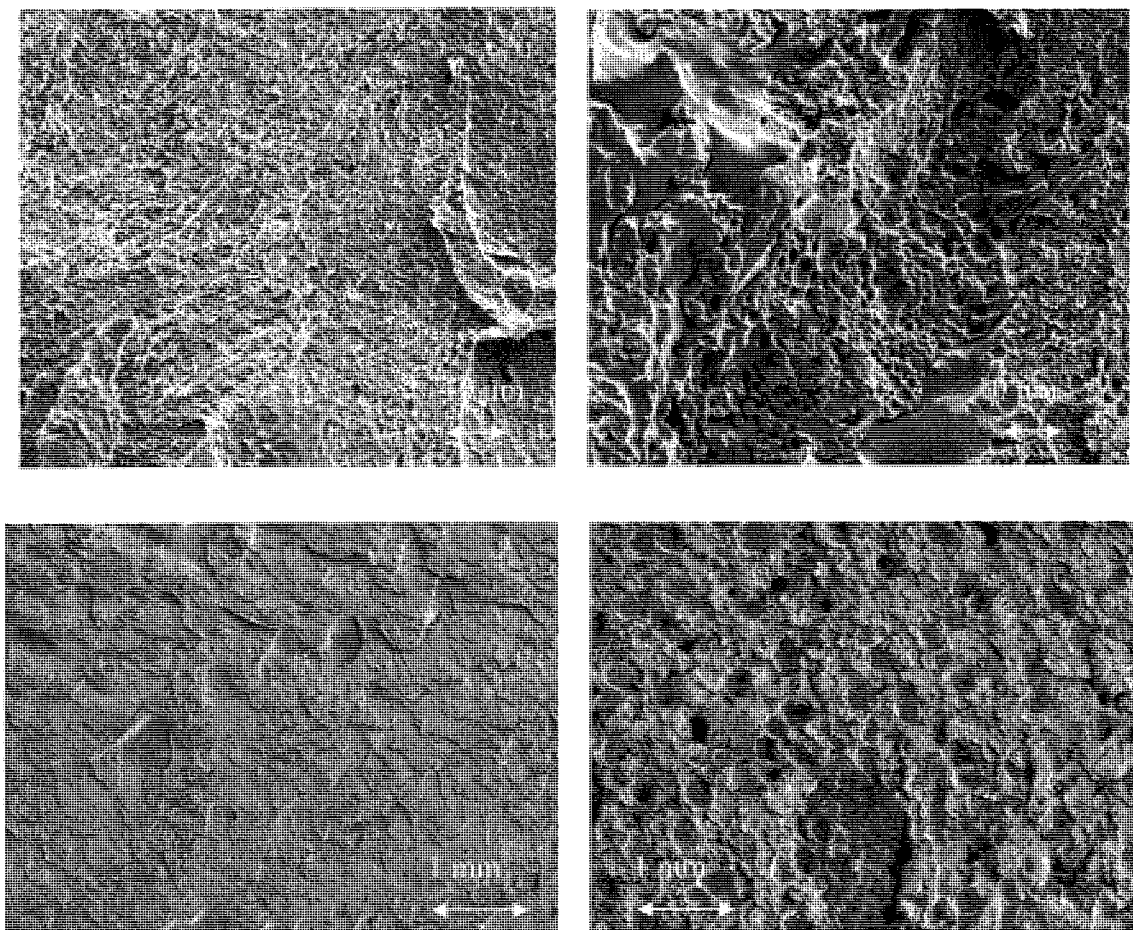


Figure 7.15. Electron images of the fracture surface for normal adhesive (left) and adhesive immersed into water before cure reaction (right).

Increased resistance of BETAMATE to the environmental factors arises from the presence of covalent interfacial bonds between epoxy and silane primer. Resistance of the adhesive joints with cured epoxy to moisture can be explained by the presence of hydrophobic components in the epoxy formulation and improved resistance in the interface region. A zinc oxide layer on the metal surface brings an additional contribution

to the durability of the BETAMATE joints. Zinc oxide like many other oxides carries hydroxyl groups on its surface. It was shown that water adsorbed on the zinc oxide partially dissociates to form OH groups on the surface and an epoxy model compound is adsorbed dissociatively on zinc oxide to form surface phenoxy compounds⁹⁰ that are not replaced by water.

Thus, appearance of micro-defects on the acoustic images of the metal/adhesive interface is an indicator of water attack before or after epoxy hardening and the presence of these defects correlates with loss of interface toughness.

7.3. Accelerated Aging of the Adhesive Bond Joints

The aim of an accelerated ageing test is to accelerate the same mechanisms of attack that work during the service-life of the bonded joint and not to induce misleading and irrelevant mechanisms. For example, it is well known that to accelerate the rate of environmental attack it is not possible to simply raise the temperature of the environment, since unrealistically high test temperatures will change the mechanisms of attack.

Specimens for these experiments were artificially aged by a chemical ageing procedure that is standard for automotive testing. Adhesive joints were exposed to several cycles of high humidity with elevated temperatures and salt spray or salt water immersion. Salt spray simulates seacoast environment, cleaning solutions, winter roads, and other contamination conditions. Details of the aging procedure are described in Chapter 4. Micro-voids at the interface are similar to the voids that appear as a result of water penetration. The number of voids at the interface is relatively small.

The result of aggressive media (temperature, humidity and, sometimes, electrolytes) exposure becomes apparent in an adhesive layer as some structural modification. Figure 7.16 represents the acoustic C-scan images of the degraded interface and bulk adhesive layer, obtained at a frequency of 50 MHz. Micro-voids are formed on the earlier stages of degradation at the interface; with time, they merge and form large delaminations at the interface (Fig. 7.17) that are shown by arrows¹³⁵. The adhesive

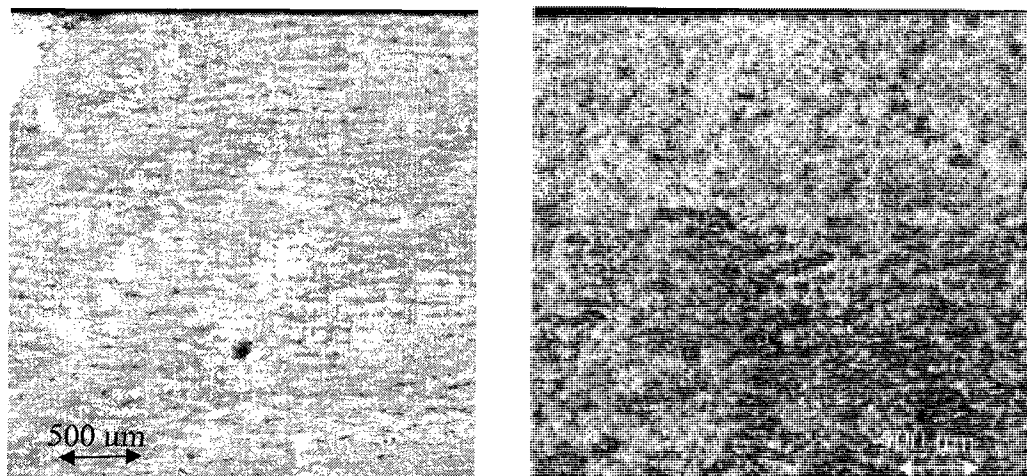


Figure 7.16. Acoustic C-scans of the steel/epoxy interface (left) and middle part of the adhesive layer (right) after accelerated aging procedure 135 (with kind permission of Springer Science and Business Media).

degradation process is usually observed together with metal corrosion in the same areas, which is shown in Fig. 7.17 as darker areas in left lower corner of the image. The internal structure of the adhesive also undergoes significant changes. Micro-voids appear in the uniform epoxy structure (Fig. 7.16 (left)). These modifications in joint structure cause loss of joint strength.

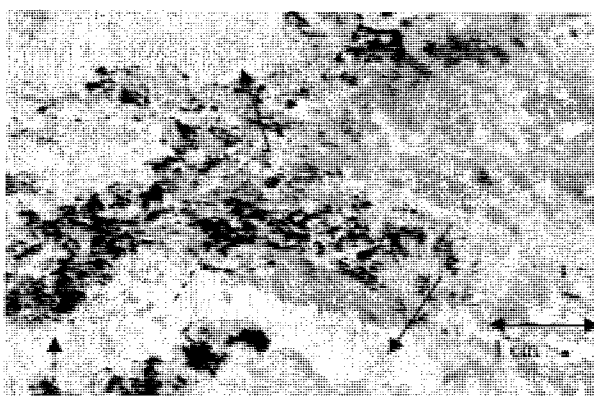


Figure 7.17. Acoustic image of the adhesive/metal interface structure at late stages of the accelerated aging. Solid arrows show delaminations on the interface which are due to lack of adhesion, dashed arrows show metal substrate degradation.

Vine¹²⁴ using a 20 MHz focused transducer, did not find any signs of the weakening of the interface of the adhesive joint under increased moisture conditions on the acoustic scans. One possible reason why the authors could not reveal any micro-

defects at the interface may be insufficient acoustic frequency; a 20 MHz acoustic lens allows resolving only the structure of 300 μ m size. Higher acoustic frequencies (25, 50 and 70 MHz) and decreasing the scanning rate allows us to reveal micro-defects as low as 30 μ m dimensions at the steel/epoxy interface.

The acoustic images of the adhesive/steel interfaces shown in Fig. 7.18 were analyzed with OriginPro 8.0 software. Conversion of the grayscale images into the pseudo-color scale allows better detection of minor variations in image brightness (Fig. 7.19). Histograms presented in Fig. 7.20 shows median shift toward higher values of the signal intensity, which corresponds to decreasing acoustic impedance. The micro-voids that appear at the interface are shown in the histogram 2 as an additional brightness peak. As images were obtained for different samples and scanning parameters and substrate conditions may vary, it is not possible to quantitatively analyze the information about

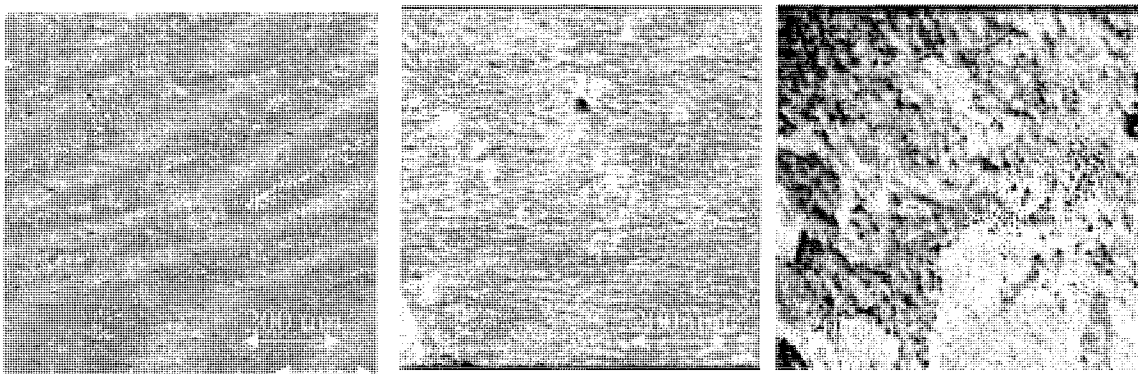


Figure 7.18. The acoustic images of the intact (left) and degraded (middle and right) steel/epoxy interface¹⁴⁶.

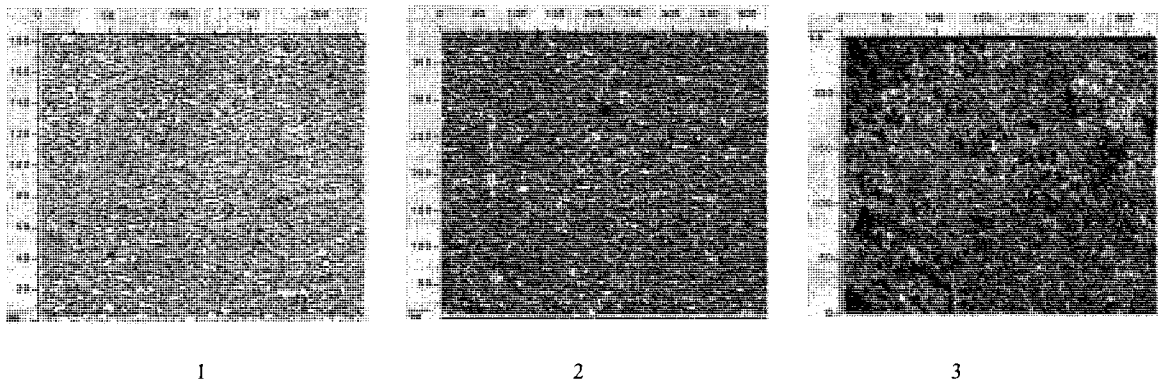


Figure 7.19. Images shown in Figure 7.18 presented in pseudo color scale.

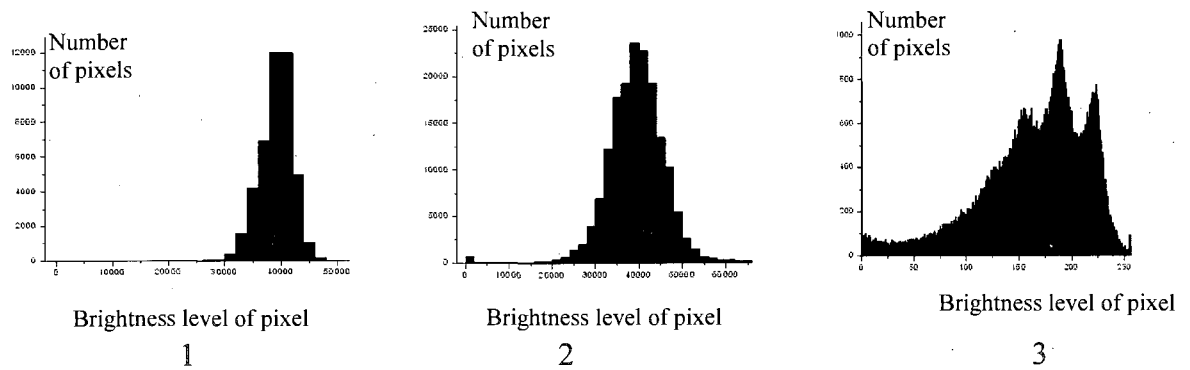


Figure 7.20. Histograms and cross-sectional profiles of the acoustic images presented at Figure 7.18.

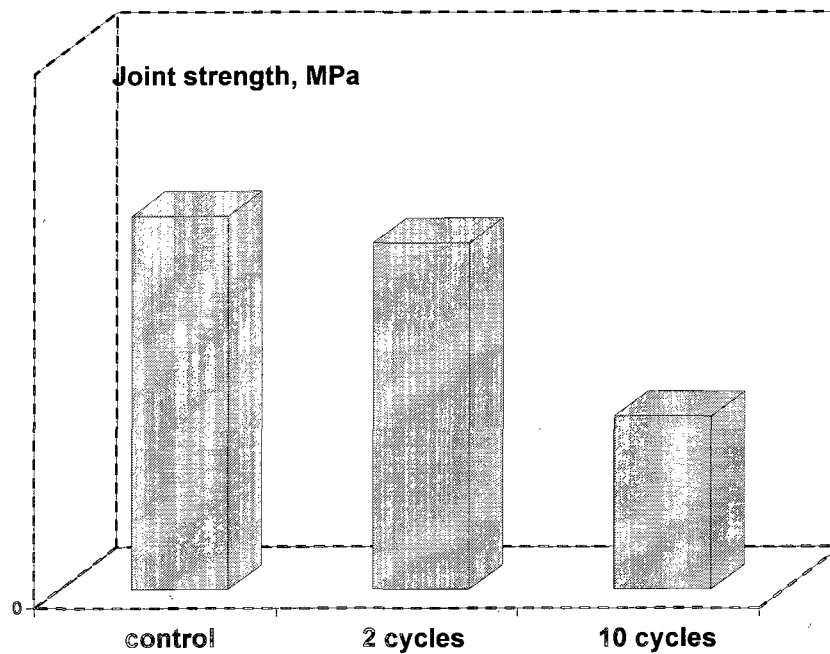


Figure 7.21. Destructive test results.

changes in the reflection coefficient and adhesive elastic modulus. A wide distribution of brightness is distinctive for histogram 3. The peak splits into three distinct regions, which correspond to the bonded area, delaminated interface and delaminated interface with corroded metal substrate. Results of the destructive tests (Fig.7.21) indicate a slight decrease in the adhesive joint strength for joints that undergo 2 cycles of degradation and 50% decrease in strength for the 8 cycles. These data correlate with the acoustic data obtained.

7.4. Effect of Stress

Adhesive joints deteriorate faster when they are under stress during service life or at the time of joint preparation. Figure 7.22 shows images of the adhesive/metal interface of the samples that were exposed to a forming operation after bonding. It is assumed that cracks were formed or round shape voids were transformed during formation operation. Regular round voids (image 1) lengthen along stress direction and merge into the net-like pattern.

Figure 7.23 represents cavities (so-called “spring effect”) in the adhesive layer that appear because the clamp that holds the adhesive joint was removed before the epoxy solidifies. As a result, the bond line area decreases significantly together with the total joint strength.

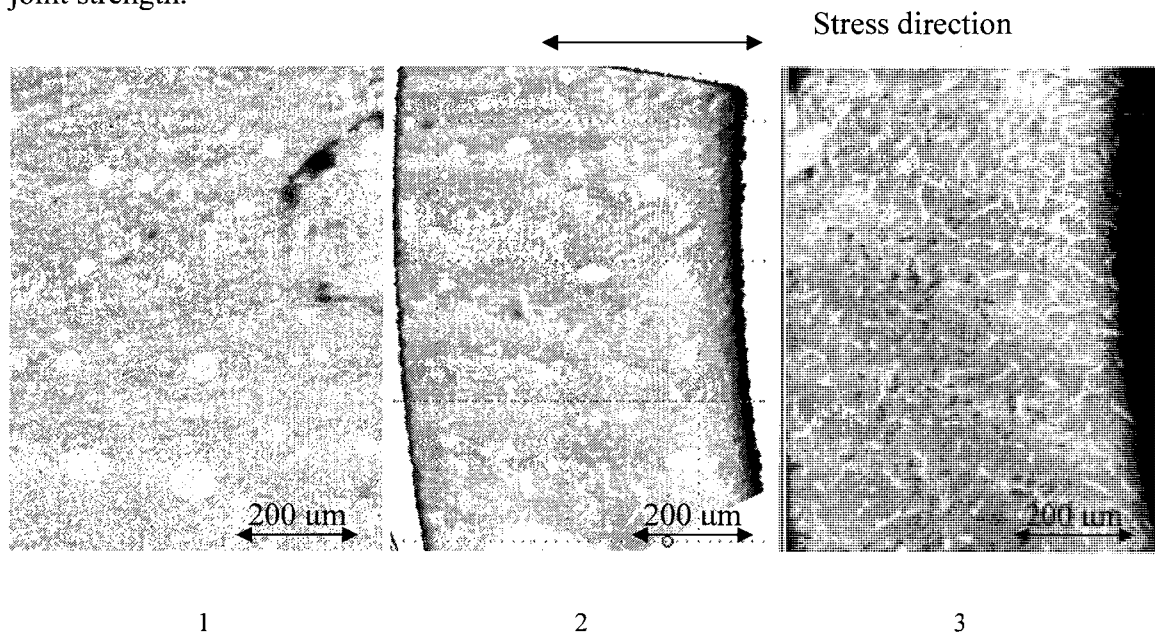


Figure 7.22. Deformation of the voids at the adhesive/metal interface due to stress. 1-stress was not applied, 2 and 3-stress was applied in the direction shown by arrow.

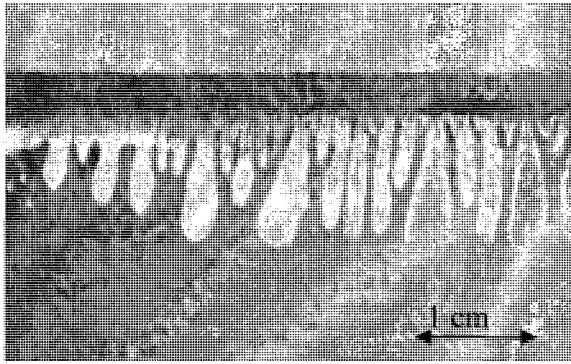


Figure 7.23. Appearance of cavities in the adhesive layer due to joint clamp been removed before adhesive solidification¹⁴⁶.

7.4.1. Normal Tensile Load for the Adhesive Bond

A special tensile stand was constructed for microscopic investigations of adhesive behavior under mechanical stress (Figure 7.24)¹³⁵. A sample consists of two steel plates with a thickness of 3 mm joined by 0.3 mm layer of a BETAMATE epoxy adhesive. A load of up to 10 kN can be applied to the bonding area of $1.5 \times 1.5 \text{ cm}^2$. The set of B- and C-scans was obtained at increasing values of the load. The bond strength is high enough to cause a deformation of the sample joint metal plates, which is visible on the C-scans

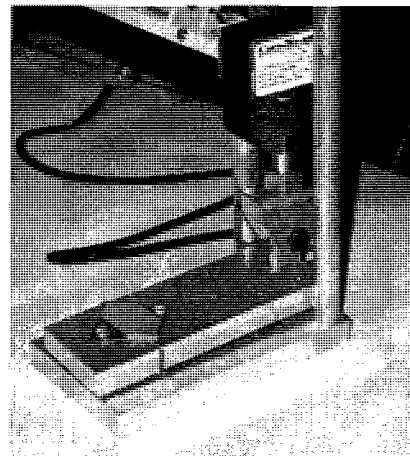
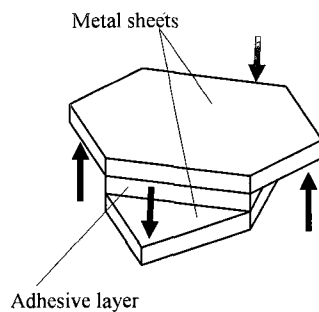


Figure 7.24. Experimental setup.

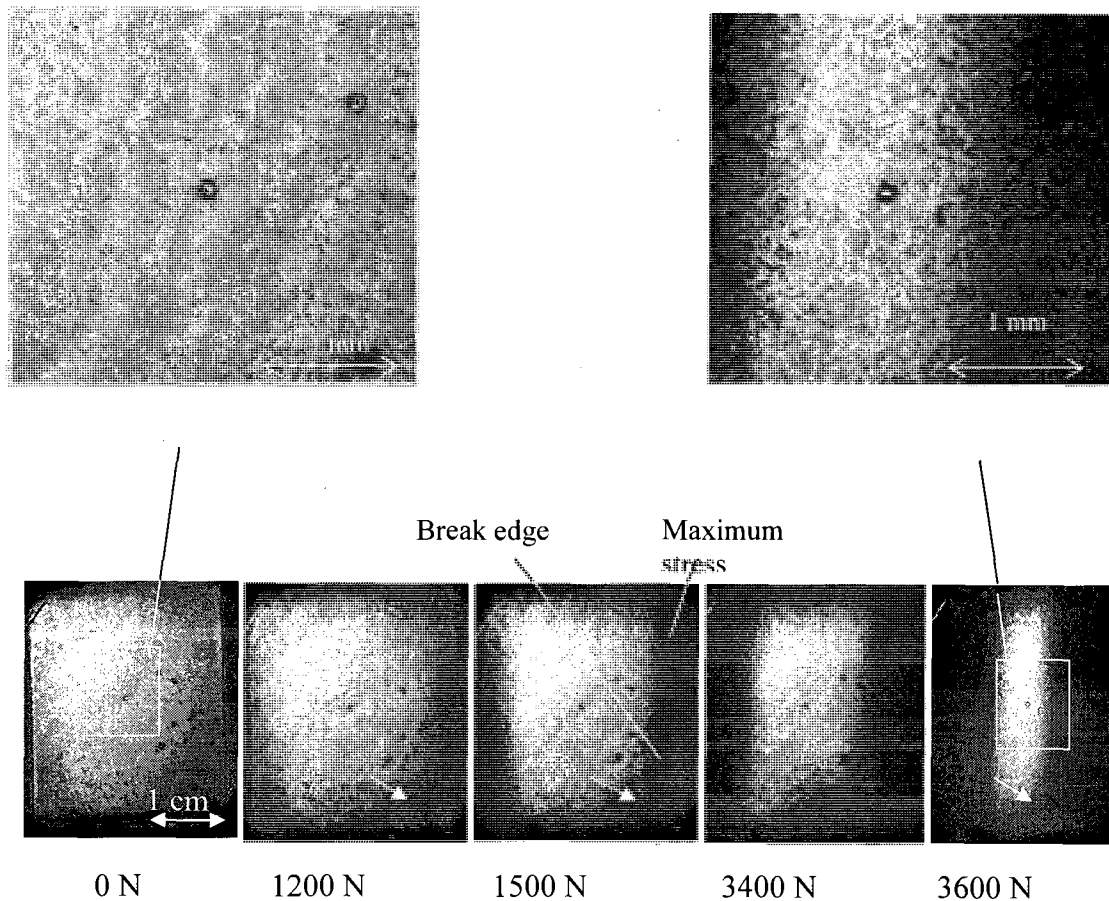


Figure 7.25. Acoustic images of the steel/epoxy interface at the increasing load¹³⁵ (with kind permission of Springer Science and Business Media).

(Figure 7.25). As a result, the tensile stress is non-uniform across the bond area. The breakage starts at the edge and gradually propagates forward to the center of the bonded area. In this case, the regions with the maximum load are located at the border between still bonded and broken areas (light and dark regions of the C-scans).

Detailed examination of these scans shows that the micro-structure of a metal-adhesive interface becomes more evident as the tensile load applied is increased. The local elastic properties of the adhesive vary in different areas of the sample. The tension load causes the expansion of the weakest and less rigid components of this structure and, accordingly, increasing the acoustic contrast of the image.

Thus, due to the mechanical nature of acoustic waves, scanning acoustic microscopy is able to detect the areas in the epoxy adhesive layer in the adhesive bonds that undergo stress effect and visualize the changes in the adhesive structure due to stress.

7.5. Joint Preparation

As discussed in Chapter 5, conditions of the polymerization reaction are among the important factors that determine the adhesive's structure and final mechanical properties of the adhesive joint. The nature of both the adhesive and the substrate also significantly influence the final properties of the adhesive joint. Proper substrate preparation is critical for the obtaining proper interaction with the epoxy adhesive and building the interface that maintains the high joint strength.

7.5.1. Contamination of the Substrate

Contamination on the substrate surface leads to the poor adhesion between metal oxides and adhesive matrix. Adhesion defects are the most complicated case for detection by any technique because the adhesive and substrate are in good contact but no attractive forces arises between the substrate and adherent.

Adhesion defects were simulated by applying TeflonTM, silicone, zinc stearate and oil layers on the steel surface. Teflon and silicone sprays are used often as molding release agents. To simulate real conditions where contamination of the substrate with grease or oil is more realistic, mineral oil was applied. Epoxy formulations with DDA are able to absorb oil from the metal surface, so an excessive amount of oil and silicone (9g/m²) was applied. BETAMATE adhesive was applied then and the joint was hardened at 180°C for 30 min.

Silicone could not provide adhesion defects; it was completely absorbed from the steel surface by the adhesive. Zinc stearate leaves thick white solid residue at the interface that hardly mimic real surface contamination. Additionally, it does not provide consistent results with adhesion defects. In the preliminary tests, joints often failed at the

steel/zinc oxide interface but not at the zinc oxide/BETAMATE interface. Thus, only samples with oil and Teflon contaminants were scanned and analyzed.

Values of the acoustic impedance for three materials used to prevent adhesion and the reflection coefficients of their interfaces with steel were calculated using Eq. (4.18) and results are presented in Table 7.1. Analysis of these data allow to conclude that oil and silicon have acoustic impedances that differ the most from the acoustic impedance of the adhesive and the reflection coefficient of steel/BETAMATE interface. Therefore, these contaminants should be visible in the images. Teflon has acoustic impedance so close to the BETAMATE one that the difference is only 3%. It is a real challenge to visualize the boundary between the materials with such close acoustic properties.

Table 7.1. Acoustic properties of the adhesion contaminants.

| | Density ρ , g/cm^3 | Sound velocity, m/s | Acoustic impedance, $\text{kgm}^{-2}\text{s}^{-1}$ | Reflection coefficient for steel/material interface |
|----------------------|-------------------------------------|---------------------------------|--|--|
| BETAMATE adhesive | 1.19 | 2360 | 3.06 | 0.875 |
| Oil | 0.854 | 1460 | 1.23 | 0.948 |
| Teflon TM | 2.14 | 1390 | 2.97 | 0.869 |
| Silicone | 0.94 | 0.988 | 0.91 | 0.961 |
| Steel | 7.8 | 5900 | 46 | n/a |

To evaluate the capability of scanning acoustic microscopy to detect adhesion problems at the interface, acoustic images were obtained with 50 MHz frequency. At this frequency, the lateral resolution of the acoustic lens is 50 μm and axial resolution is equal to 30 μm what is greater than the thickness of the layers that were applied to prevent adhesion. However, if the total reflection coefficient for thin films is different from the substrate, the film can be resolved.

The results are presented in Fig. 7.26. The contrast for Teflon layer is extremely low, but the boundary of the TeflonTM layer is visible and the image is reproducible¹. The

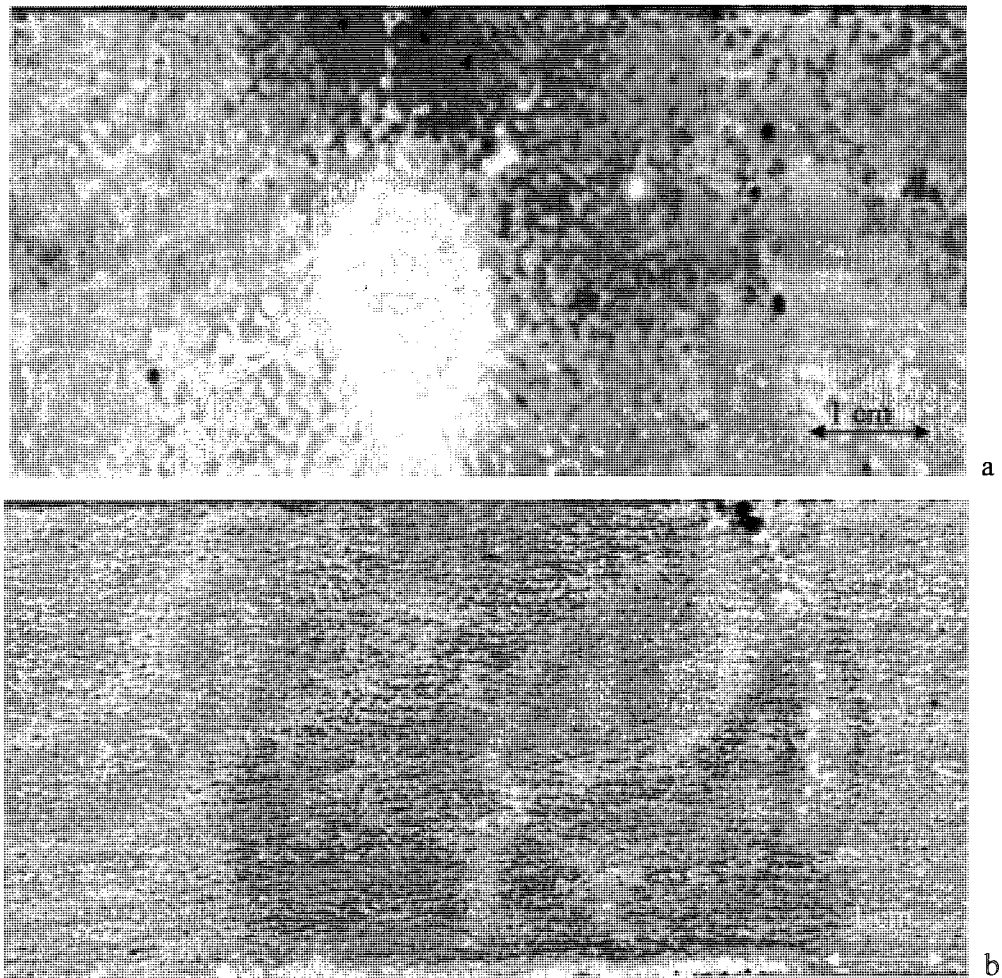


Fig. 7.26. Acoustical images of the adhesion problems caused by oil (a) and Teflon (b) contamination on the interface^{1, 146}.

Teflon layer is darker than the interface due to lower reflection coefficient. The detected area on the image corresponds to the destructive test result. As oil has a lower acoustic impedance than adhesive, it appears brighter on the acoustic images of the metal/adhesive interface (Fig. 7.26b). It is difficult to achieve full coverage of the desired area with oil because of the high ability of adhesive to remove it from the interface. Therefore the contaminated region always has an irregular shape.

7.5.2. Improper Cure Conditions

Poor cohesive strength in the adhesive joints is often a result of improper curing conditions (insufficient cure temperature or reaction duration, improper adhesive resin/hardener ratio). As discussed in Chapter 5, sound velocity and attenuation undergo significant changes during the curing reaction. Elastic properties and, accordingly, sound velocity and especially attenuation essentially differ for cured and uncured adhesive. This results in a different time of pulse arrival and signal amplitude. Therefore, regions with uncured material are detectable with acoustic microscopy. Though excessive attenuation in some materials (like epoxy) may lead to limitations of the ultrasound penetration depth, this acoustic parameter can be very useful for the detection of the material's conditions and properties. An adhesive that did not reach full reaction completion has a lower sound velocity and higher attenuation due to lower cross-link density and looks darker in the acoustic images. Fig.7.27 represents an image of the adhesive joint with cured and uncured areas of the adhesive made in transmission mode. Ultrasound passes

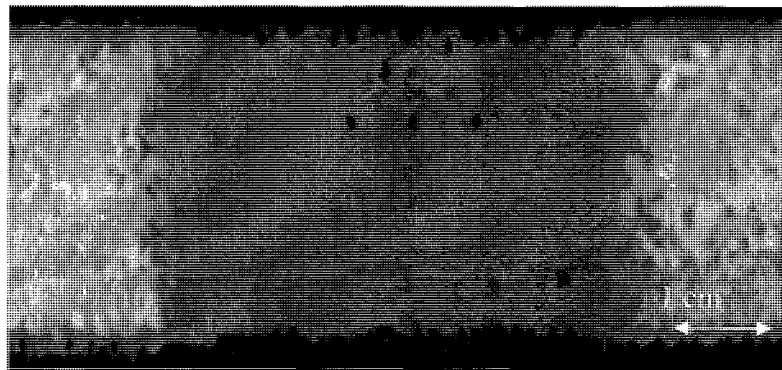


Figure.7.27. Acoustic image of the adhesive joint with uncured adhesive area.

through the material; both amplitude and position of the received signal are monitored. The amplitude of the acoustic wave that passed through the sample is mapped; thus, image shows spatial distribution of the attenuation coefficient. The image has a good contrast (30%), clearly indicating areas with cured (lighter areas) and uncured (darker region due to higher sound attenuation) material.

CHAPTER VIII

Conclusions

This research study has been examined the feasibility of using acoustic methods for evaluation of adhesive mechanical properties. Two methods were used. The first one is based on the measurement of bulk longitudinal sound velocity and attenuation during the process of the adhesive curing reaction. The second method is scanning acoustic microscopy which allows us to visualize an intact adhesive/steel interface. The motivation for this work came from the automotive industry that needs effective non-destructive methods for on-line evaluation quality of the adhesive bond joints.

The focus of this dissertation research is an investigation of viscoelastic properties of structural adhesive systems. As high cohesive strength is one of the major characteristics of structural polymers, it is important to establish correlations between an adhesive's structure and its mechanical performance.

The first step involves the development of the methodology for monitoring of the viscoelastic properties of the adhesive and finding parameters that correlate with the adhesive joint performance. In preliminary study it was shown that the acoustic method is sensitive to variations in epoxy/hardener ratio as well as to the extent of reaction.

The glass transition region was analyzed for the cured adhesive. The glass transition temperature, T_g , determined as the inflection point on the thermomechanical curve of the storage modulus L' , is found to be the closest to the T_g value determined by DSC. However, this value is difficult to measure in a commercial toughened system with a wide glass transition region. Instead, the temperature value of the peak maximum on the $\tan \delta$ curve was used as a reference point for T_g .

The reaction of epoxide polymerization was studied at different temperatures and various heating conditions (isothermal and continuous heating). As a result, correlations of the acoustic and viscoelastic parameters with molecular structure and glass transition temperature of the adhesive were demonstrated. It was found that the adhesive's

longitudinal sound velocity measured non-destructively in the joint structures by a pulse-echo acoustic method correlates with glass transition temperature and cohesive strength of the adhesive bond. Acoustic conversion of the reaction was determined for different curing temperatures. It was shown that, it is not enough to raise the temperature of the reaction just above the T_g value. Because of the wide glass transition region and limited solubility of the crystalline DDA at 100 °C, it is critical to maintain a reaction temperature of at least 140°C to form proper an adhesive structure and to reach sufficient cohesion strength.

Changes in the microstructure on the intact metal-adhesive interface were investigated during the epoxide polymerization reaction. Two-dimensional Fourier transforms allows us to determine the main sizes of the granular structure which is 200 μm . Changes in brightness of the images correspond to changes in the reflection coefficient on the adhesive/metal during the polymerization reaction. It was shown that the adhesive adjacent to the interface has Young's modulus slightly higher than the adhesive in the middle of the layer.

Conditions optimal for visualization of the major defects of the adhesive structure were determined. The capability of scanning acoustic microscopy to detect and dynamically monitor small changes in both structure of the metal/epoxy interface and bulk adhesive material was demonstrated.

Thus, acoustic methods are an effective tool for qualitative and quantitative characterization of the viscoelastic properties of adhesive systems and for estimation of the overall quality of adhesive bonds.

REFERENCES

- (1) Maeva, E.; Severina, I.; Bondarenko, S.; Chapman, G.; O'Neill, B.; Maev, R.; Severin, F. *Canadian Journal of Physics* **2004**, 82, 981-1025.
- (2) Petrie, E. M. In *Adhesives Families*; Handbook of Adhesives and Sealants; McGraw-Hill: 2000; pp 343-414.
- (3) Petrie, E. M. In *Theories of Adhesion*; Handbook of Adhesives and Sealants; McGraw-Hill: 2000; pp 49-91.
- (4) Pham, H. Q.; Marks, M. J. In *Epoxy Resins*; Mark, H. F., Ed.; Encyclopedia of Polymer Science and Technology; Wiley-Interscience: 2004; Vol. 9, pp 678-804.
- (5) Adler, L.; Rokhlin, S.; Baltazar, A. *Determination of material properties of thin layers using angle beam ultrasonic spectroscopy*; Proceedings of the IEEE Ultrasonics Symposium, 2001; Vol. 1, pp 701-704.
- (6) Chapman, G. B.; Sadler, J.; Maev, R. G.; Titov, S.; Maeva, E.; Severina, I.; Severin, F. *Ultrasonic Pulse-Echo Evaluation of Adhesive Bond in Sheet-Metal Assemblies*; in 2006 IEEE International Ultrasonics Symposium; pp.906-909.
- (7) Kinloch, A. J. In *Adhesion and Adhesives; Science and Technology*; Chapman & Hall: London, 1987; pp. 425.
- (8) Ellis, B. In *The kinetics of cure and network formation*; Ellis, B., Ed.; Chemistry and Technology of Epoxy Resins; Blackie Academic & Professional: Glasgow, UK, 1993; pp 72-116.
- (9) Ellis, B. In *Introduction to the chemistry, synthesis, manufacture and characterization of epoxy resins*; Ellis, B., Ed.; Chemistry and Technology of Epoxy Resins; Blackie Academic & Professional: Glasgow, UK, 1993; pp 1-36.
- (10) Bolger, J. C. In *Structural Adhesives for Metal Bonding*; Patrick, R. L., Ed.; Treatise on Adhesion and Adhesives; Marcel Dekker, Inc.: New York, 1973; Vol. 3, pp 2-78.
- (11) Rozenberg, B. A. *Kinetics, thermodynamics and mechanism of reactions of epoxy oligomers with amines*; In *Epoxy Resins and Composites II*; Springer Berlin / Heidelberg: 1986; pp. 113-165.
- (12) Poisson, N.; Maazouz, A.; Sautereau, H.; Taha, M.; Gambert, X. *J. Appl. Polym. Sci.* **1998**, 69, 2487-2497.
- (13) Gilbert, M. D.; Schneider, N. S.; MacKnight, W. J. *Macromol.* **1991**, 24, 360-369.
- (14) Fedtke, M.; Domaratius, F.; Pfitzmann, A. *Pol. Bulletin* **1990**, 23, 381-388.

- (15) Pfitzmann, A.; Fischer, A.; Fryauf, K.; Fedtke, M. *Pol. Bulletin* **1992**, 5, 557-564.
- (16) Gundjian, M.; Cole, K. C. *J. Appl. Polym. Sci.* **2000**, 75, 1458-1473.
- (17) Johnsen, B. B.; Olafsen, K.; Stori, A. *Int. J. Adh. Adh.* **2003**, 23, 155-163.
- (18) Fata, D.; Possart, W. *J. Appl. Polym. Sci.* **2006**, 99, 2726-2736.
- (19) Kinloch, A. J. In *Rubber-Toughened Thermosetting Polymers*; Kinloch, A. J., Ed.; Structural Adhesives: Developments in Resins and Primers; Elsevier Applied Science Publisher Ltd.: New York, USA, 1986; pp 127-162.
- (20) Özpozan, T.; Schrader, B.; Keller, S. *Spectrochimica Acta Part A: Molecular and Biomolecular Spectroscopy Section* **1997**, 53, 1-7.
- (21) Olivier, P.; Ioualalen, K.; Cottu, J. P. *J. Appl. Polym. Sci.* **1997**, 63, 745-760.
- (22) Gao, J.; Li, Y. *Polym. Int.* **2000**, 49, 1590-1595.
- (23) Gillham, J. K.; Enns, J. B. *Trends in Polymer Science* **1994**, 2, 406-419.
- (24) White, S. R.; Mather, P. T.; Smith, M. J. *Pol. Eng. and Sci.* **2002**, 42, 51-67.
- (25) Hojjati, M.; Johnston, A.; Hoa, S. V.; Denault, J. *J. Appl. Polym. Sci.* **2004**, 91, 2548-2557.
- (26) Ramis, X.; Cadenato, A.; Morancho, J. M.; Salla, J. M. *Polymer* **2003**, 44, 2067-2079.
- (27) Pindinelli, C.; Montagna, G.; Luprano, V. A. M. Maffezzoli, A. *Macromol. Symp* **2002**, 180, 73-88.
- (28) Nguyen, N. T.; Lethiecq, M.; Gerard, J. F. *Ultrasonics* **1995**, 33, 323-329.
- (29) Loinetto, F.; Rizzo, R.; Luprano, F. A. M.; Maffezzoli, A. *Materials Sci. Eng. A* **2004**, 370, 284-287.
- (30) Guyott, C. C. H.; Cawley, P. *NDT International* **1988**, 21, 233-240.
- (31) Younes, M.; Wartewig, S.; Lellinger, D. *Polymer* **1994**, 35, 5269-5278.
- (32) Mac Bain, W.; Hopkins, D. G. *J. Phys. Chem.* **1925**, 29, 88-96.
- (33) Van der Leeden, M.C.; Frens, G. *Adv. Eng. Materials* **2002**, 4, 280-289.
- (34) Fourche, G. *Poly Eng Sci* **1995**, 35, 957-967.

- (35) Lee, L. H.; In *Recent Studies in Polymer Adhesion Mechanisms*; Lee, L. H., Ed
Adhesive Bonding; Plenum Press: New York, 1991; 1-31.
- (36) Zisman, W. A. in *Recent Advances in Wetting and Adhesion*; Lee, L. H., Ed.;
Adhesion Science and Technology; Plenum Press: New York, 1975; pp 55-86.
- (37) Mittal, K. L. In *Surface Chemical Criteria for Maximum Adhesion and Their
Verification Against the Experimentally Measures Adhesive Strength Values*; Lee, L.
H., Ed.; Adhesion Science and Technology; Plenum Press: New York, 1975; pp 129.
- (38) Abbot, S. G. *Int. J. Adhesion Adhesives* **1985**, 5, 7-11.
- (39) Kumar, G.; Ramani, K. *J. Comp. Mater* **2000**, 34, 1582-1599.
- (40) Kazayawoko, M.; Balatinecz, J. J.; Matuana, L. M. *J. Materials. Sci.* **1999**, 34, 6189-
6199.
- (41) Messler, R. W.; Gene, S. *J. Thermoplast. Comp. Mater* **1998**, 11, 200-215.
- (42) Packhman, D. E.; Johnson, C. *Int. J. Adhesion Adhesives* **1994**, 14, 131-135.
- (43) Tomas, J. *Chemical Engineering Science* **2007**, 62, 1997-2010.
- (44) Ladizesry, N. H.; Ward, I. M. *J. Materials Sci.* **1989**, 24, 3763-3773.
- (45) Allen, K. W. *Int. J. Adhesion Adhesives* **1993**, 13, 67-72.
- (46) Luan, B.; Robbins, M. O. *Nature* **2005**, 435, 929-932.
- (47) Sharpe, L. H.; Schonhorn, H. In *Contact Angle, Wettability and Adhesion*, Advances
in Chemistry; American Chemical Society: Washington, 1964; Vol. Series 8, pp 189-
201.
- (48) Good, R. J.; Chaudhury, M. K.; van Oss, C. J. In *Theory of Adhesive Forces Across
Interfaces*; L.H. Lee, e., Ed.; Fundamentals of Adhesion; Plenum Press: New York,
1991; 153-173.
- (49) Fowkes, F. M. *J. Adhesion Sci. Tech.* **1987**, 1, 7-27.
- (50) Allara, D. A.; Fowker, F. M.; Noolandi, J.; Rubloff, G. W.; Tirrell, M. V. *Mat. Sci.
Engin.* **1986**, 83, 213-226.
- (51) Fowkes, F. M. *J. Phys. Chem.* **1963**, 67, 2538-2541.
- (52) Owens, D. K.; Wendt, R. C. *J. Appl. Polymer Sci.* **1969**, 13, 1741-1747.

- (53) Wu, S. In *Polymer Interface and Adhesion*; Marcel Dekker: New York, 1982; 172-177.
- (54) Della Volpe, C. C.; Brugnara, M.; Maniglio, D.; Siboni, S. *J. Colloid Interface Sci.* **2004**, *271*, 434-453.
- (55) van Oss, C. J.; Good, R. J.; Chaudhury, M. K. *Langmuir* **1988**, *4*, 884-891.
- (56) van Oss, C. J.; Good, R. J. In *Interfacial Forces in Aqueous Media*; Marcel Dekker: New York, 1994; 12-230.
- (57) Fowkes, F. M. In *Interface Acid-base/ Charge Transfer Properties*; Andrade, J. D., Ed.; Surface and Interfacial Aspects of Biomedical Polymers; Plenum Press: New York, 1985; Vol. Ch. 9,.
- (58) Good, R. J.; van Oss, C. J. Schrader, M. E., Loed, G., Eds.; *Modern Approach to Wettability: Theory and Application*; Plenum Press: New York, 1991; Vol. Ch. 1, pp.33-89.
- (59) Morra, M. *J. Colloid Interface Sci.* **1996**, *182*, 312-314.
- (60) Berg, J. C. In Berg, J. C., Ed.; *Wettability*; Dekker: New York, 1993; pp 49-75.
- (61) Della Volpe, C.; Siboni, S. *J. Colloid Interface Sci.* **1997**, *195*, 121-136.
- (62) Lee, L. *Journal of Adhesion* **2001**, *76*, 163-183.
- (63) Connor, M.; Bidaux, J.; Manson, J. E. *Journal of Materials Science* **1997**, *32*, 5059-5069.
- (64) Penn, L. S.; Defex, E. *J. Mat. Sci.* **2002**, *37*, 505-513.
- (65) Deryagin, B. V.; Smilga, V. P. *J. Appl. Phys.* **1967**, *38*, 4609-4616.
- (66) Yang, S.; Gu, L.; Gibson, R. F. *Composite structures* **2001**, *51*, 63-71.
- (67) Hays, D. A. In Lee, L. H., Ed.; *Fundamentals of Adhesion*; Plenum Press: New York, 1999; pp 56-149.
- (68) Feng, J. Q.; Hays, D. A. *Powder Technology* **2003**, *65*, 135-136.
- (69) Zhou, H. et al. *Powder Technology* **2003**, *82*, 135-136.
- (70) Czarnecki, W. S.; Schein, I. B. *J. Electrostatics* **2004**, *61*, 107-115.
- (71) Hays, D. A. *J. Adhes. Sci. Technol.* **1995**, *9*, 1063-1073.

- (72) Weaver, C. *Faraday Spec. Discuss. Chem. Soc.* , **1972**, 2, 18-25.
- (73) Mizes, H., Ott, M., Eklund, E., Hays, D.. *J. Adhesion* **2000**, 65, 11-23.
- (74) Voyutski, S. S. In *Autohesion and Adhesion of High Polymers*; Wiley-Interscience: New York, 1963; pp.1-33.
- (75) Pravatareddy, H.; Dillarad, J. G.; McGrath, J. E.; Dillard, D. A. *J. Adhesion* **1999**, 69, 83-98.
- (76) Hansen, C. M.; Just, L. *Int. Eng. Chem. Res.* **2001**, 40, 21-25.
- (77) Vasenin, R. M. In *Adhesion: Fundamentals and Practice*; McLaren: London, 1969; pp 2-29.
- (78) de Gennes, P. G. *J. Chem. Phys.* **1971**, 55, 572-579.
- (79) Doi, M.; See, H. In *Introduction to Polymer Physics*; Oxford University Press: USA, 1996; pp. 36-47.
- (80) Graessley, W. W. *Adv. Polymer Sci.* **1982**, 47, 76-117.
- (81) Bikerman, J. J. In *The Science of Adhesive Joints*; Academic Press: New York, 1968; pp.137.
- (82) Fabulyak, F. In *Molecular flexibility in the border layers*; Naukova Dumka: Kiev, 1983; pp.5-12.
- (83) Veselovsky, R. A. In *Adhesion of Polymers*; McGraw-Hill: New York, 2001; pp. 67-183.
- (84) Duprée, A. In *Theorie Mechanique de la Chaleur*; Gauthier-Villars: Paris, 1869; , pp 393.
- (85) Good, R. G. In *Measurement of adhesion of thin film*, Mittal, K. L., Ed.; Thin Film and Bulk Coating; 1978; ASTN American Society for Testing and Materials, **640**, pp 18-29.
- (86) Kalnins, M.; Ozolins, J. *Intl. J. Adhesion Adhesives* **2002**, 22, 179-185.
- (87) Sharpe, K. *The Journal of Adhesion* **1972**, 4, 51-64.
- (88) Schmidt, R.; Bell, J. *Epoxy Resins and Composites II* **1986**, 33-71.
- (89) Drzal, L. T. In *The interphase in epoxy composites*; Epoxy Resins and Composites II; Springer Berlin / Heidelberg: 1986; Vol. 75, pp 1-32.

- (90) Nakazawa, M.; Somorajai, G. A. *Applied Surface Science* **1995**, 84, 309-323.
- (91) Nakazawa, M. (. *Nippon Steel Technical Report* **1994**, 63, 16-22.
- (92) Bouchet, J.; Roche, A. *The Journal of Adhesion* **2002**, 78, 799-830.
- (93) Crompton, J. S. *J. Mater. Sci.* **1989**, 24, 1575-1581.
- (94) Nigro, J., Ishiada, H. *J Appl Polym Sci* **1989**, 38, 2191-2204.
- (95) Gaillard, F.; Hocquaux, H.; Romand, N.; Verchere, D. In Proc. of European Adhesive Congress, Karlsruhe, Germany, 1992, pp 122-127.
- (96) Kollek, H. *International Journal of Adhesion and Adhesives*, **1985**, 5, 75-80.
- (97) Maguire, J. F.; Talley, P. L.; Lipowski, M. *The Journal of Adhesion* **1994**, 45, 269-290.
- (98) Nakamae, K.; Nishino, T.; Airu, X.; Asaoka, S. *International Journal of Adhesion and Adhesives* **1995**, 15, 15-20.
- (99) Carter, R. O.; Dickie, R. A.; Holubka, J. W.; Lindsay, N. E. *Ind. Eng. Chem. Res.* **1989**, 28, 48-51.
- (100) Holubka, J. W.; Bach, R. D.; Andres, J. L. *Macromolecules* **1992**, 25, 1189-1192.
- (101) Kinzler, M.; Grunce, M.; Blank, H.; Schenkel, H.; Scheffler, I. *J. Vac. Sci. Technol.* **1992**, 10, 2691-2697.
- (102) Bremont, M.; Brockmann, W.; Guimon, M. F.; Pfister-guillouzo, G. *The Journal of Adhesion* **1993**, 41, 147-168.
- (103) Perepechko, I. In *Acoustic methods of investigating polymers*; Mir Publishers: Moscow, USSR, 1975; pp 312. Gillham, J. K.
- (104) Ferry, J. In *Viscoelastic properties of polymers*; New York : Wiley, 1980; pp 1-141.
- (105) Sperling, L. H. In *Introduction to Physical Polymer Science*; Wiley-Interscience: 2005; pp 85-168.
- (106) Ngai, K. L.; Plazek, D. J. In *Temperature Dependences of the Viscoelastic Response of Polymer Systems*; Physical Properties of Polymers Handbook; Springer: New York, 2007; pp 455-478.

- (107) Chartoff, R. P. In *Thermal Analysis*; Mark, H. F., Ed.; Encyclopedia of Polymer Science and Technology; Wiley-Interscience: 2004; Vol. 4, pp 1-86.
- (108) Parthun, M. G. Dielectric and ultrasonic studies of macromolecular growth during polymerization, McMaster University, McMaster University, 1997, .
- (109) Gillham, J. K. In *Thermosets*; Mark, H. F., Bikales, N., Overberger, C. G., Menges, G. and Kroschwitz, J., Eds.; Encyclopedia of Polymer Science and Technology; John Wiley & Sons: 1986; Vol. 4, pp 284-326.
- (110) Sinha, M.; Buckley, D. J. In *Acoustic Properties of Polymers* ; Physical Properties of Polymers Handbook; Springer: New York, 2007; pp 1021-1031.
- (111) Cheeke, J. D. N. In *Fundamentals and Applications of Ultrasonic Waves*; CRC Press: 2002; , pp 188-262.
- (112) Cawley, P. *IEEE Ultrasonics Symposium* **1992**, 767-772.
- (113) Adams, R. D.; Drinkwater, B. W.; *Int. J. Material and Product Technology* **1999**, 14, 385-398.
- (114) Szilard, J. In *Physical principles of ultrasonic testing*; Ultrasonic testing; John Wiley & Sons: New York, 1982; pp 1-24.
- (115) Gillham, J. K. In *Acoustic testing of materials*; Nondestructive testing techniques; John Wiley & Sons, Inc.: New York, 1992; pp -148-253.
- (116) Maev, R. G.; Shao, H.; Maeva, E. Y. *Materials Characterization* **1998**, 41, 97-105.
- (117) Maeva, E. Y.; Severina, I. A.; Severin, F. M.; O'Neill, B.; Maev, R.Gr. In *Some approaches of ultrasonic evaluation of the metal sheets adhesive bonds*; Review of Progress in Quantitative Nondestructive Evaluation. Proceeding of QNDE; Melville: New York, 2004, 2004; pp 937-943.
- (118) Goglio, L.; Rossetto, M. *NDT&E International* **1999**, 32, 323-331.
- (119) Goglio, L.; Rossetto, M. *Ultrasonics* **2002**, 40, 205-210.
- (120) Challis, R. E.; Freemantle, R. G.; Wilkinson, G. P.; White, J. D. H. *Ultrasonics* **1996**, 34, 315-319.
- (121) Thompson, W. J. *Journal of Applied Physics* **1950**, 21, 89-93.
- (122) Haskell, N. A. *J. Bull. Seism. Soc. Am.* **1953**, 43, 17-43.

- (123) Pollock, D. S. G. In *A Handbook of Time-Series Analysis, Signal Processing and Dynamics*; Academic Press: 1999; pp 130-184.
- (124) Vine, K.; Cawley, P.; Kinloch, A. J. *NDT &E International* **2002**, *35*, 241-153.
- (125) Moidu, A. K.; Sinclair, A. N.; Spelt, J. K. *Research in Non-destructive Evaluation* **1999**, *11*, 81-95.
- (126) Pilarski, A.; Rose, J. L. *Journal of Applied Physics* **1988**, *63*, 300-307.
- (127) Tattersall, H. G. *Journal of Applied Physics D: Applied Physics* **1973**, *6*, 819-832.
- (128) Munns, I. J.; Georgiou, G. A. *Insight* **1995**, *37*, 941-952.
- (129) Clark, A. V. J.; Hart, S. D. *Materials Evaluation* **1982**, *40*, 866-873.
- (130) Quate, C. F. *Physics Today* **1985**, *38*, 34-42.
- (131) Briggs, A. In *Acoustic Microscopy*; Monographs on the Physics and Chemistry of Materials; Claredon Press: Oxford, NY, 1992, pp 25-59.
- (132) O'Neill, B.; Maev, R. G. *Canadian Journal of Physics* **2000**, *78*, 803-821.
- (133) Zheng, Y.; Maev, R. G.; Solodov, I. Y. *Canadian Journal of Physics* **1999**, *77*, 927-967.
- (134) Severina, I. A.; Fabre, A. J.; Maeva, E. Y. *Acoustic imaging of microstructure and evaluation of the adhesive's physical, mechanical and chemical properties changes at different cure states*, 28th International Acoustical Imaging Symposium, San Diego, CA, March 20-23, 2005; in *Acoustical Imaging*; 2007 Vol. 28, Plenum publishing Corp., pp. 367-374.
- (135) Maeva, E.Y., Severina, I., Chapman II, G., Severin, F., O'Neill, B., Maev. R.Gr. *Acoustic visualization of interface deterioration in adhesive bond joints*, in 27th International Acoustic Imaging Symposium, Saarbrücken, Germany, March 24-27, 2003, *Acoustical Imaging*, V. 27, Kluwer Academic Publishers, Saarbrücken, 2004, pp.99-104.
- (136) Brown, R. In *Handbook of Polymer Testing*; Marcel Dekker Inc.: New York, 1999;pp. 485-547.
- (137) Hagemaiier, D. J. In *ASM Handbook Nondestructive Evaluation and Quality Control*; USA, 1996; Vol. 17, pp 610-758.
- (138) Cros, B.; Gigot, V.; Despaux, G. *Applied Surface Science* **1997**, *119*, 242-252.

- (139) Yamanaka, K.; Nagata, Y.; Koda, T.; Karaki, K. In *IEEE Ultrasonic Symposium*, **1990**; Vol. 2, pp 913-920.
- (140) Hadimioglu, B.; Foster, J. S. *Journal of Applied Physics* **1984**, *56*, 1976-1980.
- (141) Billson, D. R.; Hutchins, D. A. *Brit. J. NDT* **1993**, *35*, 705-709.
- (142) Drinkwater, B.; Cawley, P. *Brit. J. NDT* **1994**, *36*, 430-433.
- (143) Drinkwater, B. W.; Cawley, P. *Materials Evaluation* **1997**, *40*, 401-406.
- (144) Schindel, D. W.; Hutchins, D. A.; Grandia, W. A. *Ultrasonics* **1996**, *34*, 621-627.
- (145) Gudra, T.; Pluta, M.; Kojro, Z. *Ultrasonics* **2000**, *38*, 794-798.
- (146) E. Yu. Maeva, I. A. Severina, G. B. Chapman II, F. M. Severin, Monitoring of adhesive cure process and following evaluation of adhesive joint structure by acoustic techniques, 9th European NDT Conference (ECNDT), Berlin, Germany, September 25-27, 2006 (<http://www.ndt.net/article/ecndt2006/doc/We.2.2.4.pdf>)
- (147) Maeva, E. Y.; Severina, I.; Chapman, G. B. *Research in NDE* **2006**, *18*, 121-1338.
- (148) Hirsekorn, S.; Arnold, W. *Ultrasonics* **1998**, *36*, 491-498.
- (149) Guo, Z.; Achenbach, J. D.; Madan, A.; Martin, K.; Graham, M. E. *Thin Solid Films* **2001**, *394*, 188-200.
- (150) Parthasarathi, S.; Tittmann, B. R.; Ianno, R. J. *Thin Solid Films* **1997**, *300*, 42-50.
- (151) Frihart, C. R. *Int J Adhes Adhes* **2004**, *24*, 415-422.
- (152) Ashcroft, W. R. In *Curing Agents for Epoxy Resins*; Ellis, B., Ed.; Chemistry and Technology of Epoxy Resins; Blackie Academic & Professional: Glasgow, UK, 1993; pp 37-71.
- (153) Ochi, M.; Takahashi, R.; Terauchi, A. *Polymer* **2001**, *42*, 5151-5158.
- (154) Dutta, S.; Karak, N. *Pigment & Resin Technology* **2007**, *36*, 74-82.
- (155) Baek, J.; Park, S.; Gong, H.; Kim, W. *Macromol. Symp.* **2007**, *249-250*, 654-659.
- (156) Hawkins, J. M. U.S. Patent Patent 3,525,779.
- (157) Amitay-Sadovsky, E.; Wagner, H. D. *J. Polym. Sci. B Polym. Phys.* **1999**, *37*, 523-530.

- (158) Abedian, B.; Garcia-Godoy, F.; Garcia-Godoy, F. *J. Appl. Polym. Sci.* **2005**, *97*, 426-431.
- (159) Martínez-Burgos, J. M.; Benavente, R.; Pérez, E.; Cerrada, M. L. *J. Polym. Sci. B Polym. Phys.* **2003**, *41*, 1244-1255.
- (160) Schneider, K. *Polymer Surfaces and Interfaces* **2008**, *35*, 139-160.
- (161) Mark, J. E. In *Acoustic Properties of Polymers*; Physical Properties of Polymers Handbook; Springer: New York, 2007; pp 1021-1031.
- (162) Alig, I.; Oehler, H.; Lellinger, D.; Tadjbach, S. *Progress in Organic Coatings* **2007**, *58*, 200-208.
- (163) Melzak, K. A.; Martin, F.; Newton, M. I.; Mchale, G.; Gizeli, E. *J. Polym. Sci. B Polym. Phys.* **2002**, *40*, 1490-1495.
- (164) Kasap, S. O.; Mirchandani, V. *Measurements in Science and Technology* **1993**, *4*, 1213-1218.
- (165) Janting, J. *MEMS/NEMS* **2006**, 905-921.
- (166) Pham, H. Q.; Marks, M. J. In *Epoxy Resins*; Mark, H. F., Ed.; Encyclopedia of Polymer Science and Technology; John Wiley & Sons: 2004; Vol. Part 3: Volume 9, pp 678-704.
- (167) Morgan, R. J. In *Structure-property relations of epoxies used as composite matrices*; Epoxy Resins and Composites I; Springer: Berlin / Heidelberg, 1985; Vol. 72, pp 1-43.
- (168) Ellis, B. In *Chemistry and Technology of Epoxy Resins*; Kluwer Academic Publishers: 1993; pp 31-332.
- (169) Barral, L.; Cano, J.; López, A. J.; Lopez, J.; Nogueira, P.; Ramírez, C. *Thermochimica Acta* **1995**, 269-270, 253-259.
- (170) Maffezzoli, A.; Quarta, E.; Luprano, A. M.; Montagna, G.; Nicolais, L. *J. Appl. Pol. Sci.* **1999**, *73*, 1969-1977.
- (171) Guyott, C. C. H.; Cawley, P.; Adams, R. D. *Journal of Adhesion* **1986**, *20*, 129-159.
- (172) Freemantle, R. J.; Challis, R. E. *Meas. Sci. Technol.* **1998**, *9*, 1291-1302.
- (173) Piche, L. *IEEE 1987 Ultrasonics Symposium* **1987**, 1125-1130.
- (174) Winfree, W. P. *IEEE 1986 Ultrasonics Symposium* **1986**, 1009-1012.

- (175) Clarke, A. R.; Eberhardt, C. N. In *Microscopy Techniques for Materials Science*. Woodhead Publishing: 2002; pp 459-484.
- (176) Plazek, D. J.; Ngai, K. L. In *The Glass Temperature; Physical Properties of Polymers Handbook*; 2007; pp 187-215.
- (177) Chartoff, R. P. In *Thermal analysis of polymers*; Encyclopedia of polymer science and technology; John Wiley & Sons: 2005; pp 1-96.
- (178) Miller, A. A. *Ann. N. Y. Acad. Sci.* **1981**, 371, 322-323.
- (179) Miller, A. C.; Minko, S.; Berg, J. C. *Journal of Adhesion* **2001**, 75, 257-266.
- (180) Johari, G. P. *Ann. N. Y. Acad. Sci.* **1976**, 279, 117-140.
- (181) Oleinik, E. *Epoxy Resins and Composites IV* **1980**, 49-99.
- (182) Alers, G. A.; Flinn, P. L.; Buckley, M. J. *Material Evaluation*, **1977**, 31, 77-84.
- (183) Mimura, K.; Ito, H. *Polymer* **2002**, 43, 7559-7566.
- (184) Kamon, T.; Furukawa, H. In *Curing mechanisms and mechanical properties of cured epoxy resin*; Advances in Polymer Science, Springer: Berlin / Heidelberg, 1980; Vol. 80, pp 173-202.
- (185) Teil, H. J. *Appl. Pol. Sci.* **2004**, 93, 1774-1756.
- (186) Maeva, E. Y.; Severina, I.; Severin, F. M.; Maev, R. G. In *Application of high-resolution acoustic imaging for adhesive bond evaluation*; CD-ROM Proceedings, available at <http://www.ndt.net/abstract/wcndt2004/444.htm>: 2004;
- (187) Sinclair, A. N.; Dickstain, P. A.; Spelt, J. K.; Segal, E.; Segal, Y. In *Acoustic resonance methods for measuring dynamic elastic modulus of adhesive bonds*; Alan Wolfenden, Ed.; Dynamic Elastic Modulus Measurements in Materials; ASTM International: 1990; , pp 162-179.
- (188) Duchet, J.; Pascault, J. P. *J. Polym. Sci. B Polym. Phys.* **2003**, 41, 2422-2432.
- (189) Calleja, F. J. B.; Fakirov, S. In *Microhardness of Polymers*; Cambridge University Press: Cambridge, UK, 2000; , pp 120-236.
- (190) Safavi Ardebili, V.; Sinclair, A. N.; Spelt, J. K. *Journal of Adhesion* **2000**, 73, 385-416.
- (191) Baldan, A. *Journal of Materials Science* **2004**, 39, 4729-4797.

- (192) Bockenheimer, C.; Fata, D.; Possart, W. *J. Appl. Polym. Sci.* **2004**, *91*, 369-377.
- (193) Guimon, M. F.; Pfister-Guillouzo, G.; Bremont, M.; Brockmann, W.; Quet, C.; Chenard, J. Y. *Applied Surface Science* **1997**, *108*, 149-157.
- (194) Loh, W. K.; Crocombe, A. D.; Abdel Wahab, M. M.; Ashcroft, I. A. *International Journal of Adhesion and Adhesives* **2005**, *25*, 1-12.
- (195) Sands, J. M.; Fink, B. K.; McKnight, S. H.; Newton, C. H.; Gillespie Jr., J. W.; Palmese, G. R. *Clean Products and Processes* **2001**, *2*, 0228-0235.
- (196) Rokhlin, S. I.; Marom, D. *J. Acoust. Soc. Am.* **1986**, *80*, 585-590.
- (197) Hartshorn, S. R. In *The durability of structural adhesive joints*; Hartshorn, S. R., Ed.; Structural adhesives: chemistry and technology; Plenum Press: NY, 1986; pp 347-403.
- (198) Xiao, G. Z.; Shanahan, M. E. R. *J. Appl. Polym. Sci.* **1998**, *69*, 363-369.
- (199) Apicella, A.; Nicolais, L. In *Effect of water on the properties of epoxy matrix and composite*; Epoxy Resins and Composites I; 1985; Vol. 72, pp 69-77.
- (200) Rattana, A.; Abel, M.; Watts, J. F. *The Journal of Adhesion* **2005**, *81*, 963-988.
- (201) Brewis, D. M.; Comyn, J.; Shalash, R. J. A. *Int. J. Adhesion Adhesives* **1982**, *2*, 215-222.
- (202) Bolger, J. C.; Michaels, A. S. In *Molecular Structure and Electrostatic Interactions at Polymer-Solid Interfaces*; Weiss, P., Ed.; Interface Conversion for Polymer Coatings; Elsevier: N.Y., 1969; pp 5-43.
- (203) Handbook of Adhesives (ed. I. Skeist), Van Nostrand Reinhold, NY (1990), pp. 620
- (204) The Dow Chemical Company, *Material Safety Data Sheet for BETAMATETM* 1496V, pp.1-9.

APPENDIX A: Copyright Permissions.



COPYRIGHT TRANSFER

REN 9-08

Date: _____

The copyright, title, interest, and all rights, including subsidiary and/or derivative rights, in all languages in the work entitled:

ultrasonic analysis of the degree of cure and cohesive properties of the adhesive in a bond joint.
by *Klaerner, E. Ya., Severina, T., Chapman G. B.*

is hereby assigned and transferred to The American Society for Nondestructive Testing, Inc. (hereinafter ASNT) effective if and when the work is accepted for publication.

Furthermore, this assignment and transfer applies to all other publications or reproductions by ASNT or its licensee, in which the above work may be reproduced subsequent to its appearance in:

Research in Nondestructive Evaluation (RNDE)

ASNT reserves the right to edit this work. However, the author and/or copyright holder reserves the following rights:

1. All proprietary rights (such as patent rights) other than copyright
2. The right to make oral presentation of the same material in any form.
3. The right to grant or refuse permission to third parties to republish all or part of the work or translations thereof. Such third parties must obtain ASNT's written permission as well.
4. The right to use all or part of this work in future works of author or author's capacity as either author or editor, without charge, provided ASNT is properly credited as the source.

The author and/or copyright holder affirms that the work does not contain material the publication of which would violate any copyright, trademark, intellectual property rights or other personal or proprietary rights of any private person or entity or governmental or quasi-governmental entity. *Caution: the author is specifically reminded and cautioned that NDT processes, procedures, techniques, etc. may be the subject of U.S. government classification regulations; the unauthorized publication thereof may expose the author to prosecution under applicable federal laws. Therefore, the author must carefully verify sources of data other than those originated by the author.* In addition, the author warrants that the work has not been published previously elsewhere.

Government-funded authors only

- ☐ This is a work of the federal government and is not subject to copyright.
- ☐ This is a work for hire. The federal government retains the nonexclusive right to reproduce this work.

Signatures of all authors or copyright holders required

| | | |
|-------------------------|-------------|-------|
| Signature of author(s): | Print name: | Date: |
|-------------------------|-------------|-------|

This document, fully executed, must be received before the manuscript can be accepted for publication. If the manuscript is not published by ASNT, this copyright transfer will not take effect. Send form fax-mail e

Assistant Editor, ASNT
1711 Arlington Lane
Columbus, OH 43228-0518
(800) 222-2768 or (614) 274-6003 X205
e-mail <rndecopyright@asnt.org>



BETWEEN NATIONAL RESEARCH COUNCIL OF CANADA ("NRC") Research Press

AND: Maeva, E.; Severino, I.; Bondarenko, S.; Chapman, G.; O'Neill, B.; Maev, R.; Severin, F

(This is not a process of copyright transfer or authorized sharing of intellectual property, government or otherwise)

1. This refers to the manuscript entitled: Acoustic methods for the investigation of adhesively bonded structures: A review

(the "Manuscript"), manuscript number [redacted], written by the following

author(s): Maeva, E.; Severino, I.; Bondarenko, S.; Chapman, G.; O'Neill, B.; Maev, R.; Severin, F

for publication in: Canadian Journal of Physics

2. In consideration of NRC Research Press agreeing to publish the Manuscript, the Author(s) grant to NRC, for the full term of copyright in the Manuscript and any extensions thereto, subject to clauses 3 and 4 below, an irrevocable, royalty-free, exclusive licence in perpetuity (a) to publish, reproduce, distribute, display, and store the Manuscript in all forms, formats, and media whether now known or hereafter developed (including without limitation in print, digital or electronic form) throughout the world, (b) to translate the Manuscript into other languages, create adaptations, summaries or extracts of the Manuscript or other derivative works based on the contribution and exercise all of the rights set forth in (a) above in such translations, adaptations, summaries, extracts, and derivative works, and (c) to license others to do any or all of the above.
3. Ownership of the copyright remains with the Author(s), and provided that, when reproducing the Manuscript or extracts from it, the Author(s) acknowledge and reference publication in the Journal, the Author(s) retain the following non-exclusive rights:
 - (a) To reproduce the Manuscript in whole or in part in any printed volume (book or thesis) of which they are the author(s).
 - (b) They and any academic institution where they work at the time may reproduce the Manuscript for the purpose of course teaching.
 - (c) To post a copy of the Manuscript as submitted up to the date of acceptance, or a copy of the Manuscript as accepted for publication after peer review six months after publication of the printed edition of the Journal, on the Author(s) own Web site or institutional repository, or the Author(s) funding body's designated archive, provided that they also give a hyperlink from the Manuscript to the Journal's Web site.
 - (d) To reuse figures or tables created by them and contained in the Manuscript in other works created by them, provided the original publication in an NRC Research Press journal is acknowledged through a note or citation.
4. In consideration of the NRC agreeing to publish the Manuscript, the Author(s) also grant to NRC for the full term of copyright and any extensions thereto the same rights that have been granted in respect of the Manuscript as set out in clause 2 above, in supplementary data submitted with the manuscript to be made available on the Web site, but on a non-exclusive basis.
5. NRC acknowledges that an earlier version of work or material contained within the Manuscript may have been submitted to a pre-print service or archive such as arXiv (in accordance with that service's standard licence terms).

Canada

(200005)

1 of 2



6. The Author(s) warrant and represent that
- (a) The Author(s) are the sole authors and owners of the copyright in the material. If the material includes materials of others, the Author(s) have obtained the permission of the owners of the copyright in all such materials to enable them to grant the rights contained herein. Copies of all such permissions have been sent to the editorial or publisher's office.
 - (b) The Author(s) qualify for authorship, and the manuscript, or its equivalent, has not been submitted for publication elsewhere. If it is accepted for publication by the NRC, or its equivalent, it will not be submitted for publication elsewhere.
 - (c) All of the facts contained in the material are true and accurate.
 - (d) Nothing in the Material is obscene, defamatory, libellous, violates any right of privacy or infringes any intellectual property rights (including without limitation copyright, patent or trademark) or any other human, personal or other rights of any kind of any person or entity or is otherwise unlawful.
 - (e) Nothing in the material infringes any duty of confidentiality which any of the Author(s) may owe to anyone else or violates any contract, express or implied, of any of the Author(s), and all of the institutions in which work recorded in the material was carried out have authorized publication of the material.
7. The Author(s) authorize NRC to take such steps as it considers necessary, in its own absolute discretion and at its own expense, in the Author(s)' name and on their behalf if it believes that a third party is infringing or is likely to infringe copyright in the Manuscript, including but not limited to taking proceedings.
8. The Author(s) hereby consent to the inclusion of electronic links from the material to third-party material wherever it may be located.
9. The undersigned declares that he/she is:
à titre exclusif de la NRC
- ☐ the sole author of the Manuscript and the sole owner of the copyright in the Manuscript.
 - ☒ a co-author of the Manuscript and a part owner of the copyright in the Manuscript, in conjunction with interests held by co-authors, or their employers.
 - ☐ an agent of my employer with authority to assign the copyright in the Manuscript owned by the employer, who is:
10. Submission of this Manuscript does not guarantee publication. If the Manuscript is withdrawn, rejected, or not published within 2 years after acceptance, the licence is revoked.

Signed at on
(City, Province or State) (day, month, year)

Name & Title: Per:
(Please print) (Signature)

Reset form

Print form and sign

Canada

000000

2 of 2

Dear Madam,

With reference to your request (copy herewith) to reprint material on which Springer Science and Business Media controls the copyright, our permission is granted, free of charge, for the use indicated in your enquiry.

- I.A. Severina, A.J. Fabre and E.Yu. Maeva *Acoustic Imaging of Microstructure and Evaluation of the Adhesive's Physical, Mechanical and Chemical Properties Changes at Different Cure States* in *Acoustical Imaging V. 28*, (ed. Michael P. André), 2007, pp. 367-374

- E.Yu. Maeva I.A. Severina, G.B. Chapman II, F.M. Severin B. O'Neill, R.GR. Maev, *Acoustic Visualization of Interface Deteriorations on Adhesive Bond Joints, Acoustical Imaging V. 27* (ed. W. Arnold and S. Hirsekorn), Kluwer Academic Publishers, Netherlands, 2004, pp. 99-104

This permission

-allows you non-exclusive reproduction rights throughout the World.

-permission includes use in an electronic form, provided that content is password protected;

-at intranet;

-excludes use in any other electronic form. Should you have a specific project in mind, please reapply for permission.

-requires a full credit (Springer/Kluwer Academic Publishers book/journal title, volume, year of publication, page, chapter/article title, name(s) of author(s), figure number(s), original copyright notice) to the publication in which the material was originally published, by adding: with kind permission of Springer Science and Business Media.

The material can only be used for the purpose of defending your dissertation, and with a maximum of 100 extra copies in paper.

Permission free of charge on this occasion does not prejudice any rights we might have to charge for reproduction of our copyrighted material in the future.

Best wishes,

Nel van der Werf (Ms)

Rights and Permissions/Springer

Van Godewijckstraat 30 | P.O. Box 17

3300 AA Dordrecht | The Netherlands

tel +31 (0) 78 6576 298

fax +31 (0)78 65 76-300

tel.vanderwerf@springer.com

www.springer.com

VITA AICTORIS
INA A. SEVIARYNA

Education

- 2002-2008 **Ph.D. Candidate**, Chemistry
Department of Chemistry and Biochemistry, University of Windsor
Advisor: E. Maeva
- 1986-1991 **M.Sc. combined with B.Sc**
Lomonosov's Moscow State University, Biology Department, Moscow, Russia.
Advisor: E. P. Iordan,
thesis: Effect of synthesis stimulation of desokciribonucleotide-reductase from *Propionibacterium freidenraheii* ssp. Shermani by DNA synthesis suppression.

Awards

- 2006 Casino Windsor Cares/Gail Rosenblum Memorial Breast Cancer Research Scholarship
- 2004 Conference Travel Award
- 2004, 2005 University of Windsor Tuition Scholarship
- 2002, 2003 Visa Differential Student Fee Bursary, University of Windsor, Canada

Employment history

- 2002-2008 **Research Assistant**
Department of Physics,
University of Windsor, Windsor
- 2002-2005 **Graduate Assistant**
Department of Chemistry and Biochemistry
University of Windsor, Canada
- 1991-2002 **Research Associate**
Laboratory of Nucleic Acids Components
Institute of Microbiology, National Academy of Science, Belarus

Publications

Articles in Refereed Journals

1. E. Yu. Maeva, **I. Severina**, G. B. Chapman, Analysis of the degree of cure and cohesive properties of the adhesive in a bond joint by ultrasonic techniques, *Research in Nondestructive Evaluation*, 18, n. 2, (2007), p 121-138
2. E. Maeva, **I. Severina**, S. Bondarenko, G. Chapman, B. O'Neill, R. Maev, F. Sevarin. Acoustical Methods for Investigation of Adhesively Bonded Structures: A Review. *Canadian Journal of Physics* (2004), V. 82, pp. 981-1025
3. Barai, V.N., **Severina**, I.A., Kukharskaya, T.A., Zinchenko, A.I. "Preparative Dephosphorilation of Calcium Salts of 2'(3')-Mononucleotides with Extracellular Phosphatase from *Spicaria violacea*" *Applied Biochemistry and Microbiology*, v.36; No 1 (2000), pp.8-12

4. Barai, V.N., Zinchenko, A.I., **Bravseovich I.A.**, Mikhailopulo, I.A. "A Chemo-Enzymatic Hydrolysis of Calcium Salt of RNA to Nucleosides", *Biotechnology Techniques*, v.10, No11, (1996)

Refereed conference proceedings

1. **I. Seviaryna**, J. Farlam, G. Ghodsi, E. Maeva, Investigation of Elastic Properties and Microstructure of the Biofiber Composites with Acoustic Microscopy Methods, *10th International Conference on Progress in Biofibre Plastic Composites*, Toronto, May 12-13, 2008
2. **I. Seviaryna**, G. Ghodsi, E. Maeva, Investigation of the Structure of New Biofiber Composite Materials with Advanced Ultrasonic Imaging Methods, *2008 CAP Congress in Laval University*, Quebec, Quebec, June 8-11, 2008
3. **I. Severina**, J. Sadler, E. Maeva, F. Severin, R.Gr. Maev, Evaluation of Adhesive Physical, Chemical and Micromechanical Properties with Acoustic Imaging Methods, *29th International Symposium on Acoustical Imaging*, Shonan Village, Kanagawa, Japan, April 16-18, 2007
4. **I. Severina**, G.B. Chapman II, J. Sadler, S. Titov, E. Maeva, F. Severin, R. Gr. Maev, High Frequency Acoustic Imaging Methods for Adhesive Bond Microstructure Study and Physical, Chemical and Micromechanical Properties Evaluation, *ASNT Automotive Industry Advancements with NDT Topical Conference*, Dearborn, MI, May 16-17, 2007.
5. E. Yu. Maeva, **I. A. Severina**, G. B. Chapman II, F. M. Severin, Monitoring of adhesive cure process and following evaluation of adhesive joint structure by acoustic techniques, *9th European NDT Conference (ECNDT)*, Berlin, Germany, September 25-27, 2006 (<http://www.ndt.net/article/ecndt2006/doc/We.2.2.4.pdf>)
6. D. Watt, Y. Huang, B. Baylis, **I. Seviaryna**, E. Maeva, Measuring the Depth of Penetration of the Laser Beam in the Absorbing Material for through-Transmission Welding Processes, *ANTEC Annual Technical Conference*, Charlotte, NC, May 7-11, 2006
7. **I. A. Severina**, A. J. Fabre, and E. Yu. Maeva, Acoustic imaging of microstructure and evaluation of the adhesive's physical, mechanical and chemical properties changes at different cure states, *28th International Acoustical Imaging Symposium*, San Diego, CA, March 20-23, 2005
8. **Severina, I.**, Maeva, E. Yu. Adhesive cure monitoring with acoustic method, *16th World Conference on Nondestructive Testing*, Montreal, Canada, September 3, 2004, CD-ROM Proceedings, available at <http://www.ndt.net/abstract/wcndt2004/458.htm>
9. Maeva, E.Y., **Severina, I.**, Chapman II, G., Severin, F., O'Neill, B., Maev. R.Gr. Acoustic visualization of interface deterioration in adhesive bond joints, in *27th International Acoustic Imaging Symposium*, Saarbrücken, Germany, March 24-27, 2003, Acoustical Imaging, V. 27, Kluwer Academic Publishers, Saarbrücken, 2004, pp.99-104.

Technical Reports

1. **I. Seviaryna**, G. Ghodsi, J. Sadler, E. Maeva, R. Gr. Maev, Investigation of the acoustic properties and microstructure of the bio-based composites with acoustic techniques, Poster at The Ontario BioCar Initiative 1st Annual Research Meeting, in University of Guelph, Guelph, Canada, May 8, 2008,
2. E. Maeva, **I. Severina**, R. Maev, O'Neill, F. Severin, "The Acoustic Microscopy inspection of the adhesive bonding quality". Report for DaimlerChrysler Corp., March 30, 2002
3. E. Maeva, **I. Severina**, E. Schulhoff, Chemical Composition and Development of Ultrasonic Coupling with System Matching Impedance and Viscosity, Tessonics, 2006, Published.

4. E. Maeva, **I. Severina**, E. Schulhoff, Optimal Composition and Process of Mixing Components for Design of Ultrasonic Coupling with System Matching Impedance and Viscosity, Tessonics, 2006, Published.
5. E. Maeva, **I. Severina**, G. Chapman, Acoustical Properties of the Adhesive Bond Joints Based on Betamate 1496 Adhesive, Daimler Chrysler Corporation, 2005, Published.
6. **I. Severina**, A. Balutiu, E. Maeva, Investigation of the Internal Structure of the Adhesive/Metal Interfaces on Specimens Cured at Different Temperatures, 3M, 2005, Published.
7. **I. Severina**, E. Maeva, Patchwork Blank Sample Inspection with Acoustic Microscope, Report for Mercedes Corporation, 2004, Published.
8. **I. Severina**, E. Maeva, Acoustical Images of Specimens from a Carbon-Glass Fiber-Reinforced Composite Wheel, DaimlerChrysler Corporation, 2003, Published.
9. E. Maeva, **I. Severina**, R. Maev, B. O'Neill, F. Severin, The Acoustic Microscopy Inspection of the Adhesive Bonding Quality, Report for DaimlerChrysler Corporation, 2002, Published, March.